THE UNIVERSITY
of EDINBURGH

Investigation of the role of hepatic stellate cells in acute liver failure and hepatocarcinogenesis

Alexandra Inés Thompson

Submitted for the degree of Doctor of Philosophy

University of Edinburgh

2016

Declaration of Authorship

I declare that the work presented within this thesis was carried out by myself during the course of my PhD. It has not been submitted for any other degree or qualification. Where I have included the work of others, the sources of information are clearly stated.

Signed:……

Printed name:….....

List of Figures

Chapter 2

Chapter 3

Chapter 4

Chapter 5

Chapter 6

List of Tables

Acknowledgements

I would like to thank the many people who have contributed to the work presented in this thesis. Firstly, I would like to thank my principal supervisor, Neil Henderson, for endless support, encouragement and mentorship. I would also like to thank John Iredale, for academic mentorship and his assistance in securing a CRUK Clinical Research Training Fellowship.

Special thanks are due to Kylie Conroy, who was tirelessly patient with me in teaching laboratory techniques, and who, together with Stephen Greenhalgh, worked closely with me on developing the intravital imaging parts of the project. Thanks are also due to Mhairi Donnelly, who contributed to immunohistochemistry, and to the other members of the Henderson group, who always offered help and advice, and have been a pleasure to work with.

Dr Timothy Kendall kindly provided help with histological identification of hepatocellular carcinoma, and image analysis. Furthermore, Rebecca Aucott helped with learning immunohistochemistry and was extremely supportive throughout my PhD, in her role as laboratory manager.

I would also like to thank David Griggs, one of our US collaborators, who provided compound CWHM12 for integrin inhibitor experiments, and assisted with pharmacokinetic modelling.

I am heavily indebted to our CRUK collaborators Martin Lee and Alan Serrels, whose expertise with intravital imaging and the custom-built multiphoton microscope was invaluable. Similarly, I would like to thank Margaret Frame, David Cameron, and CRUK for funding my research.

I wish to express my gratitude to all the technicians in the animal units, and specifically to Jon Henderson, who is an enormous asset to the Henderson group, and whose kindness, diligence and meticulous colony management was immensely appreciated. Thanks also to Ken Simpson, for managing the Project Licence, and for offering welcome advice regarding paracetamol experiments.

Finally, I would like to thank my gastroenterology colleagues, friends, family, and especially Aedán, for putting up with me during this period of research.

Abstract

Introduction: Hepatic stellate cells (HSC) and myofibroblasts may be relevant stromal drivers of human hepatocellular carcinoma (HCC). It was hypothesised that targeted inhibition of αv integrin-mediated TGF-β activation, by HSC or hepatocytes, may result in reduced peri-tumoural and intra-tumoural extracellular matrix formation, and reduced hepatic carcinogenesis.
The role of HSC in acute liver injury is less well characterised. It was anticipated that integrin signalling on HSC and hepatocytes might also be relevant in the acute setting.
The emerging technique of intravital microscopy (IVM) allows detailed, real-time investigation of the cellular processes involved in hepatocyte injury, cell death and repair. It was hypothesised that this could be coupled with mouse models of HCC and acute liver injury, to perform sequential imaging under anaesthesia.
Aims: (i) To determine the effect of targeted inhibition of αv integrins on HSC and hepatocytes, during hepatocarcinogenesis, in a mouse model of HCC. (ii) To investigate the effect of targeted inhibition of αv and other integrins on HSC, hepatocytes, and liver sinusoidal endothelial cells (LSEC), during acute liver injury, in the mouse model of paracetamol-induced liver injury. (iii) To develop IVM of the liver, via an abdominal imaging window, with optimisation of surgical and imaging techniques, to allow sequential imaging of the same animal.
Methods: The diethylnitrosamine (DEN)-induced mouse model of hepatocarcinogenesis was used, and PDGFRβ-Cre;$\alpha v^{fl/fl}$ and Alb-Cre;$\alpha v^{fl/fl}$ mice were employed to deplete αv integrins on HSC and hepatocytes respectively. Tumours were harvested at 40 weeks post-DEN. Tumour size and number was evaluated in all animals.
PDGFRβ-Cre;$\alpha v^{fl/fl}$ and Alb-Cre;$\alpha v^{fl/fl}$ mice were used in the paracetamol model, to investigate the role of αv integrins in acute liver injury. PDGFRβ-Cre;$\beta 8^{fl/fl}$ and Alb-Cre;$\beta 8^{fl/fl}$ animals were also tested in this model. The role of integrins in liver sinusoidal endothelial cells (LSEC) during paracetamol-induced liver injury was evaluated using Cdh5-Cre mice.
IVM of the liver was performed by surgical implantation of an abdominal imaging window, consisting of a titanium ring and coverslip, secured in place with a purse string suture. Fluorescent reporter mice were used to identify hepatic and vascular architecture, and other label-free microscope technologies were utilised to image collagen, lipid distribution, necrotic areas and blood flow within tissues.
Results: In large cohorts of PDGFRβ-Cre;$\alpha v^{fl/fl}$, Alb-Cre;$\alpha v^{fl/fl}$, and control animals, there was no difference in mean tumour size or number, at 40 weeks. Targeted inhibition of αv integrins and β8 integrin on hepatocytes, HSC or LSEC was not protective in paracetamol-induced liver injury.
IVM of the liver can be performed on animals with HCC and throughout paracetamol-induced liver injury, to obtain high quality, real-time images of multiple cell lineages and the hepatic microenvironment.
Conclusions: The role of TGF-β in HCC pathogenesis is complex and context-dependent. Targeted loss of αv integrin did not result in reduction in tumour burden in this non-cirrhotic model of HCC. IVM of the liver is a powerful tool to quantify inflammatory infiltrates and assessment of vascular remodelling throughout the course

of acute liver injury and regeneration, providing insights into the biological processes determining recovery.

Lay summary

Cancer of the liver (hepatocellular carcinoma) is the commonest cause of death in patients with chronic scarring of the liver (cirrhosis). Over 90% of liver tumours arise in a scarred or 'fibrotic' liver, and to date there are no effective anti-fibrotic treatments to halt the development of cirrhosis. Furthermore, chemotherapy options for hepatocellular carcinoma (HCC) are limited. Only one, sorafenib, is currently licensed for advanced HCC, and this provides at best a modest survival benefit. Many new chemotherapy agents have been tested in patients with HCC, but have not been proven to improve outcome. This may partly be due to the fact that the liver tissue surrounding the tumour is abnormal and scarred; signals from this cirrhotic environment may act to support the growth of cancer cells.

The hepatic stellate cell is the major source of scarring proteins during liver injury and fibrosis. The integrin family of receptors are present on these cells, and form an important link between cells and their surrounding environment, as well as playing a role in signalling during scar formation. Using a mouse model of liver cancer, I have investigated the effect of removing an integrin protein (αv integrin) on stellate cells, and hepatocytes, to see if this protects against cancer formation.

Acute liver failure is another life-threatening condition, and paracetamol poisoning is the main cause in the UK and US. Although there is an antidote available, this is not sufficient to cure all cases, and deaths still occur. Although liver transplant is effective for severe liver failure, this is a limited resource; furthermore around half of patients meeting transplant criteria will have psychiatric or medical contraindications to this treatment. As such, there is a pressing need for alternative treatments for paracetamol-induced acute liver failure.

I have therefore investigated the effect of loss of different integrin proteins in a mouse model of paracetamol-induced acute liver failure. I have also developed a new way to study liver injury and repair, in this model. Other groups have previously shown that the liver can be imaged in live mice, by surgically placing a titanium window in the abdomen, with a glass coverslip, and secured in place with a suture. Using a microscope with powerful lasers, the animal can then be imaged under general anaesthetic. I have developed this technique in our laboratory, and modified and optimised surgical protocols. I have been able to image the same mouse over several days, allowing

assessment of biological processes occurring throughout the course of liver injury and regeneration.

To our knowledge, this technique has not been performed before in mice with liver cancer or paracetamol-induced liver failure. The use of genetically modified mice, which express different fluorescent proteins to colour specific cell types (such as stellate cells and hepatocytes) has been coupled with microscope techniques to image liver scarring and blood flow, to obtain a large amount of information from one animal, in real-time. It is hoped that this will allow further experiments to investigate the biological processes governing recovery from acute liver injury, and potentially identify new targets for development of effective drug treatments.

Publications and presentations arising from this thesis

Publications:

Thompson AI,* Conroy KP,* Henderson NC. Hepatic stellate cells: central modulators of hepatic carcinogenesis. BMC Gastroenterology. 2015: 15(63). PMID: 26489516. (*Joint first authors).

Vliegenthart AD, Shaffer JM, Clarke JI, Peeters LE, Caporali A, Bateman DN, Wood DM, Dargan PI, Craig DG, Moore JK, **Thompson AI**, Henderson NC, Webb DJ, Sharkey J, Antoine DJ, Park BK, Bailey MA, Lader E, Simpson KJ, Dear JW. Comprehensive microRNA profiling in acetaminophen toxicity identifies novel circulating biomarkers for human liver and kidney injury. Scientific Reports. 2015: 5 (15501). PMID:26013123.

Presentations:

Thompson AI, Simpson E, Simpson KJ, Iredale JP, Henderson NC. Role of αv integrin-mediated TGF-β activation in hepatocarcinogenesis. April 2016. Poster Presentation. EASL. Barcelona, Spain.

Thompson AI, Simpson E, Simpson KJ, Iredale JP, Henderson NC. Role of αv integrin-mediated TGF-β activation in hepatocarcinogenesis. March 2016. Poster Presentation. SSG/BSG Joint Spring Meeting. Edinburgh, UK.

Thompson AI, Conroy KP, Greenhalgh SN, Lee M, Simpson KJ, Iredale JP, van Rheenan J, Serrels A, Henderson NC. Real-time, sequential, intravital imaging of paracetamol-induced acute liver injury and repair. March 2016. Poster Presentation. SSG/BSG Joint Spring Meeting. Edinburgh UK. (Awarded the Derek Gillen Poster Prize).

Thompson AI, Conroy KP, Lee M, Simpson KJ, Iredale JP, van Rheenan J, Serrels A, Henderson NC. An intravital imaging approach to study acute liver injury and repair in real time. September 2015. BASL Basic Science Retreat. Newton-Abbot, UK.

Abbreviations

μm micrometer
α-SMA alpha smooth muscle actin
AIH Autoimmune hepatitis
ALD Alcoholic liver disease
ALF Acute liver failure
ALP Alkaline phosphatase
ALT Alanine transaminase
Ang Angiopoietin
AST Aspartate aminotransferase
ATP Adenosine triphosphate
B7H1 Human B7 homolog 1
BCG Bacillus Calmette-Guérin
BCLC Barcelona liver clinic cancer
BDL Bile duct ligation
CAD Computer-assisted design
CAF Cancer associated fibroblasts
CARS Coherent anti-Stokes Raman scattering
CCL_4 Carbon tetrachloride
CLL Clodronate liposomes
CM Conditioned medium
Con A Concanavalin A
Cre Cyclization recombinase
CSF1 Colony-stimulating factor 1
DAB 3,3'-diaminobezidine
DEN Diethylnitrosamine
DAMPs Damage-associated molecular patterns
DILI Drug-induced liver injury
DNA, Deoxyribonucleic acid
ECLAD Extracorporeal liver assist device
ECM Extracellular matrix
EMT, Epithelial-mesenchymal transition
eGFP Enhanced green fluorescent protein
EGF Epidermal growth factor

FAK Focal adhesion kinase

FGF Fibroblast growth factor

FLIM Fluorescent lifetime imaging microscopy

FRAP Fluorescence recovery after photobleaching

FSP Fibroblast specific protein

Fv single chain antibody variable fragment

GFAP Glial fibrillary acidic protein

GFP Green fluorescent protein

H and E Haematoxylin and eosin

HBV Hepatitis B virus

HCC Hepatocellular carcinoma

HCV Hepatitis C virus

HGF Hepatocyte growth factor

HSA Human serum albumin

HSC Hepatic stellate cell

HVP High volume plasma exchange

ICAM-1 Intercellular adhesion molecule-1

IFN-γ Interferon gamma

IGF Insulin-like growth factor

*i*NKT Invariant natural killer T cells

I/R Ischaemia reperfusion

IV Intravenous

IVM Intravital microscopy

JNK c-jun N-terminal kinase

loxP Locus of X-over in P1

LAP Latency associated peptide

LPS Lipopolysaccharide

LSEC Liver sinusoidal endothelial cells

LysM Lysozyme M

M6P Mannose-6-phosphate

MAPK Mitogen-activated protein kinases

MARS Molecular adsorbent recirculating system

MD Moderately differentiated

mGFP Membrane-targeted GFP

mRNA Messenger ribonucleic acid

miRNA Micro ribonucleic acid
MDSC Myeloid-derived suppressor cell
MHC Major histocompatibility complex
MMPs Matrix metalloproteinases
MP Multiphoton
MPT Membrane permeability transition pore
NADH nicotinamide adenine dinucleotide
NAFLD Non-alcoholic fatty liver disease
NAD(P)H nicotinamide adenine dinucleotide phosphate
NAPQI *N*-acetyl-p-benzoquinone-imine
NET Neutrophil extracellular trap
NIR Near-infrared
NO Nitric oxide
ns Nanoseconds
OCT Optimum cutting temperature
PBC Primary biliary cirrhosis
PBS Phosphate-buffered saline
PCR Polymerase chain reaction
PD Poorly differentiated
PDL-1 Programmed death ligand 1
PEG Polyethylene glycol
PML Progressive multifocal leukoencephalopathy
PI3K Phosphatidylinositol 3 kinase
PPB PDGFRβ receptor recognising peptide
PPL-g-PEG Poly-L-lysine-g-poly(ethylene glycol)
PSR Picosirius
RA Retinoic acid
RBC Red blood cells
RFP Red fluorescent protein
RGD Linear arginine-glycine-aspartic acid motif
RNA Ribonucleic acid
scAb Single chain antibody
siRNA Small interfering ribonucleic acid
SC Subcutaneous
SEM Standard error of the mean

SHIM Second harmonic imaging microscopy

SHG Second harmonic generation

SIRS Systemic inflammatory response syndrome

TAA Thioacetamide

Td tomato Tandem dimer tomato

TGF-β Transforming growth factor-beta

TIMP-1 Tissue inhibitors of metalloproteinases 1

TNF Tumour necrosis factor

TLR Toll-like receptor

TPEF Two photon excitation fluorescence

UV Ultraviolet

VEGF Vascular endothelial growth factor

WD Well-differentiated

YFP Yellow fluorescent protein

Chapter 1: Introduction

1.1 Clinical consequences of hepatic fibrosis: chronic liver disease

Cirrhosis of the liver develops as a consequence of progressive tissue fibrosis. This is a wound-healing response, arising from chronic inflammation due to sustained or repeated liver injury. Histologically, cirrhosis is defined as advanced liver fibrosis with diffuse nodular regeneration, causing marked distortion of hepatic vascular architecture.[1] Dense fibrotic septae link central veins and portal tracts. This creates a direct anastomosis between portal vessels and central veins, allowing shunting of blood. The resistance to portal blood flow leads to portal hypertension and hepatic synthetic dysfunction.[2] This can manifest clinically with decompensating events such as abdominal ascites, hepatic encephalopathy, variceal haemorrhage, and hepatorenal syndrome. Furthermore, chronic liver disease is the major risk factor for development of hepatocellular carcinoma (HCC). These complications account for much of the morbidity and mortality attributable to cirrhosis, with HCC representing the commonest cause of death in these patients.

Cirrhosis is an increasing problem, particularly in developed countries. It is the 14th commonest cause of death in adults worldwide but the fourth commonest in central Europe.[2] It is responsible for 1.03 million deaths per year worldwide,[3] and is the indication for 5500 orthotopic liver transplants each year in Europe.[4] The aetiology of cirrhosis varies geographically. In sub-Saharan Africa and most parts of Asia chronic hepatitis B virus (HBV) infection is the commonest cause, whereas in more developed countries, hepatitis C virus (HCV) infection, alcohol misuse and, increasingly, non-alcoholic liver disease predominate.

In the UK, deaths from liver disease have increased fourfold between 1980 and 2013. This has been largely attributed to increasing alcohol consumption. In contrast to improvements in health and life expectancy observed over the past 30 years for other chronic disorders such as stroke, heart disease, and many cancers, there is a highly conspicuous lack of progress in liver disease. Whilst alcohol misuse is a critical factor, there is growing concern for the long-term consequences of obesity. At present, 25% of the UK population are categorized as ‘obese’. Most of these will have non-alcoholic fatty liver disease, and up to one in 20 of the UK population will have persistent inflammation and scarring, ultimately leading to cirrhosis. Whilst effective treatments for viral hepatitis have been developed, there are still substantial pools of people infected with HBV or HCV that remain unrecognized, and dissemination of treatment is a challenge. It is projected that the prevalence of end-stage liver disease from HCV infection will continue to increase until 2020.[5]

The hepatic myofibroblast in liver fibrosis

The perisinusoidal hepatic stellate cell (HSC) is a key effector of fibrogenesis.[6] HSC are mesenchymal cells, located in the space of Disse between specialized hepatic sinusoidal endothelium and hepatocytes. These cells are characterized by their cytoplasmic storage of vitamin A (retinoid) droplets. In acute and chronic tissue injury, HSC shed their retinoid and lipid droplets, transforming to an activated, myofibroblast-like phenotype. This state is typified by expression of collagen I and alpha smooth muscle actin (α-SMA). The extracellular matrix-secreting phenotype also results in production of fibrillar collagen, elastin and fibrotic matrix deposition.[7-10] The specific origin of these cells has previously been a source of controversy. Portal myofibroblasts, circulating fibrocytes and mesenchymal stem cells, as well as peritoneal mesoepithelial cells can all give rise to a myofibroblast population.[6,11-16] However, the relative contribution of each lineage is not entirely clear. It is likely that the cellular origin is related to the site and duration of injury; Iwaisako et al performed fate-mapping experiments to show that chronic hepatotoxic (CCL_4-induced) injury preferentially activated HSC to myofibroblasts, whereas bile duct ligation (BDL) injury activated portal fibrobasts to this phenotype.[17] However, evidence suggests that HSC remain the predominant source of hepatic myofibroblasts; in Iwaisako's study, HSC contributed significantly to the myofibroblast population at later stages in the BDL model.[17]

Critical stimuli to HSC activation include transforming growth factor β1 (TGF-β1) which promotes a fibrogenic collagen-secreting phenotype, and PDGF stimulation, which promotes a proliferative phenotype.[18,19] HSC are also extremely sensitive to the extracellular components they are in direct physical contact with, which allows matrix elements to profoundly affect their behavior.[20] HSC activation is accompanied by upregulation in expression of tissue inhibitors of metalloproteinases (TIMPs), chemotactic and vasoactive factors. [21-23] The accumulation of the fibrotic scar requires both increased matrix deposition and a simultaneous reduction in matrix degradation. The major secreted TIMP, TIMP-1 inhibits the matrix degrading activities of a wide variety of matrix metalloproteinases (MMPs), shifting the balance in favour of scar deposition.[6]

Reversibility of fibrosis

It is increasingly recognized that hepatic fibrosis is a reversible process, after removal of the causative agent. This has been observed in both clinical practice and experimental fibrosis models induced by alcohol, CCL_4 and BDL.[24-27] Resolution of fibrosis is accompanied by senescence and apoptosis of myofibroblasts.[25,28] Myofibroblast apoptosis simultaneously removes a critical source of extracellular matrix deposition, as well as TIMP production, thereby reverting the balance to favour matrix degradation.

Loss of signalling from fibrogenic cytokines can lead to HSC senescence and death receptor mediated cell death.[27] Reduction in fibrogenic signals or antiviral drug therapy can result in caspase 8/caspase3-dependent apoptosis of HSC, via increased HSC expression of Fas receptor, tumour necrosis factor (TNF) receptor 1 and their ligands. Caspase-9-mediated programmed cell death is also possible, via overexpression of pro-apoptotic proteins including p53, Bax and Bcl-2.[24] Furthermore, natural killer cells and liver specific T cells are involved in resolution of fibrosis. These cells are activated by interferon-γ (IFN-γ) to induce rapid killing of HSC.[27] Additionally, myofibroblasts can regress to an inactive phenotype during resolution.[29,30]

Despite extensive human and animal examples of regression of fibrosis, it is clear that there are some irreversible components of progressive chronic injury. The development of septal fibrosis, for example, is thought to be a factor in defining the extent to which fibrosis is reversible.[31] Whilst significant remodelling (and therefore functional improvement) can occur in the context of cirrhosis if the injuring agent is removed, complete regression of all the anatomic features (such as pathological vascular shunts in portal-central septae) is unlikely to occur.[31] In clinical practice, this has implications for long-term management of the potential complications of cirrhosis, in particular ongoing HCC risk.

1.2 Clinical consequences of fibrosis: hepatocellular carcinoma

HCC is the second leading cause of cancer-mortality, and was responsible for more nearly 746 000 deaths in 2012.[32] Again, chronic hepatitis B virus infection remains the major risk factor globally, with 80% of cases occurring in eastern Asia and sub-Saharan Africa. In most countries, the mortality rate of HCC approximates the incidence, which is increasing.[33-35] This partly due to the rising prevalence of advanced fatty liver disease and chronic hepatitis C, alongside other risk factors such as hepatitis B infection and alcohol-related cirrhosis. Some progress has been made with prevention, for example emerging antiviral agents and vaccination for hepatitis B. However, the vast majority of HCC cases are associated with fibrosis, and 90% of tumours develop in cirrhotic livers.[33,34,36-39] Furthermore, liver disease severity markers correlate with tumour

formation. Currently there are no effective anti-fibrotic therapies available to halt the fibrosis-cirrhosis-HCC continuum. In the last twenty years, diabetes and obesity have emerged as significant risk factors for non-alcoholic fatty liver disease/non-alcoholic steatohepatitis. These conditions also confer increased risk of HCC, which typically is not universally associated with cirrhosis.[40] This has implications for the future; whilst the advent of directly-acting antiviral treatments for hepatitis C is expected to significantly reduce HCC incidence in HCV-infected patients,[41] conversely, metabolic risk factors are projected to increase, likely with an accompanying propensity to HCC.

Patients who present with early disease may benefit from resection, transplantation or loco-regional therapy (radiofrequency ablation or transcatheter arterial chemoembolization). At present, the Barcelona Clinic Liver Cancer (BCLC) staging system is the most widely used prognostic scoring system for HCC, having been externally validated and updated.[42,43] It is hoped that this system could be refined in future, by the incorporation of tumour marker and genetic expression profile information. At presentation, one third of patients are eligible for potentially curative therapies, and these can extend median survival times beyond 60 months.[44] However, many are unsuitable for curative treatment due to advanced malignancy, or the severity of co-existing liver disease. The multi-tyrosine kinase inhibitor sorafenib is the only available systemic chemotherapy agent with proven survival benefit for advanced stage HCC. However, it confers at best a modest overall survival benefit (from a median of eight months to eleven months) and its use is limited to those with well-preserved liver function.[33] Whilst there is scope to optimize our use of existing treatments, for example by targeting tumours earlier and combining local and systemic approaches, efforts to broaden our chemotherapy armamentarium have been disappointing. Numerous molecular therapies with robust preclinical evidence for efficacy have failed to show benefit in clinical trials. This may in part reflect the abnormal tumour microenvironment, which acts to support the persistence and growth of cancer cells, and has resulted in the peri-tumoural stroma and its cellular inhabitants becoming an intense area of study in the search for efficacious therapies for HCC.

Advances in targeted therapies for HCC

Over the past decade, genomics-based analyses of patients with HCC have identified subclasses of the disease, with respect to shared molecular features. This has allowed

an initial classification of tumours based on proliferative and non-proliferative genotypes.[45-48] Each of these groups represents approximately 50% of patients.[44] The proliferative subclass is characterized by activation of classic RAS, mTOR and/or insulin-like growth factor (IGF) signalling. It is associated with poor outcome in comparison to the non-proliferative phenotypes.[44,46-49] The proliferative subclass is subdivided into two more phenotypic groups, namely the Wnt/TGF-β group, which demonstrates activation of these pathways, and the progenitor-cell group. The progenitor cell group is in general more heterogeneous, but is characterized by expression of progenitor cell, epithelial cell adhesion molecule and keratin, and type I cytoskeletal 19 markers. These tumours tend to overexpress α-fetoprotein at early stages.[44] However, at present, there is no definitive consensus as to whether a specific molecular subclass clearly determines patient outcome. It is also difficult to design adequately powered clinical trials to study a single molecular subclass. It is currently unclear, for example, whether patients with HCC exhibiting features of the Wnt/TGF-β subclass would respond to treatment with TGF-β inhibitors.[44] Due to the challenges of investigating a single molecular subclass, interest has focused on whether gene prognostic signatures could be a better predictor of patient outcomes. These gene-expression signatures are defined by combinations of genes, that together, when dysregulated, correlate with prognosis.[50] Although up to 30 signatures from either the tumour or adjacent nontumour tissues could be prognostic indicators of HCC outcomes, the validation process needed before these can be incorporated into HCC treatment guidelines is extremely rigorous. Therefore, to date, only several have been identified for possible translation into clinical practice.[44]

In general terms, survival benefits from molecular targeted therapies might be derived from two distinct approaches. One strategy might be to treat all patients with very effective and multi-targeted therapies with acceptable toxicity (such as sorafenib) or a broad mechanism of action (e.g. immune therapies). Another approach might be to target a specific sub-group of patients, who have tumours that depend on a specific molecular pathway to survive and grow. However, treatment with highly selective agents might be limited by factors such as tumour heterogeneity, cell plasticity and potential escape pathways.[44]

Deep-genome sequencing of HCC samples has provided insights into the mutational profile of this tumour, identifying on average 30-40 mutations per tumour, of which 5-8 might be driver mutations.[44] Subsequent functional classification of mutated genes has allowed the identification of key carcinogenic signalling pathways, including the Wnt/β-catenin pathway, chromatin remodelling, oxidative stress, and signalling involving

epidermal growth factor (EGF), platelet-derived growth factor (PDGF), fibroblast growth factor (FGF), vascular endothelial growth factor (VEGF), and IGF, and intracellular mediators like RAS/RAF/MAPK and PI3K/AKT.[51,52] Pharmacologic agents are currently in development to try to target these processes. Over the last ten years, clinical trials testing chemotherapeutic drugs for HCC have yielded little more than a survival benefit for sorafenib. These trials have been reviewed in depth by Llovet et al, and the authors have commented on some lessons from the results.[44] For example, it is acknowledged that severity of liver disease is a potentially confounding factor, and that stratification for specific HCC progression end points, such as portal vein invasion and metastases must be considered. Furthermore, identification of accurate biomarkers of tumour response is highly desirable for use in future trials, so as not to miss potential benefit in subgroups of patients.[44]

Targeted therapies for HCC have historically been focused on antiangiogenic pathways. However, no drug has yet been proven to demonstrate superior efficacy or non-inferiority to sorafenib. Advances in our knowledge of the molecular heterogeneity of this tumour are now being applied to the development of newer agents, which are less restricted to antiangiogenic effects.

The TGF-β signalling pathway is one such example. This will be discussed in more detail in subsequent chapters, but part of the rationale for the development of TGF-β inhibitors for HCC is that such treatments may be expected to have positive effects on the cirrhotic liver, as well as the tumour itself. Galunisertib is a selective TGF-β tyrosine kinase inhibitor, and is currently being evaluated in patients with HCC and glioblastoma multiforme.[44] It was previously shown to block tumour migration, invasion and angiogenesis in cell culture HCC models.[53] In a randomized phase II study assessing two doses of galunisertib, a trend towards longer time to progression was observed in patients that had a greater reduction in serum α-fetoprotein and TGF-β1. Median overall survival was greater in those with a detectable α-fetoprotein response, compared to those without (21.4 months versus 6.8 months)[54] highlighting the potential for activity in selected patient groups. Neutropenia, leukopenia and fatigue were the commonest adverse events. Although α-fetoprotein and TGF-β1 may be useful markers associated with therapeutic effects, a definite predictive marker for choosing patients that are most likely to benefit from galunisertib is still required, and will be pivotal to the ongoing development and use of this agent.[44]

Other pathways of interest include FGF19/FGFR4 signalling, RAS signalling, immune checkpoint pathways and MET signalling.[44] Going forward, HCC drug development will

need to encompass testing nonspecific agents (anticipated to benefit all patients) as well as targeted treatments (evaluated by trials designed with biomarker-based enrichment) expected to benefit certain subpopulations of patients. Ultimately, it is hoped that a personalized oncology approach might be feasible, in which molecular alterations driving tumour progression could be selectively targeted in a specific individual.

1.3 Acute liver failure: clinical perspective

Acute liver failure (ALF) is a rare, but life-threatening condition. It was originally defined as the development of hepatic encephalopathy and coagulopathy in the setting of an acute liver injury, in the absence of chronic liver disease.[55] More modern definitions tend to quantify the interval between onset of symptoms and development of encephalopathy. This can help distinguish the aetiology of the liver injury, and estimate prognosis with supportive medical care alone.[56] Hyperacute cases are usually caused by paracetamol toxicity or viral infection, and encephalopathy develops within a week. Subacute cases evolve more slowly, and may result from idiosyncratic drug-induced liver injury, autoimmune or indeterminate causes. These subacute cases have a worse outcome with medical care alone, despite typically demonstrating less dramatic coagulopathy and encephalopathy.[56]

Current definitions of ALF are heterogeneous, and at present there is no clear consensus. However most studies consider an international normalized ratio >1.5 to represent coagulopathy and any grade of encephalopathy to represent ALF.[57]

Aetiology of ALF

Worldwide, ALF is more common in developing countries, where viral causes (hepatitis A, B and E) are the major precipitants. Conversely, drug-induced liver injury, such as paracetamol overdose, is the predominant cause of ALF in the developed world.[56] Whilst emergency orthotopic liver transplantation is the mainstay of treatment for ALF with poor prognostic features, there are some nontransplant therapies specific to aetiology, which will be briefly summarized below.

Hepatitis A and E are the main viral causes of ALF, although HBV infection is also a recognized cause, particularly in some Asian and Mediterranean areas. Reactivation of hepatitis B during immunosuppressive treatment for other conditions such as cancer or tuberculosis can also result in ALF. Nucleos(t)ide analogues are considered part of management in ALF secondary to hepatitis B infection, however evidence of efficacy is equivocal.[57,58] According to recent data, ribavirin can be effective in acute hepatitis E infection.[59] Rarer, viral causes of ALF include herpes simplex virus, cytomegalovirus,

Epstein-Barr viruses and parvoviruses. IV acyclovir is indicated in cases of herpes simplex.[60]

Drug-induced liver injury (DILI) resulting in ALF is either dose-dependent and predictable, such as paracetamol-induced, or idiosyncratic, probably dose-independent and unpredictable.[56] Paracetamol-induced hepatotoxicity is treated with the antidote *N*-acetylcisteine, and will be discussed in more detail in subsequent chapters. Whilst idiosyncratic DILI is a relatively rare cause of ALF, it carries significant morbidity and mortality.[61] Data from the US Drug Induced Liver Injury Network indicates that antimicrobials and herbal or dietary supplements are the major causes of DILI.[62] In a recent prospective study from this consortium, 899 out of a total of 1257 patients enrolled were considered to have probable, highly likely or definite DILI, and 10% of these died or underwent liver transplantation.[61] In cases where drug hypersensitivity forms part of the clinical picture, or an autoimmune reaction to the drug is suspected, steroids may be employed.[63]

Corticosteroids are also considered in the treatment of severe acute liver injury secondary to autoimmune hepatitis (AIH). There is a significant risk of septic complications in patients with advanced encephalopathy.[57,64] However, a subset of patients with AIH-ALF has been shown to benefit from steroids (initial MELD score <27 and low grade hepatic encephalopathy).[65]

ALF can occur during pregnancy, due to progression of acute fatty liver of pregnancy, or development of the HELLP syndrome (haemolysis, elevated liver enzymes, low platelets). Good outcomes from ALF in this context can be achieved with early delivery of the fetus.[66,67]

Ischaemic hepatitis is a condition observed in critically ill patients, secondary to cardiac, circulatory or respiratory failure. Management centres on cardiovascular support and resuscitation. There is some evidence that statin therapy prior to critical care admission may be protective, in critically ill patients with ischaemic hepatitis.[68]

Wilson's disease is a rare metabolic cause of ALF. Whilst initial treatment with penicillamine or trientine can be of benefit, the development of hepatic encephalopathy heralds extremely poor prognosis. Emergency liver transplantation is the only proven therapeutic option for ALF as a consequence of Wilson's, which is otherwise universally fatal. [57,69]

Acute Budd-Chiari syndrome can present with ALF, and may respond to venous decompression via transjugular intra-hepatic portosystemic shunt or hepatic vein stenting.[70] Other causes of ALF include neoplastic infiltration, heat-stroke and mushroom

ingestion. In 14-20% of patients with ALF, the cause is unidentified despite extensive investigations.[71] These cases are often subacute in nature, and prognosis is poor without transplantation.[56]

Pathophysiology of ALF and the systemic inflammatory response

In ALF, hepatocyte cell death is associated with a systemic inflammatory response syndrome, triggering multiorgan failure. It is now recognized that immune dysregulation is likely to be a key factor in the pathogenesis of ALF, and that an individual patients' outcome is probably determined by their innate immune response to liver injury, rather than the liver injury and hepatocyte necrosis itself.[72]

The systemic inflammatory response syndrome (SIRS) in ALF comprises fever, tachycardia, leukocytosis and increased respiratory rate. It occurs due to both systemic pro-inflammatory cytokines (including TNF-α, IL-1 and IL-6) and anti-inflammatory cytokine release (such as IL-10). It may arise from sterile inflammation or the development of sepsis. Those with initial sterile inflammation are also likely to subsequently develop sepsis. The increased risk of infection probably relates to defective functioning of immune cells, particularly of the innate immune system.

Pro-inflammatory cytokines recruit circulating neutrophils, B and T lymphocytes, and increase vascular permeability secondary to activation of vasoactive mediators, platelets, and the coagulation cascade.[73] A compensatory anti-inflammatory response syndrome is also observed, which represents a counteractive homeostatic phenomenon, to try to prevent overwhelming inflammation. This is characterized by persistently elevated levels of IL-4, IL-10 and TGF-β, as well as defective cellular immune function.[73] Changes induced in monocyte phenotype, for example, result in deactivation of these cells. Not only is there an accompanying decrease in pro-inflammatory cytokine secretion, but IL-10 production is also increased. Eventually, the homeostatic compensatory inflammatory response changes into a pathological state, where there is excessive immunosuppression, leading to increased susceptibility to infection.[73] This is likely to account for the late mortality in refractory septic shock.[74] Other causes of innate immune dysfunction include changes in gut permeability, endotoxinaemia, lipoprotein and albumin dysfunction, and toll-like receptor (TLR) expression.[72] TLR are innate pattern recognition receptors, present on multiple cell-types including neutrophils and hepatocytes. Once pathogen-associated molecular patterns bind to TLR on immune cells, an inflammatory response is initiated. Neutrophil TLR activation results in

phagocytic activity and cytokine release, but it is unclear whether this is a positive or detrimental event in patients with ALF.[75]

Whilst acute liver injury begins with hepatocyte necrosis, the molecular mechanisms causing further necrosis in the absence of ongoing injury are not fully understood.[72] Activation of c-Jun N-terminal kinase (JNK) occurs after a cascade of events initiated by oxidative stress and production of reactive oxygen species. JNK activation results in mitochondrial dysfunction causing further hepatic necrosis and release of damage-associated molecular patterns (DAMPs). These in turn activate hepatic macrophages, and can lead to the assembly of a cytosolic protein complex known as the 'inflammasome'.[76] Inflammasomes sense intracellular danger signals via NOD-like receptors. They initiate the release of the pro-inflammatory cytokines IL-1β and IL-18 via caspase-1 activation. They are able to fine-tune the inflammatory response, by responding to low-threshold signals.[76]

Specifically, the inflammasome in paracetamol-induced ALF is thought to be a critical part of the drug-mediated inflammation within the liver.[76] Jaeschke et al described paracetamol-induced liver injury in terms of three key stages: initiation, amplification and inflammation.[77] In the initiation phase, injury is triggered by production of the reactive metabolite *N*-acetyl-*p*-benzoquinone imine (NAPQI). Mitochondrial damage occurs during the amplification phase, and hepatocyte necrosis worsens. In the third inflammation phase, DAMPs released by dying hepatocytes activate the inflammasome. However the effect of this final event on the degree of hepatocyte death and overall outcome is controversial. It is also unclear whether paracetamol itself can directly cause formation of the immune cell inflammasome, or whether necrotic hepatocyte-derived DAMPs (such as DNA fragments, nuclear HMGB1 and heat shock proteins) are entirely responsible. It has been proposed that DAMPs and the inflammasome are important determinants of hepatic inflammation in response to paracetamol overdose, but their role in hepatocyte death (an early response triggered by toxic paracetamol metabolites) is likely to be limited.[76] It remains unclear as to whether the inflammasome significantly affects liver regeneration in the recovery phase of paracetamol-induced acute liver injury. This is a key question for further research.

Prediction of outcome in ALF

In clinical practice, it is important to identify patients who will benefit most from emergency orthotopic liver transplantation. Candidates for transplantation should be selected early on in the course of liver injury, because progression of multiorgan failure

leads to significant deterioration. A number of different prognostic evaluation scoring systems have been developed to aid decision-making. The presence of encephalopathy, along with patient age, coagulopathy and jaundice are key indicators of poor prognosis without transplantation.[56] The King's College Criteria represent the most well characterized scoring system.[78] In patients who fulfilled these criteria, a systematic review found that survival was found to be 24% in nontransplanted patients with paracetamol-induced ALF.[79] This highlights the urgent unmet need for novel medical therapies to improve outcome.

Experimental alternatives to orthotopic liver transplantation

Orthotopic liver transplant is a limited resource, and the development of alternative strategies to support the failing liver has been a longstanding research aim. Extracorporeal liver assist devices (ECLAD) have been anticipated for many years as a potential bridge to temporarily replace liver function, whilst awaiting transplantation or liver regeneration. These remain at an experimental stage, however, with no single system having been proven to definitively benefit patients with ALF.[56] They can be divided into biological or non-biological devices. Biological ECLAD utilize living liver cells, aiming to harness their hepatic synthetic functions and detoxification properties, for use on the blood or plasma of patients with ALF. Different sources of hepatocytes have been employed. The HepatAssist system, for example, uses porcine hepatocytes within a dialysis cartridge, before a moratorium in the use of porcine hepatocytes was put in place. The Extracorporeal Liver Assist Device uses cells derived from a human hepatoblastoma cell line.[57]

Non-biological systems in contrast, simply aim to replace the detoxification functions of the liver, without providing any synthetic function (as no living cells are involved). The Molecular Adsorbent Recirculating System (MARS) device is one of the most commonly studied non-biological machines. Here, toxic molecules are removed by plasma dialysis across an albumin-porous exchange membrane, with absorption into a number of binding columns. Whilst the use of MARS in patients with ALF has been shown to correlate with biochemical improvements, these may not be sustained. [80,81] A randomized controlled trial of MARS therapy or standard of care alone, performed in patients fulfilling poor prognosis criteria, did not demonstrate a significant survival benefit.[82] Attempts to quantify the overall potential for biological and non-biological ECLAD to improve outcome in ALF and acute on chronic liver failure have revealed conflicting results.[57] One systematic review found that non-biological support systems

reduced mortality in acute on chronic liver failure, however neither biological nor non-biological systems affected mortality in ALF.[83] However, a separate systematic review and meta-analysis investigating survival following both biological and non-biological extracorporeal liver support found that these systems did improve survival in ALF (with number needed to treat of eight) but not acute on chronic liver disease.[84]

To date, development of biological devices have been fraught with technical and logistical challenges. This may be changing, with technologic advances leading to a new generation of such devices.[81] Recently, another novel therapeutic approach has been found to confer a survival benefit; Larsen et al hypothesized that high-volume plasma exchange (HVP) might prevent the development of multiorgan failure and thereby reduce mortality in ALF, by removing deleterious plasma cytokines and adhesion molecules, replacing plasma factors and immunomodulation.[85] Whilst this does not fit the exact definition of an ECLAD, HVP does simulate some of the detoxifying purposes of hepatic support. In a prospective, randomized controlled multicenter trial, 182 patients with ALF received either HVP for three days, or standard medical therapy alone. It was found that treatment improved outcome by increasing liver transplant-free survival.[85] Patients undergoing HVP had significantly reduced circulating levels of DAMPs, TNF-α and IL-6, and reduced markers of monocyte and neutrophil activation. The immunological findings were consistent with the hypothesis that HVP suppresses SIRS associated with ALF and this was also in agreement with the observed improvement in clinically relevant critical illness scores. This study included a relatively large proportion of patients whose aetiology of ALF was paracetamol.[85] Whilst HVP represents a potentially promising adjunct to the management of ALF, further work is required to clarify which patients are most likely to benefit, and whether it remains effective in larger cohorts with more varied aetiologies.

Cell therapy

Transplantation of cells, rather than a whole organ, is in principle, an attractive idea for restoring hepatic function.[86] Repopulation of the liver with functional donor hepatocytes can be attempted by direct injection of cells into the liver, or into the spleen (from which they can subsequently migrate to the liver). In animal models of ALF, hepatocyte transplantation can improve survival.[86,87] Translating this into a clinically applicable human therapy is not straightforward however. Difficulties include limited availability of functional human hepatocytes, and resuscitating cells successfully after cryopreservation.[57]

Problems with access to hepatocytes could potentially be circumvented, for example by using stem cells, or stem cell-derived hepatocytes. In animal studies, rats transplanted with stem cell-derived hepatocyte-like cells had better survival outcomes in ALF (induced by D-galactosamine).[87] However, in humans, stem cell survival post-transplant is a challenge. At present, there is much interest in identifying a source of infinitely expandable hepatocyte-like cells, with good function, phenotypic stability and minimal risk of tumourgenicity.[86] Similarly, the development of protocols to ensure optimal cell delivery, engraftment and survival are the subject of considerable ongoing research.

2.1.1 The role of the microenvironment in HCC

The stroma is a central component of both hepatic fibrosis and carcinogenesis, and is likely a key player in the cellular and molecular mechanisms linking these processes. It remains unclear, however, whether liver fibrosis specifically promotes HCC, or if it is merely a wound-healing by-product of chronic hepatic injury and inflammation, with no direct impact on liver cancer formation.[34-39,88] Evidence would suggest the former; the identification of gene signatures from non-tumoural tissue correlating with late recurrence of HCC, supports the concept of a 'field effect' in cancer development.[33-38,88-101] The role of the microenvironment in hepatocarcinogenesis has recently been reviewed, highlighting the complex interaction between immune, angiogenic, and cancer-associated fibroblastic cells.[33-39,88,90,93,94,96,102] Hepatic stellate cells (HSC, also known as liver-specific pericytes) are the major source of extracellular matrix proteins during liver injury and fibrogenesis.[24,35,37] As master regulators of the fibrotic matrix stellate cells may therefore directly support tumourigenesis. Following liver injury, quiescent stellate cells become activated to matrix-secreting myofibroblasts; it is well established in other systems that complex intercellular signalling networks exist between tumours and tumour-associated fibroblasts, contributing to cancer initiation, growth and progression.[24,35,37,89,91,92,95,97-101] Tumour secretion of cytokines such as transforming growth factor-beta (TGF-β) stimulates myofibroblast activation, leading to profound changes in extracellular matrix (ECM) composition and organization. Therefore, HSC or HSC-secreted products may be either permissive or necessary for oncogenesis and HCC persistence. In other cancers, the identification of pathways that the tumour depends upon for growth and proliferation, so-called 'oncogenic addiction loops' has led to revolutionary therapeutic approaches. The landmark discovery of the protein kinase oncogene BCR-ABL and subsequent development of imatinib, allowed curative treatment of chronic myeloid leukaemia, and paved the way for targeted therapies in other malignancies.[103,104] Other protein kinase inhibitors have translated to clinical practice, including trastuzumab for HER2 positive breast cancer,[105,106] and several drugs for non-small-cell lung cancer: erlotinib and gefitinib in EGFR positive disease, and crizotinib in patients with ALK-rearrangements.[107-112] Targeting other non-kinase oncogenes such as RAS and MYC has proven more challenging; despite extensive genomic profiling of HCC and the identification of promising candidate pathways, targeted inhibition of a driving molecular alteration, applicable to a significant proportion of patients, remains an alluring but elusive goal.[113] Furthermore, the microenvironment

may modulate susceptibility to inhibition of specific oncogenic pathways. Straussman et al developed a co-culture system to test the ability of 23 stromal cell types to influence the susceptibility of 45 different cancer cell lines to 35 therapeutic agents.[90] They demonstrated that stroma-mediated resistance to anti-cancer drugs (especially targeted agents) is common. In particular, although melanomas expressing mutant BRAF respond to vemurafenib, hepatocyte growth factor (HGF) secretion by peri-tumoural stromal cells correlated with resistance to vemurafenib-induced cell death.[90,114,115] This illustrates the importance of stroma-derived resistance to chemotherapy, in many different organs and disease settings. Therefore, in the search for key driver mutations in HCC, the effect of the microenvironment cannot be underestimated. In clinical practice, this may mean that combinations of chemotherapeutic agents are required, to neutralize specific stromal interactions, resulting in greater overall efficacy.

2.1.2 HSC, the extracellular matrix and myofibroblast phenotype in fibrosis

It is well known that activated HSC infiltrate HCC stroma and peri-tumoural tissue, and are localized around tumour sinusoids, fibrous septae and the tumour capsule.[116-118] Activated HSC have also been identified around the periphery of dysplastic nodules within the liver.[119] Following activation to the myofibroblast phenotype, HSC secrete substantial amounts of ECM proteins into the stroma. Fibrotic matrix deposition and degradation by HSC is tightly regulated in the liver. For example, TIMP-1 secretion favours scar deposition by inhibiting the endogenous matrix-degrading activities of various MMPs. However, the balance between and TIMPs and MMPs is complex; activated HSC are also a major source of MMP-2 in vitro, elevation of which has been correlated with increased tumoural collagen I, extracellular remodelling, and HCC progression.[102,120,121]

The biomechanics of the ECM are also relevant. Differentiation of primary hepatocytes is inhibited by culture on a stiff collagen gel, with accompanying promotion of proliferation.[122,123] Increasing matrix stiffness in vitro has also been shown to directly stimulate growth of the HCC cell lines, HuH-7 and HepG2, and reduce chemotherapy-induced apoptosis.[124] Integrin β1 signalling was an integral driver of this response, via Fak, Erk, Pkb/Akt and Stat3 pathways.[124] Furthermore, stromal stiffness is self-perpetuating, causing stellate cell activation, and therefore further fibrosis.[39,125,126] Data in humans support these experimental findings. Ultrasound elastography has demonstrated that measurements of liver stiffness predict HCC development.[127-129] Similarly, established HCC exhibits further increases in matrix stiffness, more so than the peri-tumoural hepatic parenchyma.[130] The mechanical tension provided by an altered

ECM is likely to act on HCC development and progression via outside-in signalling, for example by integrins (discussed below) to support tumour growth and progression. This has also been observed in other malignancies, such as a mouse model of breast cancer.[131] Hepatocarcinogenesis in the context of cirrhosis, however, is a unique model of diseases ECM, and an ideal setting to further characterise and potentially target stromal drivers.

2.1.3 The role of HSC in HCC

The interplay between HSC biology and hepatocarcinogenesis is complex. The mechanisms by which HSC may facilitate HCC development and progression are likely to involve diverse biological processes including regulation of ECM turnover, growth factor and cytokine signalling, promotion of tumour angiogenesis and immunomodulation. These will be summarized below.

Integrins as mediators of HSC/HCC crosstalk

The integrin family of transmembrane receptors allow transduction of signals between the intracellular and extracellular environments.[132] Integrins consist of an α and β subunit, and they regulate cell adhesion, spreading, migration, proliferation and differentiation, as well as ECM deposition and remodelling. Integrins will be discussed in more detail in the following chapter, however evidence for their role in crosstalk between HSC and HCC will be considered below.

Activated HSC promote ECM deposition, via the focal adhesion kinase (FAK)-phosphatidylinositol 3-kinase (PI3K)-Akt pathway, which is a downstream effector of integrin signalling.[133] In vitro, a stiff ECM enhances integrin expression and activity, and formation of focal adhesions.[131] Activation of downstream integrin signalling within the hepatocyte may support the growth and survival of precancerous cells. Matrix stiffness has been demonstrated to correlate with differentiation and chemotherapeutic resistance of human HCC cell lines. Softer matrices abrogate hepatoma proliferation, whereas stiffer matrices promote proliferation.[124,134] An elegant in vivo study by Dong et al involved orthotopic implantation of cells from the HCC cell line McA-RH7777 into rats with different degrees of liver stiffness (achieved by treating with CCL_4 for variable lengths of time). Subsequent microarray analysis of the tumours showed a positive correlation between matrix rigidity and tumour angiogenesis.[134] Associations between collagen deposition, integrin expression and tumourigenicity have been reported in human HCC and murine HCC models.[135,136] Integrin expression in HCC cell lines is highly heterogenous.[137] This was also apparent in two mouse models of HCC; Lai et al characterized and compared

ECM protein changes occurring during tumour development in the PDGF-C overexpressing mouse (a model of HCC associated with fibrosis and angiogenesis) and in the PTEN null mouse (a model of liver tumours of mixed cholangio- and hepatocytic features).[136] They demonstrated that each model had a specific pattern of integrin expression, and commented that specific integrin-laminin interactions could be promising targets for inhibiting microenvironmental factors promoting HCC growth, in tumours with dysregulated PTEN function.[136]

The β1 integrin subfamily has been extensively studied with respect to HCC, and hepatocarcinogenesis is associated with the enhanced expression of integrins α1β1, α2β1 and α3β1, and the acquisition of a migratory phenotype by hepatocytes.[138-140] Moreover, integrin β1 expression in human HCC tissues correlated positively with ECM stiffness, pathological grade and metastasis.[141] Integrin β1 blockade in vitro significantly abrogated migration and invasion of HCC cell lines, induced by TGF-β and EGF.[140,142] This finding was supported by the work of Mizuno et al, who reported that integrin β1 overexpression enhanced HepG2 cell migration.[143] Dong et al more recently suggested that integrin β1 was involved in transduction of ECM signalling into HCC cells, culminating in downstream activation of angiogenic signalling.[134] Using a high-stiffness gel to culture HCC cell lines, Dong et al found that VEGF expression is suppressed by treatment with an integrin β1-specific antibody.[134] SERPINA5 (Protein C inhibitor), a member of the serine protease inhibitor superfamily known to have anti-metastatic and anti-angiogenic effects,[144] is down-regulated in human HCC tissues. Further assessment of its anti-tumourigenic activity demonstrated that this was mediated by effects on the fibrogenic-integrin β1 signalling pathway.[145] The relationship between integrin β1 and ECM stiffness in HCC is further highlighted in a study where resistance of the HCC cell line, Hep3B, to sorafenib, was found to be mediated by integrin β1 and its downstream effector JNK.[146]

Integrin subunits other than β1 have been found to have important roles in HCC progression. Fan et al showed that integrin α6 expression correlated strongly with HCC metastasis in humans.[147] They used a viral short hairpin RNA-mediated strategy to overexpress integrin α6 in HCC cell lines. It was found that integrin α6 could form a complex with CD151, a tetraspanin protein also associated with HCC invasion.[147] Further investigation of this in vivo indicated that the CD151/α6 complex stimulated the PI3K-Akt signalling pathway, leading to enhanced epithelial-mesenchymal transition (EMT) of HCC cell lines.[147]

Crosstalk between integrins and TGF-β signalling has also been investigated in hepatocarcinogenesis. TGF-β receptor 1 (TGF-β R1) activation has been shown to promote HCC cell invasiveness by phosphorylation of the intracellular portion of the β1 subunit of the α5β1 integrin, via Smad-2 and Smad-3. This led to an inside-out conformational change and stimulation of vascular invasion.[148] TGF-β1 has been shown to upregulate other integrins, including α3β1 and α6β1, resulting in increased tumour invasiveness.[149] Specific crosstalk between fibronectin-binding integrins and TGF-β1 can promote cell cycle progression in HCC cells, by activation of c-Src.[150] Crosstalk between integrins, growth factor receptors and ECM proteins, including collagen, have also been shown to modify downstream signal transduction pathways, such as Smad, acting in favour of hepatocyte proliferation, and ongoing HSC activation.[151,152] TGF-β1 has also been shown to affect α5β1 expression and synergistically enhance integrin-mediated FAK phosphorylation and cell adhesion in the HCC cell line SMMC-7721.[153] Integrins may therefore (via modulation of TGF-β signalling) render hepatocytes less sensitive to pro-apoptotic signals in early HCC stages, and more sensitive to tumourigenic differentiation and metastasis signals, in advanced HCC.

HSC growth factor signalling

HSC have been shown to favour HCC tumourigenicity, potentially as a result of a change in their secretory phenotype upon activation. In vitro studies, using conditioned media from activated HSC, have consistently reported increased proliferation, migration and invasion of tumour cells.[154-156] Isolation and subsequent co-culture of human intratumoural HSC with hepatoma cell lines enhanced their viability and migratory capacity.[154] Furthermore, co-transplantation with HCC cells into nude mice promoted tumour formation and growth.[157] Utilising both co-culture and conditioned media from primary human HSC, Giannelli et al found laminin-5 was a mediator of HSC-induced HCC migration via its activation of the MEK/ERK pathway.[158] This was supported by in vivo experiments, in which co-transplantation of murine activated HSC with murine HCC cells (H22 line) into immunocompetent mice resulted in significantly larger tumour volumes.[155] Moreover, implantation of human HCC cell lines (PLC and Hep3B) into nude mice did not form tumours unless activated HSC were concurrently implanted.[154] HepG2 cells did form tumours when implanted alone, however tumour growth was more rapid when co-transplanted with activated HSC.[154] Activated HSC secrete a broad range of growth factors including HGF, TGF-β, FGF, EGF, VEGF and IGF. The following sections discuss their potential contributions to HCC pathogenesis.

Hepatocyte growth factor

HGF is expressed by HSC and myofibroblasts,[159,160] and is a highly potent hepatocyte growth factor, regulating cell proliferation, migration, survival and angiogenesis.[161-164] As such, it is widely regarded as a key factor for tumour cell invasion and metastasis.[165] HGF binding to its receptor, c-MET, induces receptor homodimerization, and a subsequent phosphorylation cascade. A transmembrane receptor tyrosine kinase, c-MET is found in 20-48% of HCCs,[166-168] and has been shown to be expressed by multiple HCC lines.[154] Correlations between increased c-MET and HCC tumour size or invasiveness of HCC have been reported in some studies.[169,170] c-MET overexpression is also associated with a reduced five-year HCC survival, and a c-MET-regulated expression signature has been reported to define a subset of patients with poor prognosis and an aggressive phenotype.[170,171] Within HCC tumours, activated HSC have been found to initiate signalling pathways downstream of c-MET, including NF-κB and ERK leading to tumour proliferation and migration.[154,172]

The pro-tumourigenic activity of fibroblast-secreted HGF has also been reported in vitro. Conditioned media from isolated and activated HSC, pre-incubated with anti-HGF antibodies, was found to abrogate the proliferative and migration-inducing effects on HCC cell lines, seen in non-treated conditioned media.[154] This has also been demonstrated in cancer-associated fibroblasts (CAF) isolated from HCC, where treatment of CAF-conditioned media with an anti-HGF antibody significantly reduced HCC proliferation in Hep3B and MHCC97L cell lines.[156] Moreover, a HGF/c-MET specific antagonist, NK4, has been found to inhibit markedly the fibroblast-induced invasion of cancer cells, both in vitro and in vivo,[173-175] although this has yet to be translated into the clinical setting. Recently, PDGF-C transgenic mice were developed as a murine model of HCC, with similarities to the human disease. In this model, progressive fibrosis and cirrhosis, initiated by ectopic expression of PDGF-C, precedes hepatocyte dysplasia and eventual HCC development.[176] Analysis of livers from these animals demonstrated that expression of hepatic HGF and its receptor were elevated at the time point at which dysplastic foci are present, further suggesting a pro-tumourigenic role for HGF. Activation of HGF/c-MET signalling has also been shown to enhance HCC chemoresistance. Conditioned media from the activated HSC cell line LX-2 enhanced resistance of the HCC cell line Hep3B to the chemotherapeutic agent cisplatin, an effect mediated by HGF.[177] Tumour cells may also potentiate pro-metastatic c-MET signalling

via an autocrine mechanism involving TIMP-1, leading to downstream expression of metastasis-promoting genes.[178,179]

However, HGF signalling is not unidirectional. A high level of bi-directional crosstalk between tumour cells and stromal cells, has been reported. Nakamura et al showed that inducers of HGF are expressed in several carcinoma cell lines, including squamous cell carcinoma, human epidermoid carcinoma, human non-small cell lung cancer cells, human cholangiocarcinoma cells, and SBC-3 human small cell lung carcinoma cells.[180] These HGF inducers include interleukin (IL)-1β, FGF, PDGF and TGF-α and were reported to up-regulate HGF expression by stromal fibroblasts.[180,181] Taken together, these studies highlight that HGF and aberrant c-MET signalling have a critical role in mediating the bi-directional crosstalk between HSC and tumour cells during hepatocarcinogenesis.

TGF-β

The large latent TGF-β complex is secreted by most cell types, including human HSC and hepatocytes.[182,183] It is fixed in the ECM by tranglutaminase-dependent linkage of latent TGF-β binding protein to fibronectin and other ECM proteins, forming a reservoir of latent TGF-β. Evidence would suggest that the role of TGF-β in HCC pathogenesis may be highly context-dependent.[184] It has been postulated that defective TGF-β signalling may promote tumourigenesis secondary to reduced responsiveness to the anti-proliferative effects of TGF-β signalling.[185,186] However, whilst tumour-suppressor functions are observed in the early stages of liver damage and regeneration, TGF-β may also exacerbate tumour invasiveness and metastatic behaviour.[187] Furthermore, TGF-β and PDGF signalling crosstalk has been shown to support EMT and promote tumour growth, and the acquisition of an invasive phenotype.[188]

Autocrine TGF-β signalling has been shown to be necessary for the survival and malignancy of HCC cell lines, including Huh7 and HepG2, with exogenous TGF-β leading to growth inhibition of HCC cells.[189] Using HCC cell lines, Meindl-Beinker et al revealed a heterogeneic response to TGF-β, reflective of different stages and mechanisms of disease. Variation between cell lines in their endogenous TGF-β and Smad7 levels, and their transcriptional activity of Smad3, was related to the maintenance of TGF-β cytostatic activity. Specifically, the Hep3B, HepG2 and PLC hepatoma cell lines were found to have low TGF-β and Smad7 levels, and strong Smad3 transcriptional activity and were therefore sensitive to TGF-β cytostatic activity, representative of the early stages of chronic liver disease.[190]

Importantly, an analysis of TGF-β expression in HCC patients revealed that tumours displaying an invasive phenotype and increased recurrence were characterized by a late TGF-β signalling signature, with transcriptional activation of genes associated with matrix remodelling and cell adhesion.[191] A significant body of evidence supports the hypothesis that TGF-β-driven epithelial plasticity of neoplastic hepatocytes is a critical event in cell dissemination and intrahepatic metastasis.[192] Furthermore, a correlation between circulating levels of TGF-β1 and increased aggressiveness of HCC phenotype, has been observed in patients with HCC.[193] Hoshida et al stratified patients with HCC according to molecular pathway activation and clinical outcome. Interestingly, TGF-β activation was associated with the worst survival. Upon activation, HSC secrete, and are receptive to TGF-β signalling; I would hypothesise that TGF-β signalling could therefore be an important stromal factor in hepatocarcinogenesis.

Toll-like receptors and epiregulin

The gut microbiome is increasingly recognized as a powerful modulator of fibrosis, cirrhosis, and infectious complications in chronic liver disease. Much interest is currently focused on the translocation of bacterial pathogen-associated molecular patterns, which activate inflammatory responses through TLRs. Recently Dapito et al demonstrated that Tlr4*mut* mice (harbouring non-functional TLR4) that received diethylnitrosamine (DEN) and carbon tetrachloride (CCL_4) show 80-90% reduction in HCC tumour size and number, compared with mice expressing wild-type TLR4.[194] Gut sterilization significantly reduced this effect whereas lipopolysaccharide (LPS) treatment enhanced it, suggesting a role for the LPS-TLR4 pathway in promotion of hepatocarcinogenesis. Interestingly, alongside hepatocytes, HSC were identified as candidates for TLR4-dependent tumour promotion in the chronically injured liver. LPS and the gut microbiome were found to induce HSC activation, resulting in production of the mitogens HGF and epiregulin, which likely act on malignant hepatocytes. Epiregulin is a member of the EGF family, and results in EGF receptor and human epidermal growth factor receptor 2 activation during early stages of DEN/CCL_4 carcinogenesis, whereas it reduces hepatocyte apoptosis by NF-κB nuclear translocation during later stages.[194,195] This suggests that there may be merit in evaluating whether long-term antibiotic treatment confers any protection against HCC development. This could initially be investigated by following up patients with cirrhosis on long-term prophylaxis for spontaneous bacterial peritonitis or encephalopathy, although identifying a comparable control group may prove challenging.

HSC and angiogenesis

Angiogenesis has a critical role in HCC initiation, progression and metastasis, as reflected by the efficacy of sorafenib, which targets this process. The rapid growth pattern of malignant hepatocytes requires new vessel formation, stimulated by multiple pro-angiogenic factors. This pro-angiogenic environment in turn supports tumour progression and metastasis. The relevance of tumour vascularity is reinforced by the observation that VEGF expression progressively increases from low-grade dysplasia to early-stage HCC.[196] VEGF overexpression is also associated with high tumour grade, and vascular and portal vein invasion.[197-201] Furthermore, raised plasma VEGF and angiopoietin 2 (Ang-2) are independent predictors of poor prognosis in advanced HCC.[202]

HSC are known to secrete VEGF as well as other angiogenic factors including PDGF, MMPs, FGF, TGF-β1, EGF, angiopoietin (Ang)-1 and Ang-2.[203-205] Upon activation, HSC express multiple smooth muscle cell markers, suggesting they may act like pericytes during angiogenesis.[206,207] They also express angiogenic growth factor receptors, such as VEGF receptor, PDGF receptor and Tie-2.[208-210] In liver injury and HCC, this facilitates reciprocal signalling between HSC and endothelial cells or malignant hepatocytes and contributes towards a pro-angiogenic microenvironment. VEGF secretion by HSC can be hormonally induced by leptin, or by physical stress such as hypoxia, and is upregulated in HCC.[204,208,211] VEGF receptor upregulation also occurs during HSC activation, resulting in increased mitogenesis in response to VEGF.[37]

Conditioned media from HCC cells can activate HSC and stimulate VEGF production. Coulouarn et al co-cultured LX2 cells with HepRG HCC cells, and analysis of differential gene expression identified a gene network linked to VEGFA and MMP9.[212] This was shown to promote angiogenesis, as conditioned medium from LX2-HepaRG co-culture (but not LX2 or HepaRG medium alone) induced tubule complex formation by primary human umbilical vein endothelial cells. A gene signature of this cross-talk correlated with poor prognosis and metastasis in humans.[212]

Lin et al have also shown increased angiogenesis by activated HSC in vitro using a murine HCC cell line (H22) and rat colon microvascular endothelial cells.[213] They went on to demonstrate, in vivo, using an orthotopic HCC model, that activated HSC promote tumour vascularization via increased VEGF and possibly PDGF secretion.

Of particular interest in HCC is the interaction between malignant hepatocytes, endothelial cells and activated HSC. Torimura et al characterized expression of Ang-1, Ang-2 and Tie2 receptors in HCC cell lines (HLE and HuH-7) and human HCC cases.[214]

They concluded angiopoietin-Tie2 signalling in the vascular wall may act in favour of vessel remodelling in HCC. Ang-2 production by hepatoma cells, HSC and smooth muscle cells binds Tie2 (on HSC, smooth muscle and endothelial cells) and destabilizes connections between endothelial cells, perivascular support cells and ECM. This allows exposure to VEGF, which in these relatively hypoxic conditions, is upregulated. Proliferation of endothelial cells ensues, allowing neovascularization and further tumour growth.

Recently, it has been shown that metformin inhibits angiogenesis in vitro, in an HCC (HepG2 line) and HSC (LX2) co-culture system.[215] This was associated with reduced VEGF production. It was postulated that metformin was acting via AMPK activation, and specifically targeting HSC in this model. Indeed, inhibition of AMPK on LX2 cells (but not on HepG2 cells) using siRNA did restore VEGF levels and abrogate metformin's anti-angiogenic effect. Metformin would seem a promising candidate for human HCC treatment, but unfortunately retrospective data would suggest a lack of survival benefit.[216] However, considering the well-established tolerability of metformin, its potential HSC-mediated effect on angiogenesis merits further investigation.

Some of the factors mediating crosstalk between HSC and HCC are summarized in Figure 2.1.[184]

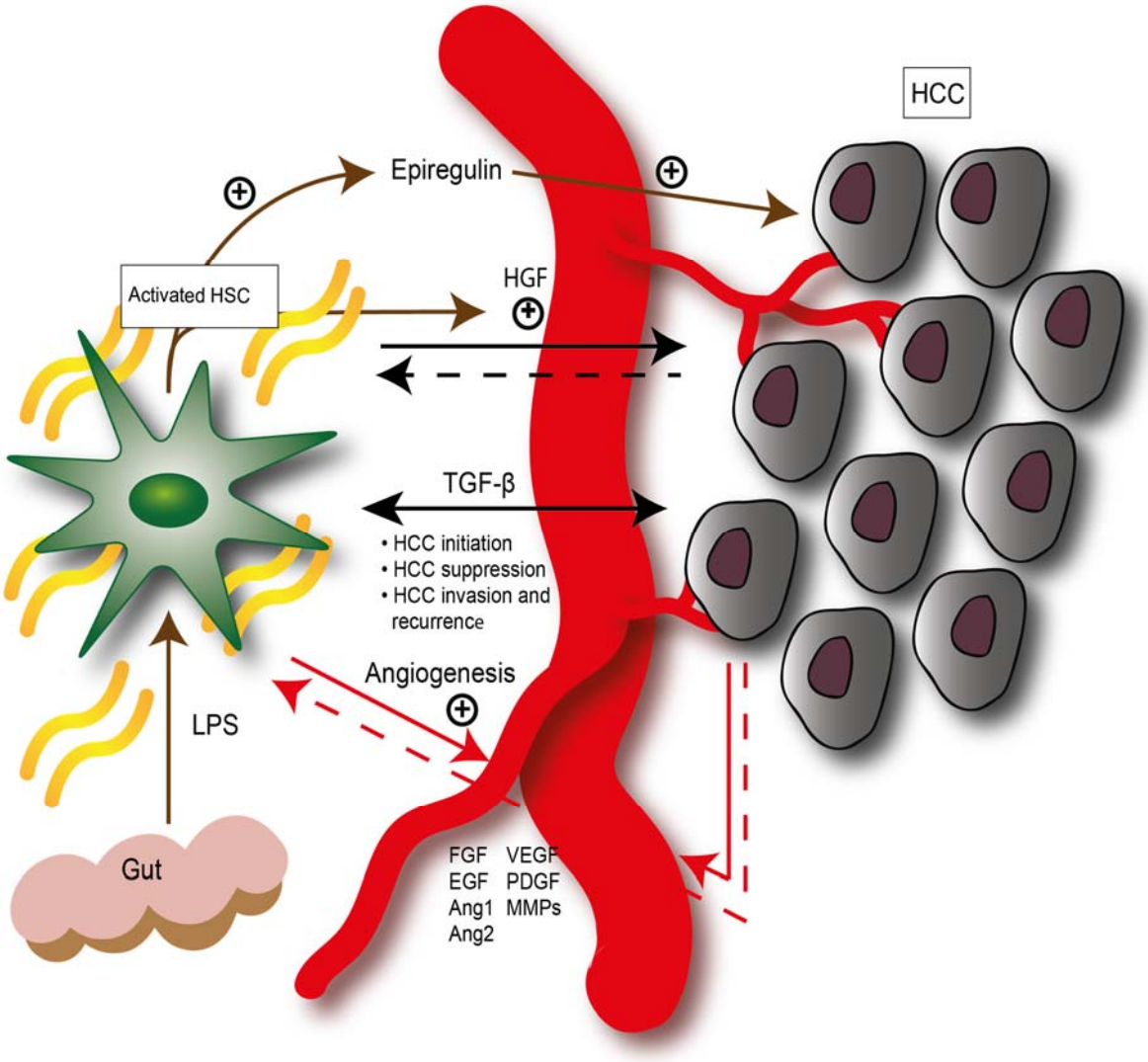

Figure 2.1 Crosstalk between HSC and HCC

Reproduced from Thompson et al 2015.[184]

HSC-secreted factors such as HGF may promote hepatocarcinogenesis. Similarly, HCC signalling results in further HGF production from activated HSC. TGF-β demonstrates both tumour-suppressive and tumour-promoting functions, depending on context. HSC produce angiogenic cytokines, supporting new vessel growth. HCC cells contribute to angiogenic signalling, and HSC also possess receptors for some of these factors. LPS induces HSC activation, resulting in epiregulin and HGF production, with mitogenic effects on HCC.

HSC and immunomodulation

Tumour immune evasion is a hallmark of cancer progression, and this process has been shown to occur in human HCC.[184] Increased levels of immunosuppressive cells (such as regulatory T-cells (Tregs)) within peripheral blood and tumours have been reported in human HCC cases.[217-219] Intratumoural Treg accumulation has also been shown to correlate with disease progression and poor prognosis in HCC.[220]

HSC themselves have immunosuppressive properties. Activated HSC have been shown in vitro and in vivo to strongly suppress T-cell responses. Furthermore, in an orthotopic rat model of HCC, intratumoural HSC number correlated with T-cell apoptosis and metastatic lung nodules.[221] Zhao et al showed that co-transplantation of HCC cells and HSC into immunocompetent mice promoted HCC proliferation and enhanced tumour angiogenesis. This was associated with inhibition of lymphocyte infiltration and apoptosis of infiltrating monocytes.[155] In another orthotopic model of HCC, activated HCC in tumour-bearing mice significantly increased Treg and myeloid-derived suppressor cell (MDSC) populations in the spleen and tumour stroma.[222] Tumours co-transplanted with HSC also had increased vascular and lymphatic vessel density.

The immunomodulatory effects of HSC in HCC may be mediated by upregulation of human B7 homolog 1 (B7-H1; programmed death ligand 1 (PDL-1)) on tumoural HSC.[223-225] B7-H1 can act as both receptor and ligand, and its immunosuppressive functions include promotion of activated T-cell apoptosis and inhibition of T-cell-mediated tumour cell apoptosis.[226-228] Its counter-receptor, PD-1, is expressed on activated (but not quiescent) T-cells, B-cells and monocytes.[229] B7-H1/PD-1 signalling has been reported to promote Treg cell induction and immunosuppressive function through down-regulation of mTor and AKT phosphorylation.[230,231] Incubation of T-cells with anti-B7-H1 monoclonal antibody in vitro resulted in a significant reduction in HSC immunomodulatory activity and HCC migration and invasion.[224]

Following on from these mechanistic studies, three monoclonal anti-PD-1 antibodies have been developed, and one against B7-H1.[232,233] Phase 1 data was promising in a range of different tumours. A Phase-1 dose escalation study in HCC, investigating the effects of anti-PD-1 therapy in patients with advanced HCC is underway (NCT01658878), preliminary results of which are anticipated at the end of this year.

Therapeutic approaches to targeting HSC and HSC signalling

HSC represent a small percentage of cells within the liver, and specific therapeutic targeting of HSC remain challenging. Recently, transgenic mice have been developed that allow reliable fluorescent labelling genetic manipulation in HSC and myofibroblasts.[234,235] These transgenic mice will hopefully prove useful not only in elucidating the molecular mechanisms in HSC that regulate the stroma-HCC interface, but also in facilitating the identification of rational, new therapeutic targets in hepatocarcinogenesis.

If a targetable, HSC-dependent pathway driving hepatocarcinogenesis is identified, cell-specific therapy is conceivable, albeit not entirely straightforward. ECM homeostasis is a key physiological process and modifying HSC functions may impair this, with potential for severe adverse effects. Practically, delivering drugs to HSC is hindered by a lack of multiple transport receptors and endocytic capacity. Furthermore, candidate compounds may include siRNA and cytokines, which have a short half-life in plasma following systemic administration hindering therapeutic efficacy.[236]

To overcome these problems, a number of groups have explored active targeting of HSC to deliver therapeutic compounds. This involves coupling the selected compound to a carrier possessing a specific receptor-binding ligand, or an antibody.

Carriers recently employed have included an antibody to the synaptophysin receptor on HSC, and a liposome specific to the vitamin A receptor on HSC.[237,238] Furthermore, Poelstra et al have used proteins substituted with a sugar moiety that binds the mannose-6-phosphate-IGFII receptor.[239] They have also utilized a peptide that binds the PDGF receptor-β,[240] to deliver a protein or an adenovirus to HSC.[241,242] An RGD-peptide which binds to RGD-binding integrins has also been used to create a carrier that accumulates in HSC.[243,244] Of note, the carrier molecules used must fit strict criteria such as low immunogenicity, and high stability, biocompatibility and selectivity, if they are to translate into clinical practice. Moreover, the target receptors on HSC should be selectively expressed and ideally upregulated during disease activity. A further challenge is the requirement for endocytosis of the construct following target receptor binding. This can be particularly problematic in the case of biological therapeutics, which usually fail to withstand the endosomal degradation process.

With these challenges in mind, Bansal et al subsequently developed a recombinant protein construct to deliver IFN-γ to HSC. This elegant system transported the signalling moiety of IFN-γ to the PDGF-receptor with a carrier molecule that was simplified and miniaturized. They found that IFN-γ could be effectively delivered to human HSC in vitro,

and to mouse HSC in vivo. Furthermore, the targeted fusion proteins were shown to ameliorate hepatic fibrosis in CCL_4-treated mice.[245-247] This suggests that directing a cytokine to HSC is a feasible and potentially tractable therapeutic approach, both in the context of developing new treatments for patients with liver fibrosis, as well as HCC. Therapeutic approaches to targeting HSC are summarized in Figure 2.2.

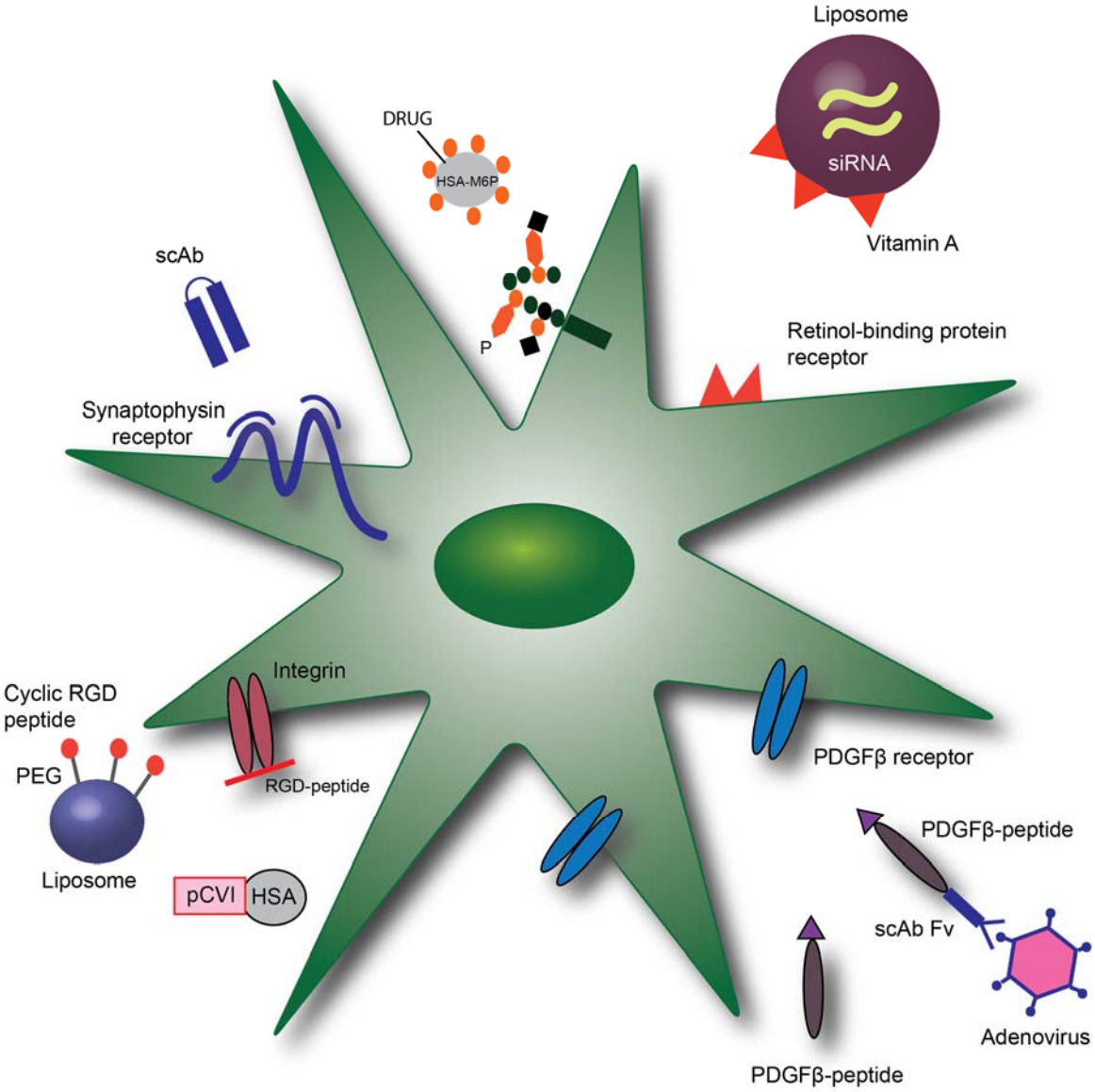

Figure 2.2 Therapeutic approaches to targeting HSC

Reproduced from Thompson et al 2015[184]

HSC have been targeted by coupling a compound to a carrier possessing either a HSC-specific receptor-binding ligand or an antibody. Carriers utilized include: a monoclonal human single chain antibody (scAb) fragment to synaptophysin; a sugar moiety that binds the mannose-6-phosphate (M6P) insulin-like growth factor receptor; a liposome specific to the vitamin A (retinol-binding protein) receptor; PDGFβ receptor recognizing peptide (PPB); an RGD peptide bound to a liposome or coupled to a human serum albumin (HSA). scAb Fv, single chain antibody variable fragment; PEG, polyethylene glycol; pCVI, 10 cyclic peptide moieties that recognize collagen type VI receptors.

2.2 Modelling HCC

The laboratory mouse is widely accepted as one of the best model systems for cancer due to ease of gene targeting methods, animal size and breeding capacity, and comparability to human biology. Models range from simple xenografts of cancer cells to immunodeficient mice, to complex genetically modified mice, and chemical carcinogenesis.

DEN is a genotoxic DNA alkylating agent. It forms mutagenic DNA adducts, and bioactivation by cytochrome P450 can produce reactive oxygen species which damage DNA, proteins and lipids, and cause hepatocyte death. It has been used since 1966 to induce HCC in rodents, and is the commonest chemical used for hepatocarcinogenesis in mice.[248,249] If injected when hepatocytes are actively proliferating (i.e. less than two weeks of age) it acts as a complete carcinogen in male, but not female mice (30% of females develop HCC).[249] If administered later, another form of tumour promotion is needed, such as phenobarbital, CCL_4, partial hepatectomy or high fat diet.[250] Consistent with human HCC, tumour development is a multi-step process, with repeated cycles of necrosis and regeneration resulting in neoplastic transformation. As dysplastic lesions progress to malignant tumours, genomic alterations accumulate. [251,252] Lesions induced by a single DEN injection often have activating H-ras mutations,[253] whereas those induced with both DEN and phenobarbital tend to demonstrate activating β-catenin mutations and genomic instability.[254,255] A limitation of this model is the lack of hepatic fibrosis in livers challenged by a solitary early postnatal DEN injection; in contrast, human HCC typically arises in the context of cirrhosis. Nonetheless, activating mutations do appear to be comparable, and gene expression profiling of the DEN model suggests there is a good overlap between the resulting mouse tumours and their human counterparts.[256]

2.3 Hypothesis and aims

HSC infiltration of human HCC may correlate with tumour collagen content and degree of differentiation.

Aims

- To characterise HSC infiltration of human HCC, using immunohistochemistry, and determine whether this correlates with tumour collagen content and degree of differentiation

2.4 Characterisation of HSC infiltration and collagen deposition in HCC

2.4.1 Materials and methods

Human HCC tissue was obtained from archived tissue held by the South East Scotland SAHSC (Scottish Academic Health Sciences Collaboration) BioResource, following appropriate ethical approval.

2.4.2 General immunohistochemistry protocol with formalin-fixed, paraffin-embedded sections

Immunohistochemistry was carried out at room temperature unless otherwise stated. Paraffin-embedded sections were de-paraffinised twice in xylene (for five minutes each time) and rehydrated in ethanol (50-100%) and distilled water. Antigen retrieval was performed at this stage (table 1) and the sections were then washed 2 x 5 minutes in phosphate buffered saline (PBS). Endogenous peroxidase activity was blocked by incubation with hydrogen peroxide (3%) solution in PBS for 10 minutes. Slides were then washed 3 x 5 minutes in PBS. Slides were then mounted into Shandon Sequenza slide racks. An endogenous avidin-biotin block (Vector Laboratories, Peterborough, UK) was performed by applying 3 drops of avidin solution to each slide for 15 minutes. Slides were then washed 3 x 5 minutes in PBS, then 3 drops of biotin reagent were applied for a further 15 minutes. Washing was repeated, 3 x 5 minutes in PBS. Non-specific protein-binding was inhibited by incubation with blocking buffer containing species-specific serum diluted (1:5) in PBS for 30 minutes. Species-specific serum was chosen to match the species in which the relevant secondary antibody was raised. Without washing, samples were then incubated with a primary antibody solution (appropriately diluted in blocking buffer) for 2 hours at room temperature

Slides were then washed 3 x 5 minutes in PBS. A secondary antibody solution appropriate to each primary antibody was made by dilution (table 1) of secondary antibody in blocking solution. Samples were incubated with secondary antibody solution for 30 minutes and then washed 3 x 5 minutes in PBS. Slides were then treated with 3 drops of Vector RTU ABC reagent for 30 minutes, and washed 3 x 5 minutes in PBS. A chromogen solution containing 3, 3'diaminobezidine (DAB) was applied to each slide for between 1-5 minutes, until a colour change was observed. This was followed by washing 3 x 5 minutes in PBS. Counterstaining was performed in Harry's haematoxylin solution (10 seconds), rinsed in running tap water and immersed in Scott's tap water (10 seconds). Sections were then rinsed in running tap water and dehydrated in graded

ethanol solutions (50-100%) 20 seconds each, and xylene for 2 x 5 minutes. Slides were mounted on glass cover slips with mounting media.

Immunohistochemistry on human and mouse HCC specimens

Immunohistochemistry was performed on formalin-fixed paraffin-embedded 5µm sections mounted on glass slides. Primary and secondary antibodies were used at different concentrations (table 1). The primary antibodies used were α-SMA and PDGFRβ. For all targets, an antigen retrieval step was performed, to unmask epitopes hidden by cross-linking formed during the fixation process.

Primary antibody	Concentration	Antigen retrieval	Secondary antibody	Concentration
Mouse anti-αSMA (Sigma A5228)	1/1000	15 minutes full power microwave (Sodium Citrate pH 6)	Goat anti-mouse IgG, Biotinylated (Vector)	1/800
Rabbit anti-PDGFRβ (Abcam 32570)	1/500	15 minutes full power microwave (Tris EDTA pH 9)	Goat anti-rabbit IgG, Biotinylated (Vector)	1/1000

Table 1: Summary of antibodies used with their concentrations, antigen retrieval and secondary antibodies

Picosirius red (PSR) staining

PSR staining was performed on 5µm liver sections. Sections were de-paraffinsied in xylene and rehydrated in ethanol (50-100%) and distilled water. Sections were then incubated for 90 minutes in saturated picric acid solution containing 0.1% Sirius red, and then 0.1% Fast green. Sections were then rinsed in distilled water to remove excess dye, and dehydrated in ethanol (50-100%) and xylene. Slides were mounted on glass cover slips with aqueous mounting media.

2.4.3 Microscopy and digital image analysis

Microscopic examination of tissue specimens was performed using an inverted Zeiss Axiovert-200 microscope and Axiovision image acquisition software (Zeiss, Heidenheim, Germany).

Digital image analysis of immunostained sections

Quantification of α-SMA, PDGFRβ and PSR immunostaining in liver specimens was performed by digital image analysis using ImageJ (National Institute of Health, USA). For each HCC sample, tumour area was identified by a pathologist, from a haematoxylin and eosin (H and E)-stained section. Whole sections were scanned in digitally, and a Wacom pad used to draw round tumours, to accurately quantify staining within HCC. Values are expressed as the total percentage area of positive staining per tumour sample. Detection thresholds were set for the brown colour of DAB or the red colour of PSR staining, from an area of intense staining; an arbitrary colour threshold range was applied.

2.5 HSC infiltration and collagen deposition in human HCC

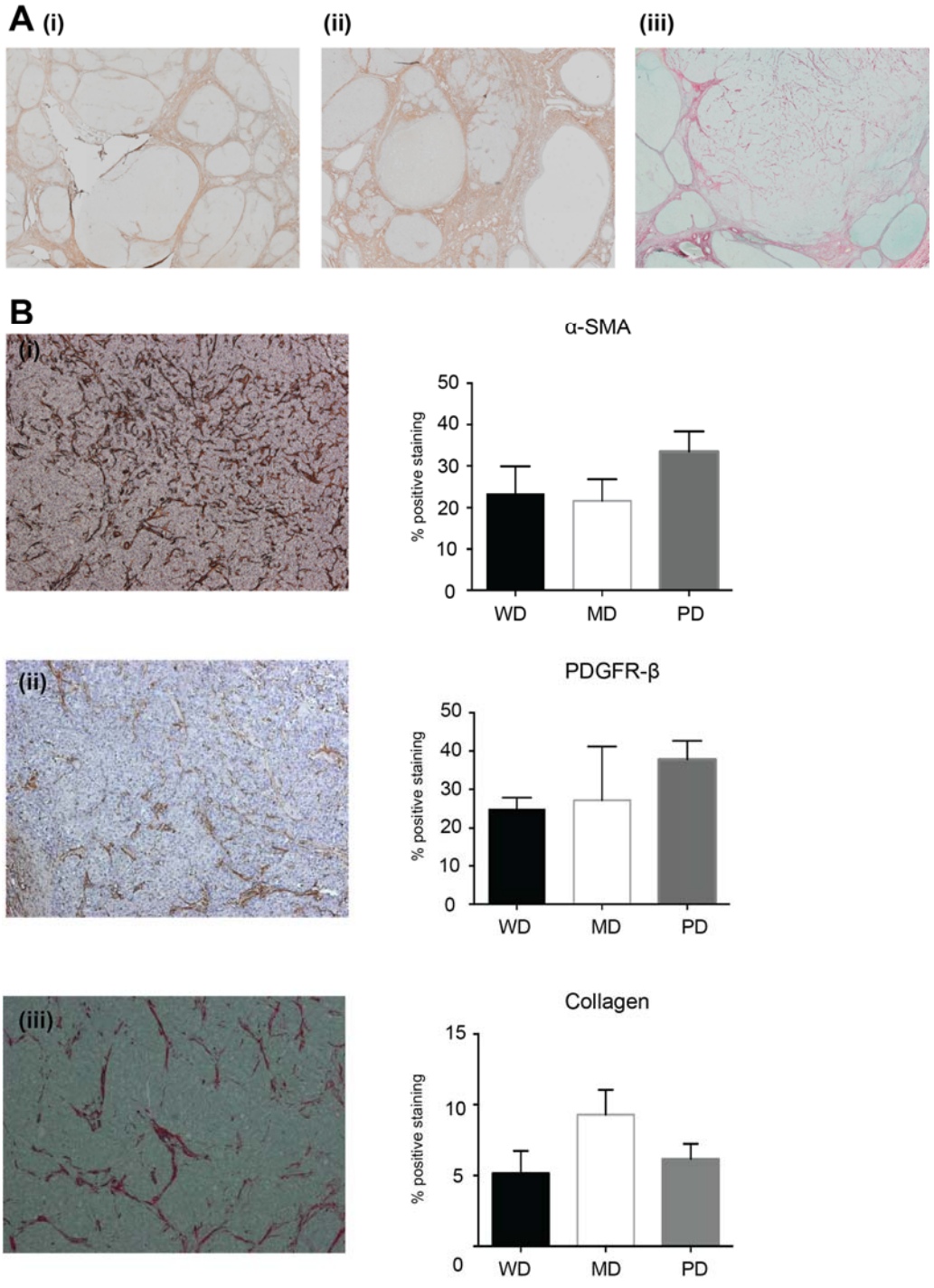

Figure 2.3 HSC infiltration and collagen deposition in human HCC

A Representative scanned images of slides of human HCC tissue stained with **(i)** α-SMA **(ii)** PDGFRβ **(iii)** PSR **B** High magnification (x20) images of intratumoural staining for markers of HSC, myofibroblasts and collagen (PSR). **(i)** α-SMA; corresponding graph

shows percentage positive immunostaining within 17 human HCC, grouped by tumour grade: well differentiated (WD) n=4, moderately differentiated (MD) n=6 and poorly differentiated (PD) n=7. **(ii)** PDGFRβ IHC of human HCC tissue (n=4 WD, n=5 MD, n=7 PD) and **(iii)** PSR IHC of collagen within human HCC tissue (n=7 WD, n=18 MD, n=13 PD).

HSC presence within human HCC shows a trend towards deteriorating tumour differentiation grade

Figure 2.3 shows IHC performed on human HCC cases, obtained from archived tissue as described above. Slides were stained for markers of activated HSC, namely α-SMA and PDGFRβ, and for the collagen marker, PSR. Sections were also stained with H and E, to establish where the areas of HCC were. Results of immunostaining are presented as percentage positive staining within the whole tumour area (mean and standard error of the mean). I found that activated HSC were distributed throughout each tumour, and not simply around the fibrous tumour capsule. In a sample of 17 HCC cases, percentage α-SMA staining was 23.50 (± 6.39) in n=4 well-differentiated (WD) tumours; 21.70 (± 5.06) in n=6 moderately differentiated (MD) tumours; 33.44 (±4.92) in n=7 poorly differentiated (PD) tumours. There was no significant difference in staining positivity between any of the tumour grades (p=0.83 WD vs MD, p=0.13 MD vs PD, p=0.25 WD vs PD).

In a sample of 16 HCC cases, percentage PDGFRβ staining was 24.95 (±2.85) in n=4 WD tumours; 27.13 (±14.07) in n=5 MD tumours; 37.8 (±4.89) in n=7 tumours. Difference in staining positivity did not reach significance between any of the tumour grades (p=0.90 WD vs MD, p=0.43 MD vs PD, p=0.10 WD vs PD). However, there did appear to be a trend towards increasing staining positivity (for both α-SMA and PDGFRβ) within tumours from low to high differentiation grade.

In a larger sample of 38 HCC cases, percentage PSR staining was 5.17 (± 1.59) in n=7 WD tumours, 9.28 (±1.76) in n=18 MD tumours, and 6.19 (±1.07) in n=13 PD tumours. These groups were not significantly different from one another (p=0.19 WD vs MD, p=0.18 MD vs PD and p=0.59 WD vs PD).

2.6 Discussion

In these experiments I stained archived human HCC sections with antibodies to markers of HSC, myofibroblasts and collagen. These tumours had all arisen in cirrhotic livers, from a variety of different aetiologies (including non-alcoholic fatty liver disease (NAFLD), alcoholic liver disease (ALD), HCV and primary biliary cirrhosis (PBC)). My sample size was slightly limited by quality of tissue; in some cases the tissue was torn or had holes. These were excluded from analysis. As the numbers were therefore relatively small, I did not look for any differences in staining between different aetiologies of liver disease, however it would be interesting to explore this in more depth in future studies.

Whilst the sample size was small, I was confident that the image analysis process was robust. For each case a pathologist independently identified the area of HCC. Each

malignant nodule was outlined on the haematoxylin and eosin-stained section; I then scanned in the antibody-stained slides and used a graphics pad to draw round the nodules, correlating these with the annotated H and E slides. This meant that for each case I could analyse percentage staining throughout the whole tumour, maximizing the intratumoural area studied.

There did appear to be a trend towards increased staining of HSC and myofibroblasts with decreasing tumour differentiation, suggesting a possible correlation between high numbers of intratumoural mesenchymal cells, and high tumour grade. However this did not reach significance, and would require analysis of larger sample sizes to fully explore this. Interestingly, this trend was not apparent when comparing collagen staining across the three tumour grade groups. Inability to tease out statistical differences may have been secondary to a range of confounding factors. For example, unfortunately I had no record of what treatments the patients had received. It is conceivable that specific tumour ablation treatments, such as trans-arterial chemoembolization, may have affected mesenchymal cell and collagen content.

The variance in staining positivity for mesenchymal cells and collagen was relatively high. Since carrying out this work, a study of 300 patients with HCC who underwent liver resection or transplantation has been performed, investigating the effect of 'stroma-rich' tumours on prognosis.[257] Patients were divided into a stroma-rich group (stroma $\geq$50% on assessment of H and E sections) and stroma-poor (stroma <50%). It was concluded that tumour-stroma ratio is an independent prognostic factor for overall survival in patients undergoing liver resection for HCC, and both overall survival and recurrence-free survival in patients who underwent liver transplantation. The authors acknowledged some limitations of this retrospective study, however felt that tumour-stroma ratio would allow improved risk stratification of patients following curative treatments.[257]

Tumour-stroma ratio has previously been shown to be an independent prognostic factor, in node-negative, premenopausal breast cancer,[258] early cervical cancer,[259] and oesophageal squamous cell carcinoma.[92] It is not entirely clear what the underlying mechanism conferring poor prognosis in a stroma-rich tumour is. Tumour-associated mesenchymal cell types (i.e. cancer-associated fibroblasts (CAF) and pericytes) have attracted much attention in recent years, in terms of their pro-tumourigenic effects and contributions to the 'hallmarks of cancer' that are required for a cell to become malignant.[260] The CAF is the dominant cell type within the tumour stroma of numerous cancers, especially breast and pancreatic.[261] CAF are heterogeneous due to their various origins, and in HCC may originate from fibroblasts and activated HSC. CAF have

also been reported to arise from bone marrow-derived progenitor cells, or transdifferentiating epithelial cells.[260] Stromal fibroblasts within tumours are characterized by (only partly) overlapping marker expression, including α-SMA, PDGF receptors, and fibroblast specific protein (FSP)-1. [262,263] This is likely to reflect distinct origins of subpopulations of CAF.[260] Tumour pericytes (contractile cells in close contact with vascular endothelial cells) also express PDGFRβ and α-SMA, and contribute to angiogenesis.[260] A CAF gene signature has been identified as predictive for response to neoadjuvant chemotherapy in breast cancer,[264] and pre-clinical studies show that CAF can mediate resistance to anti-angiogenic therapy, and targeted tyrosine kinase inhibitors.[92,260,265] They can also influence transport of drugs within tumours, by PDGF receptor-mediated regulation of interstitial fluid pressure in tumours.[266] CAF may induce EMT through paracrine TGF-β signalling, [267,268] and TGF-β is likely to be a key player in the interaction between HCC and the stroma.[269]

A large prospective study of human HCC cases would be informative, perhaps looking at markers of activated HSC and CAF, and correlating this with aetiology of liver disease and treatments. I investigated ethical approval for this, which was straightforward, however the time scale for patient recruitment would have been outwith the constraints of this project. I felt there was a considerable body of evidence implicating stromal TGF-β signalling in HCC growth and progression, and therefore decided to proceed with in vivo animal experiments to investigate this further.

Chapter 3: The role of αv integrins during hepatocarcinogenesis

3.1 The integrin family and TGF-β signalling

The integrin family of cell adhesion molecules, of which there are 24 known members in humans (noncovalent α/β heterodimers composed from 18 different α subunits and 8 β subunits) mediate many key cell-cell and cell matrix interactions implicated in fibrosis. In particular, the αv integrin subunit forms heterodimers with the β1, β3, β5, β6 or β8 subunits (Figure 3.1). Integrins are transmembrane receptors, allowing communication between the intra- and extracellular environments. They bind the ECM and cytoskeleton, thereby facilitating transduction of signals to regulate cell adhesion, migration, proliferation and differentiation, as well as ECM deposition and remodelling.[270]

When integrins bind to growth factors or ECM ligands such as collagen, laminin and fibronectin, they form membranous plaque products, known as focal adhesions. Focal adhesions activate specific intracellular effector pathways, including protein kinase C, talin, paxillin and the phosphatidylinositol 3-kinase (PI3K) and mitogen-activated protein kinases (MAPK) pathways. Downstream, integrins coordinate the fibrogenic response, and help regulate cell survival, differentiation and proliferation, control of which is often lost in cancer cells.[271,272]

Integrins are important in TGF-β signalling and secreted TGF-β is a critical regulator of fibrosis in multiple organs.[270,273-275] The three mammalian isoforms of TGF-β are synthesized as precursor proteins. These are subsequently processed by proteolytic cleavage within the endoplasmic reticulum. They are assembled as a non-covalent 'small latent complex'. This consists of a disulfide-linked homodimer of the mature cytokine (a short C-terminal fragment), which is encased within a disulfide-linked
homodimer of a larger amino terminal fragment known as the latency-associated peptide (LAP) forming the 'small latent complex'. The distinct conformation of the associated LAP homodimer (in contrast with free dimer) prevents the mature C-terminal fragment from binding to its receptors. This 'small latent complex' is modified further in the endoplasmic reticulum by disulfide linkage to latent TGF-β binding proteins. These are cross-linked to the ECM, and therefore store and tether TGF-β extracellularly, in this latent form. The latency cage can be disrupted by cellular contraction, resulting in release of mature dimer, and allowing activation of TGF-β (figure 3.1.2). The biological effects of TGF-β are mostly regulated by extracellular activation of this stored latent complex.[276-278] All three of the mammalian TGF-β isoforms mediate their effects at least partly through the intracellular SMAD pathway.

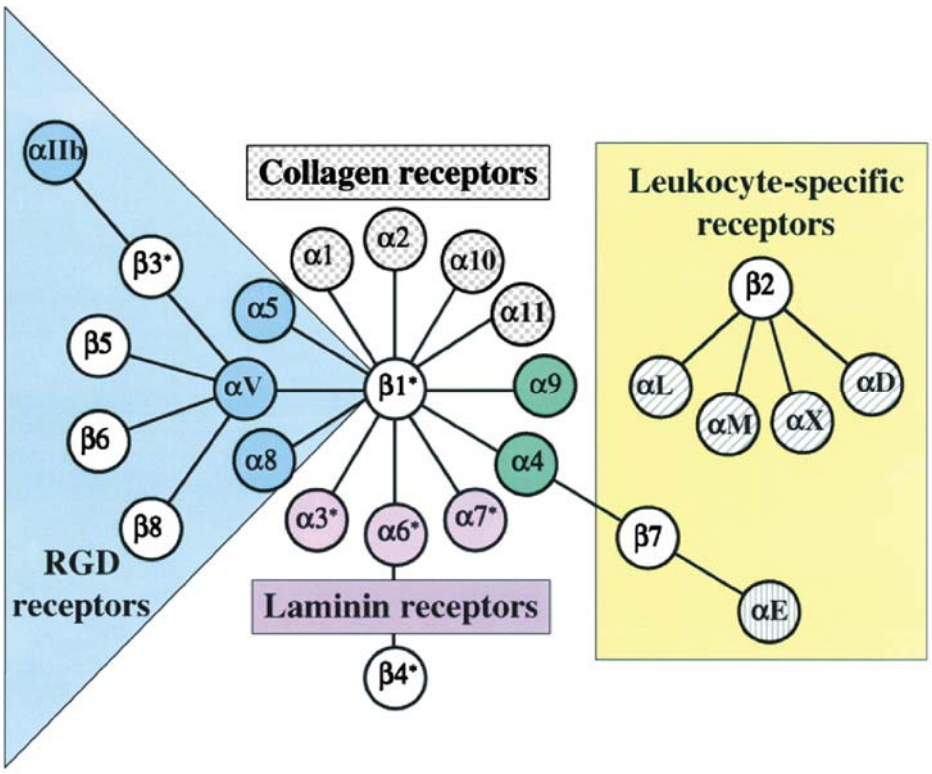

Figure 3.1 The integrin family of cell adhesion molecules

Reproduced from Hynes, Cell 2002.

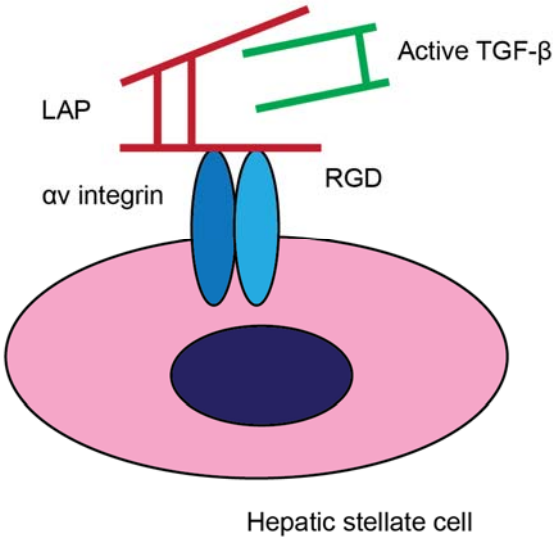

Figure 3.2 TGF-β activation by αv integrins

LAP: Latency-associated peptide

RGD: linear arginine-glycine-aspartic acid motif

They have overlapping functions, although TGF-β1 appears to be most extensively implicated in fibrogenesis. Two of the three isoforms (TGF-β1 and TGF-β3) can be activated by members of the integrin family that interact with a linear arginine-glycine-asparatic acid (RGD) motif present in an N-terminal of the LAP.[279-283] Importantly, all αv integrin heterodimers can activate TGF-β in this way. This is not the only pathway by which integrins contribute to TGF-β activation; integrin-mediated generation of mechanical force by the actin cytoskeleton can also activate latent TGF-β1.[284] Similarly, myofibroblast αv integrins can free TGF-β1 from the ECM via mechanical force. Furthermore, a stiff ECM results in more force-stimulated TGF-β1 release in comparison with a relaxed ECM, i.e. latent ECM-bound TGF-β1 can effectively be primed by the surrounding fibrotic matrix.[278,285]

αv integrins

Manipulation of specific members of the αv integrin family has been shown to have significant effects in experimental hepatic fibrosis (Table 2, adapted from Conroy et al 2016[278]). Reed et al developed a small molecule inhibitor of αvβ1, and demonstrated that this is the predominant fibrogenic αv integrin on fibroblasts, mediating adhesion to the TGF-β1 LAP.[286] The inhibitor compound c8 could reduce fibrosis in CCL_4–treated mice, to a similar degree as seen with conditional deletion of all αv integrins on myofibroblasts.[234] The reduction of phosphorylation of Smad3 (the intracellular downstream signalling effector of TGF-β) in these models provided further evidence that the antifibrotic effect is due to the inhibition of αvβ1-mediated TGF-β activation.[234,286]

Similarly, αvβ6 has been implicated in the progression of biliary fibrosis.[287] This was perhaps unsurprising, considering that hepatic expression of this integrin is low at baseline, but increased with inflammation and fibrosis.[278,287] Moreover, patients with fibrotic liver disease secondary to a wide range of aetiologies (including primary biliary cirrhosis, alcohol, viral hepatitis) have elevated αvβ6 integrin mRNA expression,[278] and in hepatitis C, the level has been shown to correlate with fibrosis stage.[288]

This is consistent with the findings from a growing body of in vivo evidence using the BDL and genetic models of acute biliary fibrosis. In the BDL model, bile duct obstruction was found to increase cholangiocyte expression of αvβ6.[287] Genetic knockout of β6 integrin resulted in a 50% reduction of biliary fibrosis in BDL-treated mice, compared with wild-type controls. Additionally, administration of an αvβ6-blocking antibody significantly reduced acute biliary fibrosis after BDL.[287] Patsenker et al then went on to show that pharmacological treatment with a small molecule inhibitor of αvβ6 (EMD527040) could

inhibit biliary fibrosis in BDL rats and Mdr2 (abcb4)$^{-/-}$ mice (another genetic model of biliary obstruction) in the context of established fibrosis.[289] More recently, Peng et al showed that αvβ6 is expressed on hepatic progenitor cells, and genetic disruption or selective targeting of αvβ6 with 3G9 antibody could inhibit progenitor cell responses in two models of chronic biliary injury (Mdr2$^{-/-}$ mice and DDC diet-treated mice) resulting in less fibrosis and, importantly, cirrhosis-associated tumourigenesis.[290]

The effect of modulation of αv integrin subunits is not universally antifibrotic however. For example, whilst αvβ6 has a convincing role in biliary fibrosis, ablation of this integrin was not protective in CCL_4-induced hepatic fibrosis.[287] This lack of effect may relate to the expression pattern of αvβ6, which is restricted to a subset of epithelial cells.[287,291,292] Therefore, αvβ6-mediated ββ activation is only very localized; any activated TGF-β generated could only be detected by cells in direct contact with the integrin-expressing cell.[279] Specifically, these αvβ6-expressing epithelial cells may be located at a substantial distance from collagen-producing myofibroblasts, responsible for tissue fibrosis.[234]

There is also evidence to suggest that some αv integrins may have a protective role in hepatic fibrosis. Pharmacological blockade of αvβ3/αvβ5 actually worsened hepatic inflammation and collagen deposition in the thioacetamide (TAA) and BDL rat models of fibrosis.[293] Inhibition of αvβ3 and αvβ5 in different organs have shown relatively inconsistent results, suggesting that there may be compensatory effects of other integrins.[278]

The effect of αvβ8 inhibition in adulthood has been less well characterized. Embryonic inhibition and blockade of both αvβ6 and αvβ8 result in perinatally lethal phenotypes similar to all of the developmental effects of loss of TGF-β1 and TGF-β3, suggesting these two integrins are critical for most or all important roles of these TGF-β isoforms in development.[294] Assessing the effect of these integrins in older animals has required the development of conditional genetic models, or specific pharmacological inhibitors. Whilst αvβ6 blocking antibodies are available, with relatively well-established pharmacokinetics, inhibitors of αvβ8 have not, to date, been easily available. There is some evidence, however, that pathological TGF-β activation in the setting of biliary atresia may be partly mediated through increased αvβ8 expression and altered MMP14 expression.[278] Liver biopsies from patients with biliary atresia have increased αvβ8 integrin expression compared with controls,[295] and both human and animal models of the disease have dysregulated MMP14 expression.[296] It has been postulated that αvβ8 can activate TGF-β1 by presenting LAP complexes to cell-surface MMPs that degrade

the LAP, allowing release of free TGF-β1.[278,297] Further investigation of this pathway in the context of liver fibrosis is required.

αv integrins are key players in the molecular pathways regulating TGF-β, and therefore fibrosis, in multiple organs including the liver. They represent attractive targets for antifibrotic therapies, although rigorous investigation of the effects of blocking individual subunits is warranted. Pan-TGF-β inhibition risks potential side effects related to loss of TGF-β activity in normal tissue homeostasis. In particular, inhibition of TGF-β1 could be pro-carcinogenic, or result in pathological autoimmunity and inflammation, due to its anti-proliferative effect on epithelial cell types, and role in immunosuppression respectively.[278,298-300] Therefore, further characterisation of the effects of individual αv integrin subunit inhibition, on specific cell-types within the liver, may allow development of targeted therapies to ameliorate fibrosis. Similarly, in view of the strong association between advanced liver fibrosis and development of HCC, it is possible that manipulation of αv integrins could also be a useful strategy in the development of new treatments for HCC.

αv integrin subunit	Model	Method of inhibition	Summary	Reference
β1	CCL_4	Small molecule inhibitor, c8	Inhibition of αvβ1significantly reduced hepatic fibrosis	Reed et al 2015[286]
β3				
β5				
β3/β5	BDL/TAA	Small molecule inhibitor, Cilengitide	Increased hepatic collagen deposition and pro-fibrogenic gene expression	Patsenker et al 2009[293]
β6	BDL	Antibody, 3G9	Reduced acute biliary fibrosis	Wang et al 2007[287]
β6	BDL	Small molecule inhibitor, EMD527040	Inhibition reduced bile duct proliferation and peribiliary collagen deposition and increased fibrolytic gene expression	Patsenker et al 2008[289]
β6	DDC	β6 function-blocking monoclonal antibody, 3G9 and β6 knockout mice	Biliary fibrosis rescued by anti-αvβ6 antibody treatment through inhibition of progenitor cell expansion	Peng et al 2016[290]
β6	CCL_4			

Abbreviations: BDL, bile duct ligation; TAA, thioacetamide; DDC, 3,5-diethoxycarbonyl-1,4-dihydrocollidine

Table 2: Effects of αv integrin inhibition in pre-clinical models of fibrosis.
Adapted from Conroy et al 2016.[278]

Anti-integrin therapies in clinical practice

There are several anti-integrin pharmaceutical agents that are used in clinical practice, or are currently being evaluated in trials. At the time of writing, there are various clinical trials in progress involving potential use of integrins as biomarkers, for example in Paget's disease (αvβ3 integrin), myocardial infarction and aortic stenosis (αvβ3 and αvβ5 integrin).

The largest area of experience with anti-integrin drugs, however, relates to therapies for inflammatory bowel disease.[301] Natalizumab is a recombinant humanized monoclonal IgG4 antibody against integrin α4, that blocks both α4β7 and α4β1.[302] It was the first anti-adhesion treatment developed in IBD, although was initially approved for relapsing multiple sclerosis.[303-306] In the gut, natalizumab disrupts the interaction between α4β7 (on leukocytes) and it's ligand MAdCAM-1 (expressed on intestinal endothelial cells).[307] This reduces the recruitment of effector T lymphocytes, which contribute to dysregulated immune responses and tissue inflammation. Natalizumab also interferes with the α4β1/VCAM-1 interaction, affecting lymphocyte migration to the CNS, providing the rationale for its efficacy in multiple sclerosis.[308] However, this is also thought to result in susceptibility to an opportunistic brain infection. Although natalizumab was able to induce and maintain clinical remission in patients with Crohn's disease,[309-311] its use was complicated by three cases of progressive multifocal leukoencephalopathy (PML).[312,313] Blocking α4β1/VCAM-1 with natalizumab prevents CNS migration of T cells, allowing reactivation of latent JC polyoma virus, and development of (typically fatal) PML.[301] This highlights potential off-target adverse effects of targeting integrins in humans.

Vedolizumab is a humanized IgG1 monoclonal antibody against α4β7 integrin, specific for the α4β7/MAdCAM-1 interaction.[307] It is therefore anticipated that the drug will not affect lymphocyte trafficking anywhere other than the gut, abrogating the risk of PML. Vedolizumab is currently licensed for induction and maintenance of remission in moderately to severely active ulcerative colitis and moderately to severely active Crohn's disease, that has failed to respond to standard immunosuppression.[314,315] It has also been suggested that this treatment could be considered in primary sclerosing cholangitis, where it is hypothesized that aberrant hepatic expression of MAdCAM-1 recruits effector cells originally activated in the inflamed gut.[316] This is hoped to be the subject of a clinical trial.

Following on from the discovery that partial inhibition of integrin αvβ6 could prevent pulmonary fibrosis in a murine (bleomycin) model, a monoclonal antibody (3G9) is now

being evaluated in humans with idiopathic pulmonary fibrosis.[317] Horan et al demonstrated that αvβ6 monoclonal antibody treatment attenuated fibrosis in the mouse model, without causing inflammation in multiple organ systems relating to TGF-β deficiency.[317] Results from human studies are awaited with interest.

Translating positive results from animal models into the development of clinically useful anti-integrin therapies is not entirely straightforward however. Integrins αvβ3 and αvβ5 are expressed abundantly in tumour-associated endothelial cells;[318,319] promising results from pre-clinical experiments in models of glioblastoma led to the development of the pentapetide integrin inhibitor cilengitide.[320] Unfortunately, when investigated in two clinical trials (to separately analyse efficacy in patients with or without a certain O^6 – methylguanine DNA methyltansferase promoter methylation) neither the 'CENTRIC'[321] nor the 'CORE'[322] trials met their primary endpoints. Subsequent immunohistochemical analysis of integrin expression patterns within the tumours included in the phase III CENTRIC trial found that αvβ3 and αvβ5 expression did not correlate with prognosis in these patients.[320] There was a weak association with improved outcome with cilengitide in the phase II CORE trial, suggesting that patient enrichment based on αvβ3 expression within tumours might be useful in future studies. However it has been suggested that agents with higher potency than cilengitide might be needed to clarify whether integrins are a worthwhile target in glioblastoma, and that downstream markers of integrin pathway activation might be more useful biomarkers to guide patient enrichment rather than integrin expression patterns alone.[320]

3.2 Targeted αv integrin depletion on HSC in HCC

Targeting HSC

Transgenic mouse technology has progressed from simple global gene knockout systems, to the development of Cre-lox technology in the 1980s.[323] This has transformed our ability to manipulate specific genes and cell lineages, to better understand their roles in the pathophysiology of liver disease. The bacteriophage P1 *cre* (cyclization recombinase) gene catalyses DNA recombination between pairs of 'locus of X-over in P1' (*loxP)* sites. The desired location of Cre expression is achieved by using cell-specific *cre* promoters. Similarly, inducible systems can temporally restrict *cre* expression. Cre can initiate deletion, inversion or translocation of the 'floxed' (flanked by *loxP*) locus depending on the location and orientation of *loxP* sites. Usually, *loxP* sites are inserted on the same chromosome, a small distance apart, and in the same orientation. This

results in excision of the floxed segment, therefore precluding the assembly of a functional gene product (Figure 3.3).[324]

Cre-lox can also be utilized to provide intrinsic cellular labelling, by cell-specific fluorescent protein expression. This is achieved by the insertion of a floxed STOP codon, meaning that transcription of the downstream sequence (in this case a fluorescent reporter construct) only occurs following Cre-mediated excision.[324] Whilst the Cre-lox approach is a sophisticated method of influencing a gene of interest, interpretation of results must incorporate consideration of potential off-target effects, or 'Cre toxicity'. Unintended Cre expression in nontargeted cell lineages can confound the conclusions drawn from gene-deletion or fate-tracing experiments.[325] The recombination efficiency (sensitivity) and expression pattern (specificity) for each Cre strain should therefore be extensively characterized prior to use.[324]

Up until recently, there was a relative lack of tools allowing consistent, specific inactivation of genes in nonparenchymal cells within the liver, such as HSC. Currently, a number of Cre drivers are available to target HSC/myofibroblasts (Table 3).

Pdgfrb-Cre mice target both quiescent HSC and activated myofibroblasts;[234] Cre is expressed under the control of a *Pdgfrb* gene fragment, driving efficient recombination in both HSC phenotypes, with high specificity. Henderson et al characterized this Cre driver extensively in both uninjured and fibrotic liver.[234] The Pdgfrb-Cre strategy was then used to demonstrate that targeted depletion of αv-containing integrin subunits on HSC protects against CCL_4-induced hepatic fibrosis. Furthermore, αv-null HSC had reduced ability to activate TGF-β. This was confirmed with use of a small-molecule inhibitor to target αv integrins, which ameliorated hepatic fibrosis in the CCL_4 model.[234]

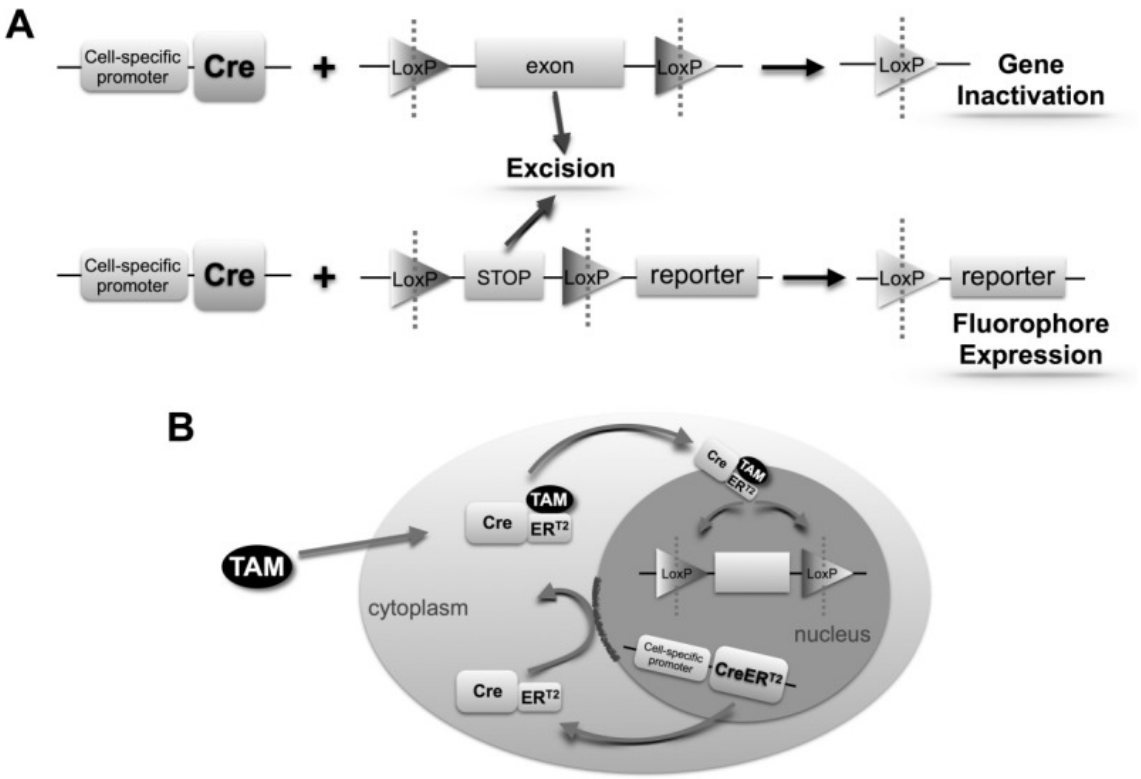

Figure 3.3 Schematic diagram of cell-specific Cre recombinase-induced gene inactivation and fluorescent reporter expression systems.

Reproduced from Greenhalgh et al 2015.[324]

A Cell-specific expression of Cre recombinase results in excision of *loxP*-flanked sequences leading to gene inactivation or fluorescent reporter expression.

B Spatiotemporal regulation of Cre activity: tamoxifen (TAM) administration permits entry of the Cre-ER^{T2} complex into the nucleus, allowing excision of *loxP*-flanked sequences.

Hepatic cell type	Cre driver	Cre system	Other cells that may be targeted	References
HSC/myofibroblast	Lrat	constitutive	VSMC	Mederacke et al 2013[235]
	Pdgfrb	Constitutive	VSMC	Henderson et al 2013[234]
Myofibroblast	α-SMA	inducible	VSMC	Michelotti et al 2013,[326] Swiderska-Syn 2014[327]
	Colα1(I)	constitutive		Kisseleva et al 2012[29]
	Colα2(I)	constitutive, inducible		Kisseleva et al 2012[29]
	Vimentin	inducible	HSC, VSMC, portal fibroblast	Troeger et al 2012[30]

Abbreviations: c, constitutive; i, inducible; VSMC, vascular smooth muscle cells

Table 3: Cre drivers that may be used to target HSC/myofibroblasts (adapted from Greenhalgh et al[324])

3.3 Hypothesis and aims

HSC αv integrins are key regulators of TGF-β activation during the stromal reaction in hepatic carcinogenesis. Targeted inhibition of αv integrin-mediated TGF-β activation by HSCs may result in less intra- and peri-tumoural ECM formation and reduced hepatic carcinogenesis.

Aims

- To investigate the role of HSC αv integrins during hepatocarcinogenesis in a mouse model of HCC, by targeted αv integrin depletion on HSC
- To also assess the role of hepatocyte αv integrins during hepatocarcinogenesis in a mouse model of HCC, by targeted αv integrin depletion on hepatocytes

3.4 DEN model of murine hepatocarcinogenesis

Animals

Animals were housed in standard sterile conditions with free access to chow and water. All procedures were undertaken in accordance with the local ethical committee.

Pdgfrb-Cre mice were a kind gift from Ralf Adams.[328] *Pdgfrb*-Cre and *Alb*-Cre[329] mice (obtained from the Jackson Laboratory) were crossed with *Itgav*$^{flox/flox}$ mice[330] (C57/BL6 background). Genotyping of all animals was performed by polymerase chain reaction.

Hepatocarcinogenesis

Male mice aged 12-14 days received a single intraperitoneal (IP) injection of DEN (25 mg/kg body weight; Sigma Chemical Co, St. Louis, MO, USA) and were sacrificed at ten months post-injection. Livers were rapidly excised and weighed. The presence and dimensions of surface nodules were evaluated and recorded. The median lobe was fixed in 10% formalin then paraffin embedded, from which 5μm slides were cut and stained with H and E. HCCs were confirmed histologically from either grossly or histologically evident nodules. A proportion of liver tissue was snap-frozen in liquid nitrogen for later analysis. A further sample was fixed in methacarn and paraffin-embedded. A last liver sample from each mouse was fixed in 4% paraformaldehyde, taken through sucrose gradients and embedded in optimum cutting temperature (OCT).

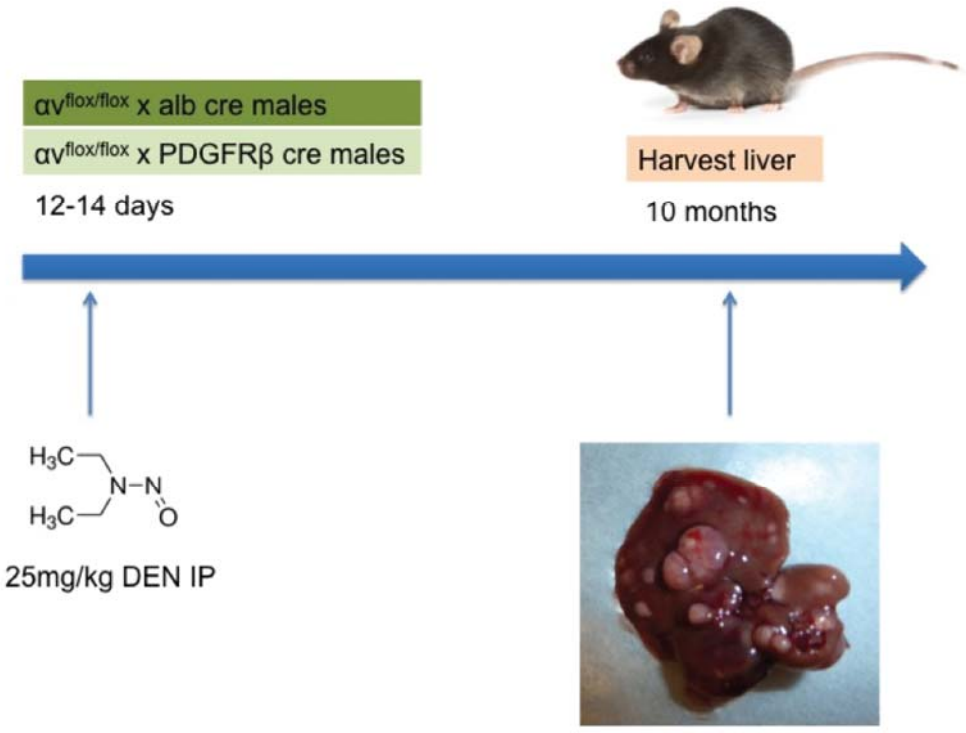

Figure 3.4 Induction of hepatocarcinogenesis: DEN injection

Male transgenic mice and cre negative controls were injected at 12-14 days of age with a once-off IP dose of 25mg/kg DEN. Animals were sacrificed and livers harvested at 10 months. Visible lesions were counted and measured with digital calipers.

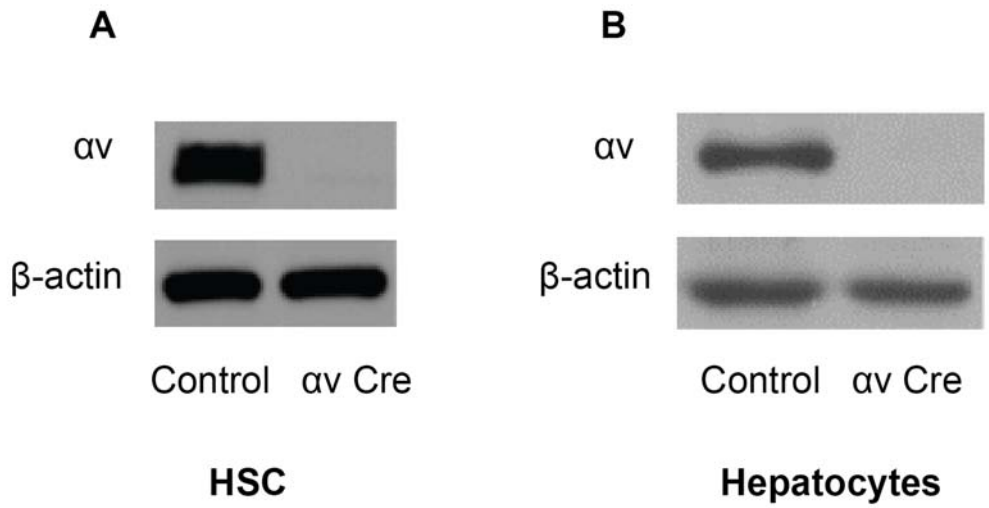

Figure 3.5 Confirmation of αv integrin loss

A Western blot for αv integrin: primary mouse HSC, PDGFRβCre$^{+/-}$;αv$^{fl/fl}$ versus cre negative control. **B** Western blot for αv integrin: primary mouse hepatocytes, AlbCre;αv$^{fl/fl}$ versus cre negative control.

3.5 Targeted αv integrin depletion on HSC in a mouse model of HCC

Loss of HSC αv integrins does not affect tumourigenesis in the DEN model of HCC

Confirmation of αv integrin loss on HSC in PDGFRβ-Cre$^{+/-}$;αv$^{fl/fl}$ positive animals was previously established by Neil Henderson by western blot (Figure 3.5). At ten months post DEN injection, virtually all animals had tumours within the harvested liver. One animal in each group had a macroscopically normal liver with no visible lesions; these were excluded from analysis. Mean lesion size in the PDGFRβ-Cre$^{+/-}$;αv$^{fl/fl}$ cohort was 7.94mm ± 1.44 (standard error of the mean, (SEM)). This cohort consisted of 18 animals. Mean lesion size in the cre negative control group was 10.34mm ± 1.33 (n=17). There was no significant difference between the two groups (p=0.23). Lesion number was also similar between the two groups: mean 12.50 ± 2.06 in PDGFRβCre;αv$^{fl/fl}$ animals, and 14.82 ± 2.45 in controls, p=0.47. Lesion number was also analysed by size, to ensure large tumours were not overrepresented in either group (Figure 3.6). Numbers of small, medium and large tumours were comparable, with no clear effect of αv integrin loss on HSC. There was no difference in liver-to-body weight ratios between the groups.

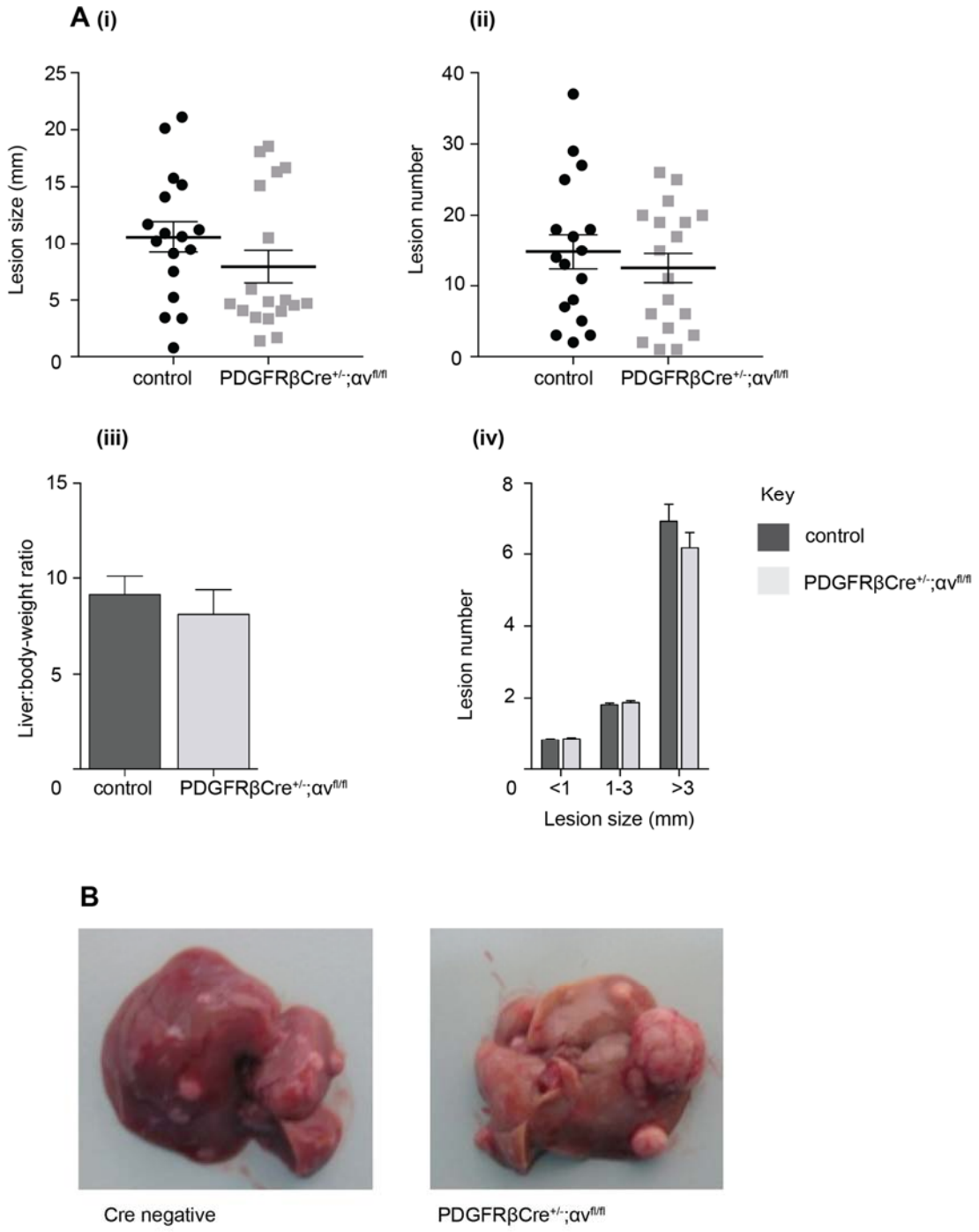

Figure 3.6 Targeted αv integrin depletion on HSC during hepatocarcinogenesis

A (i) Comparison of lesion size (measured using digital calipers) and number **(ii)**; **(iii)** liver:body-weight ratio; **(iv)** lesion numbers grouped by size

B Macroscopic photographs of harvested livers with visible lesions

3.6 Targeted αv integrin depletion on hepatocytes in HCC

Loss of αv integrins on hepatocytes does not affect tumourigenesis in the DEN model of HCC

Loss of αv integrin on hepatocytes in AlbCre$^{+/-}$;αv$^{fl/fl}$ animals was previously demonstrated by Neil Henderson (Figure 3.5).

In this experiment, two animals in the control group and one AlbCre$^{+/-}$;αv$^{fl/fl}$ animal had no visible liver lesions at ten months, and were therefore excluded from the analysis. This left 10 animals in the AlbCre$^{+/-}$;αv$^{fl/fl}$ group, and 17 controls. AlbCre$^{+/-}$;αv$^{fl/fl}$ mice showed similar lesion characteristics to control animals (mean size 11.68mm ± 1.93 compared with 9.39mm ± 3.85, p=0.52). Again, there was no difference in lesion number, mean 8.60 ± 2.14 vs 12.00 ± 1.97, p=0.28. Similarly, liver-to-body weight ratios and numbers of small, medium and large tumours were not significantly different between groups.

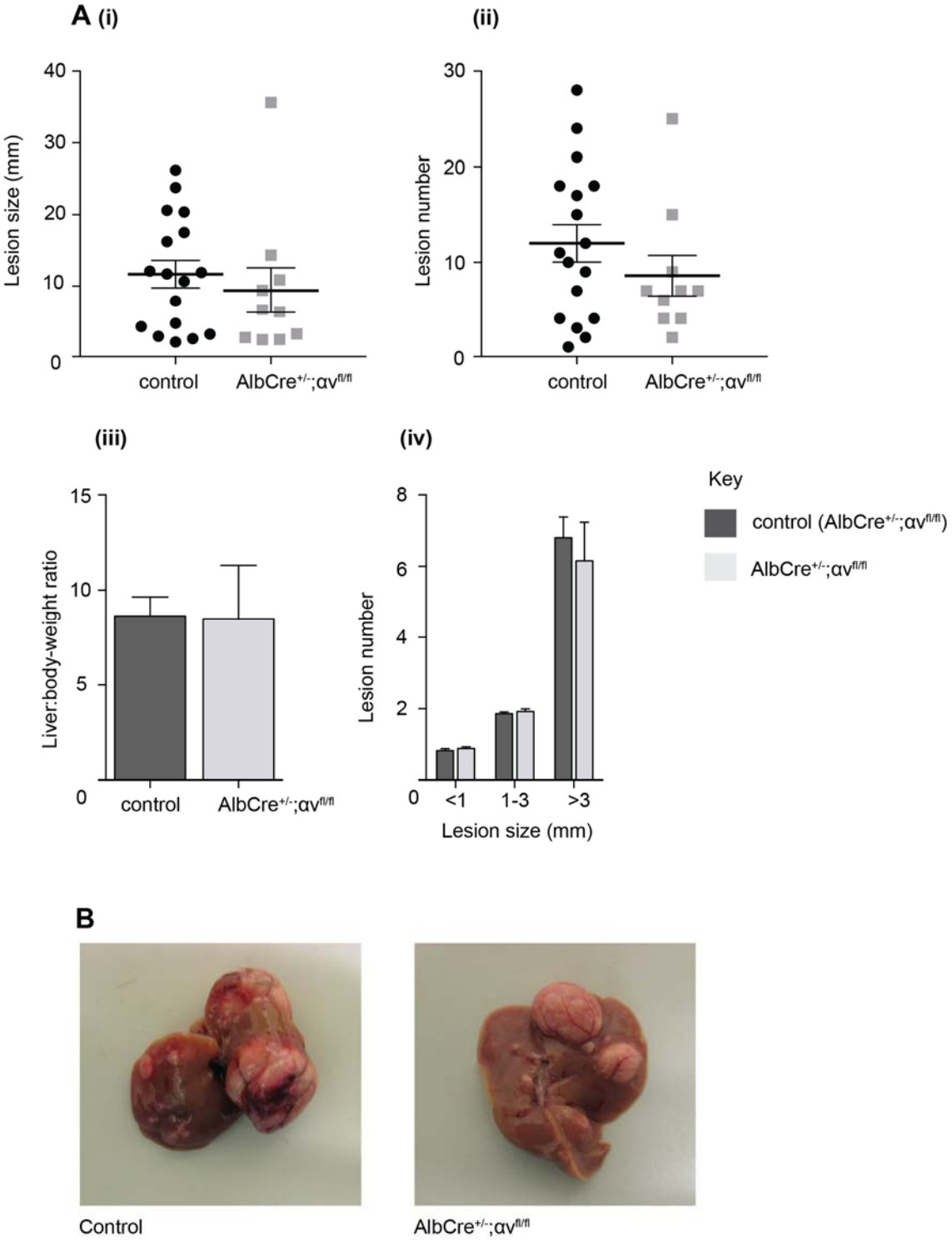

Figure 3.7 Targeted αv integrin depletion on hepatocytes during hepatocarcinogenesis

A (i) Comparison of lesion size (measured using digital calipers) and number **(ii)**; **(iii)** liver:body-weight ratio; **(iv)** lesion numbers grouped by size

B Macroscopic photographs of harvested livers with visible lesions

3.7 Discussion

The results presented demonstrate that loss of αv integrin on HSC or hepatocytes does not protect against hepatocarcinogenesis in the murine model of DEN-induced HCC. Lesion size and number were similar in large cohorts of mice with cell-specific, targeted αv loss compared with controls. This was unexpected, as I had anticipated that loss of αv integrin on HSC or hepatocytes might have reduced hepatocarcinogenesis in this model. I hypothesized this might have occurred via a TGF-β-mediated mechanism, particularly in light of evidence linking TGF-β to hepatocellular EMT and intrahepatic metastasis.[192] However, further consideration of the strengths and weaknesses of this murine model of HCC is required before drawing firm conclusions about the role of HSC and hepatocyte αv integrins and TGF-β in human HCC. The DEN model was chosen primarily because the tumours generated display similar gene expression patterns to human HCC.[256] It is a well-established model for testing the effect of specific genes using transgenic mice, or the efficacy of experimental drug treatments. However, it is a model with a long latency period, requiring ten months before reliable development of HCC. This was a limitation in terms of the time constraints of my PhD project; the lack of a robust, rapidly growing, in vivo HCC model is also a significant limitation in this field of research. Currently, implantation models of HCC are widely used, due to their much shorter latency period and lower cost.[331] Most commonly, the subcutaneous xenograft model is used, in which human HCC cells, or tumour tissue fragments, are implanted into immunodeficient mice (such as nude mice, severe combined immune deficient mice, or nonobese diabetic-severe combined immunodeficiency disease mice).[331] Cells or tissue fragments are typically implanted subcutaneously into the flank. Whilst these systems are relatively easy to set up and monitor tumour size (estimated tumour volume can be calculated every few days from caliper measurements, or by using an in vivo fluorescence imaging approach[332]) any interaction with the native hepatic parenchyma is lost. Additionally, all contributions of the hepatic microenvironment to tumour growth are eliminated, which I hypothesized might be critical in any αv integrin-mediated effects. It is recognized, for example, that spontaneous metastasis is extremely rare when HCC cells are subcutaneously implanted. Conversely, in orthotopic implantation models (where the tumour cells are injected into the liver, or tissue fragments are implanted directly into the liver of immunodeficient mice) spontaneous metastasis is reported.[331,333] Orthotopic xenograft models therefore have some advantages in terms of reproducing the microenvironment. However tumour volume can only be measured upon sacrificing the animal. There are some further technical issues; during injecting tumour cells, it is

possible that seeding along the needle track or into blood can occur, and implanting tumour tissue into the liver is more practically challenging in comparison with ectopic xenografts. Moreover, the requirement for using immunodeficient mice in all xenograft models also eliminates contributions from the host immune system, which may be highly relevant in terms of tumour progression and metastasis.

Allograft models involve injecting murine tumour cells via the portal vein or splenic vein, or orthotopic implantation of murine HCC cell lines.[331] These have the advantage of not requiring immunodeficient host mice, although it is not entirely clear how well tumour biology in these systems replicates the human disease. Kornek et al implanted murine HCC cells into fibrotic mice livers, to investigate HCC angiogenesis in animals with pre-existing fibrosis.[334] This approach mimics human HCC arising in cirrhotic liver. However, overall I felt that whilst the xenograft models were useful in terms of testing changes in tumour progression and metastasis, they were less helpful in cases where a gene might affect the early stages of tumour initiation. For these reasons, I used the chemically-induced method of hepatocarcinogenesis using the well-characterised genotoxic agent DEN. I felt this was a more faithful method to tease out any potential protective effect of loss of HSC or hepatocyte αv integrins, in transgenic, immunocompetent mice. Whilst there are a number of genetically engineered mouse models of HCC, very few constitutive or conditional expression systems have a shorter latency period than the DEN model, and not all have 100% incidence of HCCs.[331] Although one inducible expression system (a tetracycline-controlled system) resulted in liver tumours after approximately 12 weeks,[335] combining this with targeted deletion of αv integrins would require a prolonged, cumbersome breeding strategy.

Although I had reservations about engineering a second genetic manipulation in αv integrin$^{fl/fl}$ mice to try to reduce the DEN latency period, I was interested in whether combining a genetic modification with this chemical carcinogen could achieve earlier HCC formation, as this would represent a useful contribution to the field of liver cancer research. To this end, I collaborated with Dr Rachel Guest to try to generate a novel model of HCC with reduced tumour latency. Here, IP DEN administration at day 15 was combined with genetic loss of the tumour suppressor p53 in hepatocytes. The Ahcre transgenic line was used, in which cre expression is inducible from a cytochrome P450 promotor element, that is transcriptionally up-regulated in response to the lipophilic xenobiotic beta-napthoflavone. The transgene was induced by IP beta-napthoflavone at six weeks of age (i.e. p53 lost at this stage) and animals monitored for clinical signs and weight loss for 52 weeks prior to harvest (n=6 and n=6 controls). There was no significant

difference in tumour size or number at harvest, and no animals required early harvest due to clinical deterioration suggestive of advanced malignancy. Other attempts to accelerate carcinogenesis in the DEN model include phenobarbital injection,[336] expression of *foxm1b*,[337] HGF,[338] interleukin-22,[339] macrophage inflammatory protein-1 and its receptor (CCR1/CCL3).[331,340] To date, these additions to DEN alone have had relatively weak effects on tumour latency.

One limitation of the DEN model was that tumour growth could not be easily monitored prior to culling the animal. I considered magnetic resonance imaging at various time points but concluded this would not be cost-effective. I also considered sacrificing animals at different time points, such as six months, eight months and ten months. This would perhaps have demonstrated any early effect of αv integrin loss on tumour initiation, which might have been lost by ten months. However this would have required larger total animal numbers, and my experience (having culled a few animals early in a small pilot experiment) was that very few lesions were visible at six months. I felt that any small effect on tumour initiation that could have been missed by harvesting all animals at one time point would be unlikely to have significant therapeutic implications, if this effect was lost by the time the tumours had fully matured.

Another disadvantage of the DEN model was the fact that hepatocarcinogenesis occurs in a non-cirrhotic liver. Since the start of this project, Uehara et al published a protocol for co-treatment of mice with a once-off low dose DEN injection at day 14, and subsequent regular low-dose injections of CCL_4 as a pro-fibrogenic agent.[341] This resulted in hepatic fibrosis and development of adenomas at 5 months, at which point 50% of animals also had HCC lesions. The reported acceleration of tumourigenesis was relatively modest, however it perhaps recapitulates human HCC more faithfully, with lesions arising on a fibrotic background.[341,342] The time constraints of my project precluded the use of this new protocol in $\alpha v^{fl/fl}$ mice, but this would be very interesting to compare with DEN alone in future studies.

In my DEN HCC models, animals developed multiple visible lesions at ten months. It is acknowledged that, like human HCC, DEN-induced HCC occurs in a stepwise process, starting with preneoplastic foci of abnormal hepatocytes, progressing to adenoma formation and then carcinoma. I did not proceed with independent examination of the harvested livers by a histopathologist, as there was no macroscopic difference in tumour size or number, making an overall difference in propensity to HCC highly unlikely. It is therefore possible that some of the lesions counted could have been benign adenomas rather than HCC, but in the absence of a clear macroscopic phenotype, I felt that detailed

histopathological analysis was not indicated. Similarly, analysis of downstream changes in TGF-β signalling between the two groups was not performed as we had not observed a clear phenotype between the groups.

Finally, it should be considered, that the observed standard deviation for lesion number in all cohorts, was relatively large. Using my exploratory study data from the PDGFRβ-$Cre^{+/-}$;$αv^{fl/fl}$ experiment, to inform a sample size calculation, a total of 204 mice would be required to enter this two-treatment parallel-design animal study. The probability is 80% that this study would detect a treatment difference, at a two-sided 0.05 significance level, if the true difference between treatments were 3.7 lesions (25% change from the mean of the baseline population). This is based on the assumption that the common standard deviation of the response variable is 9.36. Similarly, for the $AlbCre^{+/-}$;$αv^{fl/fl}$ group, using my study data to inform a sample size calculation, a total of 208 mice would be required to enter this two-treatment, parallel-design animal study. The probability is 80% that the study would detect a treatment difference at a two-sided 0.05 significance level, if the true difference between treatments were 3 lesions (25% change from the mean of the baseline population). This is based on the assumption that the common standard deviation of the response variable is 7.7. The experiments were therefore underpowered, although this was something I could not have fully anticipated; I used sample sizes that were larger than many examples in the literature, and the time constraints of my project, combined with the long latency period of tumour formation, meant that a pilot study for a power calculation was not feasible.

In summary, the role of TGF-β in HCC pathogenesis is complex and context dependent. It may have tumour-suppressive actions in the early stages of liver injury and regeneration, but could exacerbate tumour invasiveness and metastasis during HCC progression. Targeted loss of αv integrin on HSC or hepatocytes did not result in any reduction in tumour burden in this non-cirrhotic model of hepatocarcinogenesis. However this could inform future investigation in larger cohorts. Furthermore, evaluation in a cirrhotic model of HCC may provide further insight into the role of local αv integrin-mediated TGF-β activation on stromal cells and epithelia during HCC formation.

Chapter 4: HSC and acute liver injury

4.1 Introduction

Paracetamol poisoning is the major cause of ALF in the UK and US.[56] Despite the availability of an effective antidote (*N*-acetylcysteine) and public health measures such as restricting sales, deaths from paracetamol-related acute liver failure still occur. ALF is more common with late presentation to medical attention due to unintentional overdose as opposed to deliberate self-poisoning.[56] Although orthotopic liver transplantation is effective, around 50% of patients will have psychiatric or medical contraindications precluding this treatment.[343] Eligible patients who meet criteria for transplantation are at risk of perioperative complications related to coagulopathy, organ failure, sepsis, and encephalopathy. As such, there is a pressing need for alternative treatments for paracetamol-induced acute liver failure.

Nontransplant therapies available for non-paracetamol ALF are scarce.[57] Use of N-acetylcysteine has been explored for other aetiologies, as it can improve liver oxygenation, and has antioxidant, anti-inflammatory and immunologic properties.[344] It may also improve haemodynamic parameters and cerebral perfusion pressure.[57,345,346] However, whilst N-acetylcysteine may have a role in mushroom poisoning and drug-induced liver injury resulting in ALF,[57] a meta-analysis of the safety and efficacy of the drug in adult non-paracetamol ALF found no significant overall survival benefit.[347] Other nontransplant therapies for specific aetiologies include steroids for drug-induced liver injury, and ribavirin for acute hepatitis E infection.[57] However there is currently no available medical therapy of proven benefit to all cases of ALF, regardless of aetiology.

Patient outcome is highly dependent on the extent of liver regeneration post-injury. This has prompted investigation into potential drug targets which could be manipulated to boost the regenerative response. This could be particularly relevant in paracetamol-induced ALF, where an attractive management strategy might include the co-administration of *N*-acetylcysteine with a novel hepatic regenerative agent, alongside established multi-organ supportive measures.

There has been some progress in efforts to augment the regenerative response, at least in experimental models of ALF; for example stimulation of regeneration by administration of growth factors such as VEGF has been shown to improve survival following paracetamol overdose in mice.[348] Additionally, macrophage colony-stimulating factor 1 (CSF1) could represent a promising therapeutic target.[57] Stutchfield et al showed that low serum levels of CSF1 in patients with paracetamol-induced ALF was associated with increased mortality.[349] Furthermore, CSF1-Fc (fragment, crystallizable) administration

increased innate immunity in mice after paracetamol overdose, promoting hepatic macrophage accumulation via proliferation of resident macrophages, and monocyte recruitment.[349]

HSC and acute liver injury

Innate immune dysregulation in ALF is a critical part of this pathophysiological process.[73] Much attention has therefore focused on the role of neutrophils, monocytes and macrophages, in particular the plasticity of hepatic macrophages, which can range from pro-inflammatory to pro-resolution in their functional phenotype. The contribution of non-immune, non-parenchymal cells is less well characterized. Although it has long been acknowledged that HSC play a key role in the fibrotic response to injury,[37] their function in acute liver injury is less clear.

As discussed previously, tools to reliably deplete activated HSC have only relatively recently become available. There is some evidence that these cells may be protective in acute liver injury, but a number of different cell-targeting methods and models of injury are used in these studies, and each set of results must therefore be interpreted carefully. Shen et al hypothesized that during acute liver injury depletion of activated HSC may lead to more significant liver damage and abnormal liver regeneration.[350] They used the fungal metabolite gliotoxin to induce apoptosis of activated HSC. Gliotoxin was administered two hours after paracetamol overdose in mice. Elevated ALT levels, more severe necrosis, and reduced survival were observed in the gliotoxin group. This was accompanied by reduced hepatocyte replication in this group, which was demonstrated by a reduction in hepatocyte bromodeoxyuridine (BrdU)-positivity. The authors hypothesized that HSC-derived growth factors and cytokines might be protective to hepatocytes during acute injury. However, an unconventional paracetamol dosing scheme was used in these experiments (three doses of 300mg/kg with three days in between each dose) which might have induced some chronicity of injury, perhaps modelling acute liver injury less faithfully. Furthermore, relatively small numbers (n=4 in each group) of animals were used for an experiment to check gliotoxin itself was not hepatotoxic, which may not have been adequately powered.[350]

The same group went on to investigate the roles of HSC at different activation stages, during acute liver injury.[351] Mouse HSC were cultured in vitro, to either an early stage of activation (‘initiation HSC’), or a more established activation state (‘perpetuation HSC’). Paracetamol-injured mice were then treated (in vivo) with conditioned medium (CM) from these two HSC groups. It was found that conditioned medium from the initiation HSC

was protective in terms of survival and histological grading of necrosis. This may relate to a reduction in hepatoprotective HSC-derived factors (such as IL-10 and HGF) with later stages of activation.[351]

Conversely, Stewart et al proposed that HSC contribute to hepatocellular damage during acute liver injury, using ischaemia/reperfusion and endotoxin-induced injury models.[352] Here, mice expressing HSV-thymidine kinase under the glial fibrillary acidic protein (GFAP) promoter were treated with CCL_4 to activate HSC, and render them susceptible to phosphorylated ganciclovir-induced death. Animals subsequently received 10 days ganciclovir treatment prior to undergoing acute liver injury. Injury was more pronounced in the CCL_4/ganciclovir-treated groups compared with controls.[352] However, the authors acknowledge that 10-15% of HSC do not express GFAP,[353] and this genetic marker is no longer widely accepted as a robust method of targeting HSC. [235,354] Evidence also implicates HSC in the recovery phase of acute liver injury, via generation of induced regulatory T cells (iTregs), which act to terminate inflammation and promote healing.[355] Lu et al postulated that HSC may contribute to iTreg formation by two parallel pathways. Active TGF-β, together with all-*trans* retinoic acid (RA), can induce peripheral naïve $CD4^+$ cells into functional iTregs ($CD4^+CD25^+Foxp3^+$). Therefore HSC may help generate iTregs via both MMP-mediated TGF-β activation and the retinol/RA pathway.[355] Lu et al demonstrated that TGF-β activation and iTreg induction were impaired in MMP9 and MMP13 knockout mice, and in mice with conditionally defective TGF-β signalling in CD4 T cells.[355] The same group also showed that adoptive transfer of HSC in the context of hepatic ischaemia/reperfusion injury was protective, although the underlying mechanism was not confirmed.[356] Subsequently, Feng et al went on to demonstrate that tail vein injection of HSC followed by acute thioacetamide-induced liver injury resulted in improved ALT and liver histology compared with controls.[357] Depletion of Tregs 24 hours after HSC treatment abrogated this improvement, suggesting that they are involved in the protective effects of HSC. Furthermore, in culture, HSC medium was able to induce Tregs from naïve T cells.[357] However, definitive evidence that this occurs in vivo is currently lacking.

Although these studies suggest that TGF-β may favour resolution of injury by immune mechanisms, others have suggested that TGF-β1/Smad3 signalling may have deleterious effects in drug-induced acute liver injury. Niu et al showed that TGF-β1/Smad3 signalling was increased in acute CCL_4 injury.[358] Overexpression of Smad3 (by tail vein injection of Smad3-expressing plasmids) during CCL_4 treatment resulted in worse liver injury, with increased infiltration of inflammatory cells, cytokine release and

hepatocyte apoptosis.[358] TGF-β therefore, may have distinct local and temporal effects in acute liver injury, and warrants further investigation.

Whilst Henderson et al demonstrated a clear protective role for targeted αv integrin inhibition on HSC in CCL_4-induced chronic liver injury,[234] the role of HSC and integrin-mediated TGF-β activation in acute liver injury is much less clear; in view of intriguing research suggesting that HSC may attenuate acute liver injury, I was therefore interested in investigating the effect of selectively targeting αv integrin on HSC (i.e. without blocking all HSC-mediated effects) in vivo, in this setting. I hypothesized that this might result in reduced TGF-β activation and possibly reduced injury. Similarly, I was interested in specifically targeting the β8 integrin subunit on HSC, as this specific αv integrin subfamily member (αvβ8) has been shown to have an important role in TGF-β activation in vivo in other systems.[359] Global loss of β8 integrin in mice is embryonically lethal, therefore Henderson et al conditionally depleted this on HSC, to investigate its role in chronic liver fibrosis.[234] Depletion of this integrin subunit was not found to protect against CCL_4-induced hepatic fibrosis. However, multiple αv-containing integrins might be involved in hepatic fibrogenesis and TGF-β activation by HSC. In human studies, others have found that integrin αvβ8 expression was increased in the livers of children with biliary atresia,[295] leading the authors to suggest that increased TGF-β activation via αvβ8 interactions with MMPs might contribute to the pathogenesis of this condition. Again, little is known about the effects of this integrin in acute liver injury, and therefore I investigated the role of HSC αvβ8 in acute liver injury, using a genetic approach ($PDGFR\beta Cre^{+/-};\beta 8^{fl/fl}$ mice).

Liver sinusoidal endothelial cells and acute liver injury

Liver sinusoidal endothelial cells (LSEC) are highly specialized endothelial cells that form the wall of the liver sinusoids. They are selectively permeable, allowing passage of certain molecules and cells between blood cells on one side, and hepatocytes and HSC on the other.[360] They are key drivers of liver regeneration in the context of liver injury[361,362] and have a close relationship with HSC in the space of Disse; activated HSC are wrapped round the exterior of LSEC and are thought to induce sinusoidal constriction.[363,364] Similarly, it has been suggested that LSEC could regulate blood flow by swelling, and thereby creating an inlet and an outlet sphincter.[363] They have also been shown to maintain HSC quiescence, counteracting their vasoconstrictive actions.[360,365] Following acute liver injury, they are thought to regulate the balance between hepatocyte and vascular proliferation.[360] In paracetamol-induced injury, LSEC have been identified as an early and direct target for drug toxicity. LSEC swelling, gap formation and

coalescence of fenestrae are observed as early as two hours post-paracetamol, i.e. prior to hepatocellular injury.[366] It is hypothesized that centrilobular microvascular congestion, resulting from sinusoidal wall collapse due to endothelial damage, may represent an early, significant event in the pathophysiology and progression of paracetamol-induced liver injury.[367]

The role of LSEC integrins in acute liver injury has not been studied extensively. However, interestingly, Lalor et al demonstrated that αv integrins mediate platelet adhesion to LSEC, leading to platelet and endothelial activation and leukocyte recruitment.[369] It is therefore conceivable that this could be relevant in acute liver injury, with integrin-dependent platelet adhesion resulting in sinusoidal injury, via immune cell recruitment to the activated endothelium.

4.2.1 Modelling acute liver injury

There are numerous methods to induce acute liver injury in different animal models, including ischaemia/reperfusion injury, partial hepatectomy and drug overdose. The paracetamol model of liver injury is unique in that it is directly comparable to the pathogenesis of a major cause of acute liver injury in humans, paracetamol overdose being the commonest cause of acute liver failure in the Western world. Large animal models of paracetamol overdose such as dogs or pigs allow measurement of physiological parameters including intracranial pressure and cardiac output. However the murine model facilitates understanding of the pathological mechanisms of liver injury and the immune response, as multiple immune markers and antibodies are available for this species, as well as numerous knockout mice.[370] The pathological mechanisms of liver damage in this model, and practical considerations for the experimental protocols are discussed in more detail below.

Whilst I have predominantly used the paracetamol model for the following experiments, other pharmacological agents used to induce acute liver injury in the mouse include anti-Jo-2 antibody (which rapidly leads to hepatocyte apoptosis) and CCL_4, and I have utilised these models in subsequent intravital imaging experiments.

4.2.2 Paracetamol model of acute liver injury

At therapeutic doses, paracetamol is conjugated safely with glucuronic acid or sulphate and excreted. In overdose, the drug causes massive hepatocyte necrosis, due to excessive metabolism to the reactive metabolite *N*-acetyl-p-benzoquinone-imine (NAPQI), via cytochrome P450 enzymes. Progress in characterizing the mechanisms of injury has been made using animal models. NAPQI can be scavenged through

conjugation with glutathione, and can react with protein sulhydryl groups to form adducts. These protein adducts are thought to precipitate mitochondrial dysfunction and early oxidant stress, thereby activating a number of MAP kinases. Finally, c-jun-N-terminal kinase is phosphorylated by the actions of different kinases, and subsequently translocates to the mitochondria, amplifying oxidant stress and peroxynitrite production.[344] This results in opening of the membrane permeability transition pore (MPT), with loss of membrane potential, and failure of adenosine triphosphate (ATP) synthesis. The MPT also causes mitochondrial matrix swelling, with outer membrane rupture, and liberation of intermembrane proteins, including endonuclease G and apoptosis-inducing factor. Upon translocation to the nucleus, these induce DNA fragmentation. The end result is cell necrosis.[371] The mode of paracetamol-induced cell death was traditionally thought to be via oncosis or oncotic necrosis,[371,372] although this was contested by a number of authors suggesting a major role for apoptosis. This was based on observation of DNA fragmentation and laddering,[373] cleavage of poly(ADP-ribose)polymerase,[374] DNA strand breaks detected by TUNEL assay,[375] and morphological assessment of individual hepatocytes.[376,377] These events may not be specific to apoptosis, however it is likely that both necrosis and apoptosis are important in paracetamol-induced hepatocyte death. More recently, Gujral et al found extensive, confluent, centrilobular, oncotic necrosis of up to 60% of hepatocytes in the first 24 hours following overdose.[378]

Paracetamol overdose in the mouse is a well-characterised model of acute liver injury, and is widely used for research purposes. Typically, mice are fasted for 12 hours prior to administration of IP paracetamol,[370] because maintaining normal oral intake results in only mild liver injury, poorly representative of acute liver failure. IP doses range from 300mg/kg to 750mg/kg. At 300mg/kg, spontaneous recovery and 100% survival is expected.[379] At higher doses (eg 600mg/kg) liver regeneration is significantly impaired. From 350mg/kg upwards a degree of mortality can be expected. Hepatocyte necrosis starts about one hour after paracetamol administration. Selection of an appropriate endpoint depends on the research objective. In the first five hours after injection, paracetamol metabolism and initial hepatocyte necrosis are the predominant features. From six hours onwards, immune processes are stimulated by hepatocyte necrosis.[370] Hepatocyte injury peaks at 12 hours post-paracetamol.[379] Typical endpoints are two hours (for metabolism), four hours (for intrinsic cell death pathways) and 6, 12 and 24 hours (for inflammation and immune-related responses). Liver injury can be assessed

by ALT measurement and quantification of the degree of hepatic necrosis observed histologically. The course of liver injury and resolution is relatively rapid, but dose-dependent; at 300mg/kg, in certain strains of mice, regression of injury is seen at 48 hours, and complete histological recovery and normalization of ALT is observed at 72 hours. At 600mg/kg there is approximately 25% mortality between 48-96 hours, and injury is sustained at 96 hours.[379]

4.2.3 FAS model

Programmed cell death by apoptosis is important in liver development, injury, fibrosis and carcinogenesis. Cells dying by apoptosis shrink and condense, with disassembly of the nuclear envelope, condensation and fragmentation of the nuclear chromatin, and cytoskeleton collapse. If the cell is large, the surface often breaks up into membrane-enclosed fragments, 'apoptotic bodies'. Chemical alteration of the cell surface/apoptotic bodies means neighbouring cells or macrophages can rapidly engulf them before spillage of their contents. This allows neat cell death and rapid clearance without causing a damaging inflammatory response.

Apoptosis can occur by two distinct pathways, the death receptor or extrinsic pathway, and the mitochondrial or intrinsic pathway. The DR pathway comprises ligation and/or oligomerisation of cell surface receptors to trigger the apoptotic pathway. The mitochondrial pathway is triggered by a number of intracellular stress responses including intracellular calcium changes and endoplasmic stress responses.[380]

Death receptors (DR) are cell surface receptors belonging to the tumour necrosis/nerve growth factor (TNF/NGF) receptor superfamily. DRs include Fas and TNF receptors 1 and 2, death receptor 3 and TNF-related apoptosis-inducing ligand (TRAIL) receptors 1, 2, 3, and 4. Apoptosis-inducing death receptors are often characterized by a 60-80 amino acid death domain in the cytoplasmic tail of the receptor, known as the death domain. This allows recruitment of adaptor molecules important for initiating the death signal.[380]

The Fas-Receptor (APO-1/CD95) has a single membrane-spanning domain, and is expressed in hepatocytes, cholangiocytes, activated stellate cells and Kupffer cells.[380] An alternatively spliced soluble form of the Fas-R without the transmembrane-spanning domain can also be expressed by hepatocytes. The soluble form of Fas-R may serve to bind Fas ligand on cytotoxic T cells, to minimize liver injury.[381] The Fas-R plays critical roles in hepatic homeostasis and pathophysiology; the Fas-null mouse develops liver hyperplasia likely due to growth unchecked by apoptosis.[382] Fas-R expression correlates with activity of viral hepatitis.[383-385] Inflammatory cytokines can induce and upregulate Fas-R expression, suggesting a role for Fas-R dependent liver injury.[380,386] This is

supported by the discovery that injecting mice with Fas-R agonistic antibodies causes rapid fulminant hepatic failure and death.[387]

4.2.4 Acute carbon tetrachloride

CCL_4 injection induces an oxidant-mediated hepatocyte injury. Its hepatotoxic properties have been recognized for many years,[388,389] and it has been extensively studied, mainly using chronic injection to induce liver fibrosis. Its toxicity is thought to involve the P450 cytochrome enzyme 2E1, with the production of an active metabolite.[388,390] Cell death occurs by apoptosis and necrosis, with the majority of cell damage occurring in the centrilobular region.[391] In the past, it was widely used in animal models of acute hepatic failure. However, it was found to be poorly reproducible and the clinical syndrome of acute hepatic failure was not well represented by CCL_4 intoxication (little encephalopathy and late stage hepatic coma).[390] It is therefore more commonly used for chronic fibrotic models rather than acute liver injury.

4.3 Hypothesis

HSC and LSEC αv integrins are key regulators of TGF-β activation during acute liver injury. Targeted inhibition of αv integrins on these cell types may be protective in paracetamol-induced acute liver injury.

4.4 Aims

- To investigate the specific role of hepatocyte, HSC and LSEC αv integrins in the mouse model of paracetamol-induced acute liver injury, using genetic approaches
- To investigate the effects of specific β8 integrin subunit depletion on HSC and hepatocytes, in paracetamol-induced acute liver injury.
- To gain experience with murine models of acute liver injury, in order to develop a novel, IVM approach to investigating the cellular and molecular mechanisms of hepatic injury and repair.

4.5 Materials and methods

Animals

Animals were housed in standard sterile conditions with free access to chow and water. All procedures were undertaken in accordance with the local ethical committee. Animals were between eight and 22 weeks old. Within each experiment, the maximum age difference between animals was four weeks.

Pdgfrb-Cre[328] and *Alb*-Cre[329] mice (obtained from the Jackson Laboratory) were crossed with *Itgav*$^{flox/flox}$ mice.[330] *Pdgfrb*-Cre and *Alb*-Cre animals were also crossed with *Itgb8*$^{flox/flox}$ mice.[392] All were maintained on a C57/BL6 background. Cdh5-cre-ERT2 mice (Tg(Cdh5-cre/ERT2)1Rha)[393] were a kind gift from Ralf Adams. These were crossed with *Itgav*$^{flox/flox}$ animals. Cre recombinase was induced by tamoxifen injection. Tamoxifen was prepared in corn oil (20mg/ml) and given IP 100mg/kg daily for three days, followed by three days of rest, then daily for three days.

Induction of liver injury

Paracetamol model

After an overnight fast, mice were injected IP with 300 or 350mg/kg of paracetamol, dissolved in sterile PBS, warmed to 42°C and allowed to cool prior to administration (Figure 4.2). After IP injection groups of mice were scored as follows for signs of systemic illness: clinically well (0 points), presence of piloerection (1 point), with additional hunched posture (2 points) and lack of spontaneous movement (3 points) 24 hours after paracetamol. They were harvested at 24 hours; one lobe from each liver was fixed in 10% formalin, and one in 4% paraformaldehyde. Remaining liver tissue was flash-frozen and stored at -80°C for downstream analysis. Serum was also stored at -80°C.

Serum analysis

All murine serum analyses were kindly performed by Forbes Howie (Centre for Inflammation Research, University of Edinburgh) as detailed below.

Total bilirubin

Total bilirubin was determined by the acid diazo method described by Pearlman and Lee[394] using a commercial kit (Alpha Laboratories Ltd., Eastleigh, UK) adapted for use on a Cobas Fara centrifugal analyser (Roche Diagnostics Ltd, Welwyn Garden City, UK). In this method a surfactant is used as a solubiliser. Conjugated and solubilised unconjugated bilirubin react with diazotised sulphanilic acid to produce an acid azobilirubin, the absorbance of which is proportional to the concentration of bilirubin in the sample and can be measured at 550nm. Within run precision was CV < 4% while intra-batch precision was CV < 5%.

Alanine aminotransferase (ALT)

ALT was measured using the method described by Bergmeyer et al,[395] utilising a commercial kit (Alpha Laboratories Ltd., Eastleigh, UK) adapted for use on a Cobas Fara centrifugal analyser (Roche Diagnostics Ltd, Welwyn Garden City, UK). Within run precision was CV < 4% while intra-batch precision was CV < 8%.

Aspartate aminotransferase (AST)

AST was determined by a commercial kit (Randox Laboratories, UK) adapted for use on a Cobas Fara centrifugal analyser (Roche Diagnostics Ltd, Welwyn Garden City, UK). α-oxogluterate reacts with L-aspartate in the presence of AST to form L-glutamate plus oxaloacetate. The indicator reaction utilises the oxaloacetate for a kinetic determination of nicotinamide adenine dinucleotide (NADH) consumption. Within run precision was CV < 4% while intra-batch precision was CV < 5%.

Alkaline phosphatase (ALP)

ALP was determined by a commercial kit (Randox Laboratories, UK) adapted for use on a Cobas Fara centrifugal analyser (Roche Diagnostics Ltd, Welwyn Garden City, UK). The substrate p-nitriphenyl phosphate is hydrolysed by ALP from the sample, in the presence of Magnesium ions, to form p-nitophenol which is yellow in colour and it's production can be monitored at 405 nm. Within run precision was CV < 4% while intra-batch precision was CV < 5%.

Serum albumin

Mouse serum albumin measurements were determined using a commercial serum albumin kit (Alpha Laboratories Ltd., Eastleigh, UK) adapted for use on a Cobas Fara centrifugal analyser (Roche Diagnostics Ltd, Welwyn Garden City, UK). The measurement of serum albumin is based on its quantitative binding to bromocresol green. The albumin-bromocresol green-complex absorbs maximally at 578nm, the absorbance being directly proportional to the concentration in the sample. Within run precision was CV < 2.5% while intra-batch precision was CV < 4%.

Immunohistochemistry

Formalin-fixed, paraffin-embedded sections were stained with H and E, for analysis of tissue injury.

Microscopy and digital image analysis

Microscopic examination of tissue specimens was performed using an inverted Zeiss Axiovert-200 microscope and Axiovision image acquisition software (Zeiss, Heidenheim, Germany).

Initially, histological grading of hepatic necrosis was performed by a blinded observer using H and E-stained sections, using a scoring system from 1-5 (ranging from minimal injury to severe haemorrhagic necrosis). More detailed quantification of liver injury was then performed using ImageJ (National Institute of Health, USA) and a Wacom tablet. For each H and E-stained section (in all cases the left hepatic lobe was used for sections), six consecutive fields of x5 magnification were acquired using the Axiovert-200 microscope. The Wacom tablet was used to draw round patches of necrosis, allowing quantification of the necrotic area. The non-cellular area in each field was also quantified in this way, as some of the specimens contained a substantial vascular component. The final 'percentage necrotic area' for each field was therefore calculated by subtracting the 'total necrotic area' from the 'total cellular area' (total field area minus non-cellular area). The average of the six fields quantified for each liver sample was then taken.

Inhibition of αv integrins by the novel small molecule CWHM 12

The protocol for inhibition of αv integrins by the small molecule inhibitor CWHM12 was devised in collaboration with David Griggs (Saint Louis University, St. Louis, USA). CWHM 12 was solubilized in PBS, for IP injection. The dosing regimen for the inhibitor was based on simulated pharmacokinetic profiles of CWHM 12 plasma levels following single dose and repeated dose IP administration. Following 100mg/kg IP CWHM 12 injection, drug concentration was expected to fall below the 3 uM threshold concentration after three hours, according to the simulated graph (Figures 4.3 and 4.4). Therefore in order to sustain constant integrin inhibition throughout paracetamol-induced liver injury, three-hourly dosing intervals were chosen. From simulated calculations, increasing the dose to 200mg/kg was not expected to significantly lengthen the dosing interval required. Animals were fasted prior to induction of liver injury as described above. The first IP injection of CWHM 12 (100mg/kg) was given 1 hour prior to paracetamol injection (350mg/kg). CWHM 12 was then administered 3 hourly (100mg/kg each time) for a total of 7 doses, providing 21 hours of continuous integrin inhibition.

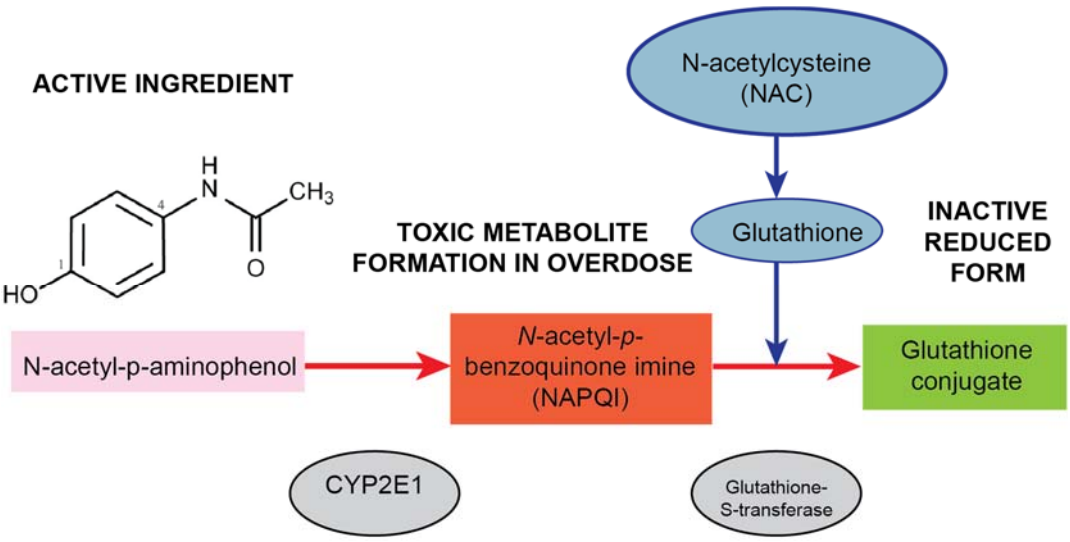

Figure 4.1 Paracetamol metabolism

Adapted from Mossanen et al 2015.[370]

N-acetyl-p-aminophenol (paracetamol) is metabolized by different isoforms of cytochrome P450 (mainly CYP2E1) leading to formation of the toxic metabolite NAPQI in hepatocytes. Glutathione binding can convert low levels of NAPQI into the inactive reduced form. In paracetamol overdose, glutathione stores are depleted, and NAPQI starts to bind mitochondrial proteins. The NAPQI protein adducts lead to hepatocyte necrosis. N-acetyl-cysteine, a glutathione precursor, is an effective treatment option following paracetamol overdose in humans.

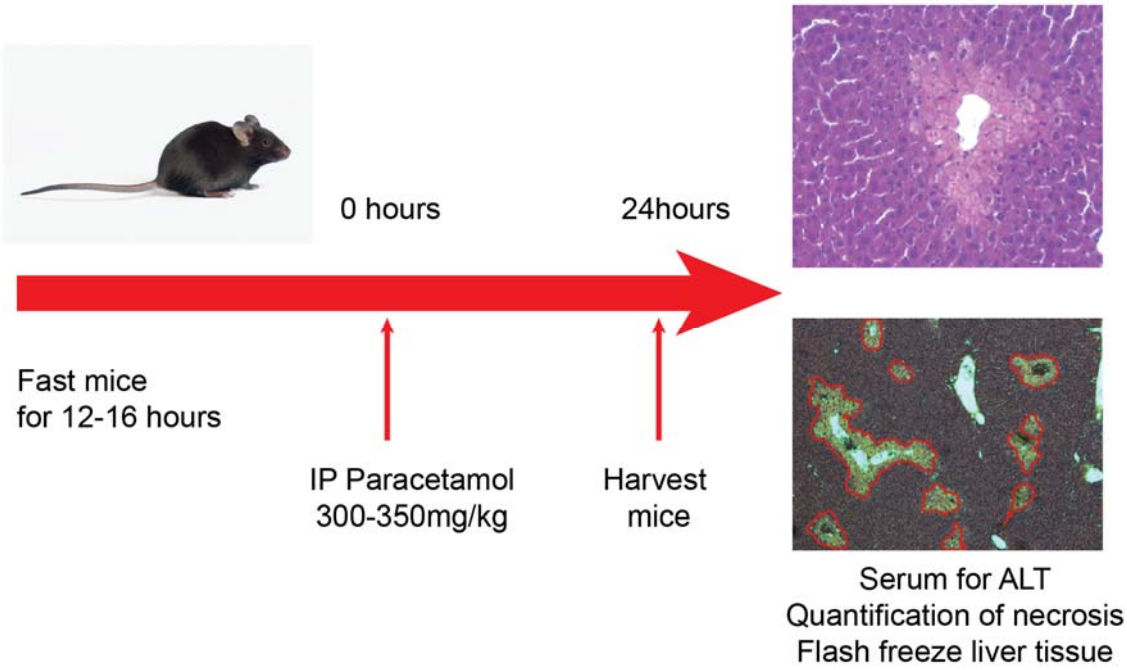

Figure 4.2 Paracetamol administration and harvesting protocol

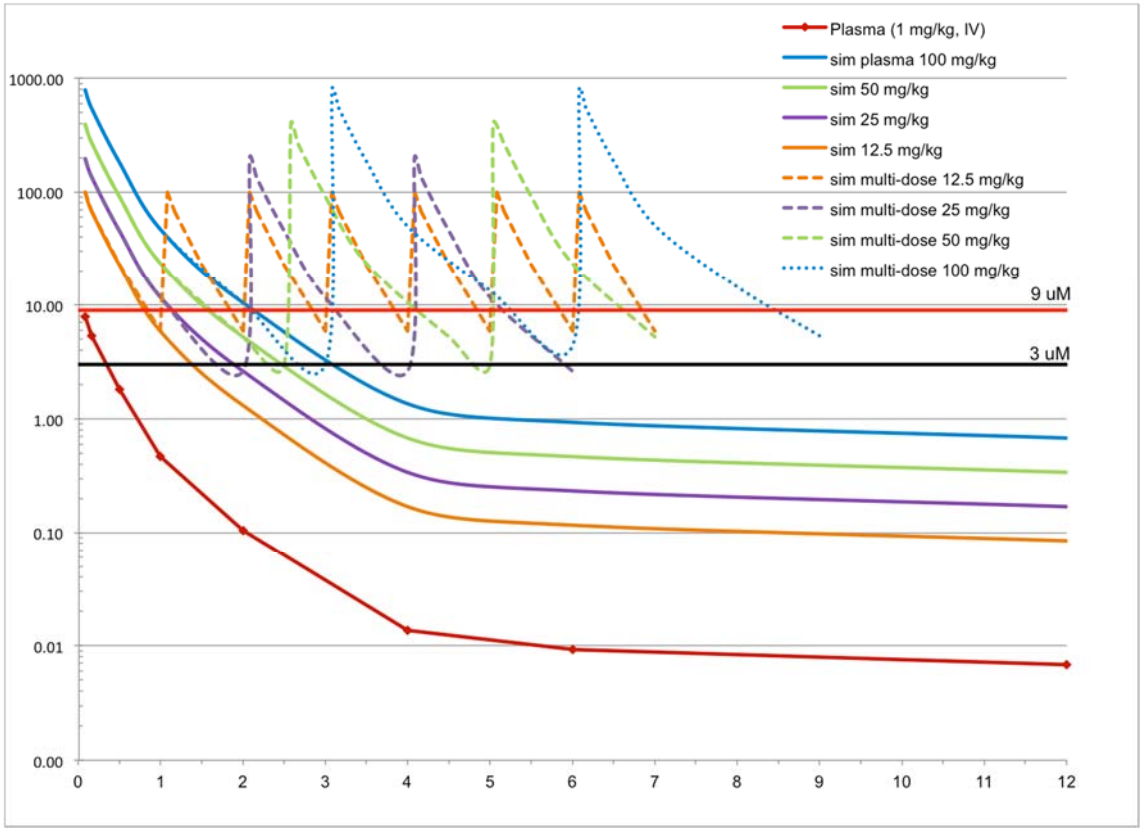

Figure 4.3 CWHM 12 Simulated plasma concentrations (uM)

Graph showing simulated plasma concentrations of CWHM 12 after single or repeated IP injections. Calculated from rat IV data. From 100mg/kg mini-pump studies, steady state mean plasma concentrations ranged from 3.58 to 9.03 uM. Simulations were based on 3uM troughs. With 100mg/kg dose every 3 hours, plasma concentration would drop below 3 uM after 9 hours. With 50mg/kg dose every 2.5 hours, plasma concentration would drop below 3 uM after 7.5 hours. With 25mg/kg dose every 2 hours. plasma concentration would drop below 3 uM after 6 hours.

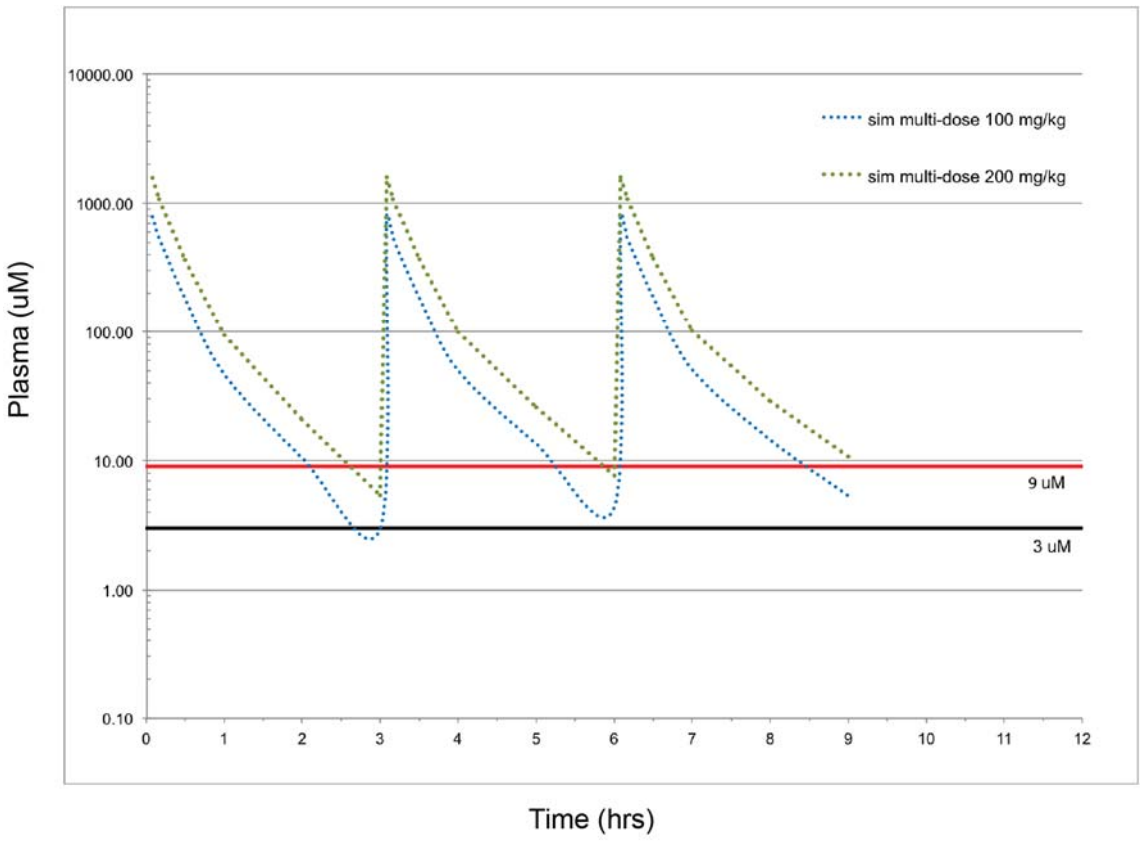

Figure 4.4 CWHM 12 Simulated plasma concentrations (uM)

Graph showing simulated plasma concentrations of CWHM12 after repeated doses. From 100 mg/kg mini-pump studies, steady state mean plasma concentrations ranged from 3.58 to 9.03 uM. Simulations were based on 3 uM troughs.100 mg/kg dose every 3 hours was projected to result in plasma levels below 3 uM after 10hr. 200 mg/kg dose every 3.5 to 4 hours was projected to result in plasma levels below 3 uM after 11 hours.

4.6 Targeted αv integrin depletion on HSC in a mouse model of paracetamol-induced acute liver injury

All experiments presented in Chapter 4 will be summarised in Confirmation of αv integrin loss on HSC in PDGFRβCre$^{+/-}$;αv$^{fl/fl}$ animals was previously established by Neil Henderson by western blot (Figure 3.5). The first acute liver injury experiment was performed using 14 week-old male mice, n=6 PDGFRβCre$^{+/-}$;αv$^{fl/fl}$ and n=6 cre negative control animals (Figure 4.5). The length of overnight fast was 16 hours. Three animals died before the intended harvest point at 24 hours. Post-mortem examination revealed macroscopically haemorrhagic liver, consistent with death from acute liver failure. From the H&E liver sections harvested at 24 hours, an initial injury score for each animal was calculated by a blinded observer. Mean injury score was 3.33 for the PDGFRβCre$^{+/-}$;αv$^{fl/fl}$ group, and 4.67 for the control group. There was a striking mortality difference: 50% mortality observed in the control group, compared with no deaths in the PDGFRβCre$^{+/-}$;αv$^{fl/fl}$ group. ALT data was unfortunately not obtained for the animals that died. Of the animals for which serum was successfully analysed, all had evidence of acute liver injury, with ALT >2000 at 24 hours. Mean ALT in the PDGFRβCre$^{+/-}$;αv$^{fl/fl}$ cohort was 6287 $\pm$ 2360 (SEM) and 7747 $\pm$ 3660 in the controls (p=0.74). Percentage necrosis was calculated from H&E sections for each harvested liver, including the animals that died. The mean percentage area of necrosis for each group was 34.00 $\pm$ 10.00 for PDGFRβCre$^{+/-}$;αv$^{fl/fl}$ animals and 64.99 $\pm$ 10.02 for controls, which did not quite reach significance (p=0.0534).

In the next experiment (Figure 4.6) I used female mice, hypothesizing that they might tolerate liver injury better than males. I therefore anticipated that all animals might survive the experiment, allowing ALT measurement in all cases. Here, n=6 (in each group) 11 week-old female mice received 350mg/kg paracetamol after a 16 hour fast. As expected, all animals survived the experiment, allowing a full set of ALT measurements to be obtained. Mean ALT was 2902 $\pm$ 721 in the PDGFRβCre$^{+/-}$;αv$^{fl/fl}$ compared with 4790 $\pm$ 1550 in the control group (p=0.30). There was an outlier in the PDGFRβCre$^{+/-}$;αv$^{fl/fl}$ group, in whom ALT was only 560 at 24 hours, suggesting less severe liver injury. This was consistent with a smaller percentage necrotic area of 44.86 in this animal. Mean percentage necrotic area was 58.07 $\pm$ 2.81 in the PDGFRβCre$^{+/-}$;αv$^{fl/fl}$ group, and 58.42 $\pm$ 3.79 in controls (p=0.94). On re-analysis of the data without this outlier, there was still no significant difference in liver injury endpoints at 24 hours between the two groups.

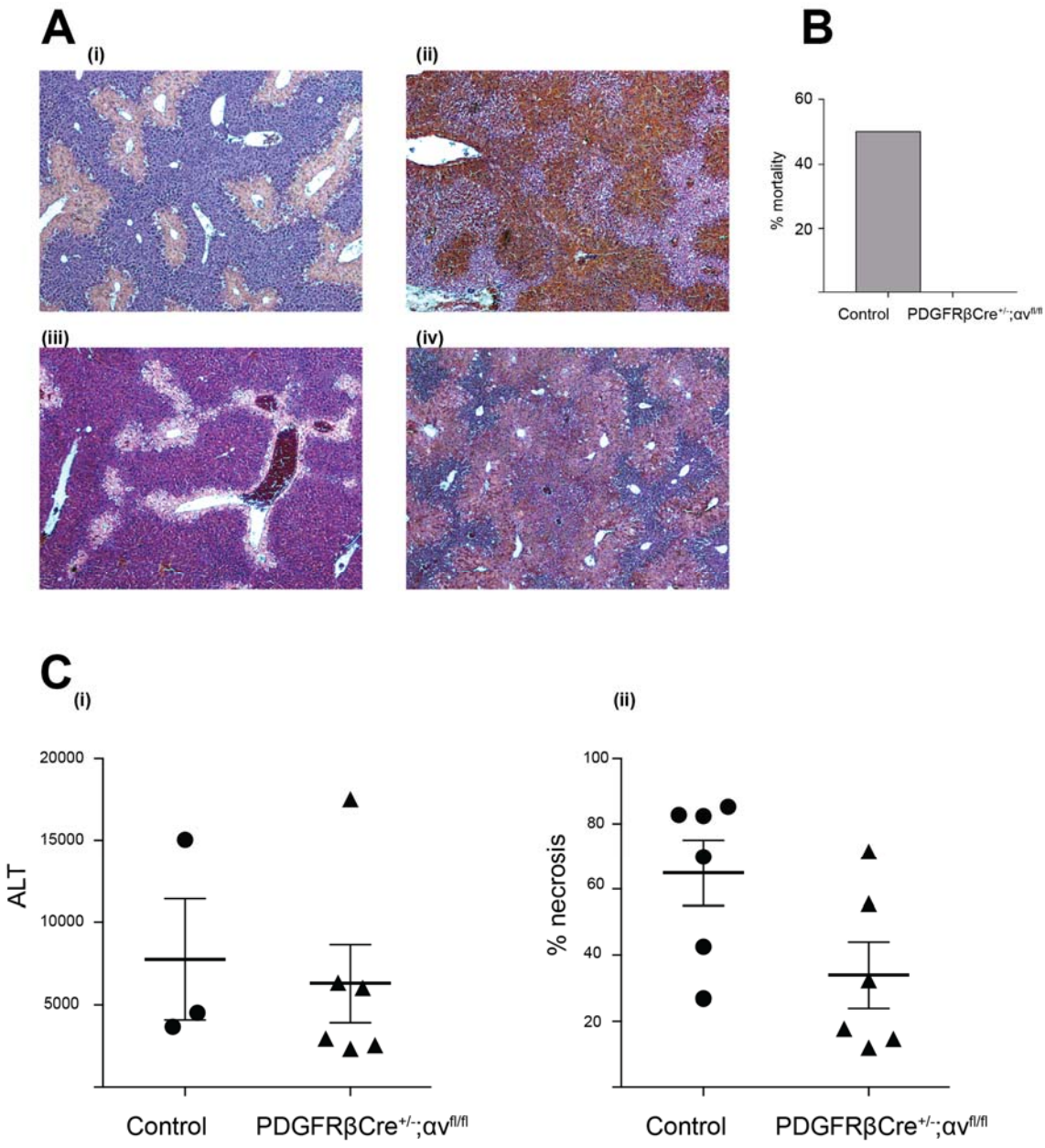

Figure 4.5 Targeted αv integrin depletion on HSC during paracetamol-induced acute liver injury

In this experiment, n=6 male animals in each group.

A H and E-stained sections (x5 magnification) of liver 24 hours post-paracetamol from **(i)** control animal showing centrilobular necrosis and **(ii)** control animal that succumbed to ALF; **(iii)** PDGFRβCre$^{+/-}$;αv$^{fl/fl}$ animals showing centrilobular necrosis and **(iv)** H and E from a PDGFRβCre$^{+/-}$;αv$^{fl/fl}$ animal with haemorrhagic necrosis. **B** Percentage mortality in each group **C (i)** Serum ALT at 24 hours post-paracetamol and **(ii)** Percentage necrosis quantified digitally from H and E sections.

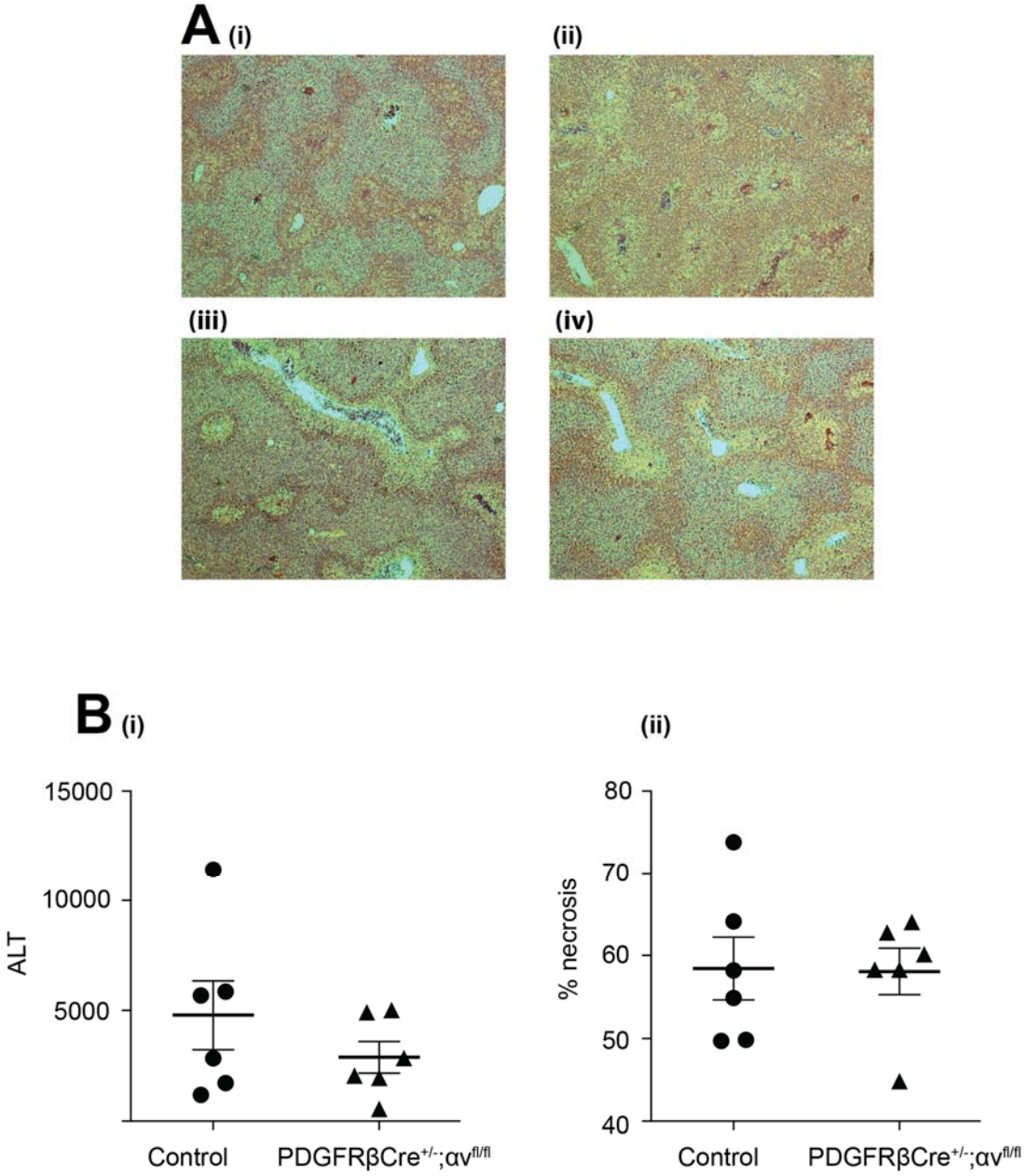

Figure 4.6 Targeted αv integrin depletion on HSC during paracetamol-induced acute liver injury

In this experiment, n=6 female animals in each group.

A H and E-stained sections of liver 24 hours post-paracetamol (x5 magnification) from **(i)** and **(ii)** control animal showing centrilobular necrosis. **(iii)** and **(iv)** PDGFRβCre$^{+/-}$;αv$^{fl/fl}$ animals showing centrilobular necrosis. **B (i)** Serum ALT at 24 hours post-paracetamol and **(ii)** Percentage necrosis quantified digitally from H and E sections.

Next, I repeated the experiment using 9 week-old male animals, but shortened the duration of the overnight fast to 12 hours, and harvested at 18 hours post-paracetamol

injection (Figure 4.7). Here, I anticipated that the younger age, shorter fast, and earlier time point for culling might result in all animals surviving to the end of the experiment, allowing ALT measurement. Group sizes were again n=6 PDGFRβCre$^{+/-}$;αv$^{fl/fl}$ and n=6 control animals. One animal in each group did, however, succumb to acute liver failure prior to the end point. This left n=5 in each cohort for ALT analysis. Mean ALT was 11580 $\pm$ 1333 in the PDGFRβCre$^{+/-}$;αv$^{fl/fl}$ group and 7212 $\pm$ 1901 in the control group (p=0.10). Mean percentage necrosis was 66.73 $\pm$ 7.192 in PDGFRβ-Cre$^{+/-}$;αv$^{fl/fl}$ animals, compared with 68.65% in controls (p=0.85).

In all three of these experiments, there was no significant difference in ALT or percentage necrosis between PDGFRβCre$^{+/-}$;αv$^{fl/fl}$ transgenic mice and cre negative controls.

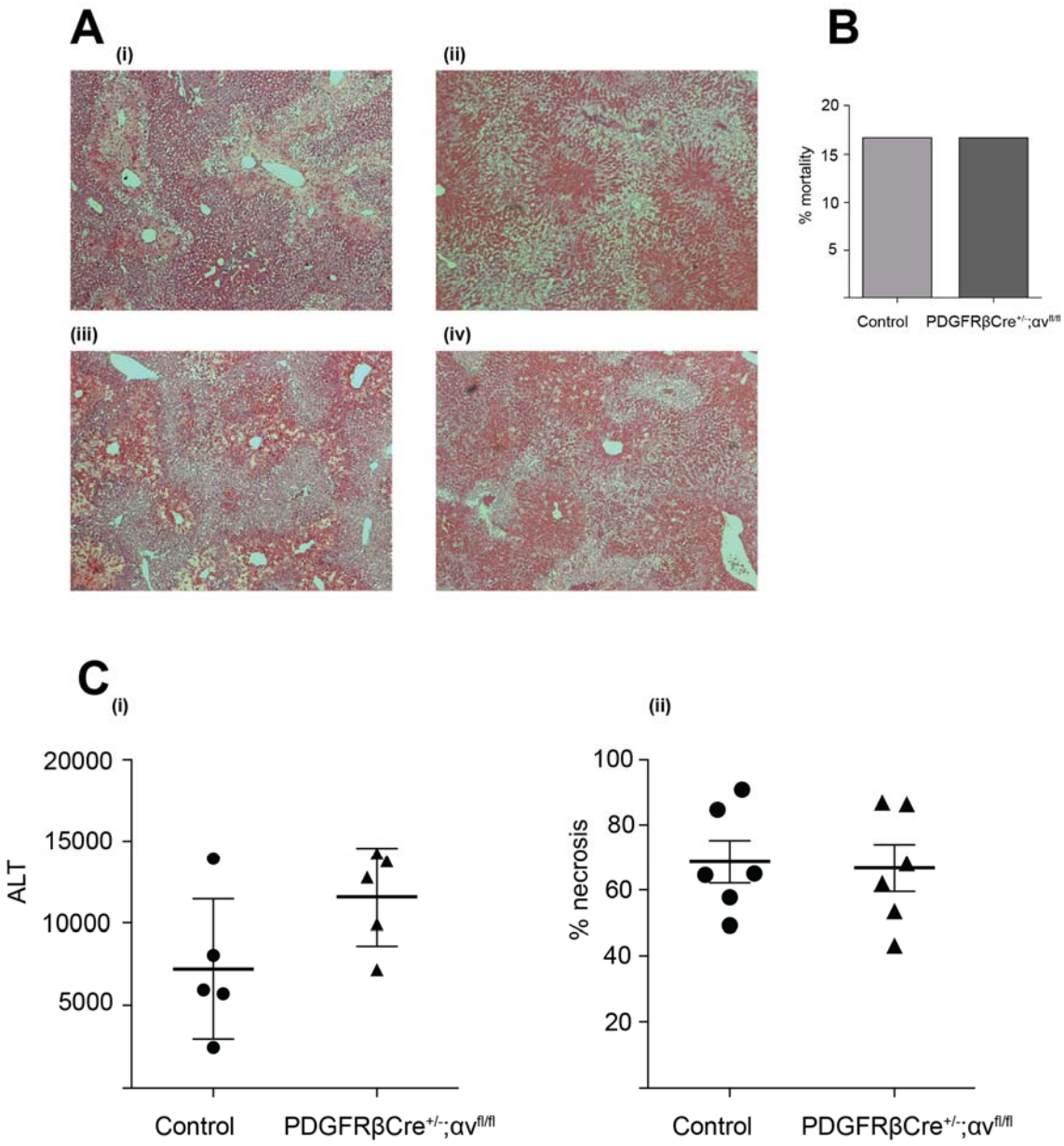

Figure 4.7 Targeted αv integrin depletion on HSC during paracetamol-induced acute liver injury

In this experiment, n=6 male animals in each group.

A H and E-stained sections of liver 18 hours post-paracetamol (x5 magnification) from **(i)** control animal showing centrilobular necrosis and **(ii)** control animal that succumbed to ALF; **(iii)** PDGFRβCre$^{+/-}$;αv$^{fl/fl}$ animal showing centrilobular necrosis and **(iv)** H and E from a PDGFRβCre$^{+/-}$;αv$^{fl/fl}$ animal that succumbed to ALF. **B** Percentage mortality in each group **C (i)** Serum ALT at 18 hours post-paracetamol and **(ii)** Percentage necrosis quantified digitally from H and E sections.

4.7 Pharmacological αv integrin blockade in a mouse model of paracetamol-induced acute liver injury

Finally, a small-molecule inhibitor of αv integrins (CWHM 12) was administered at 3-hourly intervals, to male C57/Bl6 mice (n=6 in each group), beginning one hour before paracetamol injection. The control group received PBS rather than CWHM 12. Animals were harvested at 24 hours post-paracetamol. In this experiment, there was a high overall mortality (Figure 4.8). In the treatment group 4/6 animals (83.33%) died prior to the 24-hour endpoint. In the control group 2/6 animals (33.33%) died. One animal in the treatment group had evidence of acute bowel obstruction, and one in the control group had urinary retention; these were likely to be complications from multiple IP injections. Post-mortem examination of the other animals revealed haemorrhagic liver but was otherwise unremarkable.

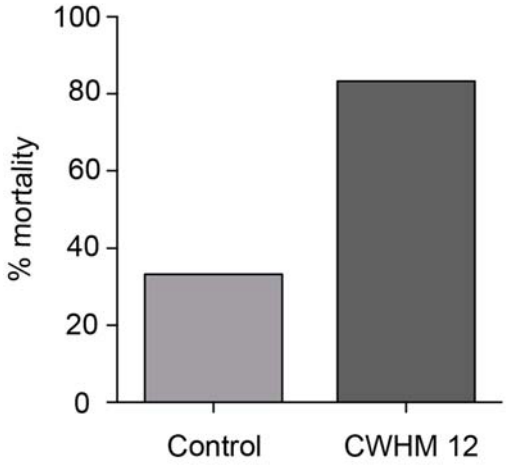

Figure 4.8 Small molecule inhibition of αv integrins during paracetamol-induced acute liver injury

Graph showing percentage mortality in each group

4.8 Targeted αv integrin depletion on hepatocytes in a mouse model of paracetamol-induced acute liver injury

Confirmation of αv integrin loss on hepatocytes in AlbCre$^{+/-}$;αv$^{fl/fl}$ animals was previously established by Neil Henderson by western blot (Figure 3.5).

In this experiment, n=6 female AlbCre$^{+/-}$;αv$^{fl/fl}$ and n=6 cre negative control animals (all 11 weeks old) received 350mg/kg paracetamol after a 16 hour fast (Figure 4.9). There was no premature mortality. Mean ALT was 6710 $\pm$ 2016 in the AlbCre$^{+/-}$;αv$^{fl/fl}$ compared with 4062 $\pm$ 1172 in controls (p=0.28). Mean percentage necrosis was 62.35 $\pm$ 3.97 in AlbCre$^{+/-}$;αv$^{fl/fl}$ animals and 54.94 $\pm$ 6.52 in controls (p=0.35).

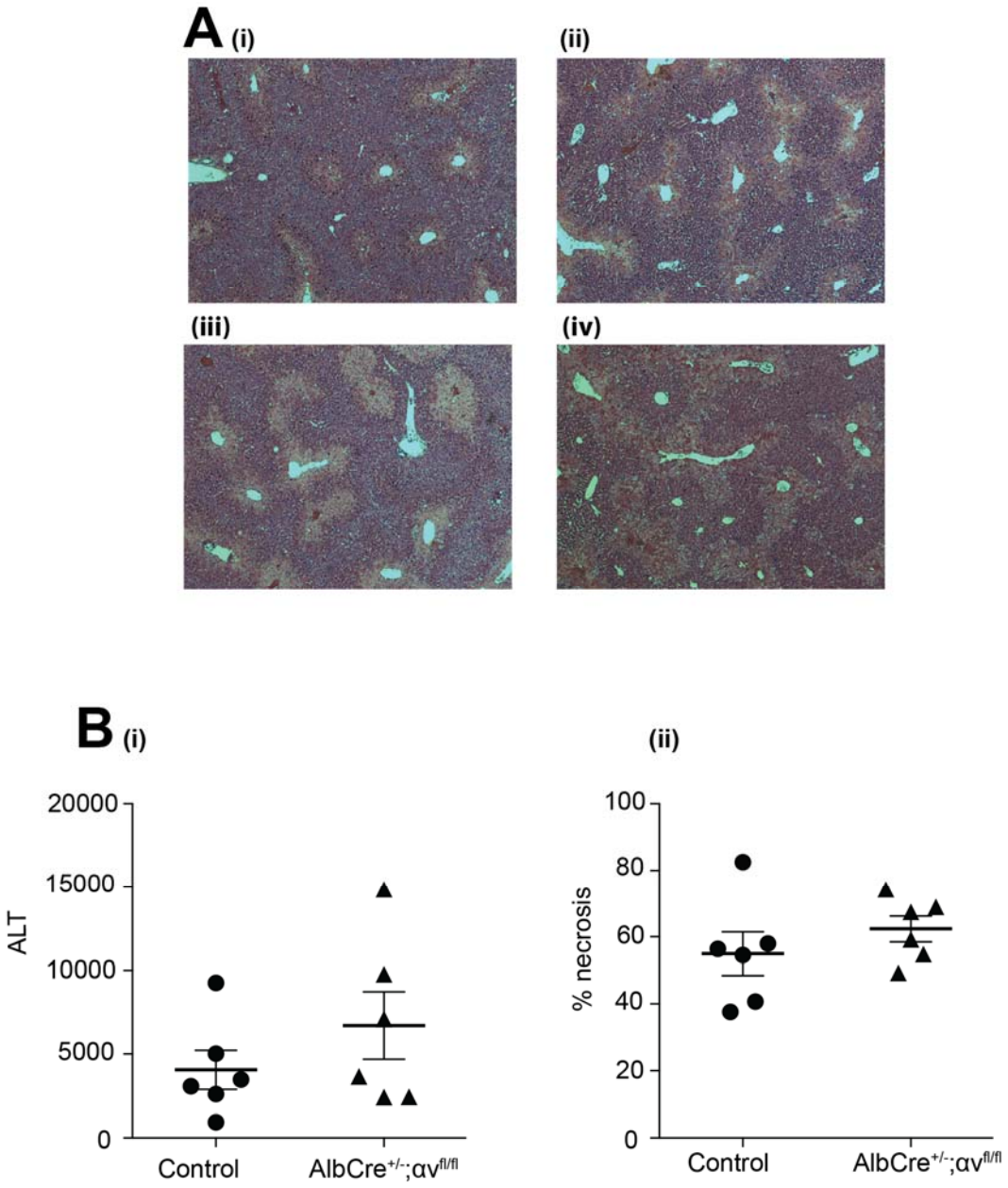

Figure 4.9 Targeted αv integrin depletion on hepatocytes during paracetamol-induced acute liver injury

In this experiment, n=6 female animals in each group.

A H and E-stained sections of liver 24 hours post-paracetamol (x5 magnification) from **(i)** and **(ii)** control animal showing centrilobular necrosis; **(iii)** and **(iv)** PDGFRβCre$^{+/-}$;αv$^{fl/fl}$ animals showing centrilobular necrosis

B (i) Serum ALT at 24 hours post-paracetamol and **(ii)** Percentage necrosis quantified digitally from H and E sections.

4.9 Targeted β8 integrin depletion on HSC in a mouse model of paracetamol-induced acute liver injury

Confirmation of β8 integrin loss on HSC in PDGFRβCre$^{+/-}$;β8$^{fl/fl}$ animals was previously established by Neil Henderson.[234] Acute liver injury was induced with 350mg paracetamol after a 16 hour fast, in 11 week-old male mice, n=5

PDGFRβCre$^{+/-}$;β8$^{fl/fl}$ and n=6 control animals (Figure 4.10). In this experiment, two control animals died prior to the 24 hour end point (33.33% mortality in the control group compared with no mortality in the PDGFRβCre$^{+/-}$;β8$^{fl/fl}$ group). Mean ALT was 2928 $\pm$ 833.1 in the PDGFRβCre$^{+/-}$;β8$^{fl/fl}$ cohort, and 8060 $\pm$ 3652 in controls (p=0.17). Mean percentage necrosis was 43.00 in PDGFRβCre$^{+/-}$;β8$^{fl/fl}$ animals, and 65.14 $\pm$ 9.80 in controls (p=0.08).

This experiment was repeated, using a larger cohort of younger male animals, and using a reduced dose of paracetamol (Figure 4.11). It was anticipated that all animals would survive to 24 hours, in order to obtain a complete set of ALT measurements. Accordingly, n=10 PDGFRβCre$^{+/-}$;β8$^{fl/fl}$ and n=10 control animals received 300mg/kg paracetamol after a 16 hour fast. Here, all animals survived.

Mean ALT was 4696 $\pm$ 700.9 in the PDGFRβCre$^{+/-}$;β8$^{fl/fl}$ group, compared with 6096 $\pm$ 853.1 in the control group (p=0.22). Mean percentage necrosis was 49.83 $\pm$ 3.848 in PDGFRβCre$^{+/-}$;β8$^{fl/fl}$ animals, and 50.29 $\pm$ 4.233 in controls (p=0.94).

4.10 Targeted β8 integrin depletion on hepatocytes in a mouse model of paracetamol-induced acute liver injury

Confirmation of β8 integrin loss on hepatocytes in AlbCre$^{+/-}$;β8$^{fl/fl}$ animals was previously performed by Neil Henderson (Figure 4.12). Acute liver injury was induced with 350mg/kg paracetamol after a 16 hour fast. Animals were 12 weeks old, with n=6 in each group (Figure 4.12). There was no early mortality in this experiment. Mean ALT was 6545 $\pm$ 929 in AlbCre$^{+/-}$;β8$^{fl/fl}$ animals and 6560 $\pm$ 628.7 in controls (p=0.10). Mean percentage necrosis was 54.01 $\pm$ 5.94 and 61.69 $\pm$ 3.75 in AlbCre$^{+/-}$;β8$^{fl/fl}$ and control animals respectively (p=0.25).

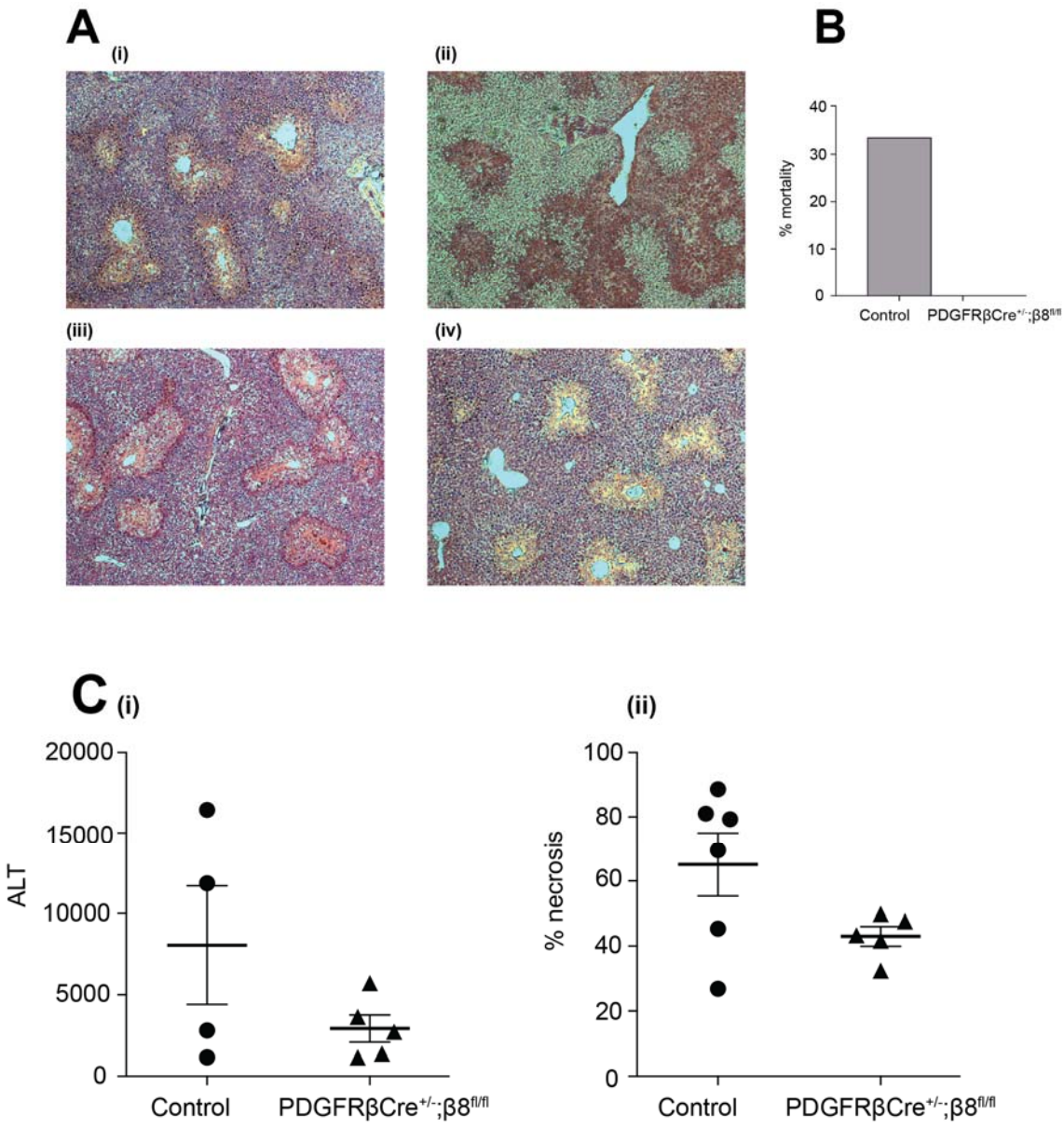

Figure 4.10 Targeted β8 integrin depletion on HSC during paracetamol-induced acute liver injury

In this experiment, n=6 control and n=5 PDGFRβCre$^{+/-}$;β8$^{fl/fl}$ male animals in each group. **A** H and E-stained sections of liver 24 hours post-paracetamol (x5 magnification) from **(i)** control animal showing centrilobular necrosis and **(ii)** control animal that succumbed to ALF showing haemorrhagic necrosis; **(iii)** and **(iv)** PDGFRβCre$^{+/-}$;β8$^{fl/fl}$ animals showing centrilobular necrosis. **B** Percentage mortality in each group **C (i)** Serum ALT at 24 hours post-paracetamol and **(ii)** Percentage necrosis quantified digitally from H and E sections.

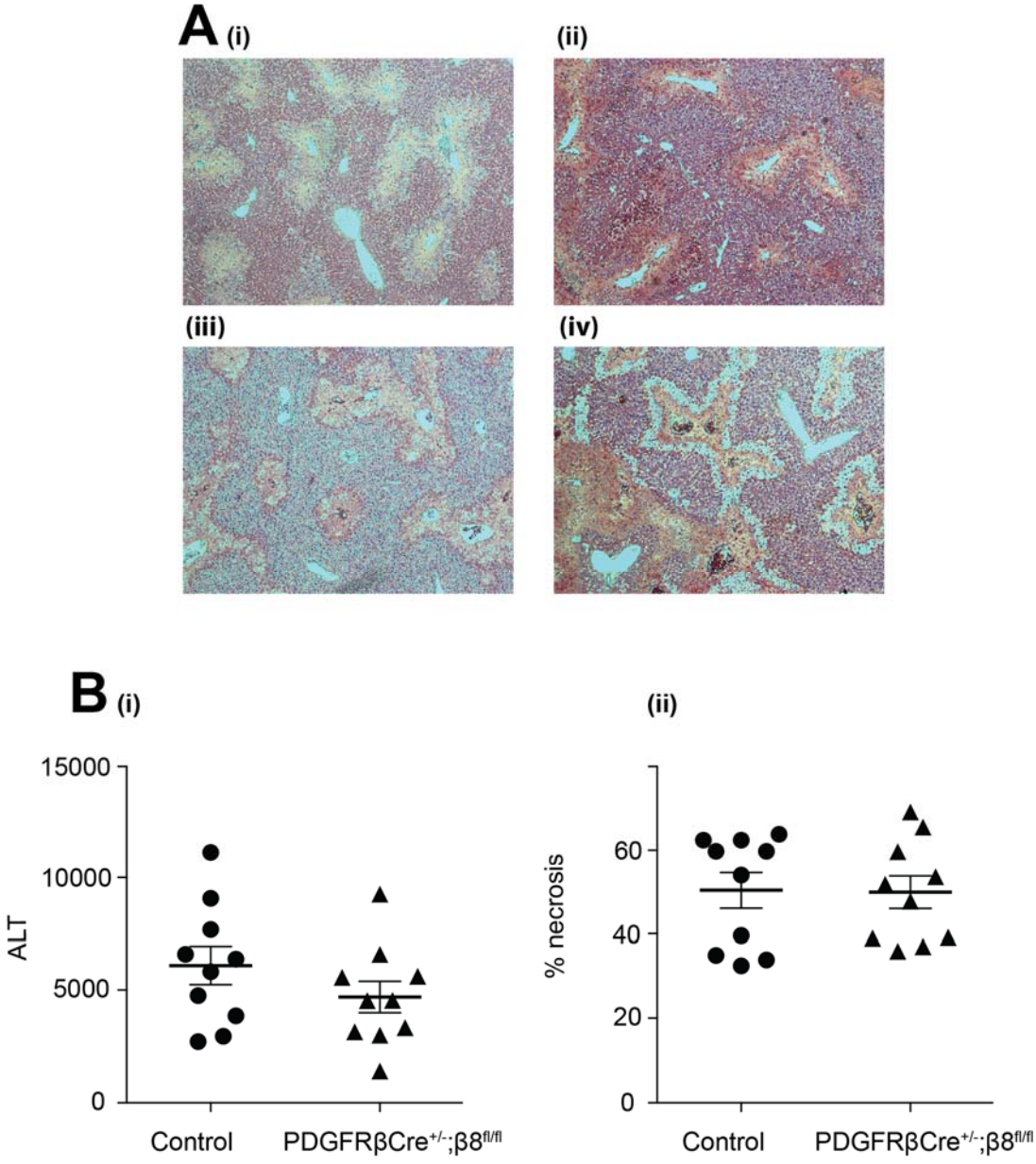

Figure 4.11 Targeted β8 integrin depletion on HSC during paracetamol-induced acute liver injury

In this experiment, n=10 male animals in each group received IP paracetamol 300mg/kg. **A** H and E-stained sections of liver 24 hours post-paracetamol (x5 magnification) from **(i)** and **(ii)** control animals showing centrilobular necrosis; **(iii)** and **(iv)** PDGFRβCre$^{+/-}$;β8$^{fl/fl}$ animals showing centrilobular necrosis. **B (i)** Serum ALT at 24 hours post-paracetamol and **(ii)** Percentage necrosis quantified digitally from H and E sections.

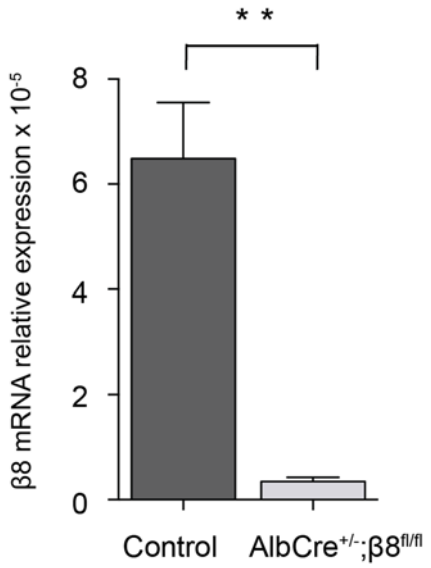

Figure 4.12 Confirmation of β8 integrin loss on hepatocytes

Graph showing β8 mRNA relative expression on hepatocytes from AlbCre$^{+/-}$;β8$^{fl/fl}$ animals and controls (AlbCre$^{-/-}$;β8$^{fl/fl}$). Primary mouse hepatocytes were isolated and β8 mRNA quantified by qRT-PCR.

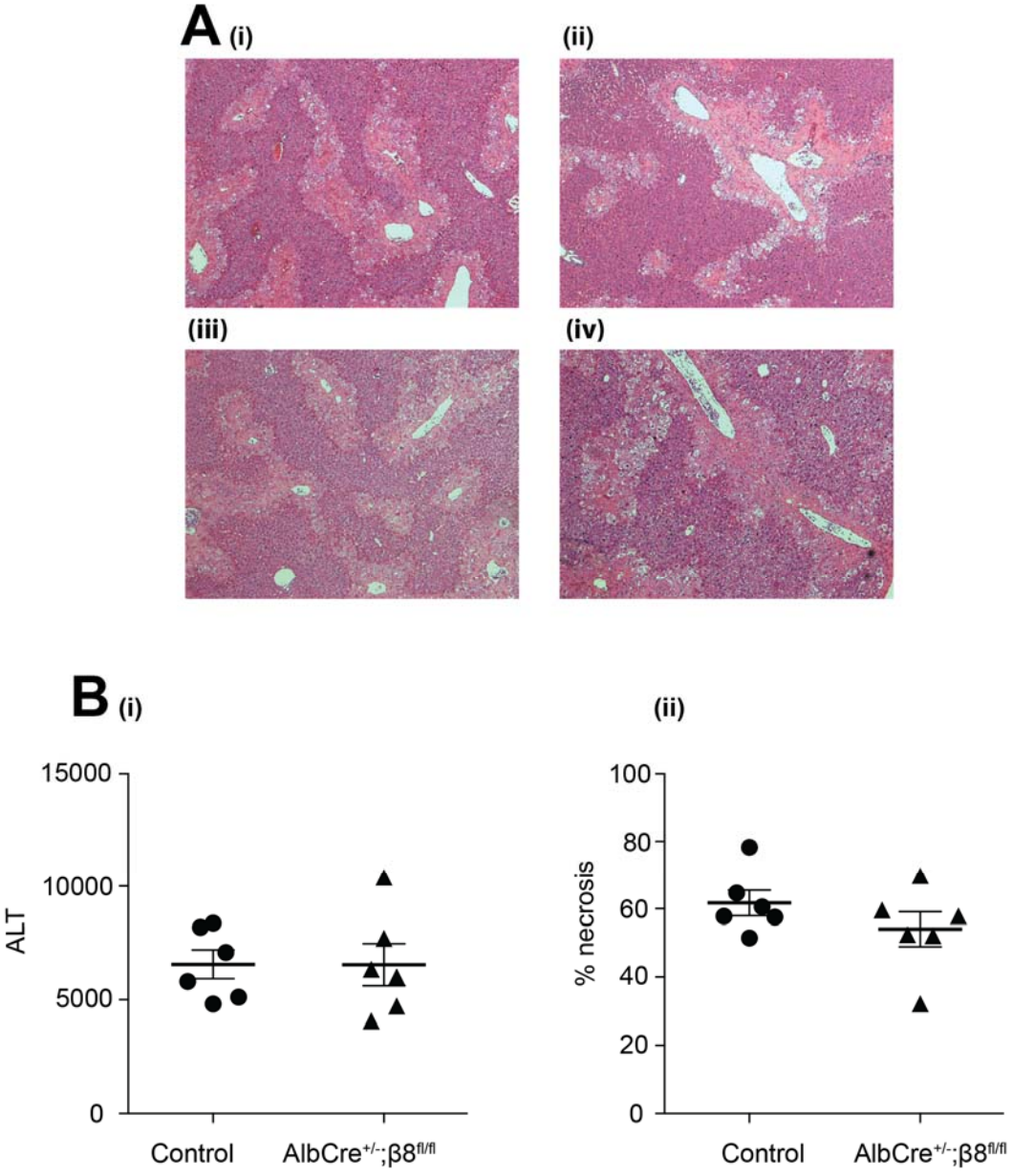

Figure 4.13 Targeted β8 integrin depletion on hepatocytes during paracetamol-induced acute liver injury

In this experiment, n=6 male animals in each group received IP paracetamol 350mg/kg.

A H and E-stained sections of liver 24 hours post-paracetamol (x5 magnification) from **(i)** and **(ii)** control animals showing centrilobular necrosis; **(iii)** and **(iv)** AlbCre$^{+/-}$;β8$^{fl/fl}$ animals showing centrilobular necrosis. **B (i)** Serum ALT at 24 hours post-paracetamol and **(ii)** Percentage necrosis quantified digitally from H and E sections.

4.11 Targeted αv integrin depletion on LSEC in a mouse model of paracetamol-induced acute liver injury

In this experiment, acute liver injury was induced with 300mg/kg paracetamol after a 16 hour fast (Figure 4.14). Mice were 13 weeks old (n=7 control and n=6 $Cdh5Cre^{+/-};\alpha v^{fl/fl}$ animals). Mean ALT was 3338 ± 942 in the $Cdh5Cre^{+/-};\alpha v^{fl/fl}$ group and 3839 ± 658.6 in controls (p=0.66). Mean percentage necrosis was 44.66 ± 6.53 in $Cdh5Cre^{+/-};\alpha v^{fl/fl}$ animals and 51.46 ± 4.46 in controls (p=0.4). All animals survived, and there was no significant difference in liver injury between the two groups.

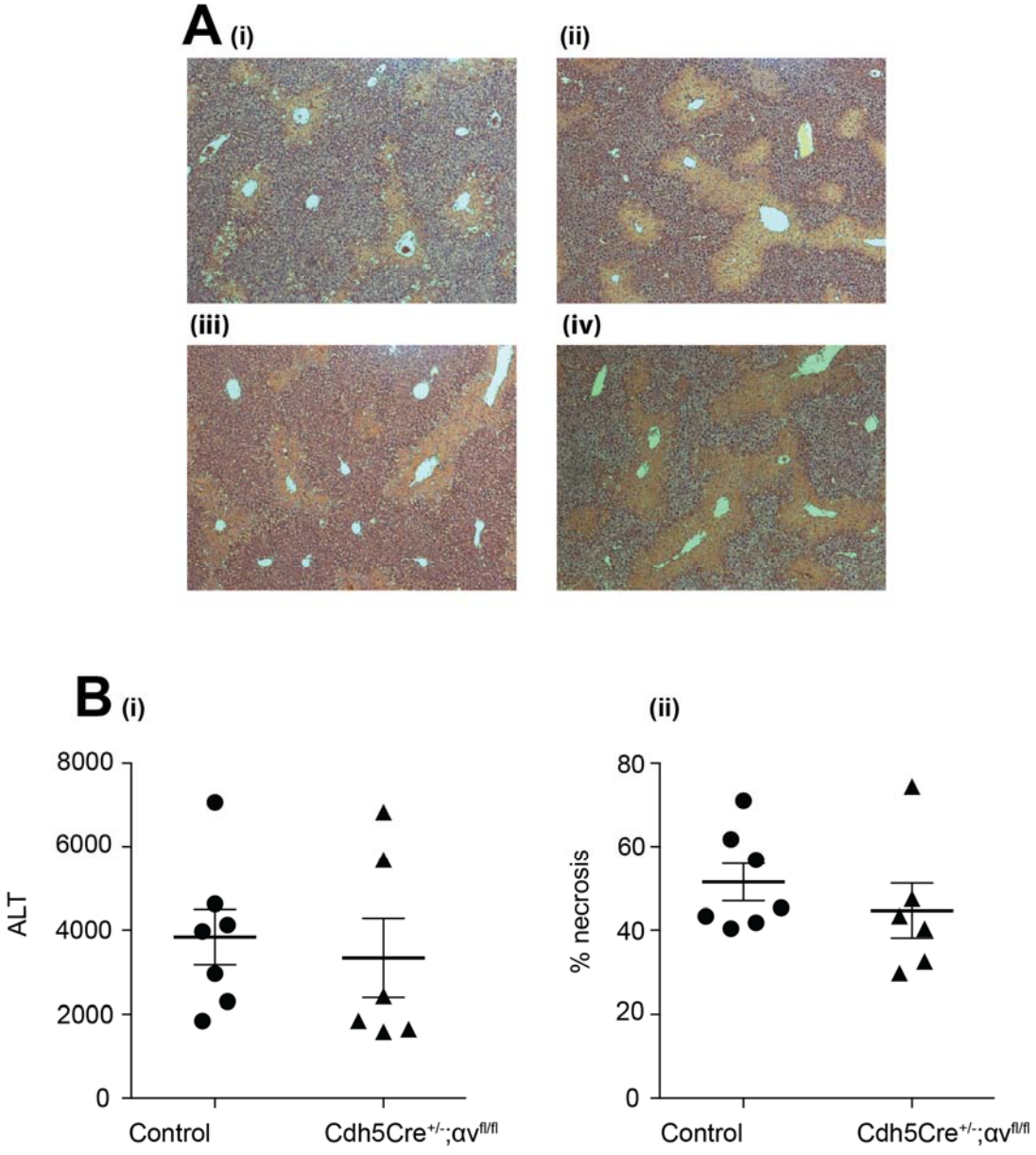

Figure 4.14 Targeted αv integrin depletion on LSEC during paracetamol-induced acute liver injury

In this experiment, n=7 control and n=6 Cdh5Cre$^{+/-}$;αv$^{fl/fl}$ male animals in each group received IP paracetamol 300mg/kg.

A H and E-stained sections of liver 24 hours post-paracetamol (x5 magnification) from **(i)** and **(ii)** control animals showing centrilobular necrosis; **(iii)** and **(iv)** Cdh5Cre$^{+/-}$;αv$^{fl/fl}$ animals showing centrilobular necrosis. **B (i)** Serum ALT at 24 hours post-paracetamol and **(ii)** Percentage necrosis quantified digitally from H and E sections.

4.12 Summary of Chapter 4 acute liver injury experiments

Table 4. Summary of Chapter 4 acute liver injury experiments

Figure no.	Transgenic mouse strain	n	Sex	Length of fast (hrs)	Paracetamol dose (mg/kg)	Harvested (hrs post-paracetamol)	Outcome: ALT (comparison with controls)	Outcome: necrosis (comparison with controls)	Mortality
4.5	PDGFRβCre$^{+/-}$;αv$^{fl/fl}$	6	M	16	350	24	p=0.74	p=0.0534	50% controls
4.6	PDGFRβCre$^{+/-}$;αv$^{fl/fl}$	6	F	16	350	24	p=0.30	p=0.94	0
4.7	PDGFRβCre$^{+/-}$;αv$^{fl/fl}$	6	M	12	350	18	p=0.10	p=0.85	16.67% each group
4.8	C57/Bl6	6	M	12	350	24	n/a	n/a	83.33% vs 33.33% controls
4.9	AlbCre$^{+/-}$;αv$^{fl/fl}$	6	F	16	350	24	p=0.28	p=0.35	0
4.10	PDGFRβCre$^{+/-}$;β8$^{fl/fl}$	5	M	16	350	24	p=0.17	p=0.08	33% controls
4.11	PDGFRβCre$^{+/-}$;β8$^{fl/fl}$	10	M	16	300	24	p=0.22	p=0.94	0
4.13	AlbCre$^{+/-}$;β8$^{fl/fl}$	6	M	16	350	24	p=0.10	p=0.25	0
4.14	Cdh5Cre$^{+/-}$;αv$^{fl/fl}$	6	M	16	300	24	p=0.66	p=0.40	0

4.13 Discussion

Although the initial acute liver injury experiment (Figure 4.5) did not reach statistical significance, I still wondered whether targeted αv integrin inhibition on HSC might confer protection in this paracetamol model. Whilst the difference in necrotic area did not quite reach significance, there did seem to be a mortality benefit in the PDGFRβCre$^{+/-}$;αv$^{fl/fl}$ group. I therefore decided to try to test the hypothesis in the context of slightly less severe injury. I was aware that a number of factors could affect the severity of liver injury in this mouse model. For example, it is well established that female mice tend to develop less hepatic necrosis than male mice, independent of their genetic background.[396] In the next experiment, therefore, female mice were used, in order to achieve 100% survival at 24 hours. This allowed ALT sampling in all animals. As expected, liver injury was slightly less severe compared with the first experiment. In the control group, mean ALT was 4790 $\pm$ 1550, and necrotic area 58.42% $\pm$ 3.794; conversely in the initial experiment using males, mean ALT was 7747 $\pm$ 3660, and necrotic area was 64.99% $\pm$ 10.02 in the control group.

In the female experiment, there appeared to be an outlier (Figure 4.6) in the PDGFRβCre$^{+/-}$;αv$^{fl/fl}$ group, which did not demonstrate significant liver injury (ALT 560, percentage necrosis 44.86). Whilst this could have been an isolated injection failure, I did observe some variety in liver injury throughout these experiments. This is consistent with the findings of others, who have presented results from large cohorts of paracetamol-treated mice, in which not all animals achieved a rise in ALT.[397] However, I did find that the variance in ALT and necrotic area improved as my experience with the model increased. Practical reasons for this might include a shortening of the injection and harvesting times with experience, meaning that animals were dosed and culled at very similar times. Additionally, the use of clean cages during the fasting period eliminated any chow deposits. Conversely, some factors were difficult to control for. For example, even if a strict fasting time is employed, animals might have different individual hepatic glutathione levels. Similarly, individual animals might have differing levels of hydration throughout induction of liver injury.

On testing the role of depletion of αv integrin on HSC in female mice during paracetamol-induced liver injury, I found no significant benefit compared with controls. I then decided to investigate this in one more experiment, using male animals, but harvesting at 18 hours. Here, the aim was to induce significant liver injury, but to harvest animals at an earlier time-point, hopefully before any animals succumbed to multiorgan failure. This was expected to allow ALT measurement in all mice. However, one animal in each group

died before 18 hours. Again, there was no difference in severity of liver injury at 18 hours between the groups.

I therefore concluded that a degree of mortality should be expected at 350mg/kg IP paracetamol. I also concluded that targeted inhibition of αv integrin on HSC during paracetamol-induced liver injury did not influence severity of liver injury, assessed by ALT and quantification of necrotic area.

In calculating adequate sample sizes for these and subsequent experiments, I used data from Mossanen et al.[370] They advised that 10 animals per group should be used for experiments using IP injection of paracetamol, in order to detect an ALT difference of 30%. For example, to detect a 50% difference in ALT, only four animals in each group would be needed. I therefore chose to use 6-10 animals for these and subsequent experiments, as a compromise between achieving sufficient power, but taking into consideration the principles of reduction and refinement, in the performance of ethical animal research.

On performing the same experiment in $AlbCre^{+/-};\alpha v^{fl/fl}$ animals vs controls, I also found no difference in severity of liver injury. I therefore decided to use a different method of αv inhibition, this time using a global systemic small molecule inhibitor. This experiment resulted in significant mortality in both groups, although more in the treatment group. However, one animal in each group died from complications of multiple IP injections. Excluding these from analysis, mortality would have been 1/5 in the control group vs 3/5 in the treatment group. It is possible that global αv integrin inhibition is detrimental during paracetamol-induced acute liver injury, however I think that the numbers are too small make meaningful conclusions from these data. A way to circumvent repeated IP injections would be to deliver CWHM 12 continuously via mini-pump. However, on the basis of my previous experiments, I did not think there was strong enough evidence for potential benefit from treatment, to warrant repeating CWHM 12 administration during acute liver injury, using this more invasive approach.

In subsequent experiments, I used similar methodology to test whether targeted inhibition of β8 integrin on HSC or hepatocytes, and αv integrin on LSEC had any effect on severity of paracetamol-induced liver injury. Because an initial experiment suggested a potential survival benefit for $PDGFR\beta Cre^{+/-};\beta 8^{fl/fl}$ animals, I repeated this with a large sample size (10 in each group), using 300mg/kg rather than 350mg/kg paracetamol. This convincingly showed no significant difference (Figure 4.11).

Overall, in this set of experiments, I found that targeted inhibition of αv integrin, or β8 integrin, on HSC or hepatocytes, and αv integrin on LSEC, did not appear to confer protection in a paracetamol-induced mouse model of acute liver injury. Although I initially observed greater mortality in the control groups compared with PDGFRβCre$^{+/-}$;αv$^{fl/fl}$ and PDGFRβCre$^{+/-}$;β8$^{fl/fl}$ animals, this was not borne out upon repetition of the experiments. I think this was an artefact secondary to the severe liver injury model used, rather than a true survival benefit. To complete these set of experiments, it would have been interesting to analyse markers of hepatic regeneration, as well as those of injury. It is possible that targeted integrin inhibition on HSC, hepatocytes or LSEC could result in a phenotype in hepatic regeneration, in the context of paracetamol-induced acute liver injury, even if differences in severity of damage are not seen. It would therefore be useful to evaluate Ki67 and BrdU staining in hepatocytes at different time points post-injury in these models.

I gained experience with the paracetamol model throughout these studies, which was important for planning IVM experiments. I found that using a dose of 300mg/kg IP paracetamol resulted in zero mortality at 24 hours (and was well-tolerated in both female and male animals) and gave acceptable liver injury. This was useful to identify a reasonable starting dose for experiments in which animals had to undergo both abdominal surgery and acute liver injury within a relatively short time period. Furthermore, I was able to use my expertise with the paracetamol model to contribute to the work of other researchers, resulting in co-author publications. I obtained serum from animals with acute liver injury for miRNA analysis. Paracetamol toxicity in mice resulted in increased miR-122-5p and miR-151a-3p and decreased miR-382-5p, which was consistent with the human data in this area.[398] These are currently being evaluated as potential biomarkers for liver injury in humans. I also performed a series of experiments administering paracetamol to C57Bl6 mice at subclinical and toxic doses, to investigate the effect of the drug on cell-cell tight junctions. By immunohistochemistry on liver sections from paracetamol-treated mice, it was demonstrated that disruption of the tight junction-associated zona occludens-1 protein correlated with modulation of hepatic ultrastructure. This was dose-dependent, and may have implications for the development of therapeutic tight junction-stabilising proteins, relevant to the clinical syndrome of human paracetamol hepatotoxicity.

5.1.1 Intravital microscopy: excitation fluorescence and label-free techniques

Intravital microscopy (IVM) is a rapidly developing technology, whereby live animals are imaged at microscopic resolution. It allows interrogation of cellular interactions in real-time, and the opportunity to investigate biological processes under nearly natural conditions. Imaging is mostly centred on the detection of fluorescence, although label-free techniques (such as the detection of second harmonic signals) complement this, and crucially, add context to cellular events.

Multiphoton (MP) microscopy is preferentially used for IVM, which facilitates fluorescent imaging at greater depths of tissue penetration.[399] The MP microscope allows selective excitation of fluorescence (Figure 5.1); a fluorophore is excited when it simultaneously absorbs two low-energy, near-infrared (NIR) photons, allowing excitation in a particular focal plane, where the two photons coincide (two-photon excitation fluorescence (TPEF)). Emission of fluorophores in wavelengths that fall in visible light or ultraviolet (UV) region can therefore be induced with low-energy NIR photons. Because the two-photon absorption only occurs in the plane of focus, background scatter from regions outside focus is minimized; this results in less photobleaching, reduced phototoxicity, and less autofluorescent signal, as compared with confocal microscopy.[400,401] TPEF can only be achieved at extremely high photon concentration in space and time, necessitating very high NIR laser intensities.[401] Ultra-short pulsed lasers have now been developed, which produce extremely high laser powers transiently, with the pulse duration ranging in the femtoseconds, and at high pulse frequency of 80-90 MHz.[402] TPEF signals can therefore be successfully generated at average laser powers lower than 5mW incident on the sample.[401,403]

A number of other microscope technologies can enhance the utility of MP imaging, including broad-band MP imaging[404,405] and optical frequency domain imaging,[406] which allow greater imaging depth, and quantification of angiogenesis, lymphangiogenesis and tissue viability respectively.[400] However, the label-free, nonlinear optical processes of second harmonic generation (SHG) and coherent anti-Stokes Raman scattering (CARS) will be focused on, as they have been applied in the following experiments.

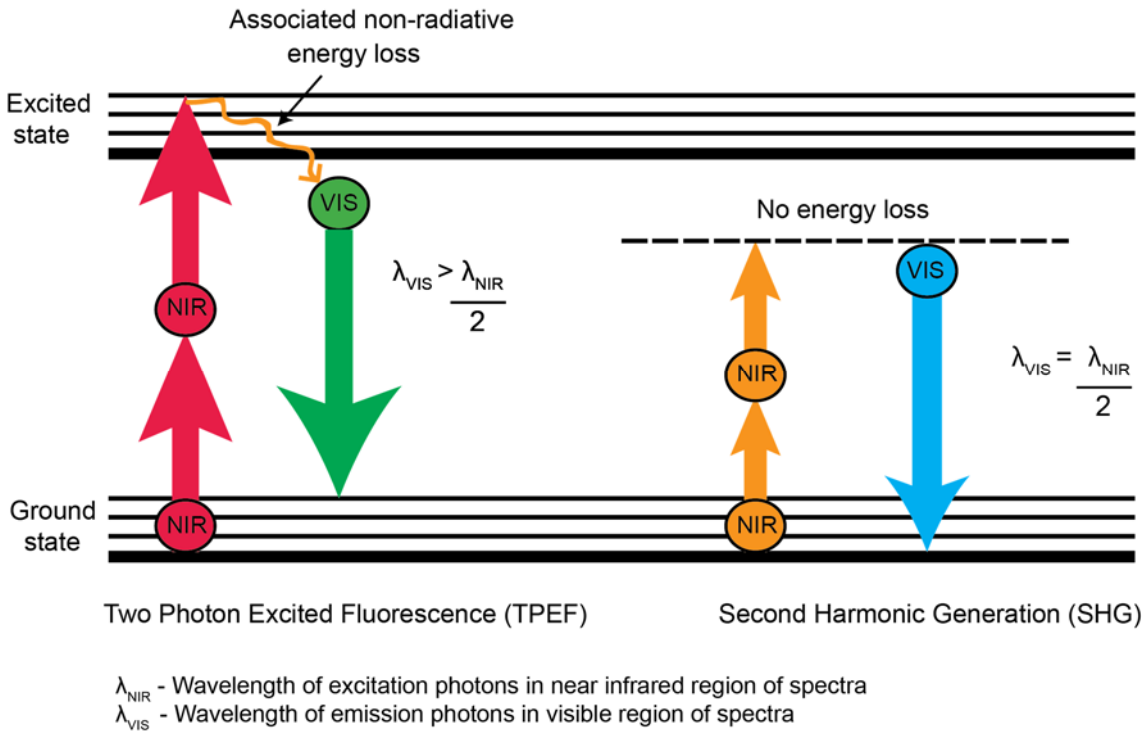

Figure 5.1 Jablonski diagram

Jablonski energy diagram demonstrating the principles of two photon excited fluorescence (TPEF) and second harmonic generation (SHG). TPEF requires the presence of an actual excited state, whilst SHG is energy-conserving, and does not. Reproduced from Thomas et al 2014.[401]

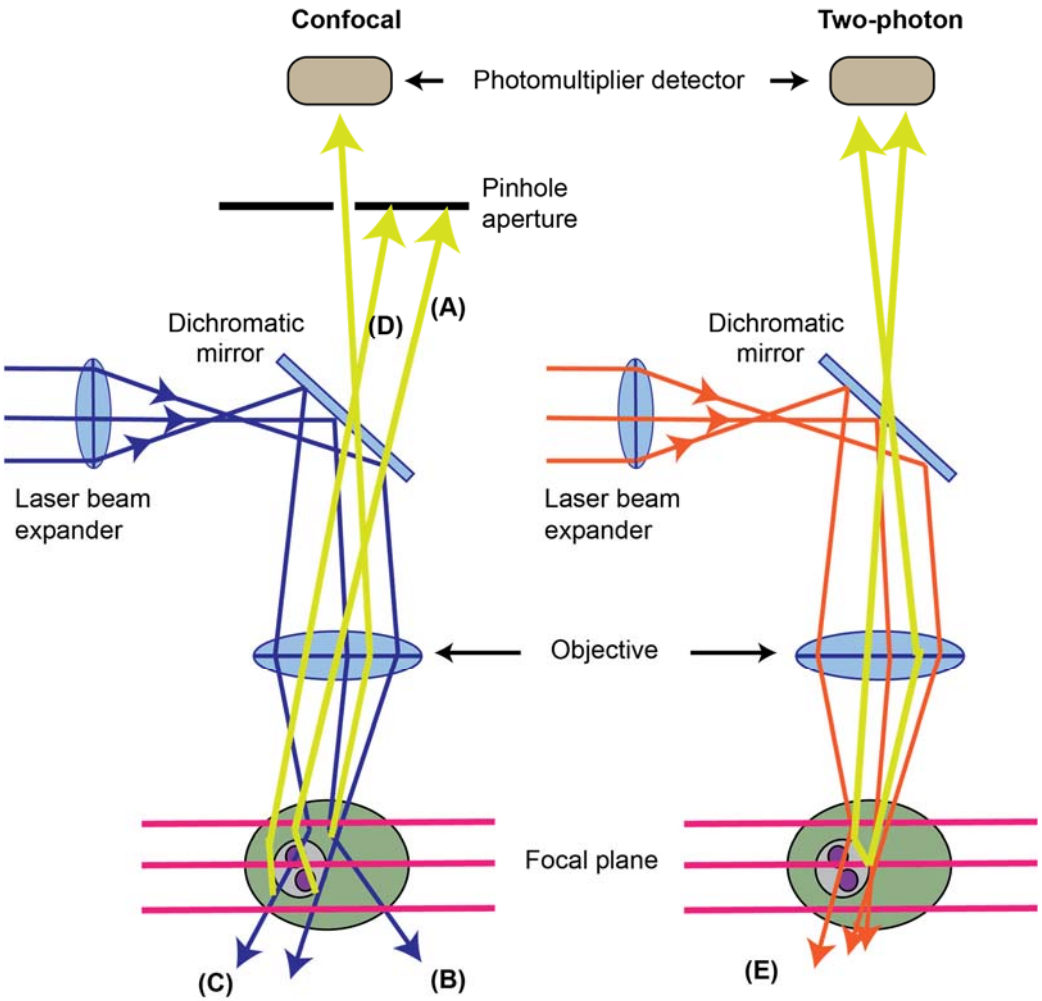

Figure 5.2 Principles of confocal and two-photon microscopy

Adapted from: http://www.microscopyu.com/articles/fluorescence/multiphoton/multiphotonintro.html

Confocal microscopy: excitation light (blue) is focused into the specimen, and the fluorescence (green) from that focal spot is captured by the objective lens, passes cleanly through the pinhole, and reaches the photomultiplier detector. However, some of the fluorescence light can be scattered as it passes back through the specimen **(A)**. This scattered fluorescence is lost and not detected. The losses reduce the detected fluorescence signal. As the excitation light passes through the specimen, it may be absorbed **(B)** or scattered before it reaches the focus **(C)**. If it is absorbed, it can generate fluorescence, but because this does not arise from the focal spot, it is not efficiently detected. However, a small portion of out-of-focus fluorescence can be scattered into the pinhole, and detected. This creates a background fog, reducing image contrast. The scattered excitation can also generate fluorescence **(C)** which can also contribute to background fog **(D)**.

Two-photon microscopy: excitation photons (red) can be scattered **(E)** like in the confocal system. However the probability of two photons being scattered simultaneously to the same specimen location is essentially zero, eliminating background fog. A greater proportion of excitation light reaches the focal plane **(F)** and **(G)**. The fluorescence generated (green) is more likely to be detected by the photomultiplier tube because no pinhole is present to block it.

Unlike other microscope systems, the MP microscope can be easily modified to detect second harmonic signals, allowing second harmonic imaging microscopy (SHIM). This is a powerful label-free technique that permits visualization of well-ordered protein structures, such as collagen, microtubules and muscle myosin.[407] SHG is a nonlinear optical effect, also known as frequency doubling. It occurs when intense laser light is passed through a highly polarizable material (such as an inorganic crystal) with a noncentrosymmetric molecular organization. The second harmonic light that is emitted from the material is exactly half the wavelength of the light being absorbed. The SHG process within the nonlinear optical material replaces two near-infrared incident photons with a single visible photon at twice the energy and half the wavelength.[401] Whilst TPEF (described above) involves an excited state, meaning some of the incoming energy is lost during relaxation, SHG does not. SHG is therefore relatively energy-conserving, and coherence of the laser light is preserved. Furthermore, the amplitude of SHG is proportional to the square of the incident light intensity, meaning SHIM has the same intrinsic optical sectioning properties as TPEF.[407] It is therefore an important three-dimensional contrast tool, allowing high-resolution imaging of protein structures such as collagen networks, without requiring excitation of fluorescent molecules.

In addition to fluorescence and SHIM, use of vibrational microscopy techniques can provide information about the exact chemical composition of tissue structures. Fluorescence microscopy is limited in chemical selectivity; there are relatively few intrinsic fluorophores, and the introduction of extrinsic fluorophores can result in unwanted alterations.[408] SHIM has inadequate sensitivity and specificity for tissue constituents other than certain protein structures. In contrast, the vibrational spectra of biological specimens provide molecular signatures, which can be utilized to identify specific biochemical tissue components.[408] The CARS technique is an important application of Raman spectroscopy, involving inelastic or ‘Raman’ scattering of monochromatic laser light.[409] The laser light is shined on a sample, and the emerging scattered light is detected. Most scattered light is of the same frequency as the excitation source (referred to as Rayleigh or elastic scattering). A small amount of the scattered light (approximately 10% of the incident light intensity) is shifted in energy from the laser frequency, because of the interaction between the incident electromagnetic waves and the vibrational energy levels of the molecules in the sample. Plotting the intensity of the shifted light against the frequency results in a Raman spectrum of the sample.[409]

The CARS process generates much stronger vibrational signals (Figure 5.3). CARS is a four-wave mixing process, where a pump, a Stokes, and a probe field, with frequencies $\omega_{pump,}$ ω_{Stokes} and ω_{probe}, induce a polarization in the sample $\mathbf{P}^{(3)}$.[409] The oscillating-induced polarization creates an anti-Stokes radiation, with a frequency $\omega_{anti\text{-}Stokes} = \omega_{pump} + \omega_{probe} - \omega_{Stokes}$. In most experiments, the pump field and probe field come from the same laser beam. The CARS signal intensity is proportional to the square modulus of the induced polarization $I_{CARS} \propto (\mathbf{P}^{(3)})^2$. The size of $\mathbf{P}^{(3)}$ is determined by the field strength of the excitation fields, and the nonlinear optical susceptibility of the material $\chi^{(3)}$. $\chi^{(3)}$ is separated into a resonant and nonresonant part. Both CARS and spontaneous Raman scattering essentially provide the same information, however because of the interference between the Raman component and the nonresonant component, the CARS spectral shape differs from the Raman lineshape. Due to the complex nature of $\chi^{(3)}$ and this interference between resonant and nonresonant background parts, CARS demonstrates a dispersive lineshape. Compared with the spontaneous Raman spectrum, the vibrational resonances show a shift of the peak to lower frequency, and the appearance of a dip at a higher frequency.[408-410]

Like SHIM, CARS microscopy allows nondestructive molecular imaging without any labelling, meaning that small molecules such as lipids or drugs can be imaged without disturbance of their molecular properties by labelling. Because the CARS signal is larger than that generated from Raman microscopy alone, high-speed vibrational imaging can be achieved. Furthermore, the CARS signals appear at a wavelength shorter than excitation wavelengths, and are therefore spectrally separated from the one-photon fluorescence background. The main limitation of CARS is the presence of a nonresonance background, arising from the electronic contribution to $\chi^{(3)}$. This background is coherently mixed with the vibrationally resonant signal, making it difficult to detect weak Raman bands. The detection of low-concentration molecules is also difficult, because the resonant CARS signal decreases quadratically with the molecular concentration. Some progress has been made in recent years however, to suppress the nonresonant background and maximize the detection sensitivity.[409]

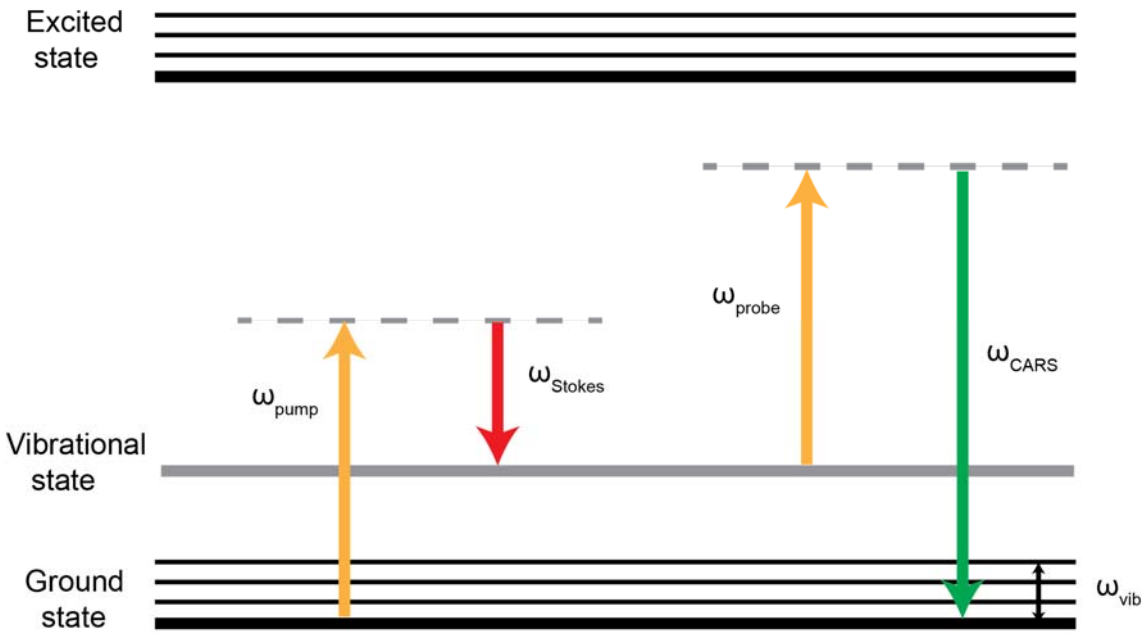

Figure 5.3 CARS energy diagram

CARS is a nonlinear four-wave mixing process, used to enhance the weak (spontaneous) Raman signal. A pump laser beam (at frequency ω_{pump}) and a Stokes laser beam (ω_{Stokes}) interact, resulting in an anti-Stokes signal at frequency $\omega_{CARS} = 2\omega_{pump} - \omega_{Stokes}$.

5.1.2 Development of IVM of the liver

Certain organ systems lend themselves particularly well to IVM via an imaging window, and there are well-established mouse models for relatively superficial tissues such as skin, (dorsal skin window chamber model[411-414]) breast, (mammary imaging window[415-417]) and brain and bone marrow (via cranial imaging window[418-420]).[421] Surgical procedures can be employed to render other organs more accessible, for example a skin incision to expose the popliteal lymph nodes,[422] and more recently, the intestine.[423,424] The maximum depth of penetration for fluorescent IVM is 1mm, meaning imaging intra-abdominal organs requires surgical exposure. The liver has traditionally been exteriorized and imaged by laser scanning or spinning disk confocal microscopy. The surgery comprises a midline laparotomy, removal of peritoneal skin and muscle, and externalization of a hepatic segment, usually the right lobe.[425-432] The mouse is anaesthetized throughout, and the liver is superfused with physiological saline. Due to the invasive surgical approach, the animal is killed at the end of imaging. This provides a good model for investigating biological processes occurring in the short term, but successful imaging has only been achieved for a maximum of six hours[433] (with the implementation of careful anaesthesia and intensive care monitoring) limiting the yield of such experiments.

For longer experimental periods, Ritsma et al devised a protocol for surgical implantation of a static abdominal imaging window, using a titanium ring and coverslip, secured in place with a purse string suture. This was used to visualize liver metastasis formation over 14 days; windows were also left in situ until dislodgement, which occurred on average after five weeks (maximum of 63 days).[421,424]

5.1.3 Application of IVM to the study of liver injury, carcinogenesis and repair

Focal liver injury

Necrotic cell death generates sterile inflammation, characterized by an influx of innate immune cells within the damaged tissue. In a landmark IVM paper, Kubes et al performed an elegant set of in vivo experiments to investigate the mechanisms governing neutrophil recruitment and migration to sites of sterile tissue injury and cell death.[430] Focal hepatic necrosis was induced in anaesthetized mice by localized thermal injury, on the exteriorized liver surface. A 0.022+/- 0.001mm^3 area of focal injury was achieved to a depth of approximately 80μm, using the tip of a heated 30-guage needle, mounted on an electro-cautery device. Necrotic cells were then labelled with propidium iodide. Using spinning disk confocal IVM with this model, the authors were able to record the kinetics

of enhanced GFP (eGFP)-labelled neutrophil migration towards the necrotic lesion. They observed that neutrophils remained intravascular during transit to sites of injury, potentially to protect healthy tissues from collateral damage en route. It was also demonstrated that neutrophils adhere and crawl inside liver sinusoids during hepatocyte death, an interaction mediated by the integrin αMβ2, and its endothelial ligand intercellular adhesion molecule-1 (ICAM-1). Furthermore, an intravascular gradient of chemokines directed neutrophils towards foci of damage, with specific chemotaxis to the necrotic area stimulated by DAMPs.[430]

Dal-Secco et al subsequently used the same focal injury model to track both neutrophils and two subsets of monocytes (with either pro-inflammatory $CCR2^{hi}CX_3CR1^{low}$ or reparative $CX_3CR1^{hi}CCR2^{low}$ phenotype) to the necrotic lesion in vivo.[434] They were able to show that $CCR2^{hi}CX_3CR1^{low}$ monocytes were recruited early to the site of damage, and formed a ring-like structure around the injury, persisting for 48hrs. Interestingly, these monocytes were converted to $CX_3CR1^{hi}CCR2^{low}$ cells in situ, showing local, cytokine-directed phenotypic switching. This conversion was required for successful repair, as evidenced by failure of clearance of necrotic debris, and inhibition of collagen redisposition within the injury, when the switch was prevented by anti-cytokine treatment.[434] This demonstrates the vast potential for in vivo imaging using IVM to improve our understanding of immune cell plasticity during liver injury and regeneration.

Hepatic ischaemia and reperfusion injury

Hepatic ischaemia-reperfusion (I/R) injury is a defect of the hepatic microcirculation, induced by the reintroduction of oxygenated blood after a period of ischaemia. The oxygenated blood causes oxidative stress, characteristically resulting in increased microvascular permeability, intracellular ATP loss, inflammatory cell infiltration, and cell death.[435] It is clinically relevant in liver transplantation (as a major cause of graft dysfunction) and hepatic resection.[436] Modelling and imaging this acute process in vivo is relatively well-established; Khandoga et al initially demonstrated that I/R induces platelet-endothelial cell interactions in the hepatic microvasculature, by IVM of an exteriorized liver lobe during the early reperfusion phase.[437] They also showed that P-selectin expressed on endothelial cells mediates the first interaction of platelets with post-ischaemic endothelium.[437] In subsequent experiments, they observed that platelet-endothelial interactions contribute significantly to microvascular I/R damage, independently of leukocyte-endothelial cell interactions.[438] Furthermore, it was shown that attenuation of platelet adhesion by administration of anti-fibrinogen antibody in vivo

(to prevent fibrinogen-mediated ICAM-1 dependent platelet-endothelial cell binding) resulted in improved sinusoidal perfusion. This was supported by a reduction in ALT and markers of apoptosis.[438]

Ongoing work using this model has provided insights into precise regulation of the routes of cell death following I/R, and has identified the platelet receptor protease-activated receptor 4,[439] and the augmenter of liver regeneration protein,[440] as two potential therapeutic targets for post-ischaemic liver injury.

Other groups have applied hepatic IVM to developing diagnostic modalities, for example to demonstrate tissue damage in vivo, in the setting of I/R injury. Thorling et al used fluorescent lifetime imaging microscopy (FLIM) in combination with MP IVM, in a rat I/R model.[441] Here, the fluorescent properties of NADH were utilized; the free and protein-bound forms of NADH have similar excitation and emission wavelengths, but can be separated by their fluorescent lifetimes (0.4-0.5 and 2.0-2.5ns respectively).[441,442] The free form of NADH is involved in the anaerobic production of ATP whereas the bound form relates to aerobic production. Therefore, changes in the free/bound ratio of NADH provides information about cellular metabolism. In this model, decreased metabolic activity (demonstrated by increased ratio of free/bound NADH) was shown during I/R injury. Similarly, MP microscopy was able to detect structural damage, in a predominantly midzonal pattern, at one hour of reperfusion.[441] In later work, they were also able to correlate I/R injury with specific fluorescent lifetime changes in NAD(P)H.[443]

The same group also investigated the transport of the fluorescent probe fluorescein, in the rat I/R model, by MP imaging after intravenous (IV) sodium fluorescein administration.[443] There was a delayed appearance and clearance of fluorescein within liver sinusoids undergoing I/R injury. This was mathematically modeled, establishing a role for in vivo MP microscopy in the study of drug distribution. It was felt that combining MP imaging with the kinetics of fluorescein uptake and clearance could potentially be employed to assess liver function intraoperatively or post-transplantation, providing a relatively non-invasive, early measure of I/R-induced damage.[443] More recently, Wang et al performed MP microscopy with FLIM on a number of different mouse models mimicking human liver diseases (including primary sclerosing cholangitis, chronic fibrosis, HCC and I/R perfusion).[444] This allowed simultaneous imaging and quantification of cellular morphology and microenvironment, and the authors anticipated that the technique could be refined to acquire real-time histology of liver disorders.[444]

Other authors have proposed the development of autofluorescent molecular imaging as another bioanalytical tool to measure I/R injury. Lu et al used the endogenous

autofluorescent properties of mitochondrial flavins to quantify cellular deoxygenation and reoxygenation. IVM of exteriorized rat liver in vivo following I/R injury showed a significant reduction in cellular autofluorescence intensity immediately after ischaemia, with a gradual return to baseline throughout reperfusion.[445] Again, it was postulated that this approach could ultimately be applied to intraoperative and postoperative assessment of organ function.

A variety of IVM studies of hepatic I/R injury have provided additional insights into cellular interactions throughout this process, and have led to experiments involving administration of biological compounds to reduce injury in these animal models.[446-450]

Acute liver injury

Drug-induced liver injury represents another attractive IVM model, allowing high-resolution imaging of cell death. Paracetamol and concanavalin-A (Con A) are the most established pharmacological agents;[432] paracetamol has the added benefit of clinical relevance to human disease, allowing comparison to the major problem of fulminant hepatic failure secondary to paracetamol overdose.

Li et al used a metallic liver window device to image mice 24 hours after paracetamol overdose (500mg/kg) by MP microscopy.[451] IV injection of fluorochromes was employed to delineate sinusoidal veins and bile canaliculi. Extent of injury was assessed by permeability of cells to dextrans or sytox green, and loss of labelling by R6G. They focused on sequential morphological changes during hepatocyte necrosis in vivo. Electron microscopy had previously demonstrated that the injured liver showed congestion, extravasation of erythrocytes into the space of Disse, dilatation of bile canaliculi and a spongy appearance of necrotic hepatocytes.[452] The authors went on to demonstrate an unexpected canalicular membrane rupture during injury in vivo, with flooding of bile back into hepatocytes.[451] Membrane rupture was accompanied by an abrupt drop in mitochondrial membrane potential, and it was hypothesized that this could indicate a point of no return in hepatocyte necrosis. Concomitant NAC administration reduced canalicular membrane rupture, potentially supporting this hypothesis. IVM was also able to demonstrate that release of hepatocellular contents from dying cells occurs in the form of dislodged blebs. These events were unable to be observed in cultured cells, because the in vivo pressure gradient between bile canaliculi and hepatocytes is not reproducible in cell culture systems. The ability to image paracetamol-induced hepatocyte death in vivo has therefore permitted the discovery of a mechanism in which elevation of bile duct pressure might contribute to induction of hepatocyte necrosis.

Whilst Li et al used IVM to further our understanding of hepatocyte biology during paracetamol overdose, other groups have harnessed the technique to demonstrate the effects of a specific pharmacological intervention on paracetamol-induced injury. Amaral et al hypothesized that ATP released from dying hepatocytes following paracetamol-induced necrosis, could contribute to progression of liver injury by immune system stimulation and modulation of cytosolic calcium levels.[453] Mice were given paracetamol by oral gavage (500mg/kg) after a 15 hour fast. Two hours later, an exogenous ATPase (apyrase) was administered to the treatment group. Liver injury was reduced in the apyrase-treated animals, with lower serum ALT and levels of pro-inflammatory cytokines. Confocal IVM of exteriorized liver also demonstrated a reduction in neutrophil recruitment to necrotic areas. Further in vitro experiments led the authors to propose that ATP may signal via purinergic receptors to increase intracellular calcium, causing direct hepatotoxicity and cell death.[453]

In an earlier experiment, Ito et al characterized the role of nitric oxide (NO) in microvascular injury, in the context of paracetamol overdose.[454] Here, IVM was employed to demonstrate liver microcirculatory dysfunction, such as impaired sinusoidal perfusion and swelling of liver sinusoidal endothelial cells (LSECs) erythrocyte infiltration to the extrasinusoidal space, and phagocytic activity of activated Kupffer cells. Using specific inhibitors of iNOS or cNOS, injury was then quantified in vivo (again via exteriorization of liver) and pre-treatment with a pharmacological inhibitor of iNOS was found to reduce paracetamol-induced liver injury, as well as hepatic microcirculatory dysfuction.[454]

More recently, DNA-binding probes (such as Sytox green, propidium iodide, DAPI) have been used to visualize and measure hepatic necrosis in vivo, allowing real-time assessment of cell death.[432,455] [428,456]

In most cases, IVM following ALI has been restricted to short, once-off imaging sessions. Heymann et al completed longer imaging sessions to investigate lymphocyte migration during acute or chronic liver injury (induced by acute or chronic IP administration of CCL_4) using CXCR6.gfp knock-in mice.[433] Here, TPEF and MP microscopy was performed on exteriorized liver. Longer imaging duration was facilitated by using intensive care monitoring, including electrocardiogram electrodes, a carbon dioxide level sensor and external temperature sensor. These measures allowed more rigorous control of anaesthesia and respiration, as well as stabilization of the circulation.

IVM has also proven valuable in discerning differential roles of immune cells in paracetamol-induced liver injury. Marques et al first demonstrated that liver injury causes

massive extracellular DNA deposition in the liver.[429] They subsequently selectively depleted Kupffer cells (KC) by intravenous clodronate liposomes (CLL) injection, and imaged after paracetamol administration. This did not result in any reduction in hepatotoxicity. However, use of anti-Ly-6G antibody to deplete circulating neutrophils did significantly reduce liver injury. Having employed IVM to show this association between neutrophil infiltration and more marked organ damage, they were able to proceed with mechanistic studies. It was found that the DNA sensor TLR9 was upregulated on neutrophils during drug-induced injury, and blockage of DNA sensing (either by knockout of TLR9 or systemic DNASE1 treatment) rescued paracetamol-induced liver injury.[429]

Bonder et al similarly investigated leukocyte signalling during drug-induced liver injury (DILI) using IVM.[457] Administration of Con A causes acute hepatitis, largely mediated by T-lymphocytes. Con A treatment resulted in increased leukocyte rolling and adhesion (in exteriorized liver postsinusoidal vessels); mice with GFP-labelled T cells were used to show that within 4 hours of Con A administration, only 20% of the leukocytes interacting and adhering in postsinusoidal venules were T cells. In fact, Con A induced early hepatic recruitment of neutrophils, without which, the drug could not recruit CD4+ T lymphocytes to the liver, abrogating injury.[457] Again, IVM permitted direct vision of these immune cells, with assessment of movement and adherence, and systematic selective depletion studies. This led to the novel realization that neutrophil recruitment is critical for the development of Con A-induced hepatitis, and that perhaps neutrophil activation may be important in patients with T cell-mediated liver diseases.[457]

This approach was also utilized by the same group to identify adhesive mechanisms required for recruitment of CD4+ lymphocytes to liver sinusoids in the context of Con A-induced liver injury.[458] Here, endogenous leukocytes were visualized by trans-illumination, whereas in vitro-differentiated T cells were labelled with rhodamine 6G ex vivo, and visualized by epi-illumination. Shear rates in postsinusoidal venules were quantified by measuring velocities of fluorescently-labelled lymphocytes, frame by frame. In vivo injection of specific antibodies led to the conclusions that CD4+ Th1 cells require α4β1-integrin for adhesion to liver sinusoidal vessels, whereas CD4+ Th2 cells need VAP-1. This work, for the first time, challenged the dogma that leukocyte-trapping within the liver during infection and inflammation was an unspecific, mechanical process, and demonstrated the importance of specific adhesion molecules, which could represent promising therapeutic targets.[432,458]

In summary, IVM of paracetamol- and Con A-induced acute liver injury has already yielded insights into hepatocyte biology during injury, and been harnessed to test the

effect of specific pharmacological agents on liver damage. Perhaps most striking is the application of IVM to studying immune cell function, recruitment and signalling in this setting. Whilst the early stages of liver injury have proven relatively straightforward to study, experiments have been limited to several hours total imaging. Some progress has been made in terms of improving animal monitoring to allow longer sessions,[433] however in vivo studies throughout the course of injury and repair are still lacking.

Infection

IVM of the liver is particularly suited to characterizing events occurring during the dissemination of pathogens via the bloodstream. Fluorescent labelling of immune cells and bacteria has allowed investigation of their interactions during infection, and mechanistic studies to visualize cellular movement in the vasculature and sinusoids in real-time. Even cellular morphology has provided new insights. KC, for example, were found to have numerous cell processes, extending into as many as five sinusoids, demonstrating their extensive filtering capacity.[459] In this paper from Paul Kubes' group,[459] the critical role of KC in limiting bacterial dissemination (in this case the spirochete *Borrelia burgdorferi*) was elegantly presented using IVM. KC activity was compared and contrasted with a subset of natural killer T cells, referred to as 'invariant natural killer T cells' (*i*NKT cells). Interestingly, depletion of KC or *i*NKT in the context of *B. burgdorferi* infection resulted in different manifestations of loss of pathogen control. Depletion of KC by CLL treatment led to large numbers of GFP-expressing *B. burgdorferi* remaining in hepatic sinusoids 12 and 24 hours after injection. These spirochetes were freely translocating, unlike in untreated mice, in which they appeared immobilized after adhesion to KC. At 72 hours, a high frequency of *B. burgdorferi* organisms were observed in the blood and liver parenchyma, in the CLL-treated mice.[459]

The role of *i*NKT cells was then assessed using *Cd1d*$^{-/-}$ mice. It had already been determined via IVM of the liver, that *B. burgdorferi* infection resulted in reduced crawling activity of iNKT cells, with subsequent arrest and clustering on KC, leading to IFN-γ production. It was therefore postulated that KC represent the main antigen presenting cells for *i*NKT in liver vasculature. In the absence of *i*NKT cells, a significant accumulation of *B. burgdorferi* occurred in joints, bladder and liver, but not in the blood. This suggested that *i*NKT cells could act to prevent the emigration of the microbes out of the vasculature.[459] The authors concluded that absence of either KC or *i*NKT cells resulted in dissemination of *B. burgdoferi*, but whilst lack of the former resulted in massive bacteraemia, loss of the latter caused pathogen dissemination to other organisms such

as the blood. This systematic IVM-based approach to examining the function of different immune cells in response to a specific pathogen produced a plethora of information relating to cell-cell interactions, cell tracking and effect on bacterial load. Importantly, the data could be analysed with key contextual information such as details of the vascular microenvironment, further enhancing the yield from each experiment.

The same group subsequently used a similar approach to characterise another novel interaction of KC, this time with platelets, during bacterial infection.[460] Initially, platelets were shown to have continuous 'touch and go' activity within liver sinusoids, in mice, under basal conditions. Platelets labelled with anti-CD49b rapidly (<1 second) touched F4/80-labelled KC lining the sinusoids, via a GPIb-dependent mechanism. Upon infection with *Bacillus cereus*, platelet-depleted animals developed bacteraemia within 4 hours, with 100% mortality. Using in vivo microscopy it was discovered that *B. cereus* trapping on KC occurred within seconds (in liver vasculature). The 'touch and go' activity of platelets then changed to sustained recruitment of platelets to the KC surface. The nature of this interaction was interrogated using high magnification and three-dimensional reconstruction in real time; platelets were found to encase trapped *B. cereus*, on KC surface, within three minutes.[460] This illustrates the potential for in vivo imaging to determine not only the nature of interactions between pathogens and immune cells, but also the actual time scale of key innate immune responses. Platelets were also shown to dock on KC following methicillin-resistant but not methicillin-sensitive *Staphylococcus aureus* infection, suggesting the platelet surveillance system may be specific to certain pathogens.[460]

Information from IVM studies has also led to revelations in our understanding of how neutrophils are recruited during endotoxaemia, and how critical the vascular endothelium is in the inflammatory response to blood-borne microbes and their products. McDonald et al performed a series of experiments aiming to dissect out the role of hepatic vascular endothelium during endotoxaemia, particularly in relation to endothelial TLR4 activation and regulation of neutrophil recruitment.[461] IVM was carried out on bone marrow chimeras and transgenic mice expressing TLR4 on selected cell populations, in the context of LPS treatment. It was demonstrated that LPS-induced TLR4 stimulation on vascular endothelium alone was enough to initiate neutrophil adhesion in hepatic sinusoids. They were also able to characterise a specific mechanism of neutrophil recruitment, showing the (interdependent) interaction between neutrophil CD44, endothelial hyaluronan and serum-derived hyaluronan-associated protein in this process. Overall, it was concluded that neutrophils accumulate in liver and lung

capillaries during endotoxaemia via active recruitment by non-leukocyte tissue resident 'sentinels' rather than hyperactivation of circulating neutrophils by LPS.[461]

The role of KC during other infections, including granuloma formation during *Mycobacterium bovis* Bacillus Calmette-Guérin (BCG) infection, has also been examined with IVM.[432] Whilst previous studies had investigated the static spatial localization of cells within mycobacteria-induced granulomas, little information was available on the dynamic cellular interactions within these immune structures. Egen et al used liver IVM throughout the granulomatous response to BCG infection, to look at host-pathogen interactions and the natural history of granuloma formation and dissolution.[462] Use of genetically modified BCG (expressing RFP) and mice with eGFP-expressing KC allowed interrogation of events immediately following infection. Gene-targeted mice expressing eGFP under control of endogenous lysozyme M promoter (LysM-eGFP) and those expressing eGFP recombined into the major histocompatibility complex (MHC) class II I-A locus (MHCII-eGFP) were used to identify KC during IVM.[462] TPEF IVM was employed to demonstrate that within one minute of IV infection, BCG became associated with the fluorescent KC population. Bone marrow chimera mice were then used to show that KC persist following BCG infection and redistribute into granulomas. Interestingly, whilst the myeloid populations moved slowly within granulomas, activated CD4+ T cells entered and migrated rapidly around the myeloid cell network. T cells were very motile within granulomas, but tended to remain within the borders of the structure. This restriction appeared to be mediated mechanically by the myeloid cell border. These experiments led the authors to propose a scenario whereby a protective granuloma environment is created by TNFα-dependent maintenance of a static scaffold of myeloid cells, supporting the migration of motile effector T cells.[462]

IVM during systemic bacteraemia has been utilized to describe the effects of specific immune cell products, such as neutrophil extracellular traps (NETs). Kolaczkowska et al extensively studied the formation and degradation of these neutrophil-derived NETs, which are composed of DNA associated with histones and proteases.[463] Whilst NETs are able to trap and kill bacteria, they are also known to cause collateral tissue damage.[464-467] IVM using spinning disk confocal microscopy of liver, during MRSA bacteraemia, demonstrated neutrophil-dependent NET formation within liver sinusoids.[463] NET release was shown to correspond with liver injury, and inhibition of von Willebrand factor (which anchored NET components to the liver vasculature) significantly reduced liver damage. It was observed that DNase treatment did not affect liver damage in this model, and real-time in vivo imaging allowed elucidation of the reasons for this;

although DNase immediately dissolved extracellular DNA, other NET components (histones and neutrophil elastase) remained attached to sinusoids i.e. DNase did not fully eliminate NETs.[463] These experiments identified potential limitations of DNase treatment (currently used in clinical practice) and it was postulated that inhibition of NET production could be beneficial. However, some of the challenges of in vivo imaging were also highlighted. For example, despite a number of different staining approaches, the authors were unable to image within necrotic areas. Hopefully, MP microscopy, with better laser penetration depths compared with confocal might overcome this problem. Furthermore, Sytox green was used to label extracellular DNA. However, on careful review of imaging, it was observed that a few KC and hepatocytes had taken up Sytox green, therefore it was essential that other NET components were concomitantly stained for (namely histones and neutrophil elastase) to ensure specificity for NET identification.[463] This emphasizes the importance of validating staining techniques and recombination efficiency/specificity of fluorescent reporter-expressing transgenic lines, before drawing conclusions from in vivo imaging.

IVM studies have also contributed to progress in our understanding of parasitic infections of the liver. In particular, Frevert et al were able to clarify the dynamics of the journey of malarial sporozoites from bloodstream to hepatocyte.[468] It had previously been unclear whether *Plasmodium* sporozoites entered the liver by passing through KC, or if they crossed directly through fenestrations in sinusoidal endothelia.[469,470] Frevert et al infected transgenic mice with *Plasmodium berghie* sporozoites by mosquito bite, then imaged exposed liver in vivo, by confocal and epifluorescence microscopy, up to depths of 50 μm. Sporozoites were detected by expressing red or green fluorophores, and endothelia or KC were identified by GFP using Tie2-GFP or lys-EGFP-ki mice respectively.[468] Sporozoites were observed gliding along the sinusoidal cell layer, then crossing it through a KC. Having entered liver parenchyma, they were then seen transmigrating through hepatocytes, moving at faster velocity, and damaging subcellular architecture. Time-lapse imaging allowed quantification of migration time (up to 15 minutes) and the longest distance covered (400-500 μm).[468] Despite shear forces of blood within vessels, the parasites were not detached from the sinusoidal cell wall, suggestion high affinity adhesion. Moreover, the parasites entered KC and hepatocytes with different patterns of motion, suggesting cell-specific invasion mechanisms. *Plasmodium* sporozoite invasion of hepatocytes had historically been problematic to study; these elegant IVM experiments allowed confirmation of a hypothesis derived from examination of fixed specimens.

Further information regarding elimination of liver-stage malaria parasites has been derived from IVM studies, especially concerning CD8+ effector T cell function.[471-473] Cockburn et al used spinning disk confocal microscopy to image mice infected with GFP-expressing *Plasmodium yoelii* sporozoites (i.e. naïve animals), or mice immunized 10 days previously with *P yoelii* radiation-attenuated sporozoites.[471] Phycoerythrin-conjugated α-CD8 antibody-labelled CD8+ T cells were injected 24 hours after sporozoite injection. In the previously immunized mice, most parasites imaged were surrounded by clusters of CD8+ cells. Mathematical modelling of cluster formation suggested that the process was non-random. Both parasite-specific CD8+ T cells and similarly activated OT-1 cells (ie non-specific CD8+ T cells) were recruited to clusters around *P yoelii* infected hepatocytes. Again, timelapse imaging data allowed mathematical modelling of cluster formation, suggesting both cell types were recruited to clusters in a positive-feedback, density-dependent fashion.[471] These observations were supported by a second study, using a slightly different model of protective immunity (again to the liver stage of malaria infection). Kimura et al[472] generated recombinant *Plasmodium berghei* expressing a fusion protein of an ovalbumin epitope, and GFP, in the parasite cytoplasm. It was then demonstrated that the ovalbumin epitope was presented by infected hepatocytes, and became a target of specific CD8+ T cells (from T cell receptor transgenic mouse line OT-1) conferring protection from liver stage *Plasmodium* infection. IVM using TPEF allowed visualization of the interaction between CD8+ T cells and infected hepatocytes, again demonstrating OT-1 cell clustering and elimination of intrahepatic parasites.[472]

Cockburn et al performed detailed imaging of the interaction between CD8+ T cells and Plasmodium-infected hepatocytes, in vivo, and were able to record parasite-killing in real time, for the first time.[471] They challenged previous findings from in vitro studies, suggesting that CD8+ T cell-mediated killing was rapid, instead observing prolonged (four hours) associations between T cells and infected hepatocytes. They also described four different parasite 'death phenotypes' characterized by distinct modes of GFP loss (e.g. sudden loss of GFP versus progressive attrition). The authors expressed confidence that loss of parasite fluorescence represented loss of viability, having considered possible confounding factors.[471] This illustrates another caveat of IVM, namely that care must be taken not to over-interpret a reduction in fluorescence from photobleaching or emigration from the field of view, as cell death.

In a further publication from the Yui group, Akbari et al[473] described an improved approach to fixing the liver, to facilitate MP IVM, focusing again on the interaction

between malaria parasites and antigen-specific CD8+ T cells during the liver-stage of malaria infection. They found inhaled isoflurane rather than injectable agents allowed better control of depth of anaesthesia. Avoidance of isoflurane overdose was recommended, as was relatively low concentration (1%) isoflurane use throughout surgery and the experiment. This served to prevent agonal breathing, which was associated with increased liver movements and image distortion. A portion of liver was exposed and fixed to gauze using adhesive glue. The liver was irrigated with PBS to avoid dehydration, and a coverslip applied, before imaging on a platform of the MP microscope. This allowed imaging for up to three hours before photobleaching. Whilst this approach only permitted relatively short imaging sessions, the optimization of anaesthesia described is particularly relevant, and becomes even more important for longer experiments, both in terms of image quality and animal welfare.

Experimental *Leishmania* infection is another parasitic disease that has been employed in conjunction with in vivo IVM of the liver, to investigate KC and CD8+ T cell dynamics, in the context of granuloma formation. Beattie et al[474] demonstrated how IVM could complement adoptive cell transfer and flow cytometry techniques, to obtain detailed information about the antigen-presenting process in parasitic infection. They were able to show for the first time, in situ, that KC act as targets for antigen recognition by granuloma-infiltrating CD8+ T cells.[474] These experiments supported the findings from Egen et al, suggesting that granulomas are not simply static tissue structures, but comprise a complex dynamic microenvironment.[425]

More recently the *Leishmania* model was used in a study to develop methods for imaging and measuring blood flow velocity within individual hepatic blood vessels, and quantitatively analyse the velocity of individual red blood cells (RBC).[475] Dasari et al described two independent imaging methods for measuring RBC velocity and blood flow speed, which could then be used to correlate blood flow parameters with parasite multiplication within the liver.[475] This technique could be applied in other infection and injury models, to gain valuable information about pathophysiological alterations in hepatic blood flow.

Cancer and metastasis

IVM techniques allow direct visualization of tumour cells interacting with their microenvironment, providing insights into the biological processes summarized by Hanahan and Weinbery as the ‘hallmarks of cancer’.[476-478] These include, for example, tumour cell ability to migrate, metastasize and induce angiogenesis. The majority of IVM

cancer research (recently reviewed and summarized by Ellenbroek and van Rheenan[478]) comprises work using well-established optical windows, such as breast, skin and brain. Sophisticated experiments have shown not only the dynamics of migratory cells within tumours, but also, for example, the regulatory role of individual proteins in migration. Canel et al combined the use of dorsal skin windows with photobleaching, photoactivation and photoswitching, to quantitatively measure tumour cell movement, proliferation and protein dynamics, in squamous cell carcinoma cells in vivo within a tumour mass.[479] Fluorescence of green-fluorescent-protein (GFP)-tagged E-cadherin was bleached in a specific area of tumour cells, and fluorescence recovery after bleaching (FRAP) was measured. Inhibition of focal adhesion kinase (FAK) increased the fluorescence recovery rate, demonstrating that FAK is a key regulator of E-cadherin activity.[479,480]

The use of photoswitchable fluorophores has enabled study of the migration of large numbers of tumour cells over multiple imaging sessions.[478] Kedrin et al expressed the photoswitchable protein Dendra2 in cells from the metastatic breast cancer line MTLn3.[416] Dendra2 expression results in green fluorescence prior to photoswitching; exposure to blue light induces an irreversible red shift.[481] Tumour cells were imaged through a mammary imaging window. Certain photoswitched regions demonstrated significant migration and invasion of the adjacent microenvironment. However there was limited migration in other regions, suggesting that the surrounding microenvironment influences cell behavior.[416]

In the liver, IVM cancer models to date have largely been confined to studying colorectal cancer metastasis or HCC by imaging inoculated cancer cell lines.

To improve our understanding of leukocyte recruitment and migration in HCC, Takeichi et al inoculated the Hep55.1C HCC cell line directly into the livers of transgenic mice (expressing eGFP-labelled leukocytes of either lymphoid or myeloid origin) via a midline incision.[482] After 12-14 days, solid, vascularized tumours of up to 10mm had grown at the implantation site. For IVM, midline incision was performed, and tumours were identified macroscopically. The tumour-bearing liver lobe was exteriorized and imaged by confocal microscopy. From timelapse images, density of perfused blood vessels was measured (visualized by IV injection of TRITC-labelled albumin) in addition to density and velocity of migrating leukocytes. Analysis of blood vessel density showed that vessel distribution was heterogeneous within HCC tissue, with areas of high and low vessel density. Quantification of eGFP fluorescence demonstrated that peritumoural blood vessels were the main site of leukocyte recruitment, in comparison to intratumoural blood

vessels, where low extravasation rates of single leukocytes were seen. The density of lymphoid leukocytes within tumour tissues was higher than that of myeloid leukocytes, and most intratumoural leukocytes migrated randomly, and changed direction many times over 30 minutes (the length of the observation period). The authors concluded that infiltration of tumour tissue by lymphoid and myeloid leukocytes in this model represented a cellular immune response against HCC, which might be further studied to elucidate mechanisms of leukocyte recruitment in this liver tumour.[482]

Tanaka et al investigated tumour angiogenesis in colorectal liver metastases in vivo, by inoculating red-fluorescent-protein (RFP)-expressing cell lines into the spleens of GFP nude mice, which then travelled to the liver.[483] The liver was then exteriorized and fixed, and imaged by two-photon laser scanning microscopy. Tumour cell arrest/adhesion, tumour cell-induced platelet aggregation, tumour cell extravasation and phagocytosis by Kupffer cells was observed using timelapse and z-stack imaging techniques. Mice were imaged at three time points, and by eight weeks, dilated and tortuous blood vessels within liver metastatic nodules were seen. Imaging more frequently using this approach was limited by the development of fibrous adhesions between the abdominal wall and liver surface. It was acknowledged that recurrent exteriorization of the liver might also affect the physiological condition of the organ.[483]

Ritsma et al pioneered the use of the AIW to demonstrate colorectal cancer metastasis formation in the liver, in real-time, over five days.[424] They identified a 'pre-micrometastasis' step, during which individual extravasated colorectal cancer tumour cells proliferate in the liver, and form a clone in which cells are highly motile, but lack contact with other tumour cells within the clone. When cell migration was inhibited in pre-micrometastases, maturation to micrometastases was abrogated, resulting in reduced metastatic load.[424]

To date, genetic or carcinogen-induced mouse models of HCC have not been imaged using the AIW technique; it is anticipated that this would be feasible, and coupled with MP microscopy, SHG and CARS, could yield a wealth of information regarding tumour biology, particularly with respect to angiogenesis and blood vessel function in this highly vascular tumour-type. Moreover, real-time imaging of the actions of anti-angiogenesis chemotherapy agents in this setting might prove illuminating in terms of understanding their anticancer efficacy or lack of benefit.

5.2 Hypothesis and aims

It was hypothesized that IVM of mouse liver, using a MP microscope, could be performed via an AIW, allowing sequential imaging of biological processes over many days. Similarly, I hypothesized that HCC induced by perinatal DEN injection could be imaged similarly, by placing the AIW on tumour tissue.

Aims

- To develop IVM of the liver, via an abdominal window, with optimization of surgical and imaging techniques, to allow sequential imaging of the liver in the same animal over several weeks.
- To optimize liver imaging of different fluorescent reporter mice strains ex vivo, including the use of SHG to visualize collagen, and CARS to demonstrate lipids, prior to live imaging.
- To image fluorescent reporter mice strains in vivo, using a variety of different models of acute or chronic liver injury and regeneration
- To demonstrate that HCC can be imaged in vivo using the AIW.

5.3 Methods

Animals

Animals were housed in standard sterile conditions with free access to chow and water. All procedures were undertaken in accordance with the local ethical committee. Animals were between 12 and 20 weeks of age. All transgenic mouse crosses are described in the results section. All mice were maintained on a C57BL/6 background. *Pdgfrb*-Cre mice were a kind gift from Ralf Adams.[328] These were crossed with Ai14 (B6;129S6-Gt(ROSA)26Sortm14(CAG-tdTomato)^{Hze}/J)[484] or mTmG (B6.129(Cg)-Gt(ROSA)26Sortm4(ACTB-tdTomato,-EGFP)^{Luo}/J)[485] mice, obtained from Jackson Laboratories. Macgreen mice (B6N.Cg-Tg(Csf1r-EGFP)1^{Hume}/J) were a kind gift from David Hume. *Alb*-Cre x confetti (albCre;Gt(ROSA)26Sor$^{tm1(CAG-Brainbow2.1)Cle}$/J) mice were obtained from the Jackson Laboratory.[329,486,487] Genotyping was performed by polymerase chain reaction (PCR). For all IVM experiments, mice aged 10-14 weeks were used, to ensure optimal liver lobe size for AIW placement.

To our knowledge, this is the first time the liver has been imaged in vivo through an AIW in the UK. A rigorous home office schedule was therefore adhered to, involving initial pilot experiments in which small numbers of animals were imaged under terminal anaesthesia. Once proof of principle was obtained that this was feasible and well-tolerated, animals were recovered post-imaging, and underwent a further imaging session at a later date. Again, once this was achieved, longer term experiments were performed, in which animals were imaged up to two weeks after initial AIW implantation.

Models of liver injury

Acute liver injury was induced by injection of anti-Fas antibody (Jo-2). Animals were injected IP with 0.5µg/g body weight of Jo-2 (purified NA/LE hamster anti-mouse CD95, 5544254, BD Bioscience, Franklin Lakes, NJ, USA) dissolved in sterile PBS. Where nuclei were labelled, the fluorescence nucleic acid stain Hoechst (33342, ThermoFisher Scientific, Walthm, MA, USA) was used. 2µg/g of Hoescht diluted in sterile PBS was injected IV, 30 minutes prior to culling, to allow incorporation into nuclei.

Chronic liver injury was induced by CCL4. Mice received 0.25µl/g diluted in olive oil, twice weekly for six weeks. IP Injections were carried out using a 27g short needle and a Hamilton glass syringe.

AIW implantation materials

Figure 5.4 shows the AIW computer-aided design (CAD) diagrams for the three different prototypes used throughout these experiments. Initial experiments utilized an AIW (modified very slightly from the specifications described by Ritsma et al in their Nature Protocols manuscript)[421] consisting of a titanium ring with a 1.3mm groove and a glass coverslip (8mm diameter, 0.13-0.17mm thickness) fixed on top, by a removable circlip (Figure 5.4 A and E(i)). Titanium alloy was chosen so the AIWs could be sterilized and reused. It was also light and therefore well-tolerated, as well as being highly biocompatible, corrosion resistant and non-inflammatory.[421] After surgical implantation of the ring (described below) a purse-string suture was employed to fix the AIW in place. This suture was concealed within the groove to prevent biting or pulling by the animals after recovery from surgery. For sequential imaging, the circlip design allowed removal of the coverslip and cleaning of any accumulated exudate beneath it, before replacement with a new coverslip. The van Rheenen group subsequently developed a larger ring with a smaller inlay to which the coverslip (12mm diameter, 0.16-0.19mm thickness) was glued (AIW-insert). This smaller AIW-insert fit into the main ring with a sliding mechanism, allowing removal with a custom-made tool (again to allow change of coverslip between imaging sessions); we were kindly permitted to use this design. Our group refined this further, by adding small grooves to the outside ring circumference (for better immobilization during imaging) and milling the underside of the ring to create a slant towards the aperture. This followed the curvature of the liver surface better, thereby minimizing the gap between the coverslip and the liver (manufactured by School of Engineering, University of Edinburgh).

Ritsma et al reported the development of exudate below the glass coverslip, which could be problematic for long-term imaging. This prompted them to coat the glass coverslip with poly-L-lysine-g-poly(ethylene glycol) (PPL-g-PEG) to prevent the development of an inflammatory or immune response against it. Therefore all glass coverslips were immersed in PPL-g-PEG 0.1mg/ml $^{-1}$ prior to use. To assemble the AIW-insert, a thin layer of cyanoacrylate glue was applied to the anterior surface, and the coverslip placed on top. Once dry, this was placed in 70% ethanol (vol/vol) for 30 minutes, then moved to a sterile laminar flow cabinet. PPL-g-PEG was then applied to the underside of the AIW-insert, and left for one hour, before being gently washed off using sterile PBS. This was allowed to dry, before being stored at 4°C for up to 14 days.

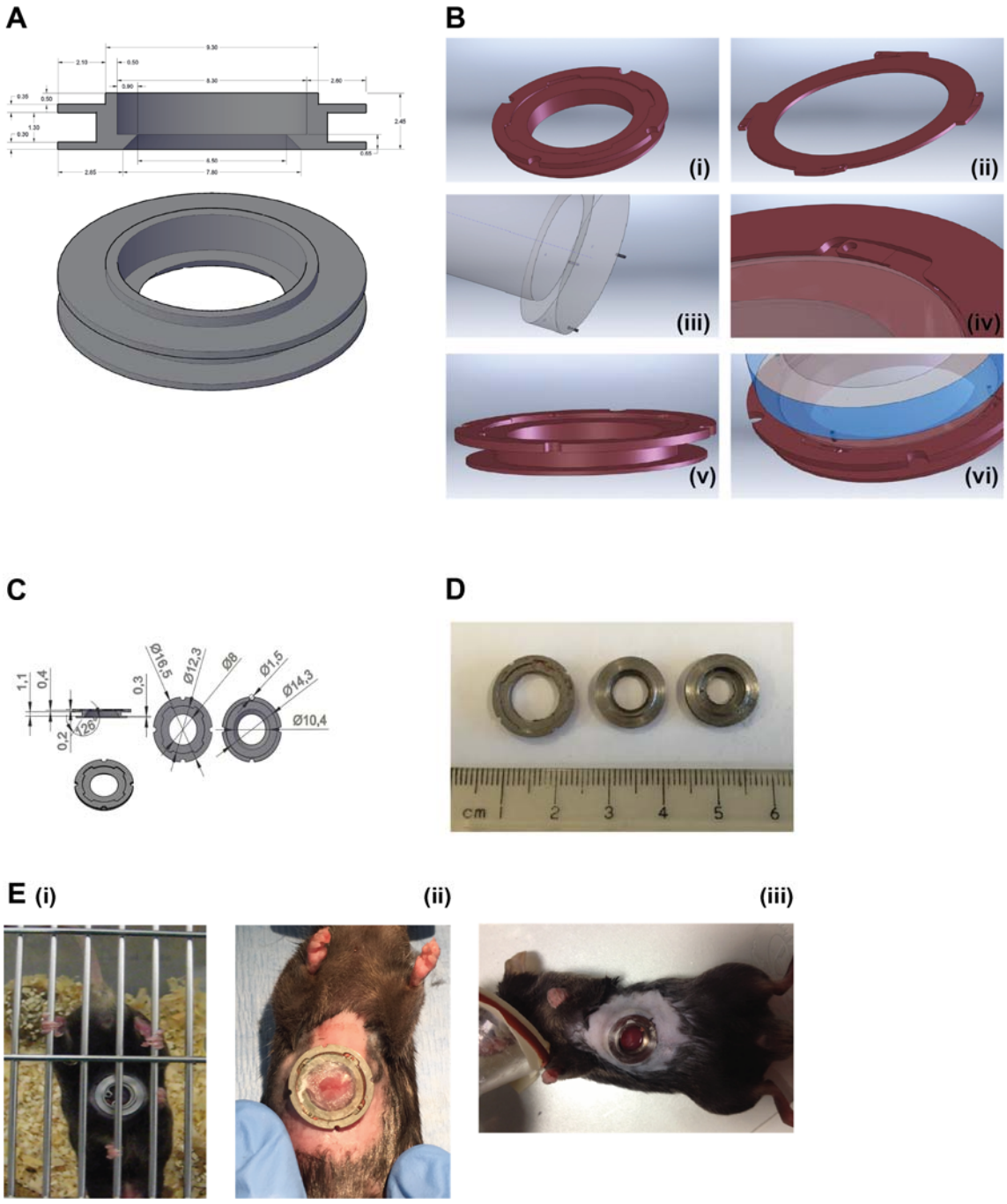

Figure 5.4 Abdominal imaging windows

A CAD drawing of the first prototype titanium AIW. A glass coverslip was placed on the inner rim of the aperture, and secured with an overlying circlip. **B** CAD drawings of the van Rheenan AIW design with a larger aperture **(i)**, and removable AIW-insert **(ii)**. A custom-built tool for changing the AIW-insert was kindly supplied by the van Rheenan group **(iii)**. **C** CAD drawings of our modified AIW design with grooves for better immobilization and domed underside. **D** (Left to right) photographs of AIW shown in **B,**

A and AIW for kidney imaging (CAD not shown). **E (i)** Still from video of well and active animal, 24 hours post-surgery. AIW pictured with circlip in situ. **(ii)** AIW from B prior to changing of AIW-insert. **(iii)** Changing coverslip with mouse briefly anaesthetized using mouth-piece.

Surgical technique

All instruments and AIW components were sterilized prior to surgery. Mice were anaesthetized by inhalation of 2% isofluorane and 2L/min oxygen flow, with induction in a Plexiglas chamber. Buprenorphine 0.1mg/kg SC was administered after induction of anaesthesia, for analgesic purposes. Anaesthesia was maintained by isofluorane inhalation through a mouthpiece, and hypothermia avoided by use of a warming pad throughout surgery. Lacrilube was applied to the eyes; abdominal hair was removed using commercially available cream and clippers. Skin was then disinfected with betadine. A midline laparotomy incision was made. Using standard aseptic surgical techniques, the caudal part of the sternum (xyphoid process) was clamped and removed, the liver mobilized and falciform ligament transected. In some cases, a cotton gauze roll was placed above the liver, under the diaphragm, aiming to cushion (and therefore minimize) movement artefact from respiration. A purse string suture was then placed, surrounding the incision. The left liver lobe was manipulated anteriorly through the incision, and the AIW glued to the liver surface. Once the glue had dried, the liver was returned intra-abdominally, and the skin and muscle layers eased into the AIW groove. The purse-string suture was tightened and tied off. Depending on the AIW prototype used, either the pre-assembled AIW-insert was then placed using the window tool (Figure 5.4 B) or the PPL-g-PEG coated coverslip was sited within the ring and held in place with a circlip. Post-operative fluids (25ml/kg saline) were administered SC at the end of the procedure, and a further SC dose of buprenorphine given if required 6-12 hours later. Mice were monitored twice daily for the first 48 hours, then daily for pain and general wellbeing.

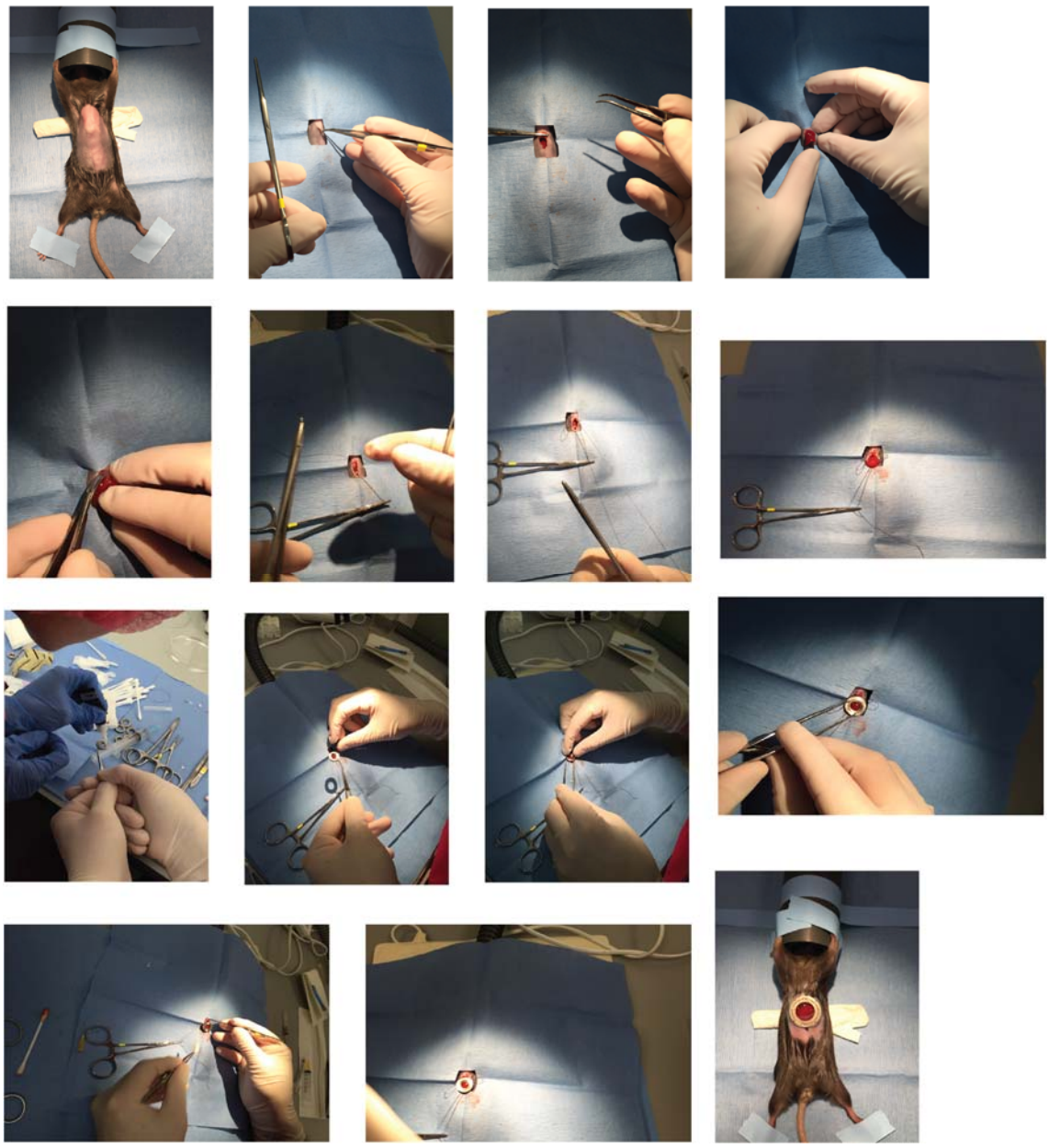

Figure 5.5 AIW surgical technique

Sequential photos from preparation of the abdomen to securing AIW in place using a purse string suture

Two-photon IVM

Imaging was performed using a custom-built microscope as described previously.[488] Briefly, a picoEmerald (APE) laser provided both a tuneable pump laser (720–990 nm, 7 ps, 80 MHz repetition rate) and a spatially overlapped second beam termed the Stokes laser (1064, nm, 5–6 ps and 80 MHz repetition rate). The laser was inserted into an Olympus FV1000 microscope coupled to an Olympus XLPL25XWMP N.A. 1.05 objective lens using a short-pass 690 nm dichroic mirror (Olympus). For general imaging the pump beam was tuned to 816.8 or 812.2 nm to generate CARS signals at 2845 cm^{-1} or 2930 cm^{-1} respectively. The various emissions were filtered in the following fashion: SHG signals were filtered using the following series of filters: FF552-Di02, FF483/639-Di01 and FF01-400/40. GFP two-photon fluorescence signals were filtered using filters: FF552-Di02, FF483/639-Di01 and FF510/84. RFP two-photon fluorescence signals were filtered using: FF552-Di02, and FF440/520-Di01 and HQ610/75m (Chroma). CARS signals were filtered using: FF552-Di02, and FF440/520-Di01 and ET687/95m (Chroma). For Confetti mice imaging the pump beam was tuned to 920.0 nm and the various fluorescences were filtered in the following fashion: CFP two-photon fluorescence was filtered using the following series of filters FF520-Di02, FF495-Di03 and FF01-466/40. GFP two-photon fluorescence signals were filtered using filters: FF520-Di02, FF495-Di03 and FF01-504/12. YFP two-photon fluorescence signals were filtered using: FF520-Di02, ET570lp (Chroma) and FF01-542/27. RFP two-photon fluorescence signals were filtered using FF520-Di02, ET570lp (Chroma) and FF01-605/15. All other filters were from Semrock.

Animals were maintained under isofluorane anaesthesia, titrated to respiratory rate, immobilised in a custom-built, heated imaging box (Figure 5.6).

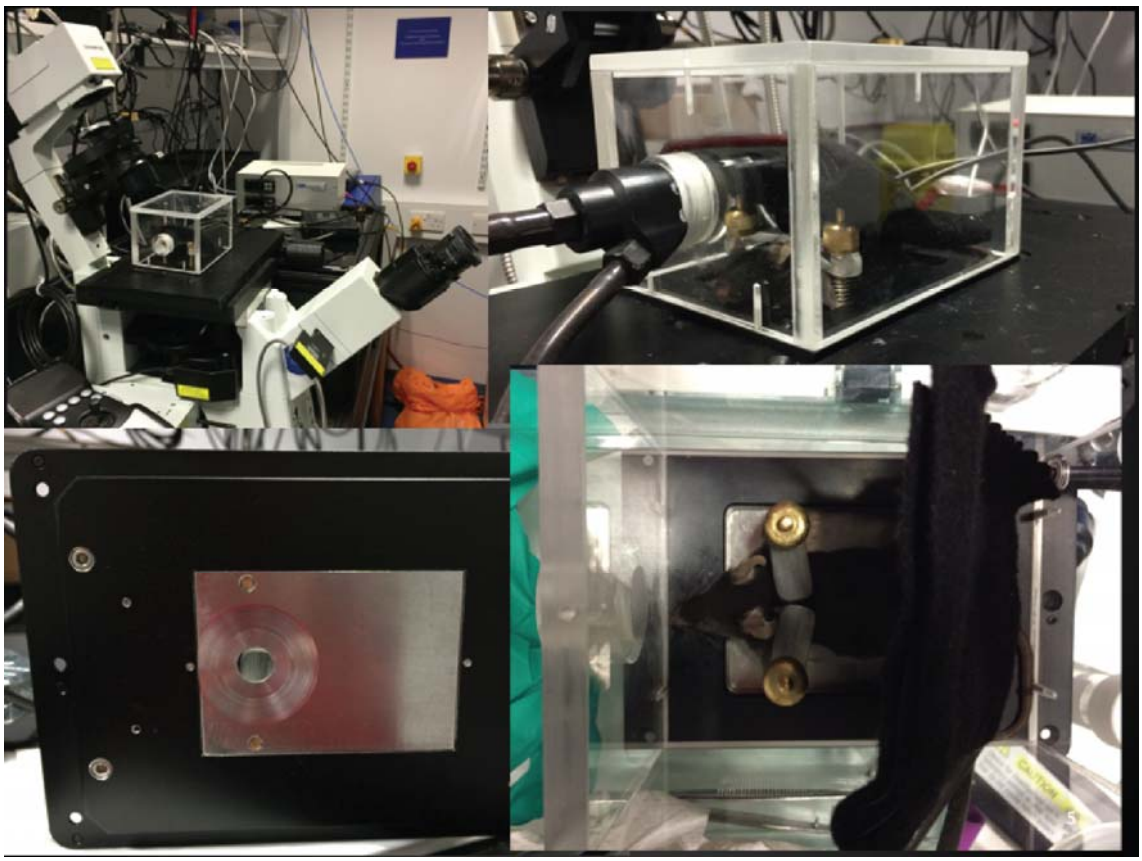

Figure 5.6 Multiphoton microscope and IVM equipment

Clockwise from left: custom-built MP microscope and imaging box. Animal anaesthetized in heated box. View from above and below box.

5.4 Results

Pdgfrb-Cre mice were crossed with mTmG reporter mice, to allow imaging of HSC under homeostatic conditions and following injury. mTmG reporter mice express membrane-targeted tandem dimer tomato (TdTomato) prior to Cre-mediated excision and membrane-targeted green fluorescent protein (mGFP) after excision).[485] Therefore, in these double-fluorescent reporter mice, all cells express membranous TdTomato (clearly outlining hepatic architecture) apart from HSC, which express mGFP. *Pdgfrb*-Cre mice were also crossed with Ai14 reporter mice (a single fluorescent reporter that expresses TdTomato after recombination).[484] In these animals, HSC TdTomato fluorescence is cytoplasmic, clearly demonstrating HSC morphology. MacGreen mice were crossed with *Alb*-Cre animals, allowing visualization of liver macrophages in green. *Alb*-Cre x confetti mice were used in the HCC model. The confetti mouse uses the Brainbow-2.1 construct, in which two invertible units are positioned in tandem.[487] Cre-mediated excision can therefore yield a total of four expression possibilities: RFP, yellow fluorescent protein (YFP), cyan or GFP. In *Alb*-Cre x confetti animals, hepatocytes stochastically express a fluorescent protein. In our experience, a proportion of cells express two fluorescent proteins, which may be explained by hepatocytes possessing multiple nuclei, resulting in more than one confetti construct per cell, or this may be secondary to *Alb*-Cre mice expressing Cre constitutively. We also observed minimal GFP reporting, which is consistent with the literature.

For all reporter mice, fluorescent MP microscopy was first performed ex vivo, to optimise laser settings. Uninjured animals were culled, livers harvested and imaged immediately in a petri dish. Figure 5.7 shows preliminary ex vivo images of uninjured PDGFRβCre$^{+/-}$;mTmG liver.

Figure 5.8 shows in vivo IVM of PDGFRβCre$^{+/-}$;mTmG. Imaging was undertaken under terminal anaesthesia. High resolution images were obtained, over a period of one hour. Initially a tile was taken to see how the liver was fixed below the AIW, and to allow selection of areas to take Z stack images from.

After establishing optimal laser settings for imaging the PDGFRβCre$^{+/-}$;mTmG line, the same experiments were performed in a model of chronic liver injury. CCL_4-treated mice were culled, and whole liver immediately imaged in a dish. Tiles and z stacks obtained demonstrated fibrotic, nodular liver tissue. The liver surface was appropriately

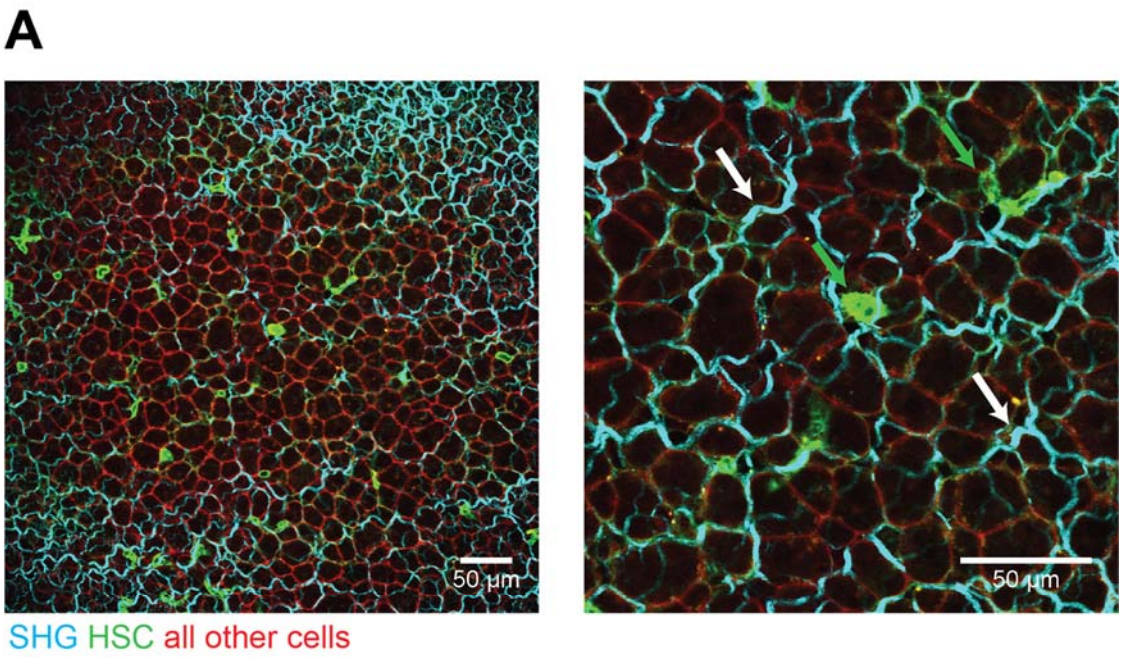

Figure 5.7 Uninjured PDGFRβCre$^{+/-}$;mTmG liver ex vivo

A Uninjured PDGFRβCre$^{+/-}$;mTmG mouse liver. Harvested whole liver imaged in a dish with MP microscope. Images taken at level of capsule and just below, with SHG demonstrating mature collagen fibrils (cyan, white arrows). HSC seen in green (green arrows) in close association with collagen. **B** Z stack images, from the same liver, starting from liver capsule and ending in hepatic parenchyma.

nodular, and uneven, resulting in black ‘holes’ in the tile (Figure 5.9 A). Expansion of GFP reporting around blood vessels was observed, due to marked HSC activation in response to injury, which also corresponded with increased SHG signal from collagen deposition. These and in vivo images (Figure 5.10) illustrate the utility of this reporter to characterise HSC location and morphology in relation to scar formation and parenchymal architecture (depicted by membranous RFP in this strain).

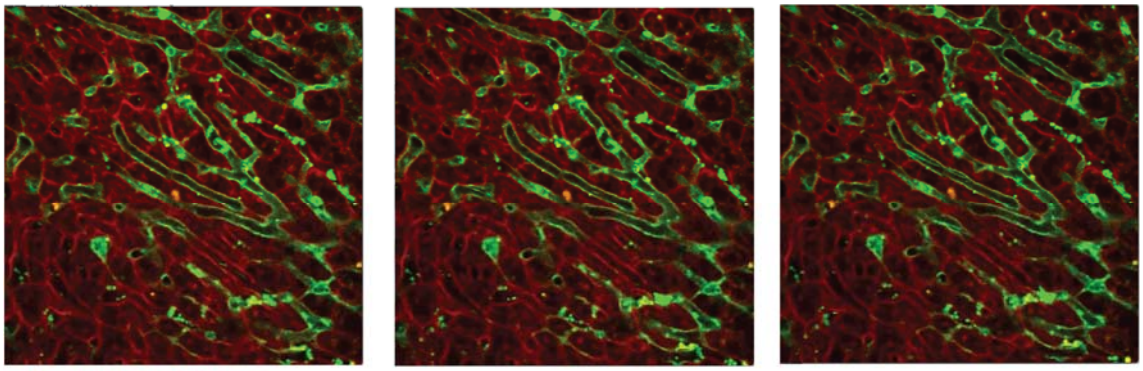

Figure 5.8 Timelapse IVM of uninjured PDGFRβCre$^{+/-}$;mTmG mouse liver under terminal anaesthesia

Sequential stills from timelapse imaging of uninjured PDGFRβCre$^{+/-}$;mTmG mouse liver under terminal anaesthesia. High resolution images were acquired over one hour. The mTmG reporter allowed characterisation of liver sinusoids and parenchymal architecture. All cell membranes (other than HSC, labelled with GFP) were labelled with RFP. It is hypothesised that this transgenic mouse might have some platelets labelled with GFP, (due to platelets transiently expressing PDGFR), which would account for small fluorescently labelled fragments flowing in large blood vessels. Work to determine the nature of these (using flow cytometry) is ongoing.

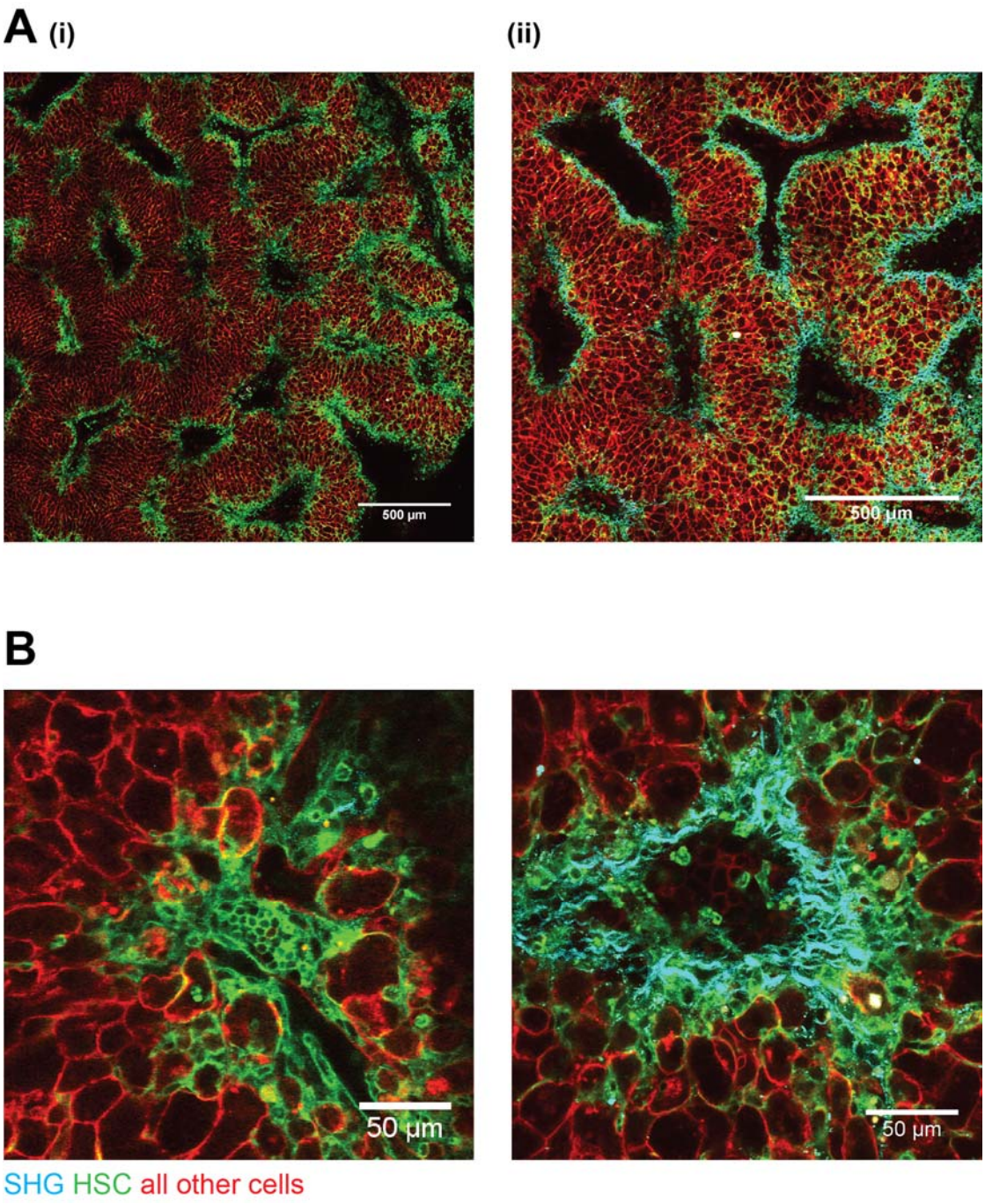

Figure 5.9 CCL_4-injured PDGFRβCre$^{+/-}$;mTmG ex vivo

A (i) PDGFRβCre$^{+/-}$;mTmG liver in a dish, after 4 weeks CCL_4 treatment. Tile showing fibrotic nodular liver with HSC expansion around blood vessels and collagen deposition. **(ii)** Z stack image through same liver. **B** Higher magnification images of CCL_4-treated liver in a dish showing HSC activation and formation of collagen scar.

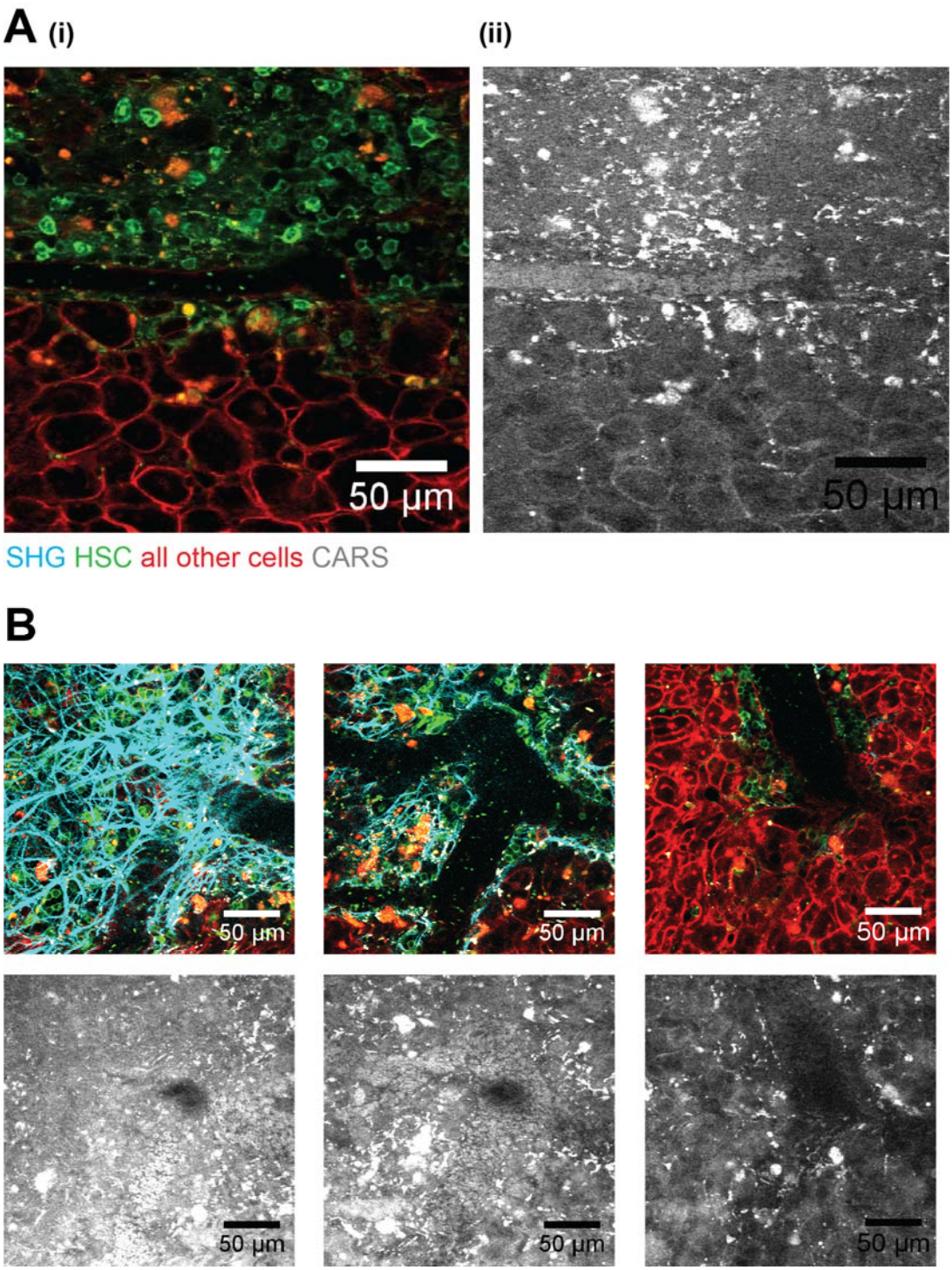

Figure 5.10 Intravital imaging of CCL_4-injured PDGFRβCre$^{+/-}$;mTmG mice

A (i) Image from chronic CCL_4-injured PDGFRβCre$^{+/-}$;mTmG mouse; timelapse in vivo imaging under terminal anaesthesia. **(ii)** CARS channel of the timelapse image, showing blood-flow through a vessel. **B** Sequential Z stack images (left to right) from the same mouse imaged in vivo, from capsule to liver parenchyma. Bottom panel shows corresponding CARS channel image.

Next, experiments were repeated using a model of acute liver injury, to examine activated HSC expansion and investigate the ability of CARS to show features of parenchymal damage. Images were taken four hours after IP injection of anti-Jo2 antibody. Ex vivo images (Figure 5.11) show HSC accumulation in close association with the collagen-rich liver capsule. Parenchymal damage was visible with destruction of hepatocyte architecture, and disruption of RFP membranous fluorescence, which corresponded with areas of haemorrhage depicted by an increase in grey CARS signal. Furthermore, CARS demonstrated an increase in hepatocyte lipid droplet content (bright white dots) which is known to occur in acute injury. The quality of in vivo timelapse imaging using this model was limited by movement artefact from respiration (Figure 5.12). This was potentially at least partly secondary to the severity of systemic illness in these animals, resulting in more gasping respiratory efforts. Subsequent in vivo imaging of acute liver injury was therefore largely focused on the paracetamol model, at well-characterized doses, known to induce hepatic injury with minimal systemic upset. Where anti-Jo2 antibody was used, the slightly earlier time point of three hours post-injection was analysed.

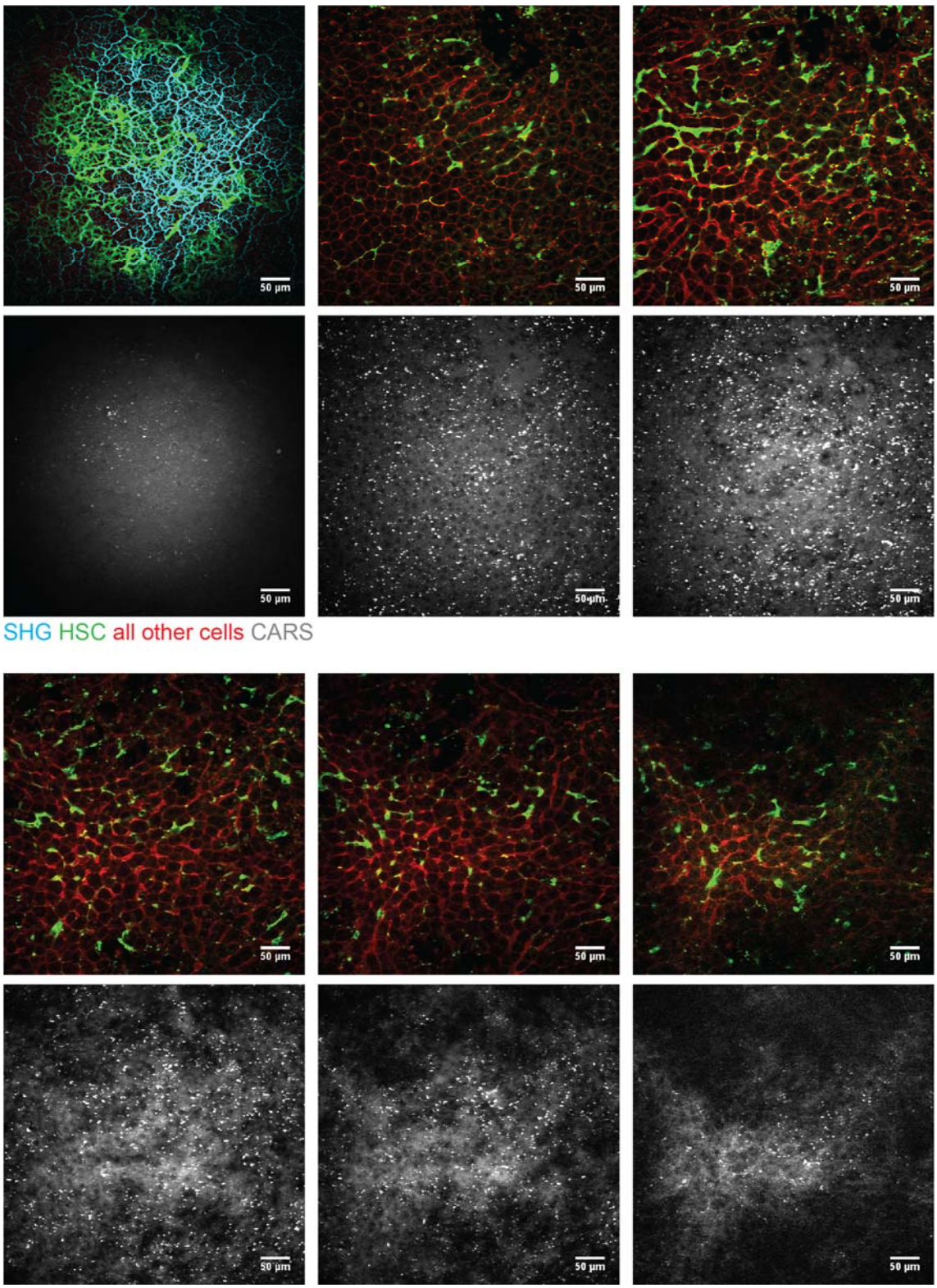

Figure 5.11 Jo-2 antibody-injured PDGFRβCre$^{+/-}$;mTmG liver ex vivo

Whole liver harvested and imaged in a dish with MP microscope. Images from a single Z stack are shown, sequentially from liver capsule (top left) to deeper within parenchyma. Top panel shows fluorescent reporters and SHG; bottom panels show corresponding

CARS image. HSC expansion is visible following injury (green). Loss of hepatic architecture is seen with a paucity of red membranous fluorescence, particularly as depth increases. This corresponds with haemorrhagic areas seen with CARS.

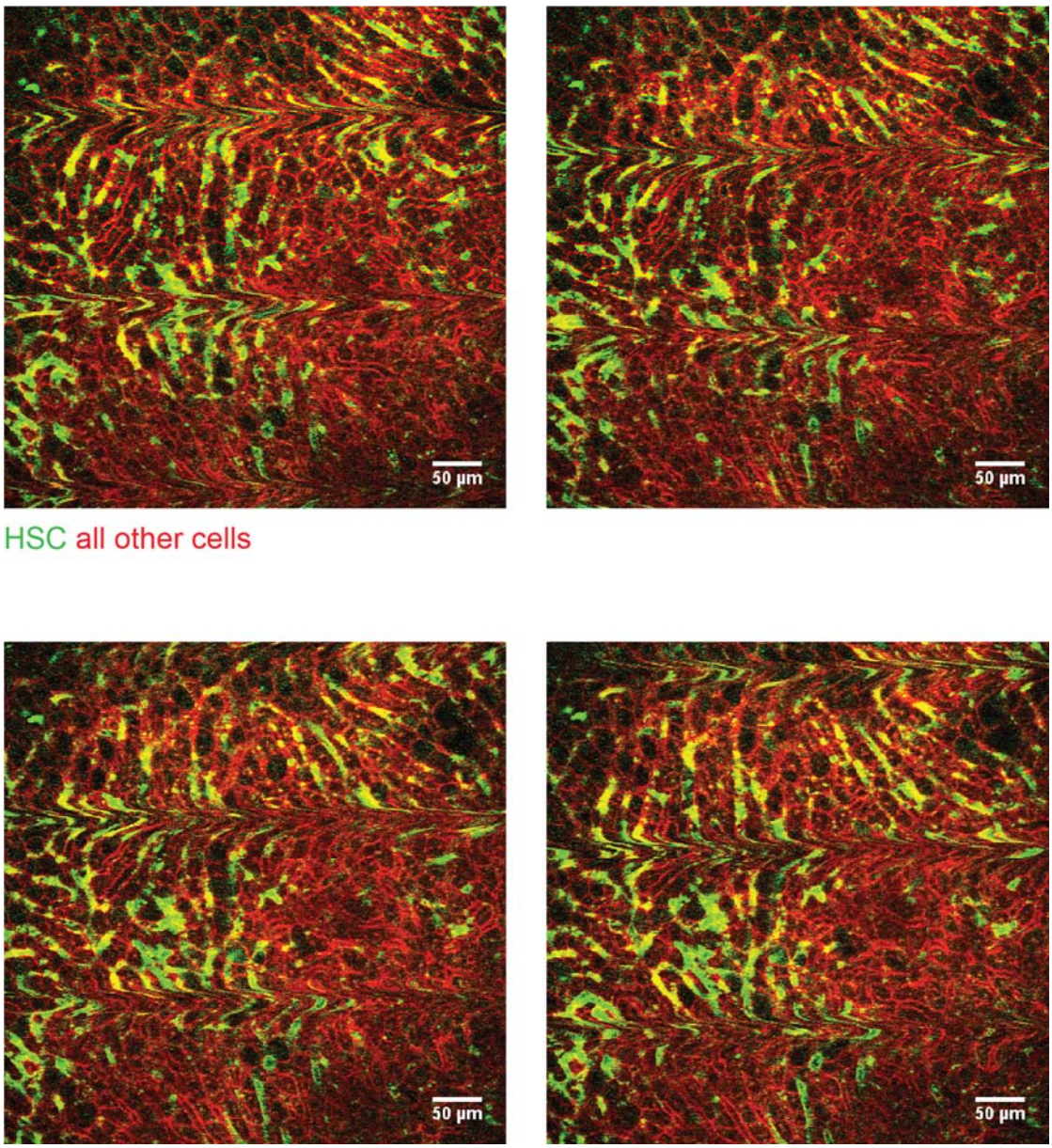

Figure 5.12 Timelapse IVM of Jo-2 antibody-injured PDGFRβCre$^{+/-}$;mTmG liver
Sequential stills from timelapse in vivo imaging under terminal anaesthesia

Having established that surgical abdominal window implantation and imaging under terminal anaesthesia was successful, we envisaged that longer imaging periods might be desirable to capture cellular events, for example HSC movement, hepatocyte division and hepatocyte necrosis. The PDGFRβCre$^{+/-}$;Ai14 reporter mouse was used in this set of experiments. This mouse labels HSC with TdTomato fluorescence.

Figure 5.14 shows consecutive stills from in vivo timelapse imaging of uninjured liver. Erythrocytes are seen clearly with strong CARS signal, in a large blood vessel. The liver was imaged for a total of three hours (all timelapse imaging) in the same field of vision. Although no specific HSC movements were visualized during this period, the cytoplasmic Ai14 fluorescence was extremely strong, and was not compromised by photobleaching, confirming the utility of this reporter for in vivo studies. The main limitation of this approach was intermittent loss of the water bubble between the microscope objective and the specimen, resulting in degradation of images and necessitating a pause to replenish the water bubble.

Once the results of these experiments had been presented to the veterinary team, it was possible to proceed with experiments involving recovery after abdominal window surgery, rather than immediate imaging under terminal anaesthesia.

In line with the suggested Home Office pilot studies, we assessed the effects (on animal welfare and imaging quality) of the mice having AIWs in for increasing lengths of time. Figure 5.16 shows timelapse IVM of PDGFRβCre$^{+/-}$;Ai14 liver, in which the AIW was surgically placed two weeks previously. Animals (n=2) were allowed to recover after window surgery, and had free access to food and water. The AIW coverslip was changed under brief anaesthesia every 48-72 hours. At two weeks they received IP anti-Jo2 antibody and were imaged three hours later. The resulting images remained of high quality, with clear HSC expansion following injury (Figure 5.16).

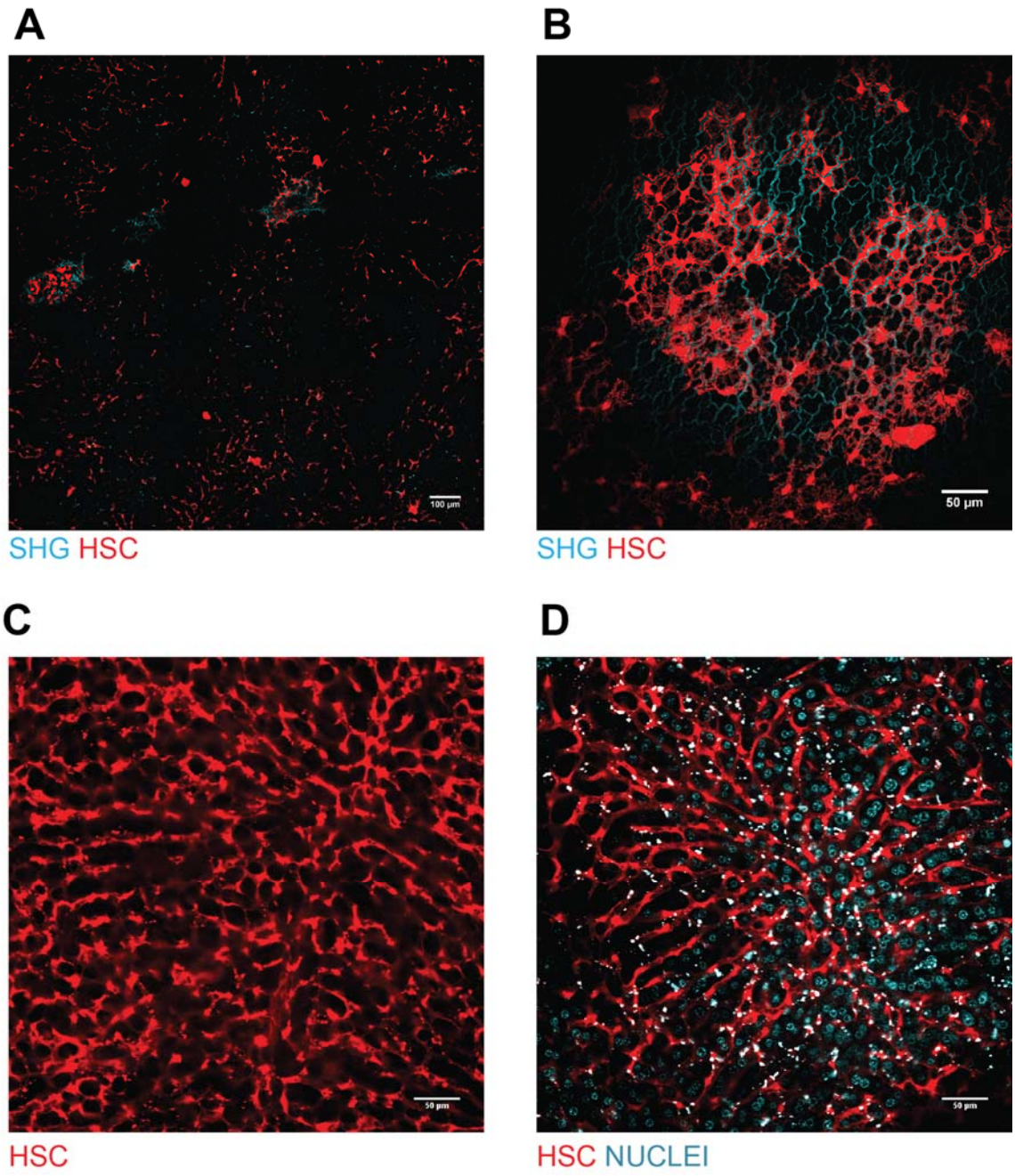

Figure 5.13 PDGFRβCre$^{+/-}$;Ai14 liver ex vivo

Whole liver harvested and imaged in a dish with MP microscope. **A** Tile of uninjured liver showing relatively sparse HSC expressing cytoplasmic Td tomato **B** High magnification image of chronic CCL_4-injured liver, at level of liver capsule (shown with cyan SHG) with high density of HSC. **C** Jo-2 antibody liver parenchyma (3 hours post-IP injection) showing marked HSC accumulation. **D** Jo-2 antibody-injured liver parenchyma with nuclear labelling by IV Hoescht injection.

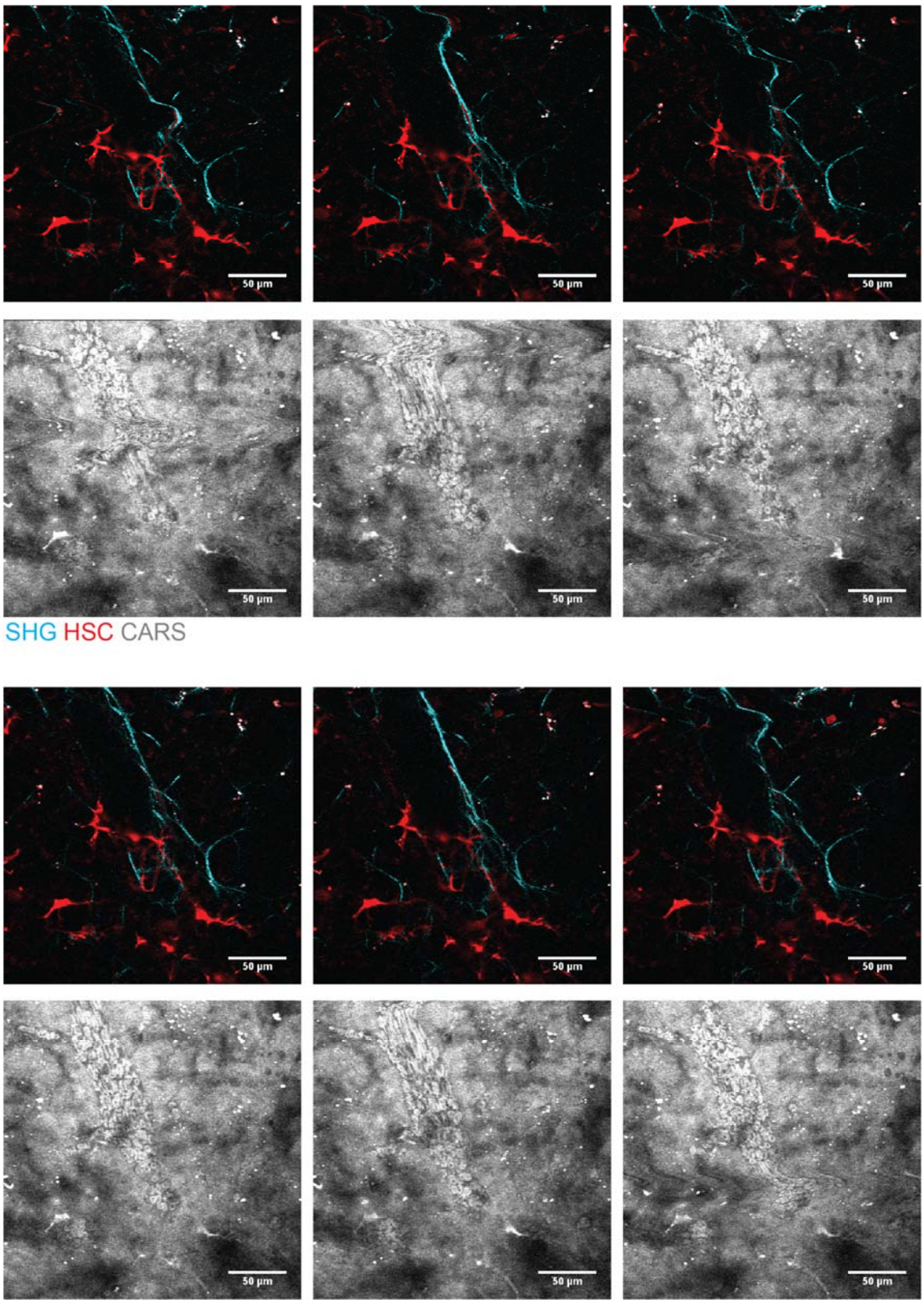

Figure 5.14 IVM of PDGFRβCre$^{+/-}$;Ai14 mouse under terminal anaesthesia
Sequential stills from timelapse imaging. Top panel shows fluorescent reporter and SHG; lower pane shows corresponding CARS image. Liver imaged for 3 hours total.

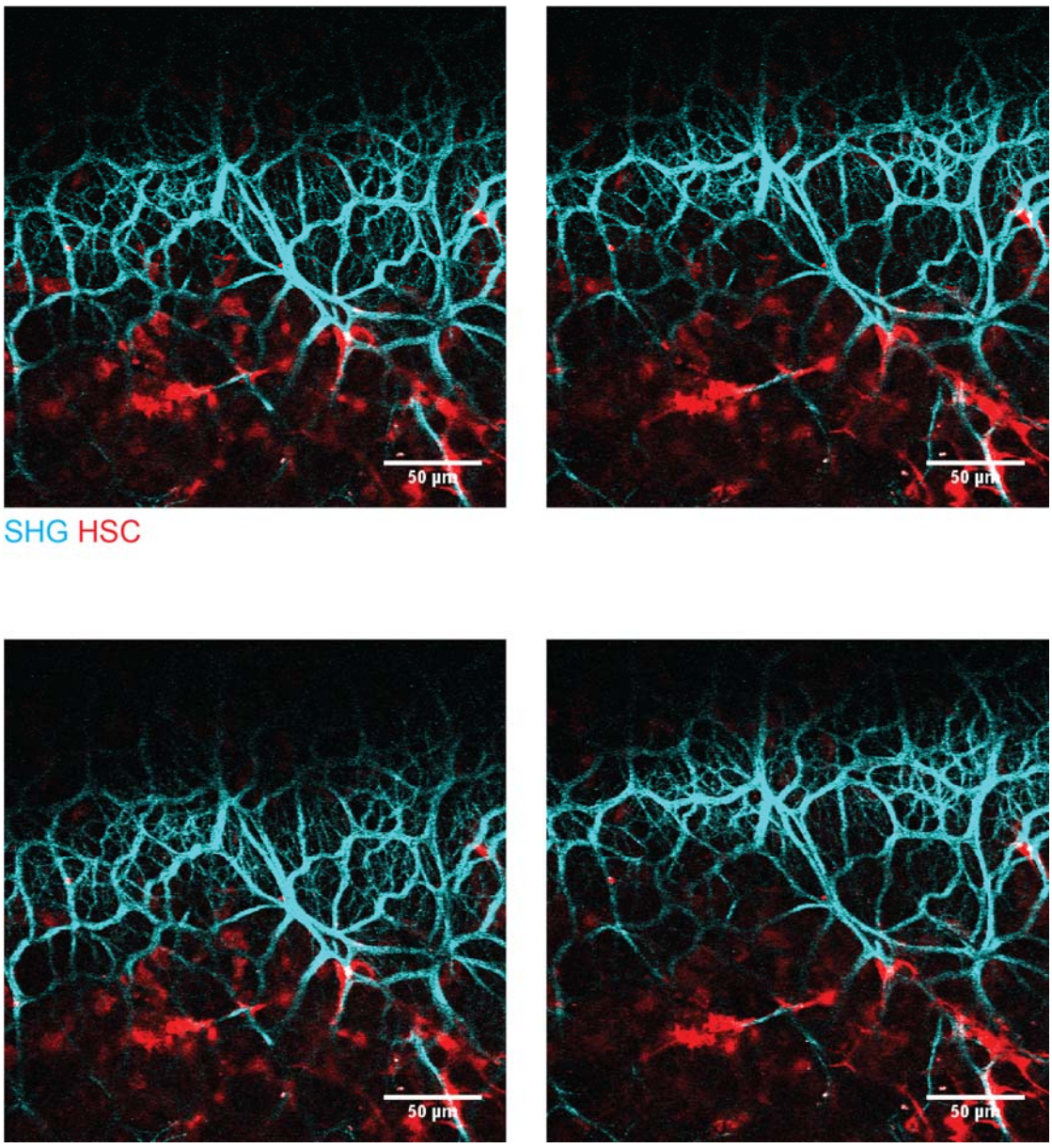

Figure 5.15 IVM of uninjured PDGFRβCre$^{+/-}$;Ai14 liver capsule under terminal anaesthesia

Sequential stills from timelapse. Collagen-rich capsule shown using SHG, with high density of HSC (shown in RFP) immediately below the capsule.

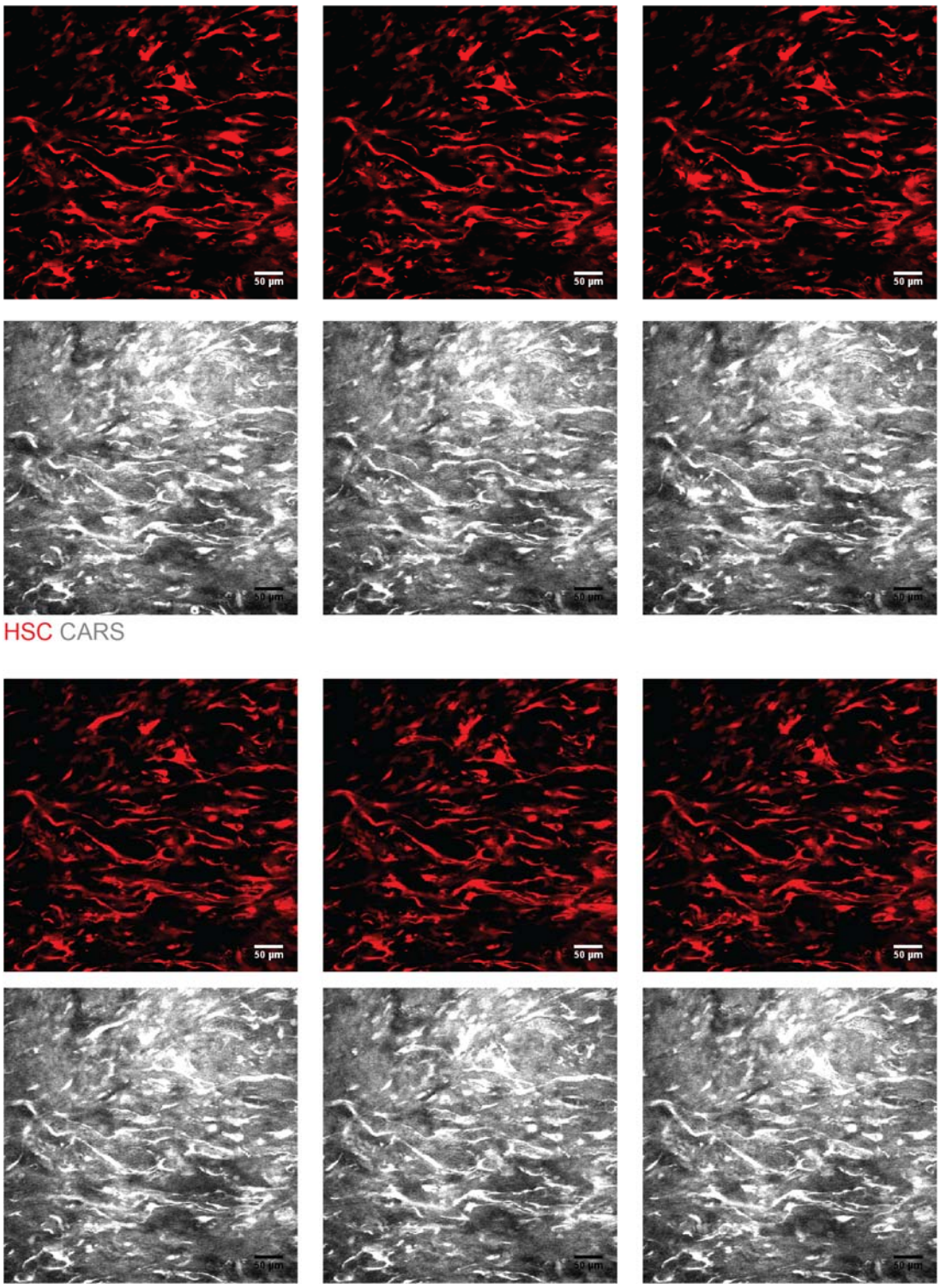

Figure 5.16 IVM of Jo-2 antibody-injured PDGFRβCre$^{+/-}$;Ai14 liver under terminal anaesthesia

Sequential stills from timelapse imaging. Top panel shows fluorescent reporter; lower panel shows corresponding CARS image. Animals imaged two weeks after AIW surgery.

Aiming to image a single mouse multiple times throughout the hepatic regenerative process, the next experiment was designed to sequentially image macrophages and their spatial relationship to collagen scar. The CCL_4 model of chronic liver injury was therefore used. Imaging of MacGreen mice was undertaken over consecutive days, following cessation of chronically-administered (twice weekly for four weeks) CCL_4 injections. In this experiment, animals underwent AIW surgery and in vivo imaging 48 hours after their last CCL_4 injection. They were allowed to recover after this first imaging session, then anaesthetized and imaged again the following day (Figure 5.17 A(i-iii)). In this preliminary experiment, the animals only underwent in vivo imaging on two days. However livers were also imaged ex vivo (48 hours and one week after the last CCL_4 injection); figure 5.7.11 B(i) shows a high density of macrophages around the collagen scar in the early time point. At one week, the macrophages appeared more uniformly distributed throughout the parenchyma. This highlights the utility of this approach for investigating immune cell migration during the fibrotic response.

Finally, to assess the potential utility of our AIW system to image cellular processes during hepatocarcinogenesis, we performed IVM of DEN-induced HCC. Figure 5.18 shows a macroscopic image of an HCC within a harvested liver. In this experiment, $AlbCre^{+/-}$;Confetti mice were used, in which hepatocytes express RFP, GFP, cyan or YFP as detailed above. Initial ex vivo images taken using the MP microscope demonstrated a number of cells expressing fluorescent proteins, which morphologically looked more like HSC than hepatocytes. This was captured at high magnification and resolution (Figure 5.18 C) and it was postulated that this could represent epithelial-mesenchymal transition within the tumour. Other ex vivo images obtained showed large patches of fluorescent cells, although at times there was degradation of fluorescence raising the possibility of necrosis within the tumours affecting fluorophore expression. Figure 5.19 demonstrates that it was possible to place an AIW on an area of HCC and perform IVM. The CARS images provide evidence that this technique could, for example, be used to analyse blood flow an angiogenesis within HCC and the surrounding parenchyma.

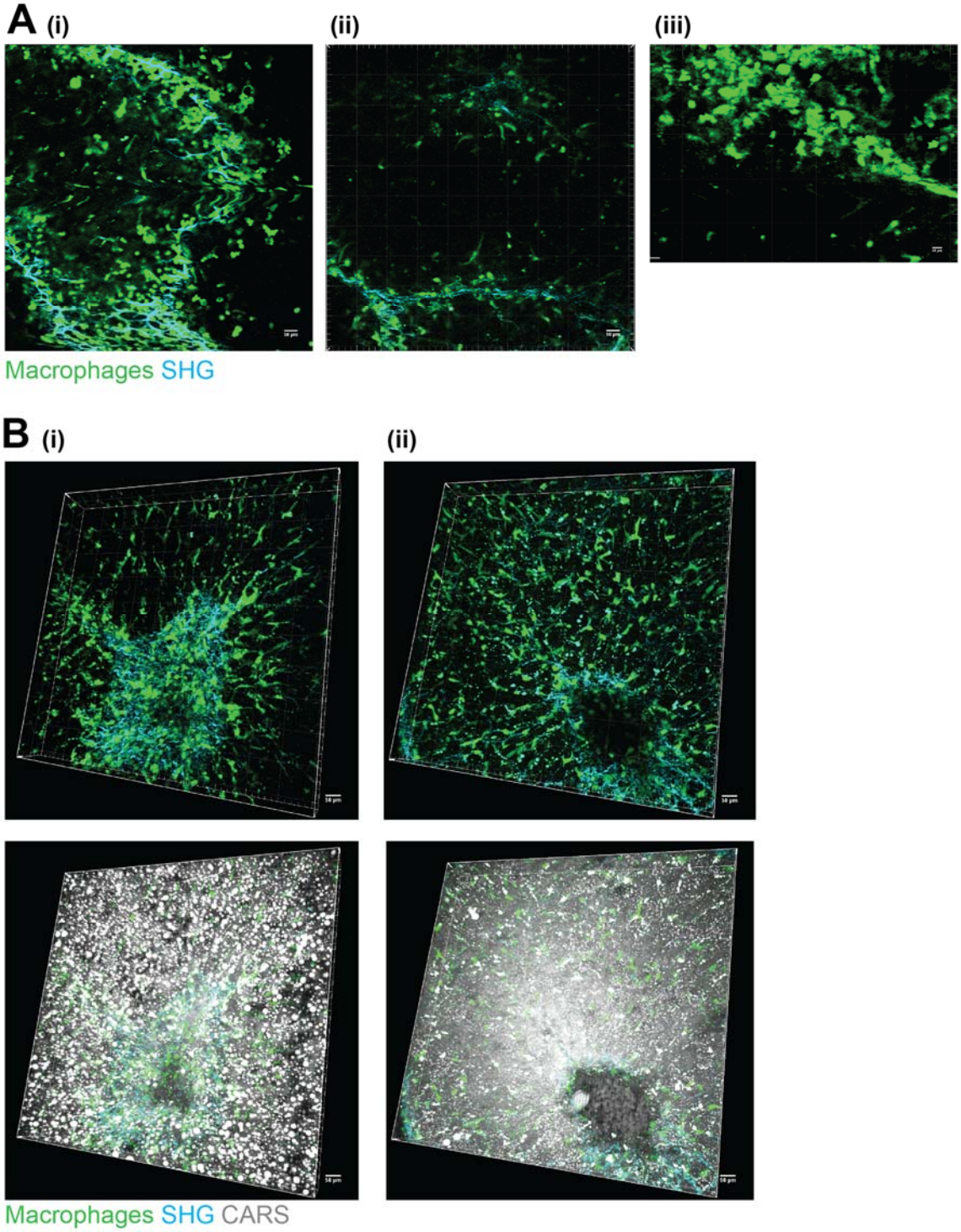

Figure 5.17 Serial imaging of CCL_4-injured MacGreen liver

A (i) Still from timelapse, in vivo imaging, day 1 post-chronic CCL_4 treatment. **(ii)** and **(iii)** Still from the same animal, imaged again in vivo the following day. **B** Ex vivo images of liver in a dish. Images reconstructed using imaris software. **(i)** Day 1 post-chronic CCL_4 treatment. Collagen scar (SHG) visible, with high macrophage density.

Lower panel image shows fat infiltration, assessed using CARS. **(ii)** Day 7 post-chronic CCL_4 treatment. Macrophages appear more evenly spread throughout the parenchyma, rather than concentrated around areas of collagen scar.

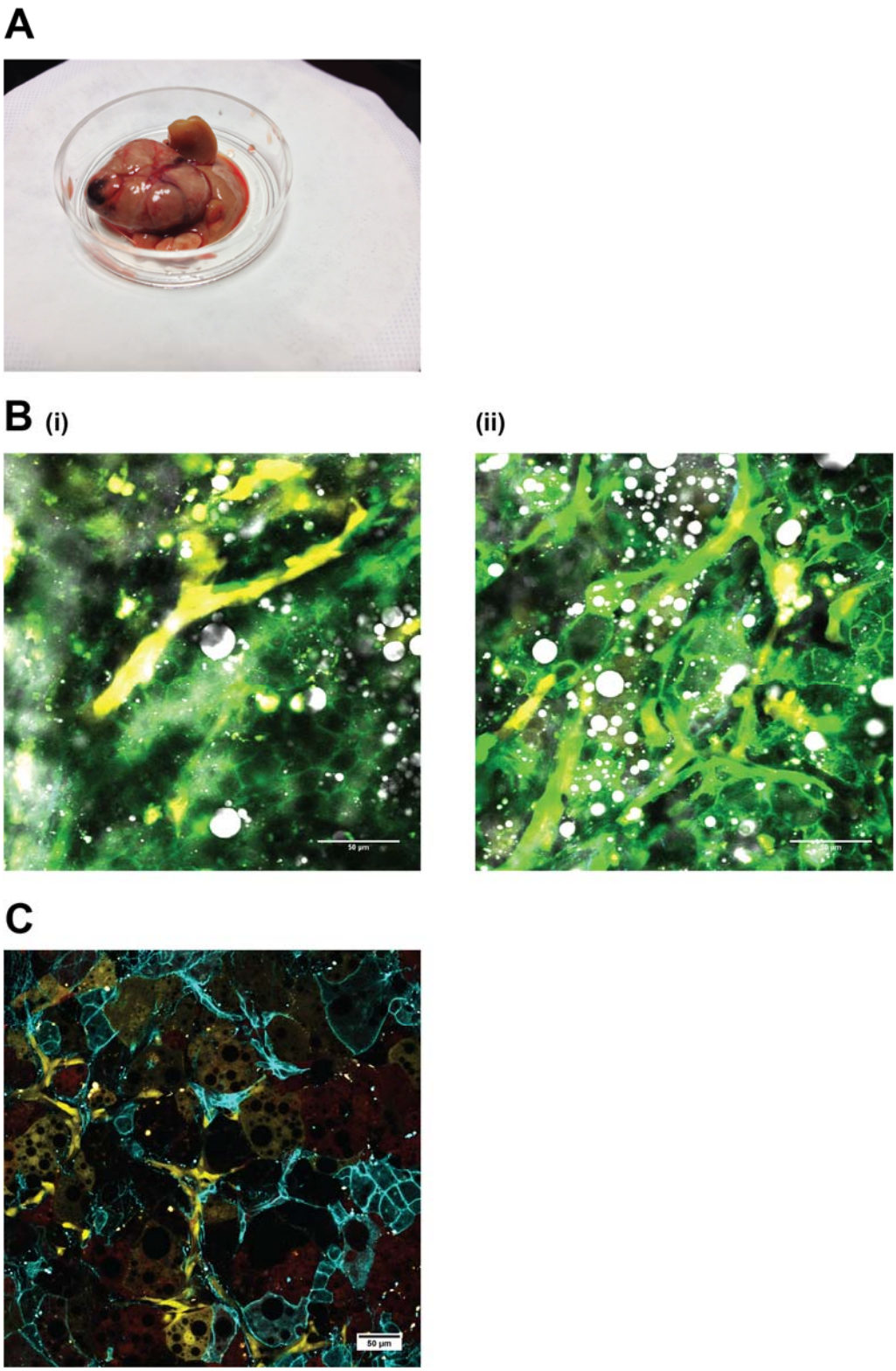

Figure 5.18 MP microscopy of DEN-induced HCC ex vivo

A Macroscopic image of HCC ex vivo **B** AlbCre$^{+/-}$;Confetti liver in a dish, harvested 10 months after DEN injection. High resolution image of liver tumour, including CARS channel showing fat droplets within the tumour. Yellow cells with apparent HSC

morphology likely represent EMT within the tumour. **C** Higher magnification image of tumour within same mouse liver, again showing probable EMT.

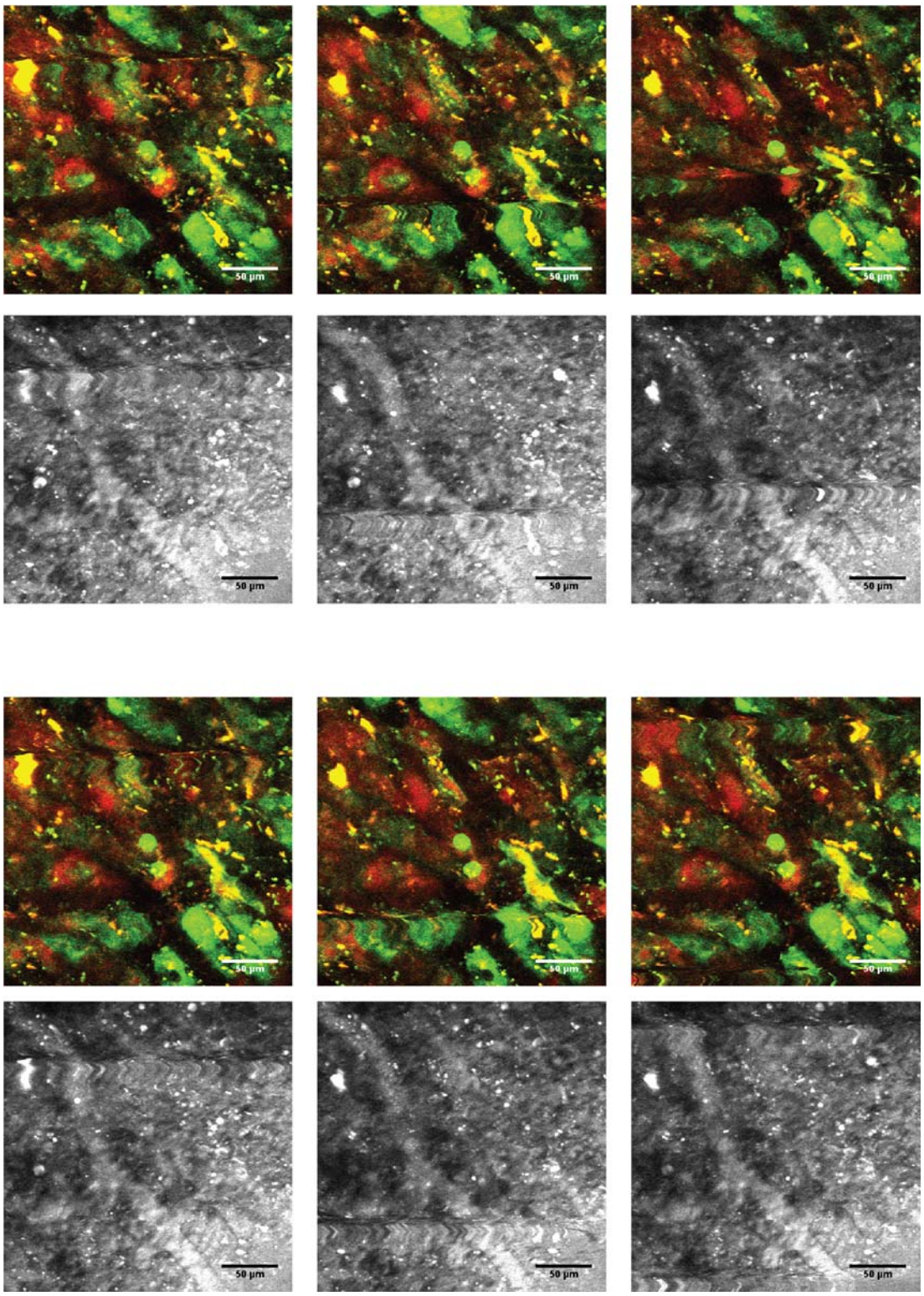

Figure 5.19 IVM of DEN-induced HCC under terminal anaesthesia

Sequential stills from timelapse of AlbCre$^{+/-}$;Confetti liver imaged in vivo, 10 months after DEN injections. Bottom panel shows corresponding CARS channel image in each case.

5.5 Discussion

The experiments presented above demonstrate that it is feasible to image mouse liver in vivo, via an AIW, in a broad range of different liver injury models. An extensive range of fluorescent reporter mice were used, in order to allowing imaging of multiple hepatic cell lineages. This is, to our knowledge, the first time this method has been employed in the UK. We therefore had to perform a series of pilot experiments, to prove the surgery and imaging were well tolerated by the mice. For each reporter mouse strain we began with imaging liver ex vivo to optimize microscope settings for detection of the specific fluorescent report in that particular strain of mouse. We progressed to live imaging under terminal anaesthesia, imaging animals after having a window in for up to 2 weeks, and finally imaging on consecutive days. The results were then presented to the veterinary Home Office team. As the animals recovered from window surgery rapidly, and tolerated subsequent anaesthesia and imaging well, we then incorporated induction of acute liver injury into our protocols, namely paracetamol overdose or partial hepatectomy. The development and utilization of these IVM models will be discussed in the following chapter.

Throughout these experiments, surgical and imaging techniques were further refined and optimised. I found that imaging quality was highly dependent on how successful AIW surgery was. This improved significantly with experience. Initially, there were two cases of wound dehiscence and therefore dislodgement of the AIW, necessitating culling of the animal. This was prevented by improvement in accurately sizing the laparotomy incision, and better placement of the purse string suture. Other than these initial complications relating to surgery, there were no problems with maintenance of the AIW in live animals; specifically the coverslips never cracked or dislodged in between imaging sessions, and no mice developed sepsis. Occasionally in early experiments, too little glue was used to fix the liver to the AIW, resulting in poor images. Achievement of a tight seal with tissue glue was imperative, to prevent introduction of fluid from the peritoneal cavity into the space below the coverslip, which restricted views and imaging quality. I also found that placing the AIW on the large left lobe of the liver (as opposed to the median lobe) minimized movement artefact. Pre-treatment of the coverslip with PEG solution prior to AIW placement was also critical to avoid thick biofilm development, rendering imaging impossible. For sequential imaging, the AIW design was modified to include a domed underside, for better apposition to the liver surface.

During imaging, I found that low-flow anaesthesia helped reduce respiratory movement-induced artefact, which was consistent with the findings of Akbari et al.[473] In conjunction

with saline boluses at the start and end of imaging, the low-flow anaesthesia also aided recovery (typically animals were feeding and grooming within ten minutes of finishing imaging sessions). Fixation of the animal in the imaging box was also important in reducing movement artefact. Therefore, we designed an improved base plate for the box, which has a more secure fixation mechanism.

Experiments in which the animals were maintained for a week or more with an AIW in situ allowed us to gain experience in deciding how often the coverslip requires to be changed during sequential IVM of the liver. We usually replaced the coverslip every 48-72 hours as longer intervals resulted in the development of a thick biofilm that could not be safely removed. At the start of imaging, the liver was examined using epifluorescence. If views were poor, the coverslip was removed (under anaesthesia and using aseptic technique) and the exudate on the liver surface gently teased away with a needle and saline washes. There were some initial problems with haemorrhage during this procedure, but with increasing operator experience this was minimised.

Timelapse imaging was often briefly limited by loss of the water droplet between the objective and the AIW. At times this occurred every five to ten minutes. This interval was lengthened by ensuring as tight a seal as possible (by optimising fixation of the animal with the imaging box) and by extra hair removal around the AIW (using hair removal cream as well as clippers) to prevent wicking away of the water droplet.

Overall, I have shown here that intravital imaging of the liver can be performed, via an AIW, multiple times in the same animal. To the best of our knowledge, this is the first time this has been achieved in the UK. Use of specific fluorescent reporter mice, coupled with label-free microscopy techniques allows interrogation of different hepatic cell lineages and their interactions with other cell types and the microenvironment. I have extensively characterised a number of different transgenic reporter mice strains, particularly those in which HSC and hepatocytes express fluorescent proteins, to inform subsequent longer term experiments focusing on cellular behaviour during acute liver injury and regeneration.

Furthermore, I have demonstrated that it is feasible to image DEN-induced HCC in vivo, via an AIW. As previously discussed, the DEN model is a well-established method of studying HCC. To the best of our knowledge, mature tumours from this model have not previously been imaged in vivo; this provides a novel opportunity to undertake experiments designed to unpick subtle differences in tumour biology and blood flow, that may only be detectable using an IVM system, and may also allow in-depth study of targeting and efficacy of novel chemotherapeutic agents, in the setting of HCC.

In summary, I have acquired significant experience in IVM, and have developed new protocols for real-time, sequential imaging of the mouse liver in a range of different injury models for the first time. The data presented serve as a strong platform on which to base our future IVM studies of liver injury, regeneration and repair.

Chapter 6: Intravital imaging of paracetamol-induced acute liver injury

6.1 Introduction

IVM experiments studying acute liver injury have, to date, been performed by exteriorization of the liver, or similar methods, allowing at most one or two short duration microscopy sessions. As discussed in the previous chapter, I hoped to develop a mouse model in which acute liver injury could be studied in vivo, sequentially, throughout the course of liver injury and repair. I was confident that the AIW approach would allow this; in particular, from my preliminary IVM experiments, I had established that crossing mTmG mice with cell specific promoters allowed clear identification of liver architecture, as well as cells of interest. In view of evidence suggesting LSEC take up paracetamol directly, I was also interested in using reporter mice in which I could image the microvasculature during liver injury, perhaps allowing quantification of angiogenesis around necrotic tissue. I therefore designed a series of experiments to first establish that the mice could tolerate acute liver injury and imaging following abdominal surgery, and then to confirm that parameters of damage and regeneration were similar with, and without, an AIW in situ. These will be presented in the following results section, along with subsequent sequential imaging experiments, using a number of different fluorescent reporter mice.

6.2 Aims

- To develop a protocol for sequential (daily) IVM of the liver, throughout the course of paracetamol-induced acute liver injury and recovery in the mouse
- To characterise the inflammatory infiltrates and regenerative response in paracetamol-induced liver injury in mice, with and without, an AIW
- To image fluorescent reporter mice strains in vivo, throughout the course of acute liver injury, aiming to capture images of the necrotic areas, surrounding vasculature and local blood flow.

6.3 Materials and methods

Animals

Animal details are as previously stated (section 5.3). Additionally, for use in the following experiments, Cdh5-cre-ERT2 mice (Tg(Cdh5-cre/ERT2)1Rha)[393] were crossed with Ai14 (B6;129S6-Gt(ROSA)26Sortm14(CAG-tdTomato)^{Hze}/J)[484] or mTmG (B6.129(Cg)-Gt(ROSA)26Sortm4(ACTB-tdTomato,-EGFP)^{Luo}/J)[485] mice, obtained from Jackson

Laboratories. Cre recombinase was induced by tamoxifen injection. Tamoxifen was prepared in corn oil (20mg/ml) and given IP 100mg/kg daily for three days, followed by three days of rest, then daily for three days.

Lastly, *Pdgfrb*-BAC-eGFP reporter mice (on a C57/Bl/6 background) were crossed with mTmG mice, and Cdh5Cre$^{+/-}$;Ai14 mice. *Pdgfrb*-BAC-eGFP (Tg(Pdgfrb-EGFP)JN169Gsat)[234] animals express one copy of a BAC transgene expressing eGFP under the control of *Pdgfrb* regulatory elements.

Immunohistochemistry on mouse liver specimens

Paraffin-embedded sections were processed for immunohistochemistry as described previously. For BrdU staining, mice were injected with 100mg/kg BrdU (Roche 10280879001, Sigma) IP, two hours before tissue harvesting. Tissue was fixed in methacarn prior to paraffin embedding. For BrdU IHC, briefly, tissue sections were deparaffinised, and exposed to 0.3% hydroxen peroxide in deionised water for 10 minutes to block endogenous peroxidase. They were then treated with hydrochloric acid, and incubated with trypsin 0.1% for 20 minutes. Slides were washed with 0.1M sodium tetraborate decahydrate (Sigma S9640) and then PBS, before blocking with M.O.M. mouse Ig blocking reagent (Vector Laboratories, PK2200). The primary antibody, mouse anti-BrdU (Dako M0744) was applied (1:40 dilution in M.O.M diluent) for 30 minutes at room temperature. The secondary antibody was M.O.M. biotinylated anti-mouse IgG reagent, diluted 1:250 in M.O.M. diluent, and left for 10 minutes at room temperature. DAB reagent was then applied, followed by counterstaining with Harry's Haematoxylin and dehydration through alcohols as previously described.

For GR1 staining, 1:750 rat monoclonal anti-GR1 (RND Mab 1037) was used as the primary antibody (left overnight) and 1:1000 goat anti-rat biotinylated IgG, (mouse adsorbed, Vector 1928) was the secondary antibody (incubated for 30 minutes at room temperature). No antigen retrieval step was required in this protocol.

Image analysis of immunostained sections

Microscopic examination of tissue specimens and digital image analysis was performed as described in section 2.4.3. Quantification of regeneration index was performed by direct cell counting (of BrdU positive hepatocytes, and total number of hepatocytes) from 20 consecutively selected high-powered fields (x20 magnification) from each liver

section. Hepatocyte regeneration index was calculated by: BrdU positive hepatocytes/total number of hepatocytes x 100.

Twenty consecutive high-powered fields from each GR1-stained liver section were also acquired. Number of GR1-positive cells (with characteristic neutrophil morphology) was counted for each high-powered field, and an average number of positive cells/field calculated for each liver.

Induction of liver injury

For experiments investigating the effect of AIW insertion on paracetamol-induced liver injury, animals underwent AIW implantation surgery (as described in section 5.3). The night after surgery, they were allowed to recover, with food and water provided ad libitum. The following evening, they were fasted for 12-16 hours, then injected with 300mg/kg IP paracetamol. Control animals did not undergo AIW insertion, but were fasted at the same time, and received the same dose of paracetamol. Animals were then culled at either 24 hours, 48 hours, or one week. One lobe from each liver was fixed in 10% formalin. For BrdU staining, one lobe was fixed in methacarn.

Serum was stored at -80°C. ALT and other liver function test analyses were performed as described in section 4.5

For sequential imaging, (Figure 6.1), animals underwent AIW implantation surgery, then allowed to recover overnight. The following evening they were fasted for 12-16 hours, then underwent baseline imaging under general anaesthetic. Imaging sessions lasted up to one hour. Animals were given supplementary IP saline at the start of imaging, then were injected IP with 300mg/kg paracetamol at the end of the imaging session. Subsequent imaging sessions were performed 24 hours later, up to a maximum of three in total. After the last imaging session, animals were culled.

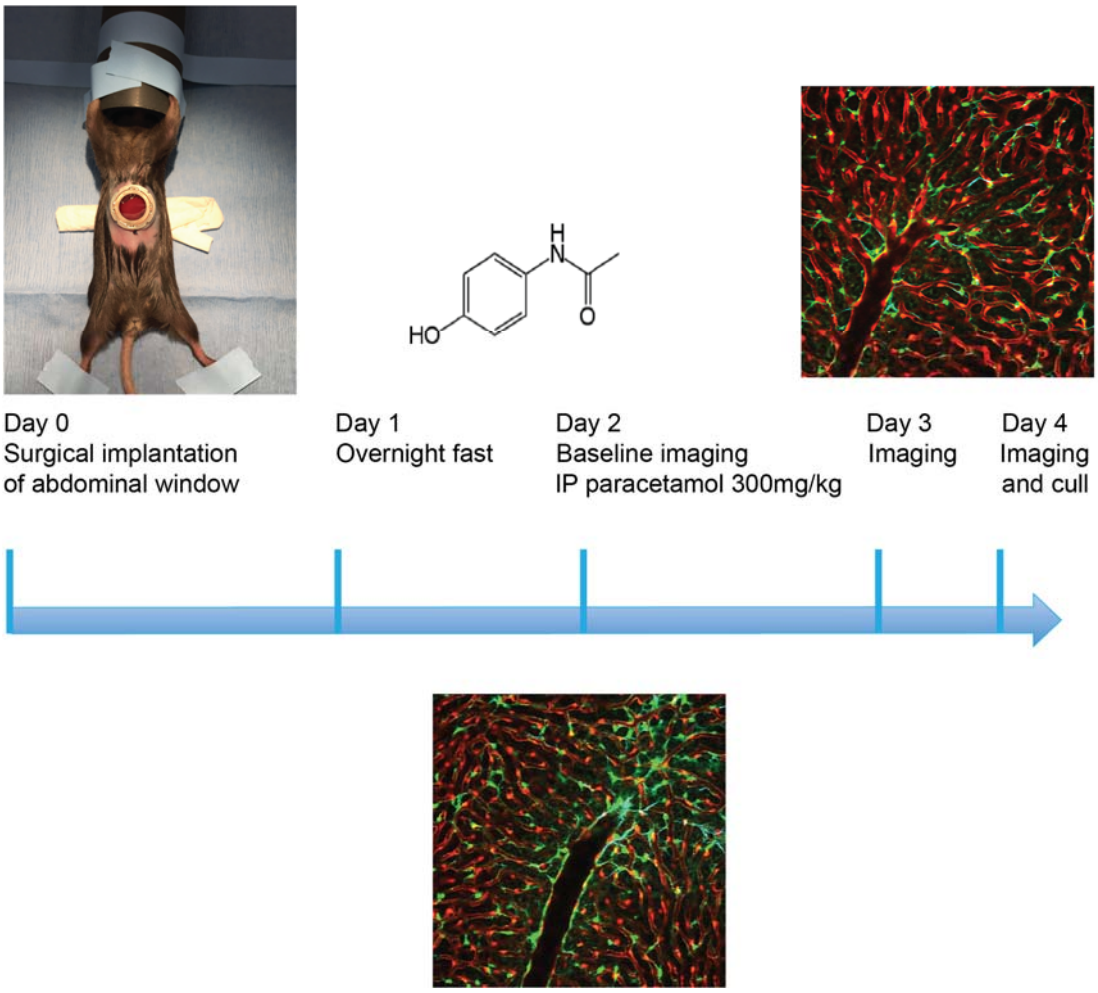

Figure 6.1 Schematic of AIW implantation, paracetamol administration, and sequential imaging

6.3 Characterisation of injury and inflammatory infiltrate following paracetamol administration, with and without abdominal window

In these experiments, animals with, and without an AIW received 300mg/kg paracetamol after an overnight fast. Animals were harvested at 24 hours, 48 hours, or one week, and markers of injury, HSC (PDGFβ), neutrophils (GR1) and regeneration (BrdU) were quantified.

Severity of paracetamol-induced liver injury is similar in animals with an AIW, to non-operated controls

Figure 6.2 shows liver function tests and quantification of injury at each time point. At 24 hours, (n=6 in each group) mean percentage necrosis was 45.75 $\pm$ 4.80 in controls, and 45.25 $\pm$ 3.10 in AIW animals, which was not significantly different (p=0.93). Similarly, at 48 hours, (n=4 in each group) mean percentage necrosis was not significantly different between groups (24.65 $\pm$ 5.89 in controls, 27.46 $\pm$ 5.25 with AIW, p=0.73). At one week, liver architecture had recovered, and there were no clear areas of necrosis to quantify. This was consistent with ALT levels, which had also returned to normal (27 $\pm$ 2.61 vs 28.5 $\pm$ 6.51, p=0.84).

Serum ALT at 24 hours was 5248 $\pm$ 856 in controls, and 4745 $\pm$ 952.8 in the AIW group (no difference, p=0.70). At 48 hours serum ALT had dropped to 472.5 $\pm$ 180.3 in controls, and 293.5 $\pm$ 49.16 in window mice. This was not significantly different (p=0.70, n=4 in each group).

Other liver function tests were all comparable at each time point, apart from ALP at 48 hours, which was higher in controls than AIW mice (175.3 $\pm$ 14.59 vs 108 $\pm$ 7.62, p=0.007). This is of uncertain significance.

Hepatic regeneration following paracetamol-induced liver injury is similar in animals with an AIW, to non-operated controls

BrdU-incorporation was quantified at 24 and 48 hours (Figure 6.3). At 24 hours, percentage BrdU-positive hepatocytes was 0.36 $\pm$ 0.12 in controls, and 0.83 $\pm$ 0.50 in AIW animals, p=0.34, n=6 in each group. At 48 hours, this had increased to 5.85 $\pm$ 1.46 in controls and 7.47 $\pm$ 2.29 in AIW mice (p=0.57, n=4 in each group).

Liver to body weight ratio was also similar at one week, suggesting liver regeneration is similar in both groups (5.46 $\pm$ 0.09 in controls and 5.96 $\pm$ 0.41 in the AIW cohort, p=0.28).

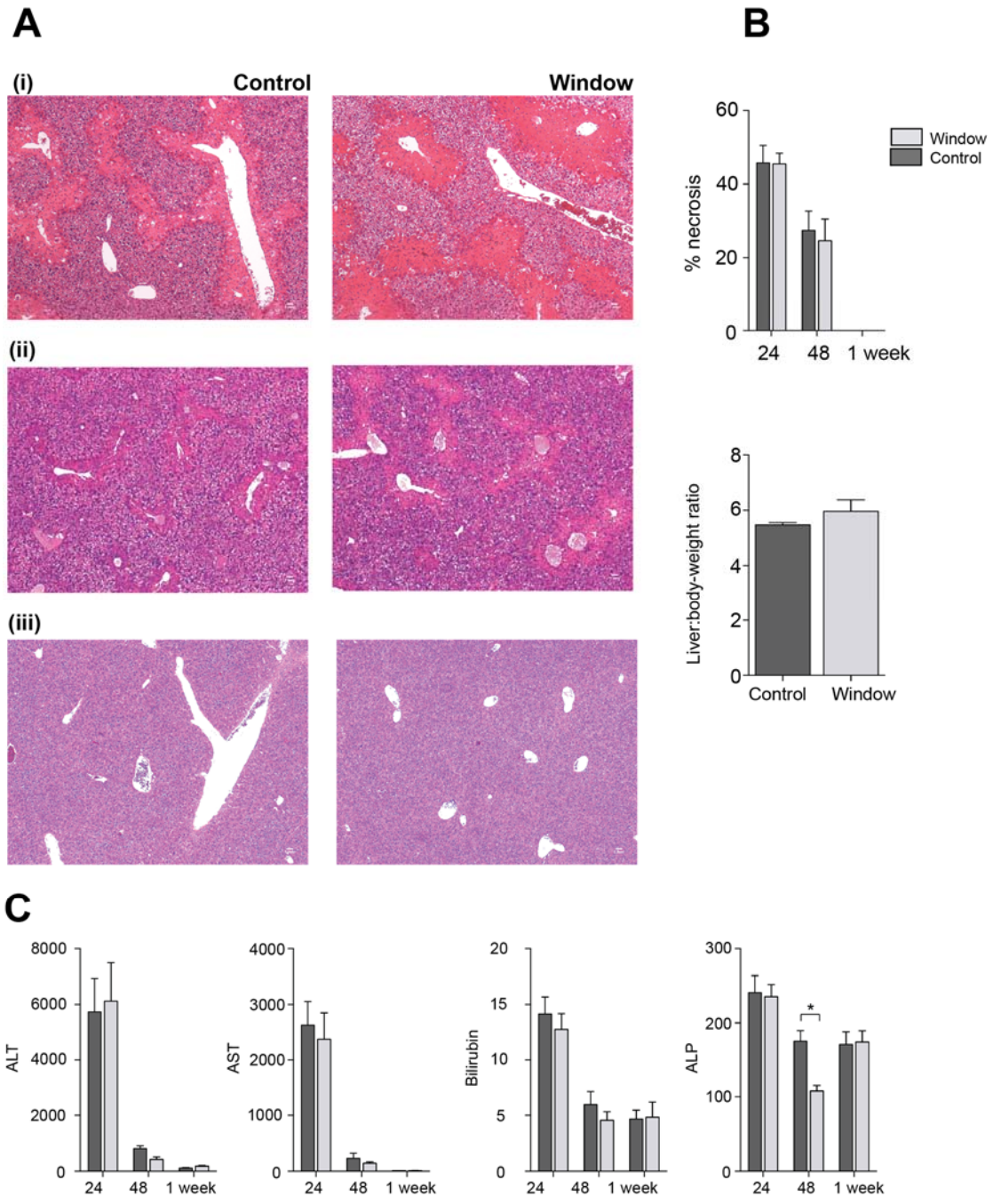

Figure 6.2 Paracetamol-induced acute liver injury with and without an AIW in situ

A Comparison of liver histology (H and E) between animals with an AIW and non-operated controls, following 300mg/kg IP paracetamol, at (i) 24 hours, (ii) 48 hours, and (iii) 1 week; (x5 magnification). **B** Graph showing percentage necrosis at 24 and 48 hours post-paracetamol, for AIW and control animals (n=6 in each group at 24 hours, n=4 in each group at 48 hours and 1 week). Graph below shows there was no difference in liver:body weight ratio at 1 week (n=4 in each group). **C** Graphs showing similar serum

bilirubin and liver enzyme levels at 24 hours, 48 hours and 1 week, in animals with an AIW and non-operated controls.

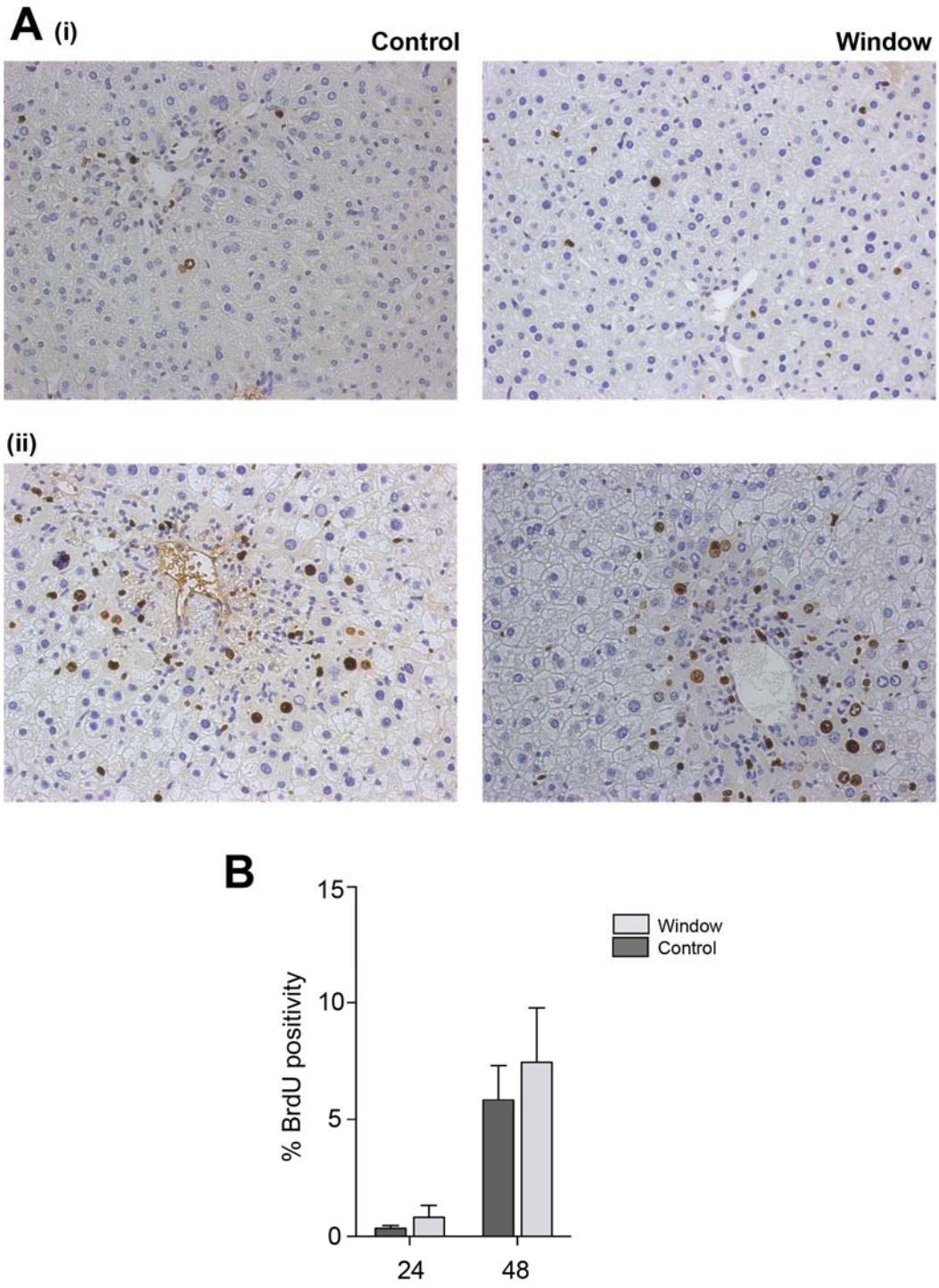

Figure 6.3 The hepatic regenerative response following paracetamol-induced acute liver injury, with and without an AIW in situ

A Comparison of BrdU staining positivity between animals with an AIW and non-operated controls, following 300mg/kg IP paracetamol at **(i)** 24 (n=6 each group) and **(ii)** 48 hours (n=4 in each group); x20 magnification. **B** Graph showing percentage BrdU positivity at 24 and 48 hours post-paracetamol.

6.4 Characterisation of quiescent and activated HSC and neutrophil infiltrate following paracetamol-induced acute liver injury in animals with an AIW, and non-operated controls

PDGFRβ staining positivity was calculated at 24 hours, 48 hours and one week following paracetamol-induced liver injury (Figure 6.4). At 24 hours, percentage staining positivity per low-powered photomicrographic field was 4.21 $\pm$ 0.39 in controls, and 5.32 $\pm$ 0.66 in AIW animals (p=0.20, n=5 controls, n=6 AIW). At 48 hours this had risen to 11.66 $\pm$ 2.68 and 9.26 $\pm$ 1.32 in controls and AIW mice respectively. This was not significantly different, p= 0.45 (n=4 in each group). By one week, PDGFRβ percentage positivity had reduced to 7.16 $\pm$ 0.78 in controls, and 5.81 $\pm$ 1.25 in the AIW group, which was again not significant, p=0.38 (n=4 controls, n=3 AIW group).

GR1 staining positivity was also calculated at 24 hours, 48 hours and one week following paracetamol-induced liver injury (Figure 6.5). At 24 hours, mean number of GR1-positive cells per high-powered field was 13.14 $\pm$ 1.13 in controls, compared with 20.24 $\pm$ 3.68 in AIW animals. This was significantly different (p=0.003, n=6 controls, n=5 AIW group). By 48 hours this difference had disappeared; GR1 positivity had reduced to 11.41 $\pm$ 2.21 in controls and 14.14 $\pm$ 1.20 in the AIW group (p=0.32).

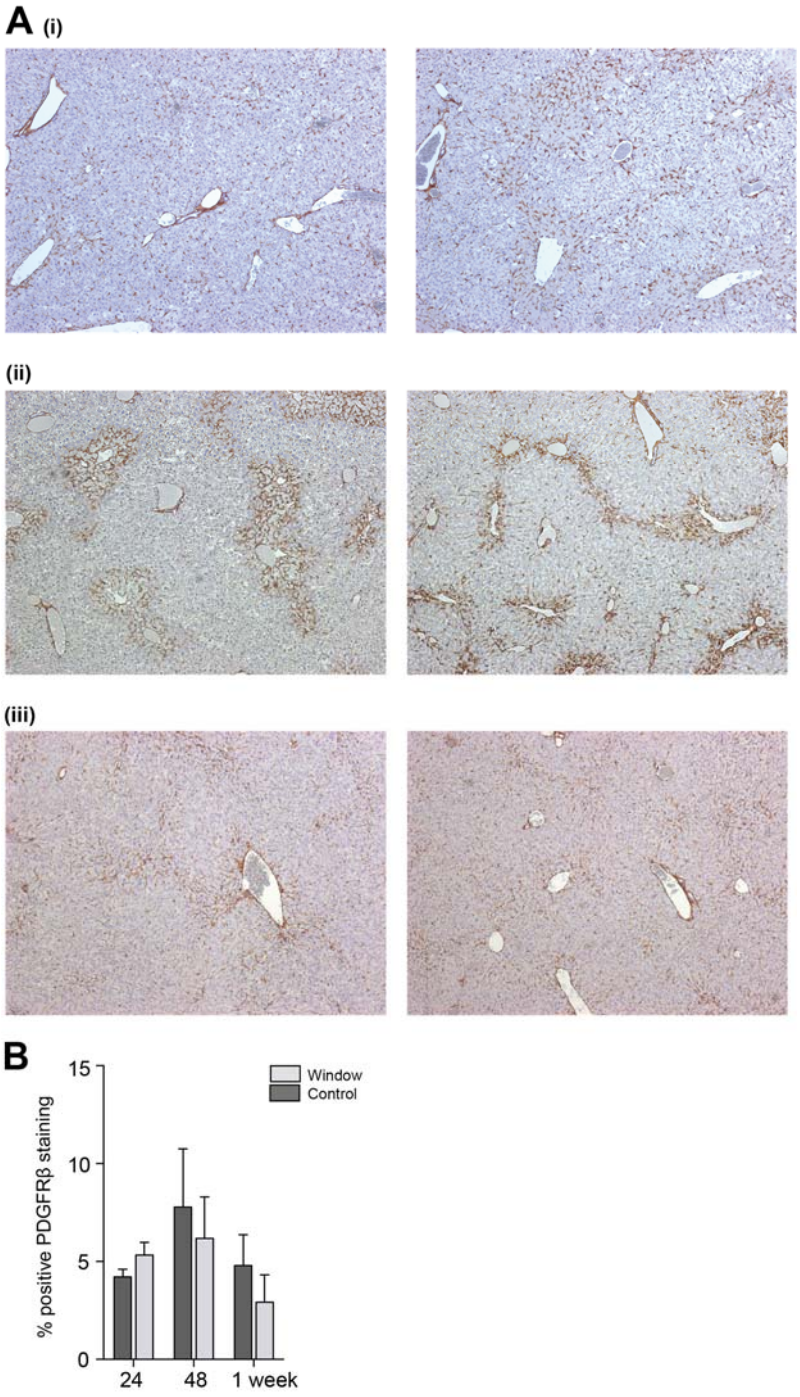

Figure 6.4 PDGFRβ staining positivity following paracetamol-induced acute liver injury, with and without an AIW in situ

A Comparison of PDGFRβ staining positivity between animals with an AIW and non-operated controls, following 300mg/kg IP paracetamol at **(i)** 24 hours (n=5 controls, n=6 AIW) **(ii)** 48 hours (n=4 in each group) and **(iii)** 1 week (n=4 controls and n=3 AIW). x5 magnification. **B** Graph showing percentage PDGFRβ staining positivity, for AIW and control animals, at 24 hours, 48 hours and 1 week.

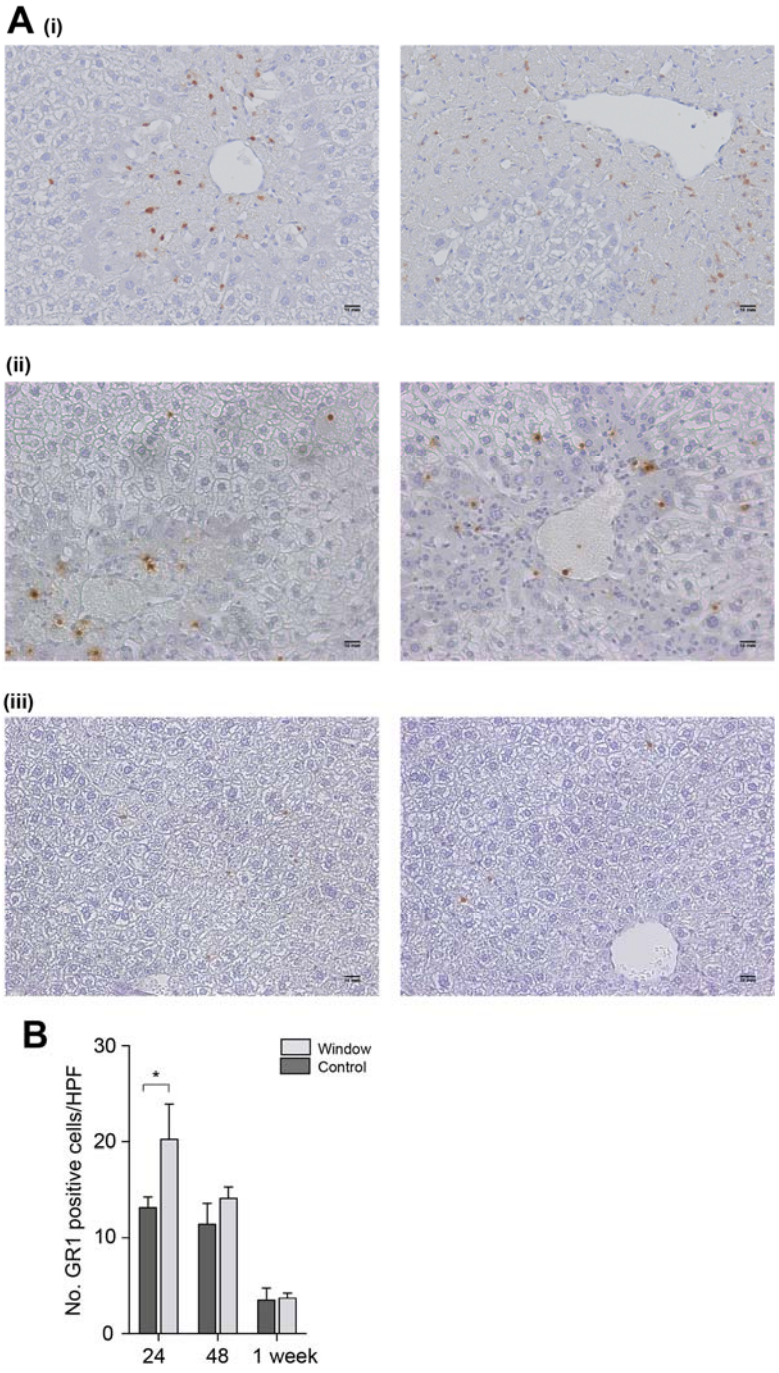

Figure 6.5 GR1 staining positivity following paracetamol-induced acute liver injury, with and without an AIW in situ

A Comparison of GR1 staining positivity between animals with an AIW and non-operated controls, following 300mg/kg IP paracetamol at **(i)** 24 hours (n=6 each group) **(ii)** 48 hours (n=4 in each group) and **(iii)** 1week (n=4 in each group). x20 magnification. **B** Graph showing number of GR1 positive cells per high-powered field (HPF), for AIW and control animals, at 24 hours, 48 hours and 1 week.

6.5 Sequential daily imaging of paracetamol-induced acute liver injury

Paracetamol-injured Cdh5Cre$^{+/-}$;Ai14 liver ex vivo

In *Cdh5*-Cre mice crossed with Ai14 reporter mice, LSEC express TdTomato. Initially, imaging after paracetamol-induced liver injuy was performed ex vivo. Whole liver was imaged in a dish, to optimise MP microscope settings, and characterise the appearance of necrotic areas with this reporter. Figure 6.6 shows uninjured and injured liver specimens. There was more autofluorescence in necrotic areas (seen in green in Figure 6.6 B (i)) and I originally hypothesised that this could be used for daily quantification of the necrotic area. However, significant background levels of hepatic autofluorescence meant that it was not possible to clearly distinguish between areas of injury and normal tissue. This transgenic mouse strain did, however, label LSEC extremely efficiently, which would be adequate for quantitative analysis of the vascular networks (Figure 6.6 B (ii) around areas of necrosis.

IVM of paracetamol-injured Cdh5Cre$^{+/-}$;Ai14 liver

In the following experiment (Figure 6.7) animals underwent AIW implantation, followed by IP paracetamol (300mg/kg) as per Figure 6.1. IVM was performed daily for three days. At each imaging timepoint, a tiled multisite image was acquired, as well as several Z stacks. 24 hours post-paracetamol, Z stacks were obtained from areas that appeared necrotic (referring back to the multisite tile to identify regions of interest). Figure 6.7 shows images taken at baseline and 24 hours after paracetamol. High magnification CARS images show centrilobular hepatocyte disruption post-injury.

Figure 6.8 shows timelapse IVM under anaesthesia, from a Cdh5Cre$^{+/-}$;Ai14 animal, 24 hours post-paracetamol. Here, an area of necrosis was initially identified from a multisite tile; a single high magnification image was then obtained, confirming there was some hepatocyte damage using CARS. A timelapse of the area was then performed, over three minutes. Blood vessel outline could be clearly seen with this Cdh5Cre$^{+/-}$;Ai14 reporter, and blood flow within vessels was visible using CARS.

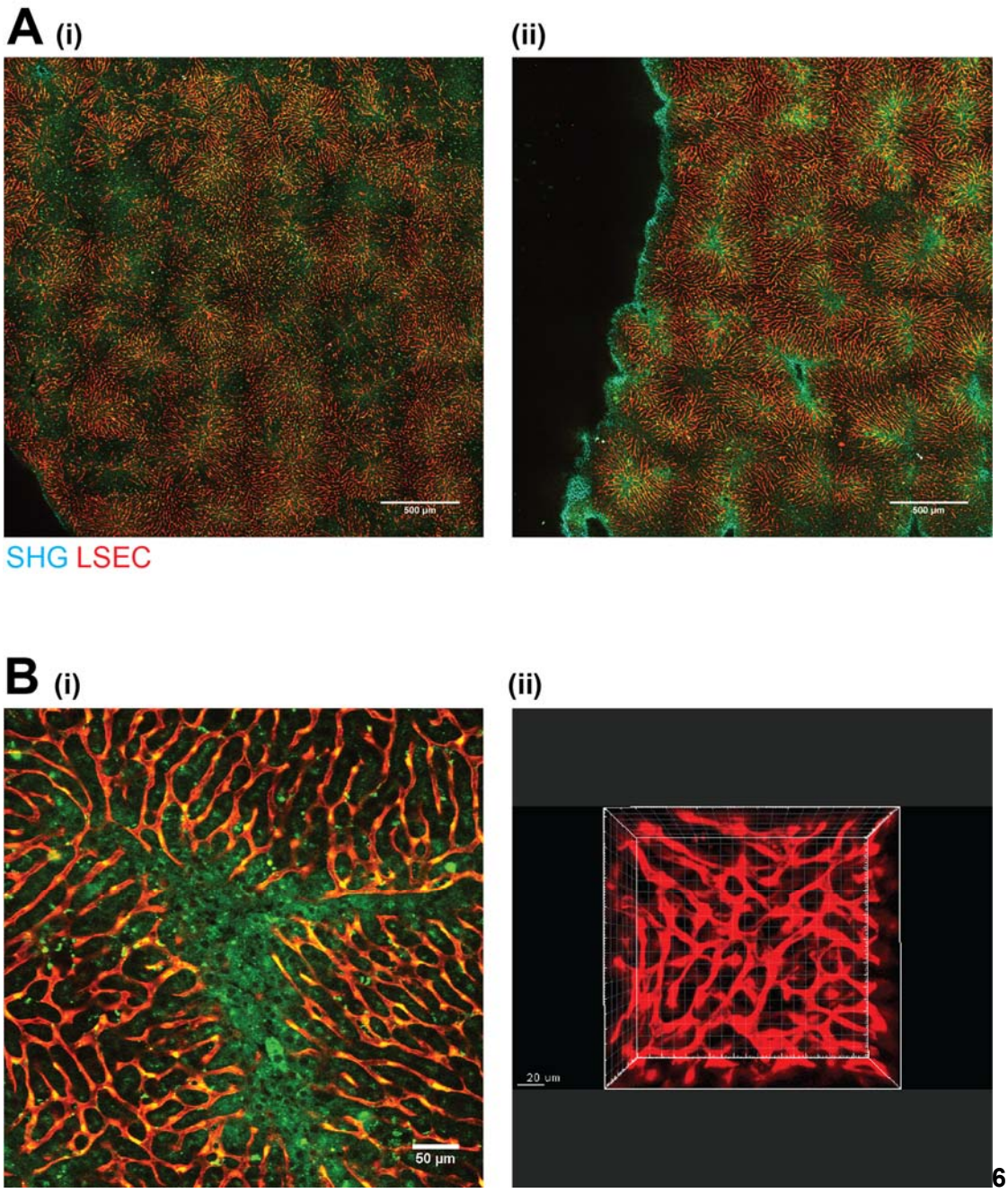

Figure 6.6 Paracetamol-injured and uninjured Cdh5Cre$^{+/-}$;Ai14 liver ex vivo

A Multisite tiled images of **(i)** uninjured and **(ii)** 24 hours post paracetamol-injured (350mg/kg) liver. **B (i)** Image from Z stack through necrotic area in paracetamol-injured liver (imaged in a dish). **(ii)** Reconstructed vascular network, from a small section of the Z stack in **(i)** acquired using Imaris software.

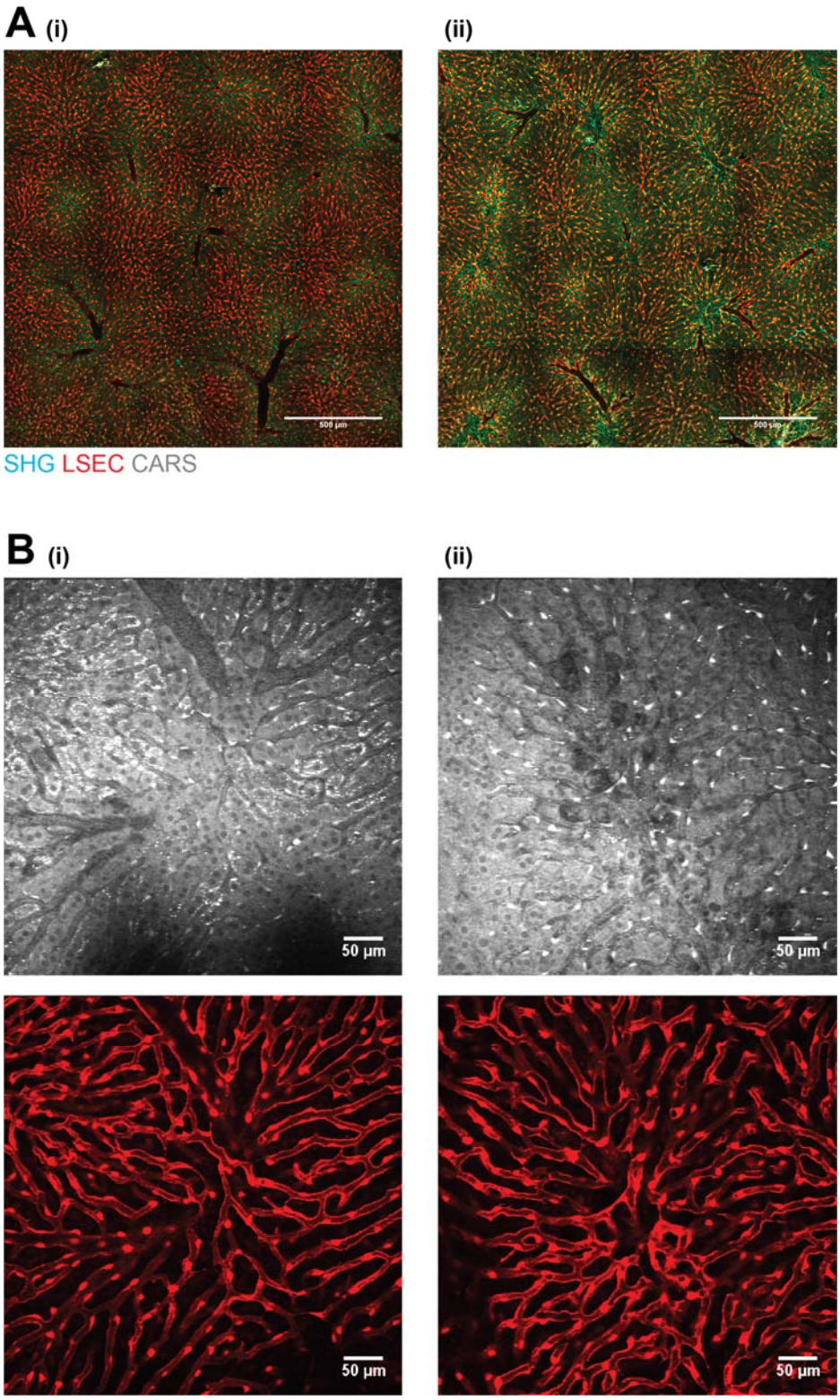

Figure 6.7 Serial IVM of Cdh5Cre$^{+/-}$;Ai14 mouse at baseline and 24 hours post-paracetamol, under anaesthesia

A Multisite tile of baseline **(i)** and injured **(ii)** liver, taken under anaesthesia. **B** Image taken from Z stack through liver (under anaesthesia) from **(i)** uninjured liver and **(ii)** 24

hours post-paracetamol, in an area of necrosis. Top panel shows CARS image, with hepatocyte damage visible in **(ii)**. Lower panel shows corresponding red channel images, depicting microvasculature using Cdh5Cre$^{+/-}$;Ai14 (LSEC) reporter.

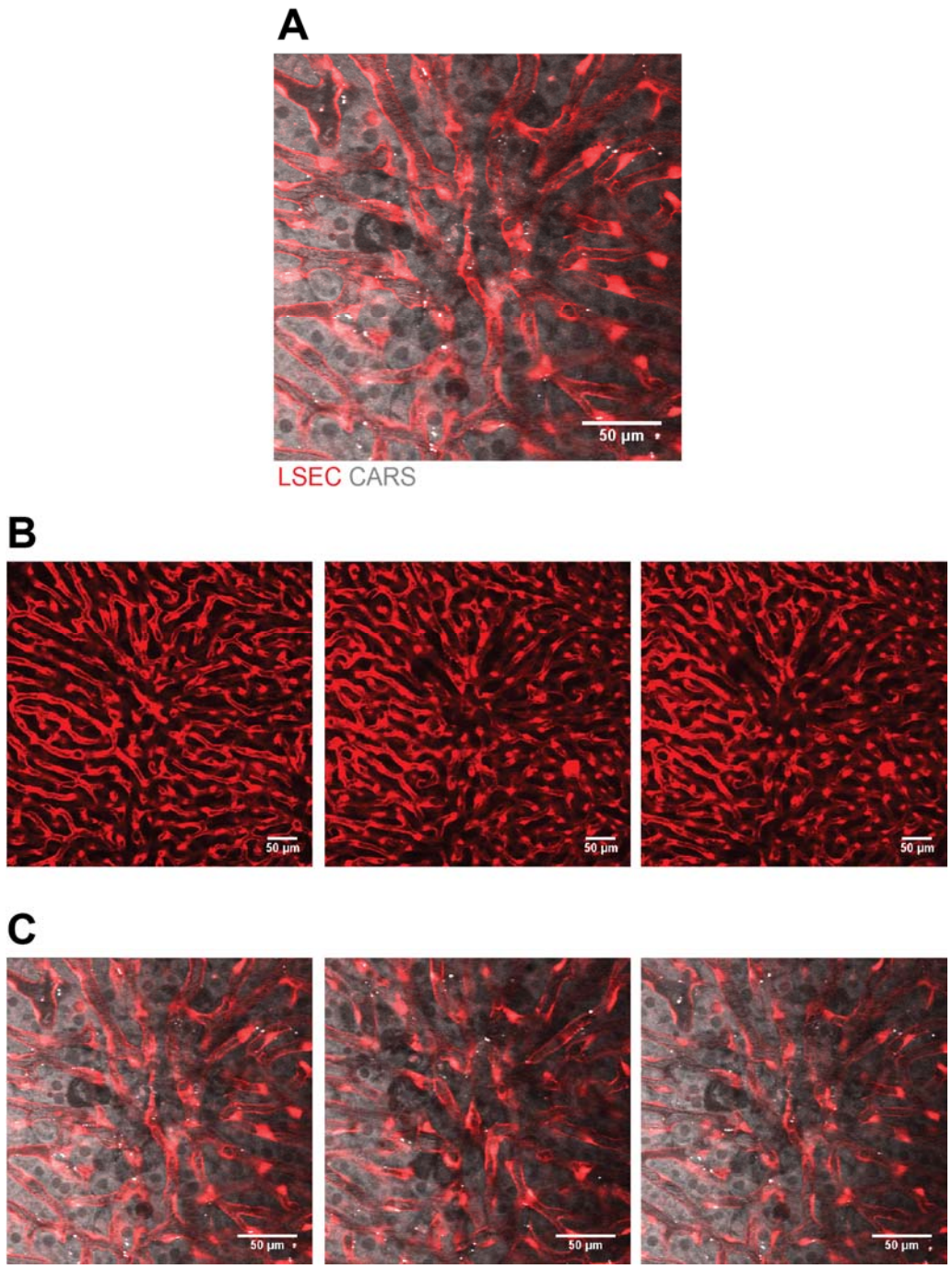

Figure 6.8 Timelapse IVM of Cdh5Cre$^{+/-}$;Ai14 mouse 24 hours post-paracetamol, under anaesthesia

A Single high magnification image of area of hepatocyte necrosis (RFP and CARS channel shown). **B** Sequential stills from timelapse imaging of same area over three minutes. **C** Corresponding timelapse images showing CARS as well as RFP channel.

IVM of paracetamol-injured Cdh5Cre$^{+/-}$Ai14;PDGFRβ-BAC-eGFP liver

Serial IVM before and after paracetamol-induced acute liver injury was also performed in Cdh5PBAG animals. In this fluorescent reporter mouse strain, LSEC are labelled red with Td tomato, and HSC are labelled with GFP. Figure 6.9 A shows multisite tiles from the same animal, taken by IVM under anaesthesia, (i) at baseline, (ii) 24 hours post-paracetamol and (iii) 48 hours post-paracetamol. This reporter strain allowed interrogation of HSC spatial relationship to LSEC (Figure 6.9 B and C).

IVM of paracetamol-injured Cdh5Cre$^{+/-}$;mTmG liver

Finally, serial IVM was performed on paracetamol-injured Cdh5Cre$^{+/-}$;mTmG animals. Here, LSEC are labelled with GFP, and all other cells express membranous RFP. Figure 6.10 A shows multisite tiles taken at 24 and 48 hours post-paracetamol. Figure 6.10 B shows single images from 3 separate Z stack images, taken from areas of hepatocyte damage.

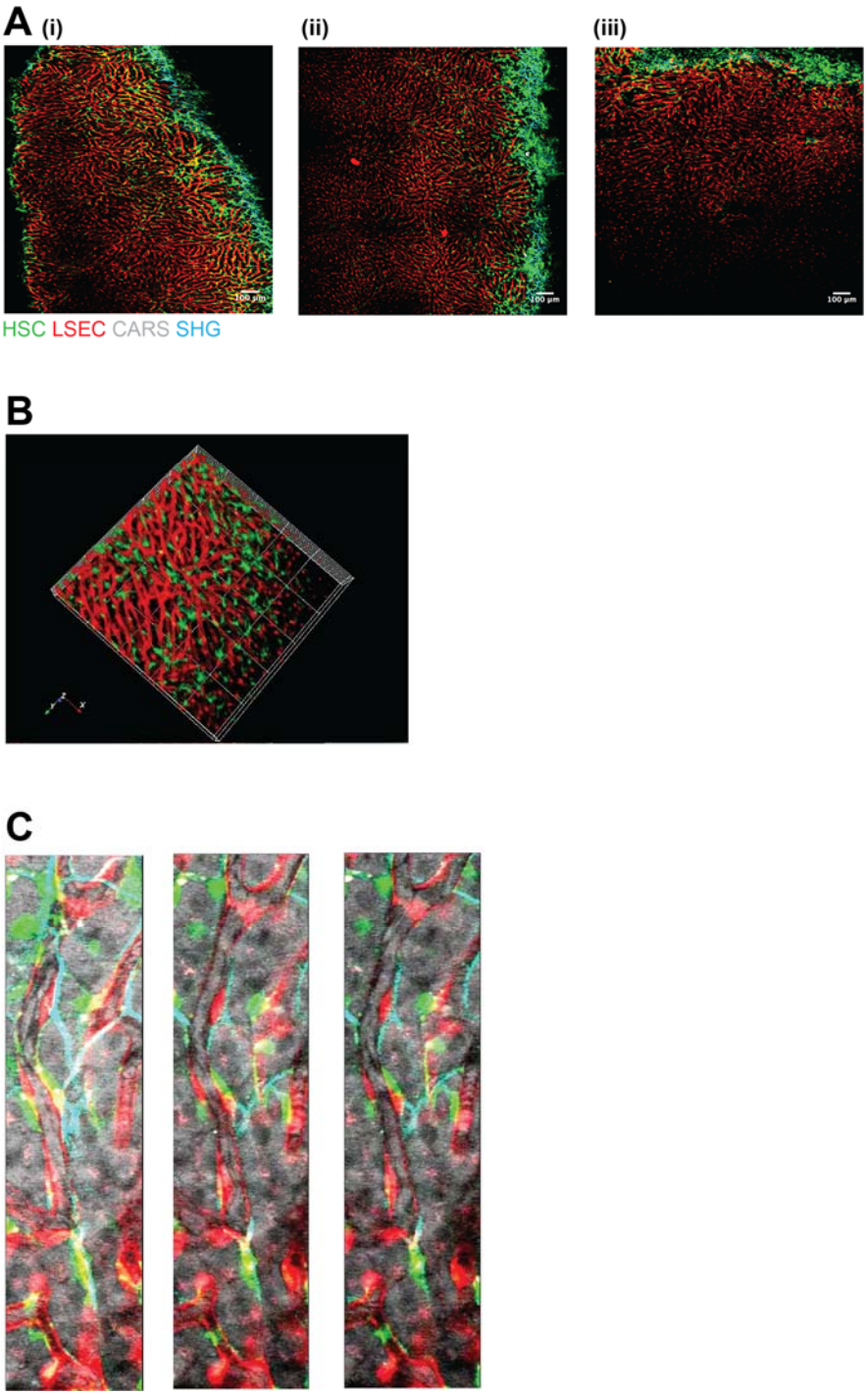

Figure 6.9 Serial IVM of Cdh5$^{+/-}$Ai14;PDGFRβ-BAC-eGFP mouse, performed under anaesthesia, before and after paracetamol-induced acute liver injury

A Multisite tiled images taken **(i)** at baseline, **(ii)** 24 hours post-paracetamol (300mg/kg) and **(iii)** 48 hours post-paracetamol. **B** 3D reconstructed image (generated from a Z stack using Imaris software), showing HSC and LSEC orientation.

C Sequential stills from a high magnification timelapse, showing blood flowing through a vessel (CARS), HSC in close proximity, and collagen using SHG.

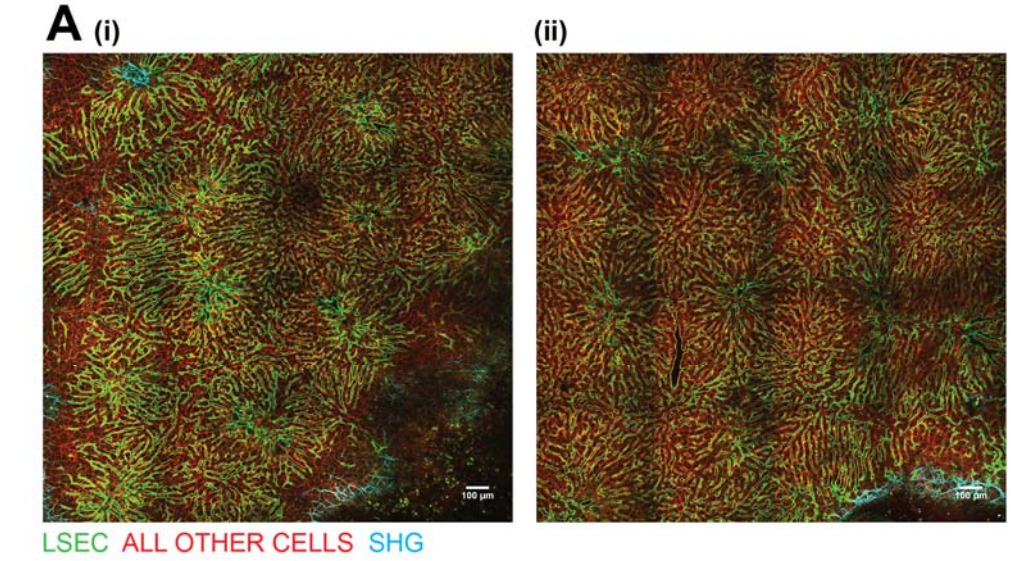

Figure 6.10 Serial IVM of Cdh5Cre$^{+/-}$;mTmG mouse, under anaesthesia, following paracetamol-induced acute liver injury

A Multisite tiles taken **(i)** 24 hours and **(ii)** 48 hours post-paracetamol induced acute liver injury (300mg/kg). **B** Single images taken from three separate Z stacks, acquired from areas of hepatocyte damage, 24 hours post-paracetamol.

6.6 Discussion

The serial IVM experiments presented above confirm that it is possible to perform daily, live imaging on a mouse undergoing paracetamol-induced liver injury. I initially completed a set of experiments investigating parameters of injury, regeneration and inflammation, in animals undergoing paracetamol-induced liver injury, with and without an AIW. This was to ensure that the window itself or abdominal surgery did not significantly affect hepatic damage, regeneration or inflammation in this model. Injury was assessed by quantification of necrotic area on H and E liver sections, and ALT. This was similar in both groups at 24 hours, 48 hours and one week. The only liver enzyme difference observed was in ALP, which was significantly lower in control animals at 48 hours. This relevance of this is uncertain, and unlikely to represent a major clinical effect. Regeneration, as assessed by BrdU staining and liver:body weight ratio at one week, was similar in both groups. PDGFRβ staining was also similar in each group. At 24 hours post-paracetamol, the neutrophil marker GR1 was slightly higher in the AIW group than controls. This is unsurprising, and may represent part of the acute response to abdominal surgery. Interestingly this effect had dissipated by 48 hours, and did not seem to affect injury or repair. Future work to fully characterise the inflammatory infiltrate in this setting could include assessment of macrophage presence at the different timepoints, by F4/80 immunohistochemistry.

At a dose of 300mg/kg, mice tolerated liver injury and daily imaging sessions (performed for up to three days). Imaging sessions typically lasted up to an hour, but it is anticipated that longer sessions could be performed if necessary, with intermittent saline boluses given SC, to replace insensible fluid losses. As previously, liver from a $Cdh5^{+/-}$;Ai14 reporter mouse was initially imaged ex vivo, to optimize the microscope settings for imaging, and obtain preliminary pictures of paracetamol damage in this strain. These confirmed that recombination was good, and that images were adequate for performing downstream analysis of the microvasculature using Imaris software.

After several serial IVM experiments using different reporter strains, it was established that imaging quality was mostly dependent on surgical factors and movement artefact from respiration. This improved with increasing experience and use of low-flow anaesthesia. Usually, six mice underwent AIW surgery at the start of a week-long experiment. This number was to ensure that there were sufficient animals available to trial red blood cell labelling, which was being optimized. Furthermore, occasionally the glue seal between the liver surface and the AIW was slightly suboptimal, meaning that images were slanted, and quality was not maintained throughout the week. At most

imaging sessions, the AIW insert was removed, and the liver surface flushed with saline. The coverslip was replaced, preventing significant biofilm development. Operating on six animals at the start provided a good sample size to obtain serial images and test IVM techniques such as red blood cell labelling.

Future work with this model includes optimising image analysis, to fully harness the potential of the different transgenic reporter mice strains. In particular, animals with LSEC fluorescent reporting are excellently suited to the quantification of vascular networks, sequentially during liver injury and repair. Improved AIW and imaging platform designs are expected to further increase the quality of in vivo imaging. It is hoped that this in vivo approach to studying acute liver injury can now be successfully applied to other models, such as partial hepatectomy, allowing comparison of different pathological processes and subsequent hepatic regeneration.

Final discussion

This research project began with an investigation into the role of αv integrins in a mouse model of HCC. It is proposed that loss of αv integrins on HSC or hepatocytes does not affect hepatocarcinogenesis in the DEN mouse model of HCC. This was an unexpected finding, but perhaps reflects the complexity of TGF-β effects in tumourigenesis. Evaluation in a cirrhotic model of HCC would complement these experiments.

The role of αv and β8 integrins on HSC and hepatocytes were then investigated in the context of paracetamol-induced acute liver injury. Integrin loss on HSC or hepatocytes did not confer protection in this model. During these experiments I gained valuable expertise in the paracetamol model, and was able to contribute animal data to the work of other researchers, resulting in publication.

The key output from this research project, however, has been the development of IVM of the liver, and the design and implementation of a new protocol for daily in vivo imaging of paracetamol-induced acute liver injury. To our knowledge, this is the first time IVM of mouse liver using an AIW has been performed in the UK, and the first time acute liver injury has been imaged daily in vivo through a window. Similarly, I have shown that it is feasible to image HCC in this fashion. Together with other members of Neil Henderson's lab, we have developed and optimised protocols for in vivo imaging; this is currently approaching a point at which we can begin to answer questions about injury and repair. For example, whilst targeted inhibition of integrins on HSC did not confer protection in paracetamol hepatotoxicity, I was interested in whether depletion of HSC throughout the course of acute liver injury might influence hepatic injury or regeneration. Using an IVM approach, and genetic targeting of HSC, sequential imaging throughout paracetamol-induced liver injury could allow detailed investigation of this research question, with quantification of interactions between different cells, and interrogation of interactions with the microenvironment, made possible by cell-specific fluorescent reporting and label-free imaging techniques.

Ultimately, however, we aim to publish our findings from our use of serial IVM in two different models of acute liver injury. Accordingly, results from sequential in vivo imaging of both paracetamol overdose and partial hepatectomy will be presented. This will be performed in transgenic mice in which hepatocytes express a distinct fluorophore depending on which stage of the cell cycle they are in, allowing assessment of regenerative aspects of hepatocyte biology, using this exciting, novel technique.

References

1. Schuppan, D. & Afdhal, N. H. Liver cirrhosis. *Lancet* **371,** 838–851 (2008).
2. Tsochatzis, E. A., Bosch, J. & Burroughs, A. K. Liver cirrhosis. *Lancet* **383,** 1749–1761 (2014).
3. Lozano, R. *et al.* Global and regional mortality from 235 causes of death for 20 age groups in 1990 and 2010: a systematic analysis for the Global Burden of Disease Study 2010. *Lancet* **380,** 2095–2128 (2012).
4. Blachier, M., Leleu, H., Peck-Radosavljevic, M., Valla, D.-C. & Roudot-Thoraval, F. The burden of liver disease in Europe: a review of available epidemiological data. *J. Hepatol.* **58,** 593–608 (2013).
5. Martin, N. K., Hickman, M., Hutchinson, S. J., Goldberg, D. J. & Vickerman, P. Combination interventions to prevent HCV transmission among people who inject drugs: modeling the impact of antiviral treatment, needle and syringe programs, and opiate substitution therapy. *Clin. Infect. Dis.* **57 Suppl 2,** S39–45 (2013).
6. Iredale, J. P., Thompson, A. & Henderson, N. C. Extracellular matrix degradation in liver fibrosis: Biochemistry and regulation. *Biochim. Biophys. Acta* **1832,** 876–883 (2013).
7. Mak, K. M. & Lieber, C. S. Lipocytes and transitional cells in alcoholic liver disease: a morphometric study. *Hepatology* **8,** 1027–1033 (1988).
8. Maher, J. J. & McGuire, R. F. Extracellular matrix gene expression increases preferentially in rat lipocytes and sinusoidal endothelial cells during hepatic fibrosis in vivo. *J. Clin. Invest.* **86,** 1641–1648 (1990).
9. Milani, S., Herbst, H., Schuppan, D., Hahn, E. G. & Stein, H. In situ hybridization for procollagen types I, III and IV mRNA in normal and fibrotic rat liver: evidence for predominant expression in nonparenchymal liver cells. *Hepatology* **10,** 84–92 (1989).
10. Pellicoro, A. *et al.* Elastin accumulation is regulated at the level of degradation by macrophage metalloelastase (MMP-12) during experimental liver fibrosis. *Hepatology* **55,** 1965–1975 (2012).
11. Asahina, K., Zhou, B., Pu, W. T. & Tsukamoto, H. Septum transversum-derived mesothelium gives rise to hepatic stellate cells and perivascular mesenchymal cells in developing mouse liver. *Hepatology* **53,** 983–995 (2011).
12. Forbes, S. J. *et al.* A significant proportion of myofibroblasts are of bone marrow origin in human liver fibrosis. *Gastroenterology* **126,** 955–963 (2004).
13. Russo, F. P. *et al.* The bone marrow functionally contributes to liver fibrosis. *Gastroenterology* **130,** 1807–1821 (2006).
14. Kisseleva, T. *et al.* Bone marrow-derived fibrocytes participate in pathogenesis of liver fibrosis. *J. Hepatol.* **45,** 429–438 (2006).
15. Kinnman, N. & Housset, C. Peribiliary myofibroblasts in biliary type liver fibrosis. *Front. Biosci.* **7,** d496–503 (2002).
16. Knittel, T. *et al.* Rat liver myofibroblasts and hepatic stellate cells: different cell populations of the fibroblast lineage with fibrogenic potential. *Gastroenterology* **117,** 1205–1221 (1999).
17. Iwaisako, K. *et al.* Origin of myofibroblasts in the fibrotic liver in mice. *Proc. Natl. Acad. Sci. U.S.A.* **111,** E3297–305 (2014).
18. Gressner, A. M., Weiskirchen, R., Breitkopf, K. & Dooley, S. Roles of TGF-beta in hepatic fibrosis. *Front. Biosci.* **7,** d793–807 (2002).
19. Pinzani, M., Gesualdo, L., Sabbah, G. M. & Abboud, H. E. Effects of platelet-derived growth factor and other polypeptide mitogens on DNA synthesis and growth of cultured rat liver fat-storing cells. *J. Clin. Invest.* **84,** 1786–1793 (1989).

20. Olsen, A. L. *et al.* Hepatic stellate cells require a stiff environment for myofibroblastic differentiation. *Am. J. Physiol. Gastrointest. Liver Physiol.* **301,** G110–8 (2011).
21. Murphy, F. R. *et al.* Inhibition of apoptosis of activated hepatic stellate cells by tissue inhibitor of metalloproteinase-1 is mediated via effects on matrix metalloproteinase inhibition: implications for reversibility of liver fibrosis. *J. Biol. Chem.* **277,** 11069–11076 (2002).
22. Iredale, J. P. *et al.* Tissue inhibitor of metalloproteinase-1 messenger RNA expression is enhanced relative to interstitial collagenase messenger RNA in experimental liver injury and fibrosis. *Hepatology* **24,** 176–184 (1996).
23. Benyon, R. C., Iredale, J. P., Goddard, S., Winwood, P. J. & Arthur, M. J. Expression of tissue inhibitor of metalloproteinases 1 and 2 is increased in fibrotic human liver. *Gastroenterology* **110,** 821–831 (1996).
24. Bataller, R. & Brenner, D. A. Liver fibrosis. *J. Clin. Invest.* **115,** 209–218 (2005).
25. Iredale, J. P. *et al.* Mechanisms of spontaneous resolution of rat liver fibrosis. Hepatic stellate cell apoptosis and reduced hepatic expression of metalloproteinase inhibitors. *J. Clin. Invest.* **102,** 538–549 (1998).
26. Issa, R. *et al.* Apoptosis of hepatic stellate cells: involvement in resolution of biliary fibrosis and regulation by soluble growth factors. *Gut* **48,** 548–557 (2001).
27. Sun, M. & Kisseleva, T. Reversibility of liver fibrosis. *Clin Res Hepatol Gastroenterol* **39 Suppl 1,** S60–3 (2015).
28. Krizhanovsky, V. *et al.* Senescence of activated stellate cells limits liver fibrosis. *Cell* **134,** 657–667 (2008).
29. Kisseleva, T. *et al.* Myofibroblasts revert to an inactive phenotype during regression of liver fibrosis. *Proc. Natl. Acad. Sci. U.S.A.* **109,** 9448–9453 (2012).
30. Troeger, J. S. *et al.* Deactivation of hepatic stellate cells during liver fibrosis resolution in mice. *Gastroenterology* **143,** 1073–83.e22 (2012).
31. Desmet, V. J. & Roskams, T. Cirrhosis reversal: a duel between dogma and myth. *J. Hepatol.* **40,** 860–867 (2004).
32. *globocan.iarc.fr*. Available at: http://globocan.iarc.fr. (Accessed: 5 August 2014)
33. Llovet, J. M. *et al.* Sorafenib in advanced hepatocellular carcinoma. *N. Engl. J. Med.* **359,** 378–390 (2008).
34. Forner, A., Llovet, J. M. & Bruix, J. Hepatocellular carcinoma. *Lancet* **379,** 1245–1255 (2012).
35. Henderson, N. C. & Iredale, J. P. Liver fibrosis: cellular mechanisms of progression and resolution. *Clin. Sci.* **112,** 265–280 (2007).
36. Bruix, J., Sherman, M.American Association for the Study of Liver Diseases. Management of hepatocellular carcinoma: an update. *Hepatology (Baltimore, Md.)* **53,** 1020–1022 (2011).
37. Friedman, S. L. Hepatic stellate cells: protean, multifunctional, and enigmatic cells of the liver. *Physiol. Rev.* **88,** 125–172 (2008).
38. European Association For The Study Of The LiverEuropean Organisation For Research And Treatment Of Cancer. EASL-EORTC clinical practice guidelines: management of hepatocellular carcinoma. *Journal of hepatology* **56,** 908–943 (2012).
39. Zhang, D. Y. & Friedman, S. L. Fibrosis-dependent mechanisms of hepatocarcinogenesis. *Hepatology* **56,** 769–775 (2012).
40. Younossi, Z. M. *et al.* Association of nonalcoholic fatty liver disease (NAFLD) with hepatocellular carcinoma (HCC) in the United States from 2004 to 2009.

Hepatology **62,** 1723–1730 (2015).
41. Morgan, R. L. *et al.* Eradication of hepatitis C virus infection and the development of hepatocellular carcinoma: a meta-analysis of observational studies. *Ann. Intern. Med.* **158,** 329–337 (2013).
42. Forner, A., Reig, M. E., de Lope, C. R. & Bruix, J. Current strategy for staging and treatment: the BCLC update and future prospects. *Semin. Liver Dis.* **30,** 61–74 (2010).
43. Reig, M. *et al.* Systemic therapy for hepatocellular carcinoma: the issue of treatment stage migration and registration of progression using the BCLC-refined RECIST. *Semin. Liver Dis.* **34,** 444–455 (2014).
44. Llovet, J. M., Villanueva, A., Lachenmayer, A. & Finn, R. S. Advances in targeted therapies for hepatocellular carcinoma in the genomic era. *Nat Rev Clin Oncol* **12,** 408–424 (2015).
45. Hoshida, Y. *et al.* Molecular classification and novel targets in hepatocellular carcinoma: recent advancements. *Semin. Liver Dis.* **30,** 35–51 (2010).
46. Chiang, D. Y. *et al.* Focal gains of VEGFA and molecular classification of hepatocellular carcinoma. *Cancer Res.* **68,** 6779–6788 (2008).
47. Boyault, S. *et al.* Transcriptome classification of HCC is related to gene alterations and to new therapeutic targets. *Hepatology* **45,** 42–52 (2007).
48. Lee, J.-S. *et al.* Classification and prediction of survival in hepatocellular carcinoma by gene expression profiling. *Hepatology* **40,** 667–676 (2004).
49. Hoshida, Y. *et al.* Integrative transcriptome analysis reveals common molecular subclasses of human hepatocellular carcinoma. *Cancer Res.* **69,** 7385–7392 (2009).
50. Hoshida, Y., Moeini, A., Alsinet, C., Kojima, K. & Villanueva, A. Gene signatures in the management of hepatocellular carcinoma. *Semin. Oncol.* **39,** 473–485 (2012).
51. Ahn, S.-M. *et al.* Genomic portrait of resectable hepatocellular carcinomas: implications of RB1 and FGF19 aberrations for patient stratification. *Hepatology* **60,** 1972–1982 (2014).
52. Totoki, Y. *et al.* Trans-ancestry mutational landscape of hepatocellular carcinoma genomes. *Nat. Genet.* **46,** 1267–1273 (2014).
53. Dituri, F. *et al.* Differential Inhibition of the TGF-β Signaling Pathway in HCC Cells Using the Small Molecule Inhibitor LY2157299 and the D10 Monoclonal Antibody against TGF-β Receptor Type II. *PLoS ONE* **8,** e67109 (2013).
54. Fairvre, S., Santoro, A. & Kelley, R. A phase 2 study of a novel transforming growth factor-beta receptor I kinase inhibitor, LY2157299 monohydrate, in patients with advanced hepatocellular carcinoma [abstract]. *J. Clin. Oncol. 32, 2014*
55. Trey, C. & Davidson, C. S. The management of fulminant hepatic failure. *Prog Liver Dis* **3,** 282–298 (1970).
56. Bernal, W. & Wendon, J. Acute liver failure. *N. Engl. J. Med.* **369,** 2525–2534 (2013).
57. Donnelly, M. C., Hayes, P. C. & Simpson, K. J. The changing face of liver transplantation for acute liver failure: Assessment of current status and implications for future practice. *Liver Transpl.* **22,** 527–535 (2016).
58. Lok, A. S. F. & McMahon, B. J. Chronic hepatitis B: update 2009. *Hepatology* **50,** 661–662 (2009).
59. Péron, J. M. *et al.* Treatment of autochthonous acute hepatitis E with short-term ribavirin: a multicenter retrospective study. *Liver Int.* **36,** 328–333 (2016).
60. Peters, D. J., Greene, W. H., Ruggiero, F. & McGarrity, T. J. Herpes simplex-induced fulminant hepatitis in adults: a call for empiric therapy. *Dig. Dis. Sci.* **45,** 2399–2404 (2000).

61. Chalasani, N. *et al.* Features and Outcomes of 899 Patients With Drug-Induced Liver Injury: The DILIN Prospective Study. *Gastroenterology* **148,** 1340–52.e7 (2015).
62. Chalasani, N. *et al.* Causes, clinical features, and outcomes from a prospective study of drug-induced liver injury in the United States. *Gastroenterology* **135,** 1924–34– 1934.e1–4 (2008).
63. Walsh, S. A. & Creamer, D. Drug reaction with eosinophilia and systemic symptoms (DRESS): a clinical update and review of current thinking. *Clin. Exp. Dermatol.* **36,** 6–11 (2011).
64. Ichai, P. *et al.* Usefulness of corticosteroids for the treatment of severe and fulminant forms of autoimmune hepatitis. *Liver Transpl.* **13,** 996–1003 (2007).
65. Mendizabal, M. *et al.* Fulminant presentation of autoimmune hepatitis: clinical features and early predictors of corticosteroid treatment failure. *Eur J Gastroenterol Hepatol* **27,** 644–648 (2015).
66. Ko, H. & Yoshida, E. M. Acute fatty liver of pregnancy. *Can. J. Gastroenterol.* **20,** 25–30 (2006).
67. Pereira, S. P., O'Donohue, J., Wendon, J. & Williams, R. Maternal and perinatal outcome in severe pregnancy-related liver disease. *Hepatology* **26,** 1258–1262 (1997).
68. Drolz, A. *et al.* Statin therapy is associated with reduced incidence of hypoxic hepatitis in critically ill patients. *J. Hepatol.* **60,** 1187–1193 (2014).
69. Devarbhavi, H. *et al.* Factors that predict mortality in children with Wilson disease associated acute liver failure and comparison of Wilson disease specific prognostic indices. *J. Gastroenterol. Hepatol.* **29,** 380–386 (2014).
70. Zahn, A. *et al.* Budd-Chiari syndrome: long term success via hepatic decompression using transjugular intrahepatic porto-systemic shunt. *BMC Gastroenterol* **10,** 25 (2010).
71. Ostapowicz, G. *et al.* Results of a prospective study of acute liver failure at 17 tertiary care centers in the United States. *Ann. Intern. Med.* **137,** 947–954 (2002).
72. Donnelly, M. C., Hayes, P. C. & Simpson, K. J. Role of inflammation and infection in the pathogenesis of human acute liver failure: Clinical implications for monitoring and therapy. *World J. Gastroenterol.* **22,** 5958–5970 (2016).
73. Antoniades, C. G., Berry, P. A., Wendon, J. A. & Vergani, D. The importance of immune dysfunction in determining outcome in acute liver failure. *J. Hepatol.* **49,** 845–861 (2008).
74. Döcke, W. D. *et al.* Monocyte deactivation in septic patients: restoration by IFN-gamma treatment. *Nat. Med.* **3,** 678–681 (1997).
75. Prince, L. R., Whyte, M. K., Sabroe, I. & Parker, L. C. The role of TLRs in neutrophil activation. *Curr Opin Pharmacol* **11,** 397–403 (2011).
76. Szabo, G. & Petrasek, J. Inflammasome activation and function in liver disease. *Nat Rev Gastroenterol Hepatol* **12,** 387–400 (2015).
77. Jaeschke, H., Williams, C. D., Ramachandran, A. & Bajt, M. L. Acetaminophen hepatotoxicity and repair: the role of sterile inflammation and innate immunity. *Liver Int.* **32,** 8–20 (2012).
78. O'Grady, J. G., Alexander, G. J., Hayllar, K. M. & Williams, R. Early indicators of prognosis in fulminant hepatic failure. *Gastroenterology* **97,** 439–445 (1989).
79. Craig, D. G. N., Ford, A. C., Hayes, P. C. & Simpson, K. J. Systematic review: prognostic tests of paracetamol-induced acute liver failure. *Aliment. Pharmacol. Ther.* **31,** 1064–1076 (2010).
80. Chiu, A., Chan, L. M. Y. & Fan, S. T. Molecular adsorbent recirculating system treatment for patients with liver failure: the Hong Kong experience. *Liver Int.* **26,** 695–702 (2006).

81. Bernal, W., Lee, W. M., Wendon, J., Larsen, F. S. & Williams, R. Acute liver failure: A curable disease by 2024? *J. Hepatol.* **62,** S112–20 (2015).
82. Saliba, F. *et al.* Albumin dialysis with a noncell artificial liver support device in patients with acute liver failure: a randomized, controlled trial. *Ann. Intern. Med.* **159,** 522–531 (2013).
83. Kjaergard, L. L., Liu, J., Als-Nielsen, B. & Gluud, C. Artificial and bioartificial support systems for acute and acute-on-chronic liver failure: a systematic review. *JAMA* **289,** 217–222 (2003).
84. Stutchfield, B. M., Simpson, K. & Wigmore, S. J. Systematic review and meta-analysis of survival following extracorporeal liver support. *Br J Surg* **98,** 623–631 (2011).
85. Larsen, F. S. *et al.* High-volume plasma exchange in patients with acute liver failure: An open randomised controlled trial. *J. Hepatol.* **64,** 69–78 (2016).
86. Forbes, S. J., Gupta, S. & Dhawan, A. Cell therapy for liver disease: From liver transplantation to cell factory. *J. Hepatol.* **62,** S157–69 (2015).
87. Ramanathan, R. *et al.* Transplantation of human stem cell-derived hepatocytes in an animal model of acute liver failure. *Surgery* **158,** 349–359 (2015).
88. Lok, A. S. *et al.* Incidence of hepatocellular carcinoma and associated risk factors in hepatitis C-related advanced liver disease. *Gastroenterology* **136,** 138–148 (2009).
89. Bhowmick, N. A., Neilson, E. G. & Moses, H. L. Stromal fibroblasts in cancer initiation and progression. *Nature* **432,** 332–337 (2004).
90. Straussman, R. *et al.* Tumour micro-environment elicits innate resistance to RAF inhibitors through HGF secretion. *Nature* **487,** 500–504 (2012).
91. Olumi, A. F. *et al.* Carcinoma-associated fibroblasts direct tumor progression of initiated human prostatic epithelium. *Cancer Res.* **59,** 5002–5011 (1999).
92. Wang, W. *et al.* Crosstalk to stromal fibroblasts induces resistance of lung cancer to epidermal growth factor receptor tyrosine kinase inhibitors. *Clin. Cancer Res.* **15,** 6630–6638 (2009).
93. Hoshida, Y. *et al.* Gene expression in fixed tissues and outcome in hepatocellular carcinoma. *N. Engl. J. Med.* **359,** 1995–2004 (2008).
94. Seitz, H. K. & Stickel, F. Risk factors and mechanisms of hepatocarcinogenesis with special emphasis on alcohol and oxidative stress. *Biol. Chem.* **387,** 349–360 (2006).
95. Eberlein, C. *et al.* E-Cadherin and EpCAM expression by NSCLC tumour cells associate with normal fibroblast activation through a pathway initiated by integrin αvβ6 and maintained through TGFβ signalling. *Oncogene* (2014). doi:10.1038/onc.2013.600
96. Hernandez-Gea, V., Toffanin, S., Friedman, S. L. & Llovet, J. M. Role of the microenvironment in the pathogenesis and treatment of hepatocellular carcinoma. *Gastroenterology* **144,** 512–527 (2013).
97. Jedeszko, C., Victor, B. C., Podgorski, I. & Sloane, B. F. Fibroblast hepatocyte growth factor promotes invasion of human mammary ductal carcinoma in situ. *Cancer Res.* **69,** 9148–9155 (2009).
98. Busch, S. *et al.* TGF-beta receptor type-2 expression in cancer-associated fibroblasts regulates breast cancer cell growth and survival and is a prognostic marker in pre-menopausal breast cancer. *Oncogene* (2013). doi:10.1038/onc.2013.527
99. Patocs, A. *et al.* Breast-cancer stromal cells with TP53 mutations and nodal metastases. *N. Engl. J. Med.* **357,** 2543–2551 (2007).
100. Nakagawa, H. *et al.* Role of cancer-associated stromal fibroblasts in metastatic colon cancer to the liver and their expression profiles. *Oncogene* **23,** 7366–7377 (2004).

101. Noskova, V., Ahmadi, S., Asander, E. & Casslén, B. Ovarian cancer cells stimulate uPA gene expression in fibroblastic stromal cells via multiple paracrine and autocrine mechanisms. *Gynecol. Oncol.* **115,** 121–126 (2009).
102. Zhou, X. *et al.* Impaired proteolysis of collagen I inhibits proliferation of hepatic stellate cells: implications for regulation of liver fibrosis. *J. Biol. Chem.* **281,** 39757–39765 (2006).
103. Druker, B. J. Inhibition of the Bcr-Abl tyrosine kinase as a therapeutic strategy for CML. *Oncogene* **21,** 8541–8546 (2002).
104. O'Brien, S. G. *et al.* Imatinib compared with interferon and low-dose cytarabine for newly diagnosed chronic-phase chronic myeloid leukemia. *N. Engl. J. Med.* **348,** 994–1004 (2003).
105. Roberts, P. J. & Der, C. J. Targeting the Raf-MEK-ERK mitogen-activated protein kinase cascade for the treatment of cancer. *Oncogene* **26,** 3291–3310 (2007).
106. Slamon, D. J. *et al.* Use of chemotherapy plus a monoclonal antibody against HER2 for metastatic breast cancer that overexpresses HER2. *N. Engl. J. Med.* **344,** 783–792 (2001).
107. Sharma, S. V., Bell, D. W., Settleman, J. & Haber, D. A. Epidermal growth factor receptor mutations in lung cancer. *Nat. Rev. Cancer* **7,** 169–181 (2007).
108. Rosell, R. *et al.* Erlotinib versus standard chemotherapy as first-line treatment for European patients with advanced EGFR mutation-positive non-small-cell lung cancer (EURTAC): a multicentre, open-label, randomised phase 3 trial. *Lancet Oncol.* **13,** 239–246 (2012).
109. Lynch, T. J. *et al.* Activating mutations in the epidermal growth factor receptor underlying responsiveness of non-small-cell lung cancer to gefitinib. *N. Engl. J. Med.* **350,** 2129–2139 (2004).
110. Soda, M. *et al.* Identification of the transforming EML4-ALK fusion gene in non-small-cell lung cancer. *Nature* **448,** 561–566 (2007).
111. Kwak, E. L. *et al.* Anaplastic lymphoma kinase inhibition in non-small-cell lung cancer. *N. Engl. J. Med.* **363,** 1693–1703 (2010).
112. Shaw, A. T. *et al.* Crizotinib versus chemotherapy in advanced ALK-positive lung cancer. *N. Engl. J. Med.* **368,** 2385–2394 (2013).
113. Luo, J., Solimini, N. L. & Elledge, S. J. Principles of cancer therapy: oncogene and non-oncogene addiction. *Cell* **136,** 823–837 (2009).
114. Chapman, P. B. *et al.* Improved survival with vemurafenib in melanoma with BRAF V600E mutation. *N. Engl. J. Med.* **364,** 2507–2516 (2011).
115. Wilson, T. R. *et al.* Widespread potential for growth-factor-driven resistance to anticancer kinase inhibitors. *Nature* **487,** 505–509 (2012).
116. Faouzi, S. *et al.* Myofibroblasts are responsible for collagen synthesis in the stroma of human hepatocellular carcinoma: an in vivo and in vitro study. *J. Hepatol.* **30,** 275–284 (1999).
117. Le Bail, B. *et al.* Osteonectin/SPARC is overexpressed in human hepatocellular carcinoma. *J. Pathol.* **189,** 46–52 (1999).
118. Dubuisson, L. *et al.* Expression and cellular localization of fibrillin-1 in normal and pathological human liver. *J. Hepatol.* **34,** 514–522 (2001).
119. Park, Y. N., Yang, C. P., Cubukcu, O., Thung, S. N. & Theise, N. D. Hepatic stellate cell activation in dysplastic nodules: evidence for an alternate hypothesis concerning human hepatocarcinogenesis. *Liver* **17,** 271–274 (1997).
120. Théret, N. *et al.* Increased extracellular matrix remodeling is associated with tumor progression in human hepatocellular carcinomas. *Hepatology* **34,** 82–88 (2001).
121. Nishio, T. *et al.* Increased expression of collagenase in the liver induces

hepatocyte proliferation with cytoplasmic accumulation of beta-catenin in the rat. *J. Hepatol.* **38,** 468–475 (2003).
122. You, J. *et al.* Characterizing the effects of heparin gel stiffness on function of primary hepatocytes. *Tissue Eng Part A* **19,** 2655–2663 (2013).
123. Semler, E. J., Lancin, P. A., Dasgupta, A. & Moghe, P. V. Engineering hepatocellular morphogenesis and function via ligand-presenting hydrogels with graded mechanical compliance. *Biotechnol. Bioeng.* **89,** 296–307 (2005).
124. Schrader, J. *et al.* Matrix stiffness modulates proliferation, chemotherapeutic response, and dormancy in hepatocellular carcinoma cells. *Hepatology* **53,** 1192–1205 (2011).
125. Wells, R. G. The role of matrix stiffness in regulating cell behavior. *Hepatology* **47,** 1394–1400 (2008).
126. Li, Z. *et al.* Transforming growth factor-beta and substrate stiffness regulate portal fibroblast activation in culture. *Hepatology* **46,** 1246–1256 (2007).
127. Masuzaki, R. *et al.* Prospective risk assessment for hepatocellular carcinoma development in patients with chronic hepatitis C by transient elastography. *Hepatology* **49,** 1954–1961 (2009).
128. Kim, D. Y. *et al.* Transient elastography-based risk estimation of hepatitis B virus-related occurrence of hepatocellular carcinoma: development and validation of a predictive model. *Onco Targets Ther* **6,** 1463–1469 (2013).
129. Wong, G. L.-H. *et al.* Liver stiffness-based optimization of hepatocellular carcinoma risk score in patients with chronic hepatitis B. *J. Hepatol.* **60,** 339–345 (2014).
130. Masuzaki, R. *et al.* Assessing liver tumor stiffness by transient elastography. *Hepatol Int* **1,** 394–397 (2007).
131. Levental, K. R. *et al.* Matrix crosslinking forces tumor progression by enhancing integrin signaling. *Cell* **139,** 891–906 (2009).
132. Legate, K. R., Wickström, S. A. & Fässler, R. Genetic and cell biological analysis of integrin outside-in signaling. *Genes Dev.* **23,** 397–418 (2009).
133. Reif, S. *et al.* The role of focal adhesion kinase-phosphatidylinositol 3-kinase-akt signaling in hepatic stellate cell proliferation and type I collagen expression. *J. Biol. Chem.* **278,** 8083–8090 (2003).
134. Dong, Y. *et al.* Increasing matrix stiffness upregulates vascular endothelial growth factor expression in hepatocellular carcinoma cells mediated by integrin β1. *Biochem. Biophys. Res. Commun.* **444,** 427–432 (2014).
135. Lee, S. K. *et al.* Integrin alpha V polymorphisms and haplotypes in a Korean population are associated with susceptibility to chronic hepatitis and hepatocellular carcinoma. *Liver Int.* **29,** 187–195 (2009).
136. Lai, K. K. Y. *et al.* Extracellular matrix dynamics in hepatocarcinogenesis: a comparative proteomics study of PDGFC transgenic and Pten null mouse models. *PLoS Genet.* **7,** e1002147 (2011).
137. Jung, C. W. *et al.* Characterization of hepatocellular carcinoma cell lines based on cell adhesion molecules. *Int. J. Mol. Med.* **29,** 1158–1164 (2012).
138. Giannelli, G. *et al.* Human hepatocellular carcinoma (HCC) cells require both alpha3beta1 integrin and matrix metalloproteinases activity for migration and invasion. *Lab. Invest.* **81,** 613–627 (2001).
139. Torimura, T. *et al.* Laminin deposition to type IV collagen enhances haptotaxis, chemokinesis, and adhesion of hepatoma cells through beta1-integrins. *J. Hepatol.* **35,** 245–253 (2001).
140. Yang, C. *et al.* Integrin alpha1beta1 and alpha2beta1 are the key regulators of hepatocarcinoma cell invasion across the fibrotic matrix microenvironment. *Cancer Res.* **63,** 8312–8317 (2003).
141. Zhao, G. *et al.* Mechanical stiffness of liver tissues in relation to integrin β1

expression may influence the development of hepatic cirrhosis and hepatocellular carcinoma. *J Surg Oncol* **102,** 482–489 (2010).
142. Fu, B.-H., Wu, Z.-Z. & Qin, J. Effects of integrin α6β1 on migration of hepatocellular carcinoma cells. *Mol. Biol. Rep.* **38,** 3271–3276 (2011).
143. Mizuno, H. *et al.* Changes in adhesive and migratory characteristics of hepatocellular carcinoma (HCC) cells induced by expression of alpha3beta1 integrin. *Biochim. Biophys. Acta* **1780,** 564–570 (2008).
144. Sil, H., Sen, T. & Chatterjee, A. Fibronectin-integrin (alpha5beta1) modulates migration and invasion of murine melanoma cell line B16F10 by involving MMP-9. *Oncol. Res.* **19,** 335–348 (2011).
145. Jing, Y. *et al.* SERPINA5 inhibits tumor cell migration by modulating the fibronectin-integrin β1 signaling pathway in hepatocellular carcinoma. *Mol Oncol* **8,** 366–377 (2014).
146. Nguyen, T. V., Sleiman, M., Moriarty, T., Herrick, W. G. & Peyton, S. R. Sorafenib resistance and JNK signaling in carcinoma during extracellular matrix stiffening. *Biomaterials* **35,** 5749–5759 (2014).
147. Ke, A.-W. *et al.* CD151 amplifies signaling by integrin α6β1 to PI3K and induces the epithelial-mesenchymal transition in HCC cells. *Gastroenterology* **140,** 1629–41.e15 (2011).
148. Fransvea, E., Mazzocca, A., Antonaci, S. & Giannelli, G. Targeting transforming growth factor (TGF)-betaRI inhibits activation of beta1 integrin and blocks vascular invasion in hepatocellular carcinoma. *Hepatology* **49,** 839–850 (2009).
149. Giannelli, G. *et al.* Transforming growth factor-beta1 triggers hepatocellular carcinoma invasiveness via alpha3beta1 integrin. *Am. J. Pathol.* **161,** 183–193 (2002).
150. Kim, H.-P. *et al.* TGF-beta1-mediated activations of c-Src and Rac1 modulate levels of cyclins and p27(Kip1) CDK inhibitor in hepatoma cells replated on fibronectin. *Biochim. Biophys. Acta* **1743,** 151–161 (2005).
151. Matsuzaki, K. Smad phosphoisoform signals in acute and chronic liver injury: similarities and differences between epithelial and mesenchymal cells. *Cell Tissue Res.* **347,** 225–243 (2012).
152. Hayashida, T. Integrins modulate cellular fibrogenesis at multiple levels; Regulation of TGF-β signaling. *Endocr Metab Immune Disord Drug Targets* **10,** 302–319 (2010).
153. Cai, T., Lei, Q. Y., Wang, L. Y. & Zha, X. L. TGF-beta 1 modulated the expression of alpha 5 beta 1 integrin and integrin-mediated signaling in human hepatocarcinoma cells. *Biochem. Biophys. Res. Commun.* **274,** 519–525 (2000).
154. Amann, T. *et al.* Activated hepatic stellate cells promote tumorigenicity of hepatocellular carcinoma. *Cancer Sci.* **100,** 646–653 (2009).
155. Zhao, W. *et al.* Activated hepatic stellate cells promote hepatocellular carcinoma development in immunocompetent mice. *Int. J. Cancer* **129,** 2651–2661 (2011).
156. Jia, C.-C. *et al.* Cancer-associated fibroblasts from hepatocellular carcinoma promote malignant cell proliferation by HGF secretion. *PLoS ONE* **8,** e63243 (2013).
157. Sun, B. *et al.* Intratumoral hepatic stellate cells as a poor prognostic marker and a new treatment target for hepatocellular carcinoma. *PLoS ONE* **8,** e80212 (2013).
158. Santamato, A. *et al.* Hepatic stellate cells stimulate HCC cell migration via laminin-5 production. *Clin. Sci.* **121,** 159–168 (2011).
159. Guirouilh, J., Castroviejo, M., Balabaud, C., Desmoulière, A. & Rosenbaum, J.

Hepatocarcinoma cells stimulate hepatocyte growth factor secretion in human liver myofibroblasts. *Int. J. Oncol.* **17,** 777–781 (2000).
160. Guirouilh, J. *et al.* Expression of hepatocyte growth factor in human hepatocellular carcinoma. *J. Hepatol.* **34,** 78–83 (2001).
161. Efimova, E. A. *et al.* Effects of human hepatocyte growth factor on the proliferation of human hepatocytes and hepatocellular carcinoma cell lines. *Eur Surg Res* **36,** 300–307 (2004).
162. Monvoisin, A. *et al.* Direct evidence that hepatocyte growth factor-induced invasion of hepatocellular carcinoma cells is mediated by urokinase. *J. Hepatol.* **30,** 511–518 (1999).
163. Suzuki, A. *et al.* Hepatocyte growth factor promotes cell survival from fas-mediated cell death in hepatocellular carcinoma cells via Akt activation and Fas-death-inducing signaling complex suppression. *Hepatology* **32,** 796–802 (2000).
164. Schmidt, C. *et al.* Scatter factor/hepatocyte growth factor is essential for liver development. *Nature* **373,** 699–702 (1995).
165. Matsumoto, K. & Nakamura, T. Hepatocyte growth factor and the Met system as a mediator of tumor-stromal interactions. *Int. J. Cancer* **119,** 477–483 (2006).
166. Suzuki, K. *et al.* Expression of the c-met protooncogene in human hepatocellular carcinoma. *Hepatology* **20,** 1231–1236 (1994).
167. Kiss, A., Wang, N. J., Xie, J. P. & Thorgeirsson, S. S. Analysis of transforming growth factor (TGF)-alpha/epidermal growth factor receptor, hepatocyte growth Factor/c-met,TGF-beta receptor type II, and p53 expression in human hepatocellular carcinomas. *Clin. Cancer Res.* **3,** 1059–1066 (1997).
168. Breuhahn, K., Longerich, T. & Schirmacher, P. Dysregulation of growth factor signaling in human hepatocellular carcinoma. *Oncogene* **25,** 3787–3800 (2006).
169. Boix, L. *et al.* c-met mRNA overexpression in human hepatocellular carcinoma. *Hepatology* **19,** 88–91 (1994).
170. Kaposi-Novak, P. *et al.* Met-regulated expression signature defines a subset of human hepatocellular carcinomas with poor prognosis and aggressive phenotype. *J. Clin. Invest.* **116,** 1582–1595 (2006).
171. Ueki, T., Fujimoto, J., Suzuki, T., Yamamoto, H. & Okamoto, E. Expression of hepatocyte growth factor and its receptor c-met proto-oncogene in hepatocellular carcinoma. *Hepatology* **25,** 862–866 (1997).
172. Luedde, T. & Schwabe, R. F. NF-κB in the liver--linking injury, fibrosis and hepatocellular carcinoma. *Nat Rev Gastroenterol Hepatol* **8,** 108–118 (2011).
173. Date, K. *et al.* Inhibition of tumor growth and invasion by a four-kringle antagonist (HGF/NK4) for hepatocyte growth factor. *Oncogene* **17,** 3045–3054 (1998).
174. Heideman, D. A. M. *et al.* Inhibition of angiogenesis and HGF-cMET-elicited malignant processes in human hepatocellular carcinoma cells using adenoviral vector-mediated NK4 gene therapy. *Cancer Gene Ther.* **12,** 954–962 (2005).
175. Son, G. *et al.* Blockage of HGF/c-Met system by gene therapy (adenovirus-mediated NK4 gene) suppresses hepatocellular carcinoma in mice. *J. Hepatol.* **45,** 688–695 (2006).
176. Wright, J. H. *et al.* Paracrine activation of hepatic stellate cells in platelet-derived growth factor C transgenic mice; evidence for stromal induction of hepatocellular carcinoma. *Int. J. Cancer* (2013). doi:10.1002/ijc.28421
177. Yu, G. *et al.* Hepatic stellate cells secreted hepatocyte growth factor contributes to the chemoresistance of hepatocellular carcinoma. *PLoS ONE* **8,** e73312 (2013).

178. Kopitz, C. *et al.* Tissue inhibitor of metalloproteinases-1 promotes liver metastasis by induction of hepatocyte growth factor signaling. *Cancer Res.* **67,** 8615–8623 (2007).
179. Schelter, F. *et al.* Tumor cell-derived Timp-1 is necessary for maintaining metastasis-promoting Met-signaling via inhibition of Adam-10. *Clin. Exp. Metastasis* **28,** 793–802 (2011).
180. Nakamura, T., Matsumoto, K., Kiritoshi, A., Tano, Y. & Nakamura, T. Induction of hepatocyte growth factor in fibroblasts by tumor-derived factors affects invasive growth of tumor cells: in vitro analysis of tumor-stromal interactions. *Cancer Res.* **57,** 3305–3313 (1997).
181. Hasina, R. *et al.* Autocrine and paracrine motility factors and their involvement in invasiveness in a human oral carcinoma cell line. *Br. J. Cancer* **80,** 1708–1717 (1999).
182. Meyer, D. H., Bachem, M. G. & Gressner, A. M. Modulation of hepatic lipocyte proteoglycan synthesis and proliferation by Kupffer cell-derived transforming growth factors type beta 1 and type alpha. *Biochem. Biophys. Res. Commun.* **171,** 1122–1129 (1990).
183. Roth, S., Schurek, J. & Gressner, A. M. Expression and release of the latent transforming growth factor beta binding protein by hepatocytes from rat liver. *Hepatology* **25,** 1398–1405 (1997).
184. Thompson, A. I., Conroy, K. P. & Henderson, N. C. Hepatic stellate cells: central modulators of hepatic carcinogenesis. *BMC Gastroenterol* **15,** 63 (2015).
185. Morris, S. M. *et al.* TGF-β signaling alters the pattern of liver tumorigenesis induced by Pten inactivation. *Oncogene* **0,** (2014).
186. Yang, L. *et al.* Transforming growth factor-β signaling in hepatocytes promotes hepatic fibrosis and carcinogenesis in mice with hepatocyte-specific deletion of TAK1. *Gastroenterology* **144,** 1042–1054.e4 (2013).
187. Meindl-Beinker, N. M., Matsuzaki, K. & Dooley, S. TGF-β signaling in onset and progression of hepatocellular carcinoma. *Dig Dis* **30,** 514–523 (2012).
188. van Zijl, F. *et al.* Hepatic tumor-stroma crosstalk guides epithelial to mesenchymal transition at the tumor edge. *Oncogene* **28,** 4022–4033 (2009).
189. Mu, X. *et al.* TGF-β signaling is often attenuated during hepatotumorigenesis, but is retained for the malignancy of hepatocellular carcinoma cells. *PLoS ONE* **8,** e63436 (2013).
190. Dzieran, J. *et al.* Comparative analysis of TGF-β/Smad signaling dependent cytostasis in human hepatocellular carcinoma cell lines. *PLoS ONE* **8,** e72252 (2013).
191. Coulouarn, C., Factor, V. M. & Thorgeirsson, S. S. Transforming growth factor-beta gene expression signature in mouse hepatocytes predicts clinical outcome in human cancer. *Hepatology* **47,** 2059–2067 (2008).
192. Giannelli, G. *et al.* The rationale for targeting TGF-β in chronic liver diseases. *Eur. J. Clin. Invest.* **46,** 349–361 (2016).
193. Giannelli, G., Bergamini, C., Fransvea, E., Sgarra, C. & Antonaci, S. Laminin-5 with transforming growth factor-beta1 induces epithelial to mesenchymal transition in hepatocellular carcinoma. *Gastroenterology* **129,** 1375–1383 (2005).
194. Dapito, D. H. *et al.* Promotion of hepatocellular carcinoma by the intestinal microbiota and TLR4. *Cancer Cell* **21,** 504–516 (2012).
195. Darnaud, M., Faivre, J. & Moniaux, N. Targeting gut flora to prevent progression of hepatocellular carcinoma. *J. Hepatol.* **58,** 385–387 (2013).
196. Park, Y. N., Kim, Y. B., Yang, K. M. & Park, C. Increased expression of vascular endothelial growth factor and angiogenesis in the early stage of

multistep hepatocarcinogenesis. *Arch. Pathol. Lab. Med.* **124,** 1061–1065 (2000).
197. Yamaguchi, R. *et al.* Expression of vascular endothelial growth factor in human hepatocellular carcinoma. *Hepatology* **28,** 68–77 (1998).
198. Li, X. M., Tang, Z. Y., Zhou, G., Lui, Y. K. & Ye, S. L. Significance of vascular endothelial growth factor mRNA expression in invasion and metastasis of hepatocellular carcinoma. *J. Exp. Clin. Cancer Res.* **17,** 13–17 (1998).
199. Yao, D.-F. *et al.* Quantitative analysis of vascular endothelial growth factor, microvascular density and their clinicopathologic features in human hepatocellular carcinoma. *HBPD INT* **4,** 220–226 (2005).
200. Zhou, J. *et al.* Expression of platelet-derived endothelial cell growth factor and vascular endothelial growth factor in hepatocellular carcinoma and portal vein tumor thrombus. *J. Cancer Res. Clin. Oncol.* **126,** 57–61 (2000).
201. Zhu, A. X., Duda, D. G., Sahani, D. V. & Jain, R. K. HCC and angiogenesis: possible targets and future directions. *Nat Rev Clin Oncol* **8,** 292–301 (2011).
202. Llovet, J. M. *et al.* Plasma biomarkers as predictors of outcome in patients with advanced hepatocellular carcinoma. *Clin. Cancer Res.* **18,** 2290–2300 (2012).
203. Corpechot, C. *et al.* Hypoxia-induced VEGF and collagen I expressions are associated with angiogenesis and fibrogenesis in experimental cirrhosis. *Hepatology* **35,** 1010–1021 (2002).
204. Aleffi, S. *et al.* Upregulation of proinflammatory and proangiogenic cytokines by leptin in human hepatic stellate cells. *Hepatology* **42,** 1339–1348 (2005).
205. Taura, K. *et al.* Hepatic stellate cells secrete angiopoietin 1 that induces angiogenesis in liver fibrosis. *Gastroenterology* **135,** 1729–1738 (2008).
206. Wirz, W. *et al.* Hepatic stellate cells display a functional vascular smooth muscle cell phenotype in a three-dimensional co-culture model with endothelial cells. *Differentiation* **76,** 784–794 (2008).
207. Kang, N., Gores, G. J. & Shah, V. H. Hepatic stellate cells: partners in crime for liver metastases? *Hepatology* **54,** 707–713 (2011).
208. Ankoma-Sey, V., Wang, Y. & Dai, Z. Hypoxic stimulation of vascular endothelial growth factor expression in activated rat hepatic stellate cells. *Hepatology* **31,** 141–148 (2000).
209. Borkham-Kamphorst, E. *et al.* Pro-fibrogenic potential of PDGF-D in liver fibrosis. *J. Hepatol.* **46,** 1064–1074 (2007).
210. Novo, E. *et al.* Proangiogenic cytokines as hypoxia-dependent factors stimulating migration of human hepatic stellate cells. *Am. J. Pathol.* **170,** 1942–1953 (2007).
211. Torimura, T. *et al.* Increased expression of vascular endothelial growth factor is associated with tumor progression in hepatocellular carcinoma. *Hum. Pathol.* **29,** 986–991 (1998).
212. Coulouarn, C. *et al.* Hepatocyte-stellate cell cross-talk in the liver engenders a permissive inflammatory microenvironment that drives progression in hepatocellular carcinoma. *Cancer Res.* **72,** 2533–2542 (2012).
213. Lin, N. *et al.* Role of activated hepatic stellate cells in proliferation and metastasis of hepatocellular carcinoma. *Hepatol. Res.* (2014). doi:10.1111/hepr.12356
214. Torimura, T. *et al.* Overexpression of angiopoietin-1 and angiopoietin-2 in hepatocellular carcinoma. *J. Hepatol.* **40,** 799–807 (2004).
215. Qu, H. & Yang, X. Metformin inhibits angiogenesis induced by interaction of hepatocellular carcinoma with hepatic stellate cells. *Cell Biochem. Biophys.* **71,** 931–936 (2015).
216. Bhat, M. *et al.* Metformin does not improve survival in patients with hepatocellular carcinoma. *World J. Gastroenterol.* **20,** 15750–15755 (2014).

217. Ormandy, L. A. *et al.* Increased populations of regulatory T cells in peripheral blood of patients with hepatocellular carcinoma. *Cancer Res.* **65,** 2457–2464 (2005).
218. Fu, J. *et al.* Increased regulatory T cells correlate with CD8 T-cell impairment and poor survival in hepatocellular carcinoma patients. *Gastroenterology* **132,** 2328–2339 (2007).
219. Facciabene, A., Motz, G. T. & Coukos, G. T-regulatory cells: key players in tumor immune escape and angiogenesis. *Cancer Res.* **72,** 2162–2171 (2012).
220. Chen, K.-J. *et al.* Intratumoral regulatory T cells alone or in combination with cytotoxic T cells predict prognosis of hepatocellular carcinoma after resection. *Med. Oncol.* **29,** 1817–1826 (2012).
221. Xia, Y.-H. *et al.* T-cell apoptosis induced by intratumoral activated hepatic stellate cells is associated with lung metastasis in hepatocellular carcinoma. *Oncol. Rep.* **30,** 1175–1184 (2013).
222. Zhao, W. *et al.* Hepatic stellate cells promote tumor progression by enhancement of immunosuppressive cells in an orthotopic liver tumor mouse model. *Lab. Invest.* **94,** 182–191 (2014).
223. Chen, C.-H. *et al.* In vivo immune modulatory activity of hepatic stellate cells in mice. *Hepatology* **44,** 1171–1181 (2006).
224. Xia, Y. *et al.* Inhibition of T-cell responses by intratumoral hepatic stellate cells contribute to migration and invasion of hepatocellular carcinoma. *Clin. Exp. Metastasis* **28,** 661–674 (2011).
225. Muhanna, N., Horani, A., Doron, S. & Safadi, R. Lymphocyte-hepatic stellate cell proximity suggests a direct interaction. *Clin. Exp. Immunol.* **148,** 338–347 (2007).
226. Azuma, T. *et al.* B7-H1 is a ubiquitous antiapoptotic receptor on cancer cells. *Blood* **111,** 3635–3643 (2008).
227. Dong, H. *et al.* Costimulating aberrant T cell responses by B7-H1 autoantibodies in rheumatoid arthritis. *J. Clin. Invest.* **111,** 363–370 (2003).
228. Kuipers, H. *et al.* Contribution of the PD-1 ligands/PD-1 signaling pathway to dendritic cell-mediated CD4+ T cell activation. *Eur. J. Immunol.* **36,** 2472–2482 (2006).
229. Keir, M. E., Butte, M. J., Freeman, G. J. & Sharpe, A. H. PD-1 and its ligands in tolerance and immunity. *Annu. Rev. Immunol.* **26,** 677–704 (2008).
230. Ni, L. *et al.* PD-1 modulates regulatory T cells and suppresses T-cell responses in HCV-associated lymphoma. *Immunol. Cell Biol.* **89,** 535–539 (2011).
231. Francisco, L. M. *et al.* PD-L1 regulates the development, maintenance, and function of induced regulatory T cells. *J. Exp. Med.* **206,** 3015–3029 (2009).
232. McDermott, D. F. & Atkins, M. B. PD-1 as a potential target in cancer therapy. *Cancer Med* **2,** 662–673 (2013).
233. Brahmer, J. R. *et al.* Phase I study of single-agent anti-programmed death-1 (MDX-1106) in refractory solid tumors: safety, clinical activity, pharmacodynamics, and immunologic correlates. *J. Clin. Oncol.* **28,** 3167–3175 (2010).
234. Henderson, N. C. *et al.* Targeting of αv integrin identifies a core molecular pathway that regulates fibrosis in several organs. *Nat. Med.* **19,** 1617–1624 (2013).
235. Mederacke, I. *et al.* Fate tracing reveals hepatic stellate cells as dominant contributors to liver fibrosis independent of its aetiology. *Nat Commun* **4,** 2823 (2013).
236. Poelstra, K., Beljaars, L. & Melgert, B. N. Cell-specific delivery of biologicals: problems, pitfalls and possibilities of antifibrotic compounds in the liver. *Drug*

Discov. Today **18,** 1237–1242 (2013).
237. Elrick, L. J. *et al.* Generation of a monoclonal human single chain antibody fragment to hepatic stellate cells--a potential mechanism for targeting liver anti-fibrotic therapeutics. *J. Hepatol.* **42,** 888–896 (2005).
238. Sato, Y. *et al.* Resolution of liver cirrhosis using vitamin A-coupled liposomes to deliver siRNA against a collagen-specific chaperone. *Nat. Biotechnol.* **26,** 431–442 (2008).
239. Klein, S. *et al.* HSC-specific inhibition of Rho-kinase reduces portal pressure in cirrhotic rats without major systemic effects. *J. Hepatol.* **57,** 1220–1227 (2012).
240. Moreno, M. *et al.* Reduction of advanced liver fibrosis by short-term targeted delivery of an angiotensin receptor blocker to hepatic stellate cells in rats. *Hepatology* **51,** 942–952 (2010).
241. Beljaars, L., Weert, B., Geerts, A., Meijer, D. K. F. & Poelstra, K. The preferential homing of a platelet derived growth factor receptor-recognizing macromolecule to fibroblast-like cells in fibrotic tissue. *Biochem. Pharmacol.* **66,** 1307–1317 (2003).
242. Schoemaker, M. H. *et al.* PDGF-receptor beta-targeted adenovirus redirects gene transfer from hepatocytes to activated stellate cells. *Mol. Pharm.* **5,** 399–406 (2008).
243. Beljaars, L. *et al.* Successful targeting to rat hepatic stellate cells using albumin modified with cyclic peptides that recognize the collagen type VI receptor. *J. Biol. Chem.* **275,** 12743–12751 (2000).
244. Du, S.-L. *et al.* Cyclic Arg-Gly-Asp peptide-labeled liposomes for targeting drug therapy of hepatic fibrosis in rats. *J. Pharmacol. Exp. Ther.* **322,** 560–568 (2007).
245. Bansal, R., Prakash, J., De Ruiter, M. & Poelstra, K. Targeted recombinant fusion proteins of IFNγ and mimetic IFNγ with PDGFβR bicyclic peptide inhibits liver fibrogenesis in vivo. *PLoS ONE* **9,** e89878 (2014).
246. Bansal, R., Prakash, J., De Ruiter, M. & Poelstra, K. Interferon gamma peptidomimetic targeted to hepatic stellate cells ameliorates acute and chronic liver fibrosis in vivo. *J Control Release* **179,** 18–24 (2014).
247. Bansal, R. *et al.* Novel engineered targeted interferon-gamma blocks hepatic fibrogenesis in mice. *Hepatology* **54,** 586–596 (2011).
248. Rajewsky, M. F., Dauber, W. & Frankenberg, H. Liver carcinogenesis by diethylnitrosamine in the rat. *Science* **152,** 83–85 (1966).
249. Newell, P., Villanueva, A., Friedman, S. L., Koike, K. & Llovet, J. M. Experimental models of hepatocellular carcinoma. *J. Hepatol.* **48,** 858–879 (2008).
250. Bakiri, L. & Wagner, E. F. Mouse models for liver cancer. *Mol Oncol* **7,** 206–223 (2013).
251. Farazi, P. A. & DePinho, R. A. Hepatocellular carcinoma pathogenesis: from genes to environment. *Nat. Rev. Cancer* **6,** 674–687 (2006).
252. Thorgeirsson, S. S. & Grisham, J. W. Molecular pathogenesis of human hepatocellular carcinoma. *Nat. Genet.* **31,** 339–346 (2002).
253. Chen, B. *et al.* Dose-dependent ras mutation spectra in N-nitrosodiethylamine induced mouse liver tumors and 4-(methylnitrosamino)-1-(3-pyridyl)-1-butanone induced mouse lung tumors. *Carcinogenesis* **14,** 1603–1608 (1993).
254. Aleksic, K. *et al.* Evolution of genomic instability in diethylnitrosamine-induced hepatocarcinogenesis in mice. *Hepatology* **53,** 895–904 (2011).
255. Aydinlik, H., Nguyen, T. D., Moennikes, O., Buchmann, A. & Schwarz, M. Selective pressure during tumor promotion by phenobarbital leads to clonal outgrowth of beta-catenin-mutated mouse liver tumors. *Oncogene* **20,** 7812–7816 (2001).

256. Lee, J.-S. *et al.* Application of comparative functional genomics to identify best-fit mouse models to study human cancer. *Nat. Genet.* **36,** 1306–1311 (2004).
257. Lv, Z. *et al.* Tumor-stroma ratio is a prognostic factor for survival in hepatocellular carcinoma patients after liver resection or transplantation. *Surgery* **158,** 142–150 (2015).
258. Dekker, T. J. A. *et al.* Prognostic significance of the tumor-stroma ratio: validation study in node-negative premenopausal breast cancer patients from the EORTC perioperative chemotherapy (POP) trial (10854). *Breast Cancer Res. Treat.* **139,** 371–379 (2013).
259. Liu, J. *et al.* Tumor-stroma ratio is an independent predictor for survival in early cervical carcinoma. *Gynecol. Oncol.* **132,** 81–86 (2014).
260. Pietras, K. & Ostman, A. Hallmarks of cancer: interactions with the tumor stroma. *Exp. Cell Res.* **316,** 1324–1331 (2010).
261. Kalluri, R. & Zeisberg, M. Fibroblasts in cancer. *Nat. Rev. Cancer* **6,** 392–401 (2006).
262. Sugimoto, H., Mundel, T. M., Kieran, M. W. & Kalluri, R. Identification of fibroblast heterogeneity in the tumor microenvironment. *Cancer Biol. Ther.* **5,** 1640–1646 (2006).
263. Anderberg, C. *et al.* Paracrine signaling by platelet-derived growth factor-CC promotes tumor growth by recruitment of cancer-associated fibroblasts. *Cancer Res.* **69,** 369–378 (2009).
264. Farmer, P. *et al.* A stroma-related gene signature predicts resistance to neoadjuvant chemotherapy in breast cancer. *Nat. Med.* **15,** 68–74 (2009).
265. Crawford, Y. *et al.* PDGF-C mediates the angiogenic and tumorigenic properties of fibroblasts associated with tumors refractory to anti-VEGF treatment. *Cancer Cell* **15,** 21–34 (2009).
266. Pietras, K. *et al.* Inhibition of PDGF receptor signaling in tumor stroma enhances antitumor effect of chemotherapy. *Cancer Res.* **62,** 5476–5484 (2002).
267. Calon, A., Tauriello, D. V. F. & Batlle, E. TGF-beta in CAF-mediated tumor growth and metastasis. *Semin. Cancer Biol.* **25,** 15–22 (2014).
268. Reichl, P., Haider, C., Grubinger, M. & Mikulits, W. TGF-β in epithelial to mesenchymal transition and metastasis of liver carcinoma. *Curr. Pharm. Des.* **18,** 4135–4147 (2012).
269. Gupta, D. K., Singh, N. & Sahu, D. K. TGF-β Mediated Crosstalk Between Malignant Hepatocyte and Tumor Microenvironment in Hepatocellular Carcinoma. *Cancer Growth Metastasis* **7,** 1–8 (2014).
270. Hynes, R. O. Integrins: bidirectional, allosteric signaling machines. *Cell* **110,** 673–687 (2002).
271. Patsenker, E. & Stickel, F. Role of integrins in fibrosing liver diseases. *Am. J. Physiol. Gastrointest. Liver Physiol.* **301,** G425–34 (2011).
272. Wallace, M. C. & Friedman, S. L. Hepatic fibrosis and the microenvironment: fertile soil for hepatocellular carcinoma development. *Gene Expr.* **16,** 77–84 (2014).
273. Ignotz, R. A. & Massagué, J. Transforming growth factor-beta stimulates the expression of fibronectin and collagen and their incorporation into the extracellular matrix. *J. Biol. Chem.* **261,** 4337–4345 (1986).
274. Roberts, A. B. *et al.* Transforming growth factor type beta: rapid induction of fibrosis and angiogenesis in vivo and stimulation of collagen formation in vitro. *Proc. Natl. Acad. Sci. U.S.A.* **83,** 4167–4171 (1986).
275. Leask, A. & Abraham, D. J. TGF-beta signaling and the fibrotic response. *FASEB J.* **18,** 816–827 (2004).
276. Gleizes, P. E. *et al.* TGF-beta latency: biological significance and mechanisms

of activation. *Stem Cells* **15,** 190–197 (1997).
277. Munger, J. S. *et al.* Latent transforming growth factor-beta: structural features and mechanisms of activation. *Kidney Int.* **51,** 1376–1382 (1997).
278. Conroy, K. P., Kitto, L. J. & Henderson, N. C. αv integrins: key regulators of tissue fibrosis. *Cell Tissue Res.* (2016). doi:10.1007/s00441-016-2407-9
279. Munger, J. S. *et al.* The integrin alpha v beta 6 binds and activates latent TGF beta 1: a mechanism for regulating pulmonary inflammation and fibrosis. *Cell* **96,** 319–328 (1999).
280. Mu, D. *et al.* The integrin alpha(v)beta8 mediates epithelial homeostasis through MT1-MMP-dependent activation of TGF-beta1. *J. Cell Biol.* **157,** 493–507 (2002).
281. Annes, J. P., Rifkin, D. B. & Munger, J. S. The integrin alphaVbeta6 binds and activates latent TGFbeta3. *FEBS Lett.* **511,** 65–68 (2002).
282. Wipff, P.-J., Rifkin, D. B., Meister, J.-J. & Hinz, B. Myofibroblast contraction activates latent TGF-beta1 from the extracellular matrix. *J. Cell Biol.* **179,** 1311–1323 (2007).
283. Asano, Y., Ihn, H., Yamane, K., Jinnin, M. & Tamaki, K. Increased expression of integrin alphavbeta5 induces the myofibroblastic differentiation of dermal fibroblasts. *Am. J. Pathol.* **168,** 499–510 (2006).
284. Shi, M. *et al.* Latent TGF-β structure and activation. *Nature* **474,** 343–349 (2011).
285. Klingberg, F. *et al.* Prestress in the extracellular matrix sensitizes latent TGF-β1 for activation. *J. Cell Biol.* **207,** 283–297 (2014).
286. Reed, N. I. *et al.* The αvβ1 integrin plays a critical in vivo role in tissue fibrosis. *Sci Transl Med* **7,** 288ra79 (2015).
287. Wang, B. *et al.* Role of alphavbeta6 integrin in acute biliary fibrosis. *Hepatology* **46,** 1404–1412 (2007).
288. Popov, Y. *et al.* Integrin alphavbeta6 is a marker of the progression of biliary and portal liver fibrosis and a novel target for antifibrotic therapies. *J. Hepatol.* **48,** 453–464 (2008).
289. Patsenker, E. *et al.* Inhibition of integrin alphavbeta6 on cholangiocytes blocks transforming growth factor-beta activation and retards biliary fibrosis progression. *Gastroenterology* **135,** 660–670 (2008).
290. Peng, Z.-W. *et al.* Integrin αvβ6 critically regulates hepatic progenitor cell function and promotes ductular reaction, fibrosis, and tumorigenesis. *Hepatology* **63,** 217–232 (2016).
291. Breuss, J. M., Gillett, N., Lu, L., Sheppard, D. & Pytela, R. Restricted distribution of integrin beta 6 mRNA in primate epithelial tissues. *J. Histochem. Cytochem.* **41,** 1521–1527 (1993).
292. Breuss, J. M. *et al.* Expression of the beta 6 integrin subunit in development, neoplasia and tissue repair suggests a role in epithelial remodeling. *J. Cell. Sci.* **108 (Pt 6),** 2241–2251 (1995).
293. Patsenker, E. *et al.* Pharmacological inhibition of integrin alphavbeta3 aggravates experimental liver fibrosis and suppresses hepatic angiogenesis. *Hepatology* **50,** 1501–1511 (2009).
294. Aluwihare, P. *et al.* Mice that lack activity of alphavbeta6- and alphavbeta8-integrins reproduce the abnormalities of Tgfb1- and Tgfb3-null mice. *J. Cell. Sci.* **122,** 227–232 (2009).
295. Iordanskaia, T. *et al.* Integrin β-8, but not β-5 or -6, protein expression is increased in livers of children with biliary atresia. *J. Pediatr. Gastroenterol. Nutr.* **59,** 679–683 (2014).
296. Iordanskaia, T. *et al.* Dysregulation of upstream and downstream transforming growth factor-β transcripts in livers of children with biliary atresia and fibrogenic

gene signatures. *J. Pediatr. Surg.* **48,** 2047–2053 (2013).
297. Araya, J. *et al.* Squamous metaplasia amplifies pathologic epithelial-mesenchymal interactions in COPD patients. *J. Clin. Invest.* **117,** 3551–3562 (2007).
298. Shull, M. M. *et al.* Targeted disruption of the mouse transforming growth factor-beta 1 gene results in multifocal inflammatory disease. *Nature* **359,** 693–699 (1992).
299. Kulkarni, A. B. *et al.* Transforming growth factor beta 1 null mutation in mice causes excessive inflammatory response and early death. *Proc. Natl. Acad. Sci. U.S.A.* **90,** 770–774 (1993).
300. Yaswen, L. *et al.* Autoimmune manifestations in the transforming growth factor-beta 1 knockout mouse. *Blood* **87,** 1439–1445 (1996).
301. Khanna, R., Mosli, M. H. & Feagan, B. G. Anti-Integrins in Ulcerative Colitis and Crohn's Disease: What Is Their Place? *Dig Dis* **34,** 153–159 (2016).
302. Andrian, Von, U. H. & Engelhardt, B. Alpha4 integrins as therapeutic targets in autoimmune disease. *N. Engl. J. Med.* **348,** 68–72 (2003).
303. Balcer, L. J. *et al.* Natalizumab reduces visual loss in patients with relapsing multiple sclerosis. *Neurology* **68,** 1299–1304 (2007).
304. Miller, D. H. *et al.* A controlled trial of natalizumab for relapsing multiple sclerosis. *N. Engl. J. Med.* **348,** 15–23 (2003).
305. O'Connor, P. W. *et al.* Randomized multicenter trial of natalizumab in acute MS relapses: clinical and MRI effects. *Neurology* **62,** 2038–2043 (2004).
306. Polman, C. H. *et al.* A randomized, placebo-controlled trial of natalizumab for relapsing multiple sclerosis. *N. Engl. J. Med.* **354,** 899–910 (2006).
307. Lobatón, T., Vermeire, S., Van Assche, G. & Rutgeerts, P. Review article: anti-adhesion therapies for inflammatory bowel disease. *Aliment. Pharmacol. Ther.* **39,** 579–594 (2014).
308. Yednock, T. A. *et al.* Prevention of experimental autoimmune encephalomyelitis by antibodies against alpha 4 beta 1 integrin. *Nature* **356,** 63–66 (1992).
309. Ghosh, S. *et al.* Natalizumab for active Crohn's disease. *N. Engl. J. Med.* **348,** 24–32 (2003).
310. Sandborn, W. J. *et al.* Natalizumab induction and maintenance therapy for Crohn's disease. *N. Engl. J. Med.* **353,** 1912–1925 (2005).
311. Targan, S. R. *et al.* Natalizumab for the treatment of active Crohn's disease: results of the ENCORE Trial. *Gastroenterology* **132,** 1672–1683 (2007).
312. Berger, J. R. Progressive multifocal leukoencephalopathy and newer biological agents. *Drug Saf* **33,** 969–983 (2010).
313. Van Assche, G. *et al.* Progressive multifocal leukoencephalopathy after natalizumab therapy for Crohn's disease. *N. Engl. J. Med.* **353,** 362–368 (2005).
314. Feagan, B. G. *et al.* Vedolizumab as induction and maintenance therapy for ulcerative colitis. *N. Engl. J. Med.* **369,** 699–710 (2013).
315. Sandborn, W. J. *et al.* Vedolizumab as induction and maintenance therapy for Crohn's disease. *N. Engl. J. Med.* **369,** 711–721 (2013).
316. Halilbasic, E., Fuchs, C., Hofer, H., Paumgartner, G. & Trauner, M. Therapy of Primary Sclerosing Cholangitis--Today and Tomorrow. *Dig Dis* **33 Suppl 2,** 149–163 (2015).
317. Horan, G. S. *et al.* Partial inhibition of integrin alpha(v)beta6 prevents pulmonary fibrosis without exacerbating inflammation. *Am. J. Respir. Crit. Care Med.* **177,** 56–65 (2008).
318. Gladson, C. L. & Cheresh, D. A. Glioblastoma expression of vitronectin and the alpha v beta 3 integrin. Adhesion mechanism for transformed glial cells. *J. Clin.*

Invest. **88,** 1924–1932 (1991).
319. Schnell, O. *et al.* Imaging of integrin alpha(v)beta(3) expression in patients with malignant glioma by [18F] Galacto-RGD positron emission tomography. *Neuro-oncology* **11,** 861–870 (2009).
320. Weller, M. *et al.* Cilengitide in newly diagnosed glioblastoma: biomarker expression and outcome. *Oncotarget* **7,** 15018–15032 (2016).
321. Stupp, R. *et al.* Cilengitide combined with standard treatment for patients with newly diagnosed glioblastoma with methylated MGMT promoter (CENTRIC EORTC 26071-22072 study): a multicentre, randomised, open-label, phase 3 trial. *Lancet Oncol.* **15,** 1100–1108 (2014).
322. Nabors, L. B. *et al.* Two cilengitide regimens in combination with standard treatment for patients with newly diagnosed glioblastoma and unmethylated MGMT gene promoter: results of the open-label, controlled, randomized phase II CORE study. *Neuro-oncology* **17,** 708–717 (2015).
323. Nagy, A. Cre recombinase: the universal reagent for genome tailoring. *Genesis* **26,** 99–109 (2000).
324. Greenhalgh, S. N., Conroy, K. P. & Henderson, N. C. Cre-ativity in the liver: transgenic approaches to targeting hepatic nonparenchymal cells. *Hepatology* **61,** 2091–2099 (2015).
325. Heffner, C. S. *et al.* Supporting conditional mouse mutagenesis with a comprehensive cre characterization resource. *Nat Commun* **3,** 1218 (2012).
326. Michelotti, G. A. *et al.* Smoothened is a master regulator of adult liver repair. *J. Clin. Invest.* **123,** 2380–2394 (2013).
327. Swiderska-Syn, M. *et al.* Myofibroblastic cells function as progenitors to regenerate murine livers after partial hepatectomy. *Gut* **63,** 1333–1344 (2014).
328. Foo, S. S. *et al.* Ephrin-B2 controls cell motility and adhesion during blood-vessel-wall assembly. *Cell* **124,** 161–173 (2006).
329. Postic, C. *et al.* Dual roles for glucokinase in glucose homeostasis as determined by liver and pancreatic beta cell-specific gene knock-outs using Cre recombinase. *J. Biol. Chem.* **274,** 305–315 (1999).
330. Lacy-Hulbert, A. *et al.* Ulcerative colitis and autoimmunity induced by loss of myeloid alphav integrins. *Proc. Natl. Acad. Sci. U.S.A.* **104,** 15823–15828 (2007).
331. He, L., Tian, D.-A., Li, P.-Y. & He, X.-X. Mouse models of liver cancer: Progress and recommendations. *Oncotarget* **6,** 23306–23322 (2015).
332. Ge, Y.-Y. *et al.* MicroRNA-100 promotes the autophagy of hepatocellular carcinoma cells by inhibiting the expression of mTOR and IGF-1R. *Oncotarget* **5,** 6218–6228 (2014).
333. Killion, J. J., Radinsky, R. & Fidler, I. J. Orthotopic models are necessary to predict therapy of transplantable tumors in mice. *Cancer Metastasis Rev.* **17,** 279–284 (1998).
334. Kornek, M. *et al.* 1,2-dioleoyl-3-trimethylammonium-propane (DOTAP)-formulated, immune-stimulatory vascular endothelial growth factor a small interfering RNA (siRNA) increases antitumoral efficacy in murine orthotopic hepatocellular carcinoma with liver fibrosis. *Mol. Med.* **14,** 365–373 (2008).
335. Shachaf, C. M. *et al.* MYC inactivation uncovers pluripotent differentiation and tumour dormancy in hepatocellular cancer. *Nature* **431,** 1112–1117 (2004).
336. Tamano, S., Merlino, G. T. & Ward, J. M. Rapid development of hepatic tumors in transforming growth factor alpha transgenic mice associated with increased cell proliferation in precancerous hepatocellular lesions initiated by N-nitrosodiethylamine and promoted by phenobarbital. *Carcinogenesis* **15,** 1791–1798 (1994).
337. Kalinichenko, V. V. *et al.* Foxm1b transcription factor is essential for

development of hepatocellular carcinomas and is negatively regulated by the p19ARF tumor suppressor. *Genes Dev.* **18,** 830–850 (2004).
338. Horiguchi, N. *et al.* Hepatocyte growth factor promotes hepatocarcinogenesis through c-Met autocrine activation and enhanced angiogenesis in transgenic mice treated with diethylnitrosamine. *Oncogene* **21,** 1791–1799 (2002).
339. Jiang, R. *et al.* Interleukin-22 promotes human hepatocellular carcinoma by activation of STAT3. *Hepatology* **54,** 900–909 (2011).
340. Yang, X. *et al.* Essential contribution of a chemokine, CCL3, and its receptor, CCR1, to hepatocellular carcinoma progression. *Int. J. Cancer* **118,** 1869–1876 (2006).
341. Uehara, T., Pogribny, I. P. & Rusyn, I. The DEN and CCl4 -Induced Mouse Model of Fibrosis and Inflammation-Associated Hepatocellular Carcinoma. *Curr Protoc Pharmacol* **66,** 14.30.1–10 (2014).
342. Uehara, T. *et al.* Molecular mechanisms of fibrosis-associated promotion of liver carcinogenesis. *Toxicol. Sci.* **132,** 53–63 (2013).
343. Rosner, B. *Fundamentals of Biostatistics*.
344. Henderson, N. C. *et al.* Critical role of c-jun (NH2) terminal kinase in paracetamol- induced acute liver failure. *Gut* **56,** 982–990 (2007).
345. Walsh, T. S., Hopton, P., Philips, B. J., Mackenzie, S. J. & Lee, A. The effect of N-acetylcysteine on oxygen transport and uptake in patients with fulminant hepatic failure. *Hepatology* **27,** 1332–1340 (1998).
346. Harrison, P. M., Wendon, J. A., Gimson, A. E., Alexander, G. J. & Williams, R. Improvement by acetylcysteine of hemodynamics and oxygen transport in fulminant hepatic failure. *N. Engl. J. Med.* **324,** 1852–1857 (1991).
347. Wendon, J. A., Harrison, P. M., Keays, R. & Williams, R. Cerebral blood flow and metabolism in fulminant liver failure. *Hepatology* **19,** 1407–1413 (1994).
348. Hu, J., Zhang, Q., Ren, X., Sun, Z. & Quan, Q. Efficacy and safety of acetylcysteine in 'non-acetaminophen' acute liver failure: A meta-analysis of prospective clinical trials. *Clin Res Hepatol Gastroenterol* **39,** 594–599 (2015).
349. Donahower, B. C. *et al.* Human recombinant vascular endothelial growth factor reduces necrosis and enhances hepatocyte regeneration in a mouse model of acetaminophen toxicity. *J. Pharmacol. Exp. Ther.* **334,** 33–43 (2010).
350. Stutchfield, B. M. *et al.* CSF1 Restores Innate Immunity After Liver Injury in Mice and Serum Levels Indicate Outcomes of Patients With Acute Liver Failure. *Gastroenterology* **149,** 1896–1909.e14 (2015).
351. Shen, K. *et al.* Depletion of activated hepatic stellate cell correlates with severe liver damage and abnormal liver regeneration in acetaminophen-induced liver injury. *Acta Biochim. Biophys. Sin. (Shanghai)* **43,** 307–315 (2011).
352. Chang, W.-J. *et al.* Early activated hepatic stellate cell-derived molecules reverse acute hepatic injury. *World J. Gastroenterol.* **21,** 4184–4194 (2015).
353. Stewart, R. K. *et al.* A novel mouse model of depletion of stellate cells clarifies their role in ischemia/reperfusion- and endotoxin-induced acute liver injury. *J. Hepatol.* **60,** 298–305 (2014).
354. Geerts, A. History, heterogeneity, developmental biology, and functions of quiescent hepatic stellate cells. *Semin. Liver Dis.* **21,** 311–335 (2001).
355. Yang, L. *et al.* Fate-mapping evidence that hepatic stellate cells are epithelial progenitors in adult mouse livers. *Stem Cells* **26,** 2104–2113 (2008).
356. Lu, L. *et al.* Restoration of intrahepatic regulatory T cells through MMP-9/13-dependent activation of TGF-β is critical for immune homeostasis following acute liver injury. *J Mol Cell Biol* **5,** 369–379 (2013).
357. Feng, M. *et al.* Adoptive transfer of hepatic stellate cells ameliorates liver ischemia reperfusion injury through enriching regulatory T cells. *Int. Immunopharmacol.* **19,** 267–274 (2014).

358. Feng, M. *et al.* Adoptive transferred hepatic stellate cells attenuated drug-induced liver injury by modulating the rate of regulatory T cells/T helper 17 cells. *Clin. Immunol.* **165,** 12–18 (2016).
359. Niu, L. *et al.* Involvement of TGF-β1/Smad3 Signaling in Carbon Tetrachloride-Induced Acute Liver Injury in Mice. *PLoS ONE* **11,** e0156090 (2016).
360. Travis, M. A. *et al.* Loss of integrin alpha(v)beta8 on dendritic cells causes autoimmunity and colitis in mice. *Nature* **449,** 361–365 (2007).
361. Poisson, J. *et al.* Liver sinusoidal endothelial cells: physiology and role in liver diseases. *J. Hepatol.* (2016). doi:10.1016/j.jhep.2016.07.009
362. DeLeve, L. D. Liver sinusoidal endothelial cells and liver regeneration. *J. Clin. Invest.* **123,** 1861–1866 (2013).
363. Wang, L. *et al.* Liver sinusoidal endothelial cell progenitor cells promote liver regeneration in rats. *J. Clin. Invest.* **122,** 1567–1573 (2012).
364. McCuskey, R. S. Morphological mechanisms for regulating blood flow through hepatic sinusoids. *Liver* **20,** 3–7 (2000).
365. Rockey, D. The cellular pathogenesis of portal hypertension: stellate cell contractility, endothelin, and nitric oxide. *Hepatology* **25,** 2–5 (1997).
366. DeLeve, L. D., Wang, X. & Guo, Y. Sinusoidal endothelial cells prevent rat stellate cell activation and promote reversion to quiescence. *Hepatology* **48,** 920–930 (2008).
367. Ito, Y., Bethea, N. W., Abril, E. R. & McCuskey, R. S. Early hepatic microvascular injury in response to acetaminophen toxicity. *Microcirculation* **10,** 391–400 (2003).
368. Badmann, A. *et al.* TRAIL enhances paracetamol-induced liver sinusoidal endothelial cell death in a Bim- and Bid-dependent manner. *Cell Death Dis* **3,** e447 (2012).
369. Lalor, P. F., Herbert, J., Bicknell, R. & Adams, D. H. Hepatic sinusoidal endothelium avidly binds platelets in an integrin-dependent manner, leading to platelet and endothelial activation and leukocyte recruitment. *Am. J. Physiol. Gastrointest. Liver Physiol.* **304,** G469–78 (2013).
370. Mossanen, J. C. & Tacke, F. Acetaminophen-induced acute liver injury in mice. *Lab. Anim.* **49,** 30–36 (2015).
371. Cohen, S. D. & Khairallah, E. A. Selective protein arylation and acetaminophen-induced hepatotoxicity. *Drug Metab. Rev.* **29,** 59–77 (1997).
372. Pumford, N. R., Halmes, N. C. & Hinson, J. A. Covalent binding of xenobiotics to specific proteins in the liver. *Drug Metab. Rev.* **29,** 39–57 (1997).
373. Ray, S. D., Kamendulis, L. M., Gurule, M. W., Yorkin, R. D. & Corcoran, G. B. Ca2+ antagonists inhibit DNA fragmentation and toxic cell death induced by acetaminophen. *FASEB J.* **7,** 453–463 (1993).
374. Zhang, H. *et al.* Reduction of liver Fas expression by an antisense oligonucleotide protects mice from fulminant hepatitis. *Nat. Biotechnol.* **18,** 862–867 (2000).
375. Lawson, J. A., Fisher, M. A., Simmons, C. A., Farhood, A. & Jaeschke, H. Inhibition of Fas receptor (CD95)-induced hepatic caspase activation and apoptosis by acetaminophen in mice. *Toxicol. Appl. Pharmacol.* **156,** 179–186 (1999).
376. Ray, S. D., Mumaw, V. R., Raje, R. R. & Fariss, M. W. Protection of acetaminophen-induced hepatocellular apoptosis and necrosis by cholesteryl hemisuccinate pretreatment. *J. Pharmacol. Exp. Ther.* **279,** 1470–1483 (1996).
377. Ray, S. D. & Jena, N. A hepatotoxic dose of acetaminophen modulates expression of BCL-2, BCL-X(L), and BCL-X(S) during apoptotic and necrotic death of mouse liver cells in vivo. *Arch. Toxicol.* **73,** 594–606 (2000).
378. Gujral, J. S., Knight, T. R., Farhood, A., Bajt, M. L. & Jaeschke, H. Mode of cell

death after acetaminophen overdose in mice: apoptosis or oncotic necrosis? *Toxicol. Sci.* **67,** 322–328 (2002).
379. Bhushan, B. *et al.* Pro-regenerative signaling after acetaminophen-induced acute liver injury in mice identified using a novel incremental dose model. *Am. J. Pathol.* **184,** 3013–3025 (2014).
380. Faubion, W. A. & Gores, G. J. Death receptors in liver biology and pathobiology. *Hepatology* **29,** 1–4 (1999).
381. Krams, S. M. *et al.* Human hepatocytes produce an isoform of FAS that inhibits apoptosis. *Transplantation* **65,** 713–721 (1998).
382. Adachi, M. *et al.* Enhanced and accelerated lymphoproliferation in Fas-null mice. *Proc. Natl. Acad. Sci. U.S.A.* **93,** 2131–2136 (1996).
383. Mochizuki, K. *et al.* Fas antigen expression in liver tissues of patients with chronic hepatitis B. *J. Hepatol.* **24,** 1–7 (1996).
384. Galle, P. R. *et al.* Involvement of the CD95 (APO-1/Fas) receptor and ligand in liver damage. *J. Exp. Med.* **182,** 1223–1230 (1995).
385. Hayashi, N. & Mita, E. Fas system and apoptosis in viral hepatitis. *J. Gastroenterol. Hepatol.* **12,** S223–6 (1997).
386. Giordano, C. *et al.* Potential involvement of Fas and its ligand in the pathogenesis of Hashimoto's thyroiditis. *Science* **275,** 960–963 (1997).
387. Ogasawara, J. *et al.* Lethal effect of the anti-Fas antibody in mice. *Nature* **364,** 806–809 (1993).
388. Hübner, G. [Ultrastructural liver damage caused by direct action of carbon tetrachloride in vivo and in vitro]. *Virchows Arch Pathol Anat Physiol Klin Med* **339,** 187–197 (1965).
389. Smith, D. H. Carbon tetrachloride toxicity. *Br Med J* **2,** 1434 (1965).
390. Rahman, T. M. & Hodgson, H. J. Animal models of acute hepatic failure. *Int J Exp Pathol* **81,** 145–157 (2000).
391. Shi, J., Aisaki, K., Ikawa, Y. & Wake, K. Evidence of hepatocyte apoptosis in rat liver after the administration of carbon tetrachloride. *Am. J. Pathol.* **153,** 515–525 (1998).
392. Proctor, J. M., Zang, K., Wang, D., Wang, R. & Reichardt, L. F. Vascular development of the brain requires beta8 integrin expression in the neuroepithelium. *J. Neurosci.* **25,** 9940–9948 (2005).
393. Wang, Y. *et al.* Ephrin-B2 controls VEGF-induced angiogenesis and lymphangiogenesis. *Nature* **465,** 483–486 (2010).
394. Pearlman, F. C. & Lee, R. T. Detection and measurement of total bilirubin in serum, with use of surfactants as solubilizing agents. *Clin. Chem.* **20,** 447–453 (1974).
395. Bergmeyer, H. U., Scheibe, P. & Wahlefeld, A. W. Optimization of methods for aspartate aminotransferase and alanine aminotransferase. *Clin. Chem.* **24,** 58–73 (1978).
396. Mohar, I. *et al.* Acetaminophen-induced liver damage in mice is associated with gender-specific adduction of peroxiredoxin-6. *Redox Biol* **2,** 377–387 (2014).
397. Dear, J. W. *et al.* Cyclophilin A is a damage-associated molecular pattern molecule that mediates acetaminophen-induced liver injury. *J. Immunol.* **187,** 3347–3352 (2011).
398. Vliegenthart, A. D. B. *et al.* Comprehensive microRNA profiling in acetaminophen toxicity identifies novel circulating biomarkers for human liver and kidney injury. *Sci Rep* **5,** 15501 (2015).
399. Denk, W., Strickler, J. H. & Webb, W. W. Two-photon laser scanning fluorescence microscopy. *Science* **248,** 73–76 (1990).
400. Pittet, M. J. & Weissleder, R. Intravital imaging. *Cell* **147,** 983–991 (2011).

401. Thomas, G., van Voskuilen, J., Gerritsen, H. C. & Sterenborg, H. J. C. M. Advances and challenges in label-free nonlinear optical imaging using two-photon excitation fluorescence and second harmonic generation for cancer research. *J. Photochem. Photobiol. B, Biol.* **141,** 128–138 (2014).
402. Spence, D. E., Kean, P. N. & Sibbett, W. 60-fsec pulse generation from a self-mode-locked Ti:sapphire laser. *Opt Lett* **16,** 42–44 (1991).
403. Palero, J. A., de Bruijn, H. S., van der Ploeg van den Heuvel, A., Sterenborg, H. J. C. M. & Gerritsen, H. C. Spectrally resolved multiphoton imaging of in vivo and excised mouse skin tissues. *Biophys. J.* **93,** 992–1007 (2007).
404. Andresen, V. *et al.* Infrared multiphoton microscopy: subcellular-resolved deep tissue imaging. *Curr. Opin. Biotechnol.* **20,** 54–62 (2009).
405. Condeelis, J. & Weissleder, R. In vivo imaging in cancer. *Cold Spring Harb Perspect Biol* **2,** a003848 (2010).
406. Vakoc, B. J. *et al.* Three-dimensional microscopy of the tumor microenvironment in vivo using optical frequency domain imaging. *Nat. Med.* **15,** 1219–1223 (2009).
407. Campagnola, P. J. & Loew, L. M. Second-harmonic imaging microscopy for visualizing biomolecular arrays in cells, tissues and organisms. *Nat. Biotechnol.* **21,** 1356–1360 (2003).
408. Evans, C. L. *et al.* Chemical imaging of tissue in vivo with video-rate coherent anti-Stokes Raman scattering microscopy. *Proc. Natl. Acad. Sci. U.S.A.* **102,** 16807–16812 (2005).
409. Cheng, J.-X. Coherent anti-Stokes Raman scattering microscopy. *Appl Spectrosc* **61,** 197–208 (2007).
410. Potcoava, M. C., Futia, G. L., Aughenbaugh, J., Schlaepfer, I. R. & Gibson, E. A. Raman and coherent anti-Stokes Raman scattering microscopy studies of changes in lipid content and composition in hormone-treated breast and prostate cancer cells. *J Biomed Opt* **19,** 111605 (2014).
411. Lehr, H. A., Leunig, M., Menger, M. D., Nolte, D. & Messmer, K. Dorsal skinfold chamber technique for intravital microscopy in nude mice. *Am. J. Pathol.* **143,** 1055–1062 (1993).
412. Palmer, G. M. *et al.* In vivo optical molecular imaging and analysis in mice using dorsal window chamber models applied to hypoxia, vasculature and fluorescent reporters. *Nat Protoc* **6,** 1355–1366 (2011).
413. Perentes, J. Y. *et al.* In vivo imaging of extracellular matrix remodeling by tumor-associated fibroblasts. *Nat. Methods* **6,** 143–145 (2009).
414. Brown, E. B. *et al.* In vivo measurement of gene expression, angiogenesis and physiological function in tumors using multiphoton laser scanning microscopy. *Nat. Med.* **7,** 864–868 (2001).
415. Gligorijevic, B., Kedrin, D., Segall, J. E., Condeelis, J. & van Rheenen, J. Dendra2 photoswitching through the Mammary Imaging Window. *J Vis Exp* (2009). doi:10.3791/1278
416. Kedrin, D. *et al.* Intravital imaging of metastatic behavior through a mammary imaging window. *Nat. Methods* **5,** 1019–1021 (2008).
417. Shan, S., Sorg, B. & Dewhirst, M. W. A novel rodent mammary window of orthotopic breast cancer for intravital microscopy. *Microvasc. Res.* **65,** 109–117 (2003).
418. Pan, F. & Gan, W.-B. Two-photon imaging of dendritic spine development in the mouse cortex. *Dev Neurobiol* **68,** 771–778 (2008).
419. Yuan, F. *et al.* Vascular permeability and microcirculation of gliomas and mammary carcinomas transplanted in rat and mouse cranial windows. *Cancer Res.* **54,** 4564–4568 (1994).
420. Kienast, Y. *et al.* Real-time imaging reveals the single steps of brain

metastasis formation. *Nat. Med.* **16,** 116–122 (2010).
421. Ritsma, L. *et al.* Surgical implantation of an abdominal imaging window for intravital microscopy. *Nat Protoc* **8,** 583–594 (2013).
422. Mempel, T. R., Henrickson, S. E. & Andrian, Von, U. H. T-cell priming by dendritic cells in lymph nodes occurs in three distinct phases. *Nature* **427,** 154–159 (2004).
423. Xu, C., Shen, Y., Littman, D. R., Dustin, M. L. & Velázquez, P. Visualization of mucosal homeostasis via single- and multiphoton intravital fluorescence microscopy. *J. Leukoc. Biol.* **92,** 413–419 (2012).
424. Ritsma, L. *et al.* Intravital microscopy through an abdominal imaging window reveals a pre-micrometastasis stage during liver metastasis. *Sci Transl Med* **4,** 158ra145 (2012).
425. Egen, J. G. *et al.* Intravital imaging reveals limited antigen presentation and T cell effector function in mycobacterial granulomas. *Immunity* **34,** 807–819 (2011).
426. Wong, C. H. Y., Jenne, C. N., Lee, W.-Y., Léger, C. & Kubes, P. Functional innervation of hepatic iNKT cells is immunosuppressive following stroke. *Science* **334,** 101–105 (2011).
427. McDonald, B. *et al.* Interaction of CD44 and hyaluronan is the dominant mechanism for neutrophil sequestration in inflamed liver sinusoids. *J. Exp. Med.* **205,** 915–927 (2008).
428. Marques, P. E. *et al.* Imaging liver biology in vivo using conventional confocal microscopy. *Nat Protoc* **10,** 258–268 (2015).
429. Marques, P. E. *et al.* Hepatic DNA deposition drives drug-induced liver injury and inflammation in mice. *Hepatology* **61,** 348–360 (2015).
430. McDonald, B. *et al.* Intravascular danger signals guide neutrophils to sites of sterile inflammation. *Science* **330,** 362–366 (2010).
431. Hickey, M. J. & Westhorpe, C. L. V. Imaging inflammatory leukocyte recruitment in kidney, lung and liver--challenges to the multi-step paradigm. *Immunol. Cell Biol.* **91,** 281–289 (2013).
432. Marques, P. E., Oliveira, A. G., Chang, L., Paula-Neto, H. A. & Menezes, G. B. Understanding liver immunology using intravital microscopy. *J. Hepatol.* **63,** 733–742 (2015).
433. Heymann, F. *et al.* Long term intravital multiphoton microscopy imaging of immune cells in healthy and diseased liver using CXCR6.Gfp reporter mice. *J Vis Exp* (2015). doi:10.3791/52607
434. Dal-Secco, D. *et al.* A dynamic spectrum of monocytes arising from the in situ reprogramming of CCR2+ monocytes at a site of sterile injury. *J. Exp. Med.* **212,** 447–456 (2015).
435. Montalvo-Jave, E. E., Escalante-Tattersfield, T., Ortega-Salgado, J. A., Piña, E. & Geller, D. A. Factors in the pathophysiology of the liver ischemia-reperfusion injury. *J. Surg. Res.* **147,** 153–159 (2008).
436. Gracia-Sancho, J., Casillas-Ramírez, A. & Peralta, C. Molecular pathways in protecting the liver from ischaemia/reperfusion injury: a 2015 update. *Clin. Sci.* **129,** 345–362 (2015).
437. Khandoga, A. *et al.* P-selectin mediates platelet-endothelial cell interactions and reperfusion injury in the mouse liver in vivo. *Shock* **18,** 529–535 (2002).
438. Khandoga, A. *et al.* Platelet adhesion mediated by fibrinogen-intercelllular adhesion molecule-1 binding induces tissue injury in the postischemic liver in vivo. *Transplantation* **74,** 681–688 (2002).
439. Mende, K. *et al.* Targeting platelet migration in the postischemic liver by blocking protease-activated receptor 4. *Transplantation* **97,** 154–160 (2014).
440. Khandoga, A. *et al.* Augmenter of liver regeneration attenuates inflammatory

response in the postischemic mouse liver in vivo. *J. Surg. Res.* **192,** 187–194 (2014).
441. Thorling, C. A. *et al.* Multiphoton microscopy can visualize zonal damage and decreased cellular metabolic activity in hepatic ischemia-reperfusion injury in rats. *J Biomed Opt* **16,** 116011 (2011).
442. Bird, D. K. *et al.* Metabolic mapping of MCF10A human breast cells via multiphoton fluorescence lifetime imaging of the coenzyme NADH. *Cancer Res.* **65,** 8766–8773 (2005).
443. Thorling, C. A. *et al.* Intravital multiphoton microscopy can model uptake and excretion of fluorescein in hepatic ischemia-reperfusion injury. *J Biomed Opt* **18,** 101306 (2013).
444. Wang, H. *et al.* Real-time histology in liver disease using multiphoton microscopy with fluorescence lifetime imaging. *Biomed Opt Express* **6,** 780–792 (2015).
445. Lu, H.-H. *et al.* Molecular imaging of ischemia and reperfusion in vivo with mitochondrial autofluorescence. *Anal. Chem.* **86,** 5024–5031 (2014).
446. Schlegel, M. *et al.* Inhibition of neogenin dampens hepatic ischemia-reperfusion injury. *Crit. Care Med.* **42,** e610–9 (2014).
447. Jellestad, L. *et al.* Inhibition of glycogen synthase kinase (GSK)-3-β improves liver microcirculation and hepatocellular function after hemorrhagic shock. *Eur. J. Pharmacol.* **724,** 175–184 (2014).
448. Kim, J.-S. *et al.* Carbamazepine suppresses calpain-mediated autophagy impairment after ischemia/reperfusion in mouse livers. *Toxicol. Appl. Pharmacol.* **273,** 600–610 (2013).
449. Tamura, T., Kondo, T., Ogawa, K., Fukunaga, K. & Ohkohchi, N. Protective effect of heme oxygenase-1 on hepatic ischemia-reperfusion injury through inhibition of platelet adhesion to the sinusoids. *J. Gastroenterol. Hepatol.* **28,** 700–706 (2013).
450. Junnarkar, S. P. *et al.* Attenuation of warm ischemia-reperfusion injury in the liver by bucillamine through decreased neutrophil activation and Bax/Bcl-2 modulation. *J. Gastroenterol. Hepatol.* **25,** 1891–1899 (2010).
451. Li, F.-C. *et al.* Apical membrane rupture and backward bile flooding in acetaminophen-induced hepatocyte necrosis. *Cell Death Dis* **2,** e183 (2011).
452. Walker, R. M., Racz, W. J. & McElligott, T. F. Scanning electron microscopic examination of acetaminophen-induced hepatotoxicity and congestion in mice. *Am. J. Pathol.* **113,** 321–330 (1983).
453. Amaral, S. S. *et al.* Altered responsiveness to extracellular ATP enhances acetaminophen hepatotoxicity. *Cell Commun. Signal* **11,** 10 (2013).
454. Ito, Y., Abril, E. R., Bethea, N. W. & McCuskey, R. S. Role of nitric oxide in hepatic microvascular injury elicited by acetaminophen in mice. *Am. J. Physiol. Gastrointest. Liver Physiol.* **286,** G60–7 (2004).
455. Pires, D. A. *et al.* Interleukin-4 deficiency protects mice from acetaminophen-induced liver injury and inflammation by prevention of glutathione depletion. *Inflamm. Res.* **63,** 61–69 (2014).
456. Gomides, L. F. *et al.* Murine model to study brain, behavior and immunity during hepatic encephalopathy. *World J Hepatol* **6,** 243–250 (2014).
457. Bonder, C. S., Ajuebor, M. N., Zbytnuik, L. D., Kubes, P. & Swain, M. G. Essential role for neutrophil recruitment to the liver in concanavalin A-induced hepatitis. *J. Immunol.* **172,** 45–53 (2004).
458. Bonder, C. S. *et al.* Rules of recruitment for Th1 and Th2 lymphocytes in inflamed liver: a role for alpha-4 integrin and vascular adhesion protein-1. *Immunity* **23,** 153–163 (2005).
459. Lee, W.-Y. *et al.* An intravascular immune response to Borrelia burgdorferi

involves Kupffer cells and iNKT cells. *Nat. Immunol.* **11,** 295–302 (2010).
460. Wong, C. H. Y., Jenne, C. N., Petri, B., Chrobok, N. L. & Kubes, P. Nucleation of platelets with blood-borne pathogens on Kupffer cells precedes other innate immunity and contributes to bacterial clearance. *Nat. Immunol.* **14,** 785–792 (2013).
461. McDonald, B., Jenne, C. N., Zhuo, L., Kimata, K. & Kubes, P. Kupffer cells and activation of endothelial TLR4 coordinate neutrophil adhesion within liver sinusoids during endotoxemia. *Am. J. Physiol. Gastrointest. Liver Physiol.* **305,** G797–806 (2013).
462. Egen, J. G. *et al.* Macrophage and T cell dynamics during the development and disintegration of mycobacterial granulomas. *Immunity* **28,** 271–284 (2008).
463. Kolaczkowska, E. *et al.* Molecular mechanisms of NET formation and degradation revealed by intravital imaging in the liver vasculature. *Nat Commun* **6,** 6673 (2015).
464. McDonald, B., Urrutia, R., Yipp, B. G., Jenne, C. N. & Kubes, P. Intravascular neutrophil extracellular traps capture bacteria from the bloodstream during sepsis. *Cell Host Microbe* **12,** 324–333 (2012).
465. Branzk, N. *et al.* Neutrophils sense microbe size and selectively release neutrophil extracellular traps in response to large pathogens. *Nat. Immunol.* **15,** 1017–1025 (2014).
466. Saffarzadeh, M. *et al.* Neutrophil extracellular traps directly induce epithelial and endothelial cell death: a predominant role of histones. *PLoS ONE* **7,** e32366 (2012).
467. Xu, J. *et al.* Extracellular histones are major mediators of death in sepsis. *Nat. Med.* **15,** 1318–1321 (2009).
468. Frevert, U. *et al.* Intravital observation of Plasmodium berghei sporozoite infection of the liver. *PLoS Biol.* **3,** e192 (2005).
469. Pradel, G., Garapaty, S. & Frevert, U. Proteoglycans mediate malaria sporozoite targeting to the liver. *Mol. Microbiol.* **45,** 637–651 (2002).
470. Shin, S. C., Vanderberg, J. P. & Terzakis, J. A. Direct infection of hepatocytes by sporozoites of Plasmodium berghei. *J. Protozool.* **29,** 448–454 (1982).
471. Cockburn, I. A. *et al.* In vivo imaging of CD8+ T cell-mediated elimination of malaria liver stages. *Proc. Natl. Acad. Sci. U.S.A.* **110,** 9090–9095 (2013).
472. Kimura, K. *et al.* CD8+ T cells specific for a malaria cytoplasmic antigen form clusters around infected hepatocytes and are protective at the liver stage of infection. *Infect. Immun.* **81,** 3825–3834 (2013).
473. Akbari, M., Kimura, K., Houts, J. T. & Yui, K. Intravital imaging of the immune responses during liver-stage malaria infection: An improved approach for fixing the liver. *Parasitol. Int.* (2016). doi:10.1016/j.parint.2016.02.011
474. Beattie, L. *et al.* Dynamic imaging of experimental Leishmania donovani-induced hepatic granulomas detects Kupffer cell-restricted antigen presentation to antigen-specific CD8 T cells. *PLoS Pathog.* **6,** e1000805 (2010).
475. Dasari, S., Weber, P., Makhloufi, C., Lopez, E. & Forestier, C.-L. Intravital Microscopy Imaging of the Liver following Leishmania Infection: An Assessment of Hepatic Hemodynamics. *J Vis Exp* e52303 (2015). doi:10.3791/52303
476. Hanahan, D. & Weinberg, R. A. The hallmarks of cancer. *Cell* **100,** 57–70 (2000).
477. Hanahan, D. & Weinberg, R. A. Hallmarks of cancer: the next generation. *Cell* **144,** 646–674 (2011).
478. Ellenbroek, S. I. J. & van Rheenen, J. Imaging hallmarks of cancer in living mice. *Nat. Rev. Cancer* **14,** 406–418 (2014).

479. Canel, M. *et al.* Quantitative in vivo imaging of the effects of inhibiting integrin signaling via Src and FAK on cancer cell movement: effects on E-cadherin dynamics. *Cancer Res.* **70,** 9413–9422 (2010).
480. Serrels, A. *et al.* Real-time study of E-cadherin and membrane dynamics in living animals: implications for disease modeling and drug development. *Cancer Res.* **69,** 2714–2719 (2009).
481. Chudakov, D. M., Lukyanov, S. & Lukyanov, K. A. Tracking intracellular protein movements using photoswitchable fluorescent proteins PS-CFP2 and Dendra2. *Nat Protoc* **2,** 2024–2032 (2007).
482. Takeichi, T., Engelmann, G., Mocevicius, P., Schmidt, J. & Ryschich, E. 4-dimensional intravital microscopy: a new model for studies of leukocyte recruitment and migration in hepatocellular cancer in mice. *J. Gastrointest. Surg.* **14,** 867–872 (2010).
483. Tanaka, K. *et al.* In vivo time-course imaging of tumor angiogenesis in colorectal liver metastases in the same living mice using two-photon laser scanning microscopy. *J Oncol* **2012,** 265487 (2012).
484. Madisen, L. *et al.* A robust and high-throughput Cre reporting and characterization system for the whole mouse brain. *Nat. Neurosci.* **13,** 133–140 (2010).
485. Muzumdar, M. D., Tasic, B., Miyamichi, K., Li, L. & Luo, L. A global double-fluorescent Cre reporter mouse. *Genesis* **45,** 593–605 (2007).
486. Snippert, H. J. *et al.* Intestinal crypt homeostasis results from neutral competition between symmetrically dividing Lgr5 stem cells. *Cell* **143,** 134–144 (2010).
487. Weissman, T. A., Sanes, J. R., Lichtman, J. W. & Livet, J. Generating and imaging multicolor Brainbow mice. *Cold Spring Harb Protoc* **2011,** 763–769 (2011).
488. Lee, M. *et al.* In vivo imaging of the tumor and its associated microenvironment using combined CARS/2-photon microscopy. *IntraVital* **4,** (2015).